

Cover Page



Universiteit Leiden



The handle <http://hdl.handle.net/1887/58921> holds various files of this Leiden University dissertation.

Author: Handgraaf, H.J.M.

Title: Intraoperative fluorescence imaging : clinical translation of targeted and non-targeted tracers

Issue Date: 2018-01-09

**INTRAOPERATIVE
INTRAOPERATIVE
FLUORESCENCE
FLUORESCENCE
IMAGING** HEIN HANDGRAAF

Clinical translation of targeted and non-targeted tracers



INTRAOPERATIVE FLUORESCENCE IMAGING

INTRAOPERATIVE FLUORESCENCE IMAGING

Clinical translation of targeted and non-targeted tracers

© H.J.M. Handgraaf 2017

COVER PHOTO
Annemarie Handgraaf

DESIGN
Caroline de Lint (caro@delint.nl)

ISBN
978-90-9030728-2

All rights reserved. No part of this thesis may be reproduced, distributed or transmitted in any form or by any means, without prior written permission of the author.

The research described in this thesis was financially supported by the Center for Translational Molecular Imaging, Dutch Cancer Society, European Research Council and National Institutes of Health.

The publication of this thesis was financially supported by the foundation Centre for Human Drug Research, Leiden, The Netherlands.

PROEFSCHRIFT

Ter verkrijging van de graad van Doctor aan de Universiteit Leiden, op gezag van Rector Magnificus prof. mr. C.J.J.M. Stolker, volgens besluit van het College voor Promoties te verdedigen op dinsdag 9 januari 2018
Klokke 16:15 uur

DOOR

Henricus Johannes Marinus Handgraaf
Geboren te Boxtel
In 1988

PROMOTORES

Prof. dr. C.J.H. van de Velde
Prof. dr. J. Burggraaf

CO-PROMOTOR

Dr. A.L. Vahrmeijer

LEDEN PROMOTIECOMMISSIE

Prof. dr. L.F. de Geus-Oei
Prof. dr. ir. B.P.F. Lelieveldt
Prof. dr. C.W.G.M. Löwik (Erasmus Medisch Centrum, Rotterdam)
Dr. K. Bosscha (Jeroen Bosch Ziekenhuis, 's-Hertogenbosch)

1	Outline of the thesis	
PART I. INTRODUCTION TO FLUORESCENCE IMAGING		
2	Current and future intraoperative imaging strategies to increase radical resection rates in pancreatic cancer surgery	12
3	Real-time near-infrared fluorescence guided surgery in gynecologic oncology: a review of the current state of the art	27
4	Identification of malignant tumors in the liver	45
PART II. NON-TARGETED TRACERS		
5	Intraoperative near-infrared fluorescence imaging of multiple pancreatic neuroendocrine tumors: a case report	63
6	Intraoperative near-infrared fluorescence imaging of tumor border and sentinel lymph nodes in rectal cancer	69
7	Long-term follow-up after near-infrared fluorescence-guided resection of colorectal liver metastases: a retrospective multicenter analysis	81
8	Staging laparoscopy combined with ultrasonography and near-infrared fluorescence imaging to detect occult pancreatic metastases	99
PART III. TARGETED TRACERS		
9	Detecting tumor-positive resection margins after oral cancer surgery by spraying a fluorescent tracer activated by gamma-glutamyltranspeptidase	115
10	Real-time near-infrared fluorescence imaging using CRGD-ZW800-1 for multiple cancer types	133
11	Real-time near-infrared fluorescence imaging of ZW800-1 and CRGD-ZW800-1: a translational study in healthy volunteers	153
PART IV. SUMMARY AND APPENDICES		
12	Summary and discussion	171
13	Nederlandse samenvatting	183
	Curriculum vitae	189
	List of publications	190
	Dankwoord	192

CHAPTER 1

Outline of the thesis

Surgery is the cornerstone of curative treatment of many malignancies. Incomplete resection of tumors and avoidable iatrogenic damage during surgery increase morbidity and mortality rates in patients. Although advances in preoperative imaging modalities have improved adequate patient selection and surgical planning, during procedures surgeons mainly rely on inspection and palpation. It is often very difficult to distinguish between fibrotic, inflamed, or malignant tissues. Inspection and palpation are highly subjective and have low sensitivity for detecting cancer, especially for subcentimeter lesions. This thesis describes intraoperative near-infrared fluorescence (NIRF) imaging: a promising technique that enhances contrast of certain structures during surgery and improves thereby their detectability. It uses targeted and non-targeted fluorescent tracers in combination with dedicated NIRF imaging systems.

Part I outlines current challenges and solutions to locate tumors and other tissue types during various surgical procedures. **Chapter 1** describes pancreatic cancer surgery. With the currently available techniques it remains very difficult to distinguish between malignant, inflamed and healthy tissue. As a consequence, up to 75% of the resections is incomplete. This will lead to (local) recurrences and a worse prognosis. New technologies, including NIRF imaging could be a solution. **Chapter 2** contains a review of the use of NIRF imaging during gynecological procedures. Indocyanine green (ICG) improves visual detection of sentinel lymph nodes compared to standard methodology. Methylene blue can be used to detect ureters, even if they are not yet fully exposed. Tumor-targeted tracers allow the detection of ovarian cancer metastases. **Chapter 3** describes the identification of hepatic tumors. ICG is cleared via the liver, but accumulates in a rim around hepatic malignancies. Healthy liver tissue clears ICG within one day after intravenous administration, while tumors remain visible by a characteristic fluorescent bullseye. This way, preoperatively diagnosed tumors as well as otherwise undetectable tumors can be detected.

Part II addresses the clinical use of non-targeted fluorophores. **Chapter 4** describes a patient with multiple pancreatic neuroendocrine tumors due to multiple endocrine neoplasia type 1 (MEN1) syndrome. Although the mechanism is not fully understood, methylene blue accumulates in certain tumors, including neuroendocrine tumors and parathyroid adenomas. In this chapter, it was attempted to identify neuroendocrine tumors with NIRF imaging and a low dose methylene blue. **Chapter 5** assesses the feasibility to mark tumors with ICG. During laparoscopic rectal cancer surgery it is often difficult to localize the tumor. Gastroenterologists mark the location currently with ink. Ink is however not always visible during surgery, for example when the spot is covered by tissue or blood. In this study, it was tested if the tumor's location was detected earlier by NIRF imaging or by ink. **Chapter 6** aimed to demonstrate if NIRF imaging during resection of colorectal

liver metastases affects the total procedure time, the amount of resected tissue and the complication rates. Moreover, the effect of NIRF imaging on survival of patients is currently unknown. A key unanswered question is whether the metastases additionally identified by NIRF are indicative of otherwise undetectable, widespread metastases in the liver or if patients are in fact cured by resecting these lesions. This study evaluated the long-term follow-up after NIRF-guided resections of colorectal liver metastases. In **chapter 7** it is attempted to increase the yield of staging laparoscopy in patients with pancreatic or periampullary cancer. The hypothesis is that NIRF imaging combined with laparoscopic ultrasound will detect more occult metastases compared to inspection alone. Accuracy of inspection, laparoscopic ultrasound and NIRF imaging was assessed in 25 patients with pancreatic or periampullary cancer.

Part III addresses the application of targeted fluorophores. In **chapter 8** a fluorescent tracer that becomes fluorescent only when activated by gamma-glutamyltranspeptidase (GGT) is investigated. GGT is overexpressed on several tumor types, including squamous cell carcinoma of the oral cavity. Activatable tracers can minimize nonspecific background fluorescence, because unbound tracers are not fluorescent. Furthermore, spraying such tracers on resected tissue instead of intravenous administration eliminates the risk of adverse events in patients and does not require expensive and time-consuming translational studies. **Chapter 9** describes CRGD, a protein targeting integrins associated with neoangiogenesis, conjugated to the 800 nm fluorophore ZW800-1. CRGD-ZW800-1 has the potential to visualize multiple tumor types. Several nonclinical *in vitro* and *in vivo* experiments are required prior to a first-in-human study. **Chapter 10** discusses the first-in-human studies of ZW800-1 and CRGD-ZW800-1. Safety, tolerability and pharmacokinetics of doses up to 5.0 mg ZW800-1 and 0.005 mg/kg CRGD-ZW800-1 are tested in two separate studies in healthy volunteers.

Finally, **part IV** provides a summary and discussion of the results and describes the future perspectives of fluorescence imaging.

PART I

INTRODUCTION TO FLUORESCENCE IMAGING

CHAPTER 2

Current and future
intraoperative imaging
strategies to increase radical
resection rates in pancreatic
cancer surgery *Biomed Res Int. 2014; 2014:890230*

HJM HANDGRAAF, MC BOONSTRA, AR VAN ERKEL, BA BONSING, H PUTTER,
CJH VAN DE VELDE, AL VAHRMEIJER, JSD MIEOG

ABSTRACT

Prognosis of patients with pancreatic cancer is poor. Even the small minority that undergoes resection with curative intent has low 5-year survival rates. This may partly be explained by the high number of irradical resections, which results in local recurrence and impaired overall survival. Currently, ultrasonography is used during surgery for resectability assessment and frozen-section analysis is used for assessment of resection margins in order to decrease the number of irradical resections. The introduction of minimal invasive techniques in pancreatic surgery has deprived surgeons from direct tactile information. To improve intraoperative assessment of pancreatic tumor extension, enhanced or novel intraoperative imaging technologies accurately visualizing and delineating cancer cells are necessary. Emerging modalities are intraoperative near-infrared fluorescence imaging and freehand nuclear imaging using tumor-specific targeted contrast agents. In this review, we performed a meta-analysis of the literature on laparoscopic ultrasonography and we summarized and discussed current and future intraoperative imaging modalities and their potential for improved tumor demarcation during pancreatic surgery.

INTRODUCTION

Surgery is the cornerstone of curative intended treatment of pancreatic cancer [1]. However, resection of pancreatic cancer is only suitable for a minority of patients [2, 3]. Pancreatic cancer surgery is only conducted when there is a reasonable chance of complete removal of all cancer cells (radical resection), as irradical resection does not improve survival, but elicit procedure-related morbidity and mortality [4]. Consequently, pancreatic cancer is known for its high mortality and low 5-year survival of only 6% [5].

Despite recent advances in preoperative imaging modalities, such as computed tomography (CT) and magnetic resonance imaging (MRI), the preoperative assessment of resectability is limited due to difficult differentiation of necrosis, fibrosis and edematous tissue from malignant tumor cells, especially after neo-adjuvant therapy [6-9]. The combination of endoscopic ultrasonography (EUS) and laparoscopic ultrasonography improves resectability assessment [10, 11]. However, microscopic involvement of resection margins (R1 resection) is reported up to 75% of cases, which results in local recurrences and decreased overall survival [12-17]. Therefore, intraoperative imaging strategies accurately visualizing pancreatic cancer cells are highly necessary. Preoperative imaging of pancreatic cancer using CT, MRI, single-photon emission CT (SPECT), positron emission tomography (PET) and EUS enhance surgical planning, but translating these results to the operating room is difficult due to altered body positioning, tissue manipulation by the surgeon and lack of sensitivity for subcentimeter lesions. When laparotomy is performed, careful palpation and inspection can yield more information about tumor localization. Minimal-invasive techniques have become important in daily clinical practice, but limit tactile feedback.

In conclusion, there is a dire need for imaging techniques accurately visualizing and delineating pancreatic cancer during surgery. This review discusses current techniques that are used to assess pancreatic tumor extension during surgery and evaluates the most promising future imaging techniques (Figure 1).

CURRENT STRATEGIES

Ultrasonography during surgery

Ultrasonography (US) is a safe and inexpensive modality that can be used for determination of resectability and identification of metastases (Figure 1A) [18-21]. Besides percutaneous application, US is also used during laparoscopy (laparoscopic ultrasonography, LUS) and open surgery (intraoperative ultrasonography, IOUS). Compared to palpation and visual inspection, US is less sensitive for surface evaluations but outperforms in examination of the interior of organs and to determine blood flow in vasculature [22]. Its user-dependency is a limitation; substantial

training and experience are required for generating and interpreting useful images during pancreatic cancer surgery. Furthermore, ultrasound waves are unable to penetrate through air or gas, hampering the visibility of structures and organs located behind hollow organs. But, by slight compression or by imaging from another side, this limitation can mostly be overcome.

Various studies have evaluated the role of LUS in predicting tumor resectability during staging laparoscopy [23-39]. The term 'resectability' is used to indicate if radical resection (RO) of the tumor is technically possible in the absence of vascular involvement and distant metastases. Staging laparoscopy combined with LUS is not always used to determine resectability, since it is debated whether this approach should be offered routinely, selectively or not at all to those who appear resectable during their preoperative work-up.[38, 40] We performed an extensive review of the literature and pooled the available data in a meta-analysis. We included seventeen studies published between 1995 and 2011. We excluded individual patients from the meta-analysis if: pancreatic cancer was preoperative considered to be unresectable [27, 29, 34, 36, 38], patients did not undergo LUS, but only laparoscopy [34, 36, 37]; patients declined surgery [31, 37]; and if patients were diagnosed with other pathology than pancreatic cancer [31, 32, 35, 37]. In two studies on selective use of LUS, it was not possible to extract the subpopulation of patients that received LUS assessment [41, 42]. Therefore, these studies were not included. In total, data on 1,255 patients undergoing LUS were available for the meta-analysis. A random effect model was chosen due to significant heterogeneity between studies. Pooled sensitivity of LUS for determining unresectable disease was 76% (95% CI = 65-87%) and negative predictive value, the proportion of patients correctly diagnosed with resectable disease, was 82% (95% CI = 75-88%) (Figure 2). The variance between studies may partly be explained by a difference in *a priori* probability, potentially as a result of patient selection by different preoperative imaging modalities. Furthermore, different criteria for unresectability were used.

We were unable to find any study on the use of IOUS in determining resectability, except some outdated literature, which reported success with IOUS in visualizing non-palpable pancreatic masses [43]. Besides assessing localization and characteristics of the primary tumor, US can also be used for the detection of previously unnoticed metastases. Sensitivity of laparoscopy combined with LUS reached 100% in detecting hepatic and peritoneal metastases in a study of 26 patients with pancreatic cancer compared with percutaneous US, CT or EUS [44].

US is a useful intraoperative imaging technique and provides valuable information about size, localization and characteristics of lesions. By intraoperative suspicion of unresectability, LUS can aid in avoiding futile resections, and even more when combined with pretherapeutic EUS [10, 11, 36, 45]. However, little literature exists about the value of US-guided surgery in reducing positive resection margins in pancreatic cancer surgery.

Intraoperative frozen-section analysis

Intraoperative frozen-section analysis (IFSA) of the margins in the pancreatic neck is commonly performed and currently considered as the most important method for intraoperative assessment of the resection margin (Figure 1B). It is a safe, fast and easy to perform, however, it requires significant processing and evaluating time [46]. Additional resection in case of positive resection margins seems logical, but several studies describe no significant survival benefit after re-resection [47-49]. However, no standardized protocol for frozen sections of pancreatic cancer resection margins was described in the studies. The use of non-standardized methods for histopathological analysis greatly influences the reporting of resection margin status [13, 17, 50]. This may explain the low sensitivity of only 33% in evaluating final resection margin status using IFSA [46]. Due to this inconsistent reporting, little is known on the relation between exact tumor location within the pancreas and margin involvement. When standardized protocols are used, IFSA can potentially be a good method for resection margin assessment. However, IFSA will not provide visual and real-time feedback.

FUTURE STRATEGIES

Contrast-enhanced ultrasonography

Ultrasonography is very usable during pancreatic surgery, hence improvements such as contrast-enhanced US (CEUS) are currently being studied. CEUS uses intravenously administered microbubbles, which allow better determination of vessel infiltration and improved visualization of tumor margins during percutaneous imaging [51-54]. Furthermore, CEUS has already shown to help differentiate between chronic pancreatitis and ductal carcinoma [55]. Finally, CEUS can potentially help in identifying more hepatic metastases [56]. During open resection of colorectal liver metastases, the use of CEUS was of significant value in assessing adequate margins and detecting additional lesions. Preoperative CEUS results are encouraging, translation to the operation room is required to fully study the added value of CEUS during pancreatic cancer surgery.

Fluorescence-guided surgery

Fluorescence-guided surgery has emerged as a novel intraoperative modality to assist surgeons to visualize tumors, sentinel lymph nodes and vital structures in real-time (Figure 1C) [57]. Near-infrared (NIR) light (700 - 900 nanometers) can penetrate through several millimeters tissue, revealing targets below the tissue surface [58]. Consequently, NIR fluorescence imaging is currently a surface technique.

At present only two NIR fluorophores are FDA approved and can be used in the clinical setting, namely indocyanine green and methylene blue. Both fluorophores are non-specific and are mainly used for sentinel lymph node mapping, bile duct imaging and ureter visualization [57]. Indocyanine green has shown to accumulate around hepatic metastasis of pancreatic and colorectal cancers, probably due to retention of indocyanine green in compressed hepatocytes, which is shown by a fluorescent rim [59, 60]. In 16% of patients undergoing pancreatic resection without preclinical detected hepatic metastases, fluorescence imaging revealed micrometastases of at least 1.5 mm, which was confirmed by histopathological examination. By revealing undetected hepatic metastases, NIR fluorescence imaging can further decrease the rate of futile pancreatic resections. Furthermore, although its mechanism is unknown, we and others showed that methylene blue tends to accumulate in neuroendocrine tumors, including pancreatic insulinomas [61, 62]. However, due to the non-specificity no tumor-specific targeting can be expected of ICG and MB, as was shown by our group in pancreatic carcinomas [63]. To obtain the full advantages of NIR fluorescence imaging for pancreatic cancer visualization, tumor specific NIR conjugated ligands need to be designed and tested.

The biological tumor make-up can be used to visualize pancreatic tumors. In the last decades, research on pancreas carcinoma proteomics gained more attention. An increasing number of differentially expressed proteins are identified (<http://www.pancreasexpression.org>). Although very promising, these biomarker studies focus mainly on diagnosis or prevention and not necessarily on biomarkers which can be used to recognize malignant cells and to function as tumor-specific target. Potential biomarker for these approaches must possess additional characteristics, such as homogenic expression, upregulation of more than ten times compared to the surrounding tissue and localization on the cellular membrane for better accessibility. Ideally, these biomarkers can also recognize precursor lesions, early stages and distinguish between pancreatic cancer and inflammation.

Until now, no membrane-bound biomarkers are validated in the clinic, but recent literature show very promising results in preclinical studies. Various forms of CEA, integrins, BRCA1 and tumor-associated glycoprotein-17 (TAG-17) are over-expressed on pancreatic tumor cells while C-MET, EPCAM and CXCR-4 are also used as pancreatic cancer stem cell markers [64, 65]. Biomarkers from the plasmin(ogen) cascade are frequently associated with early stage invasion and cell dissociation [66]. The urokinase receptor (UPAR) is highly upregulated on pancreatic tumors, is associated with tumor invasion and its soluble variant differentiates between pancreatic adenocarcinomas and chronic pancreatitis [67, 68].

Very promising pre-clinical results are already reported for pancreatic cancer specific molecular targets like CEA, MMPs, claudin-4, RGD and cholecystokinin-2 receptor [69-73]. The focus within the field is currently shifting towards clinical translation and the first successful in-human results of tumor targeted probes has

already been published, although this study is concerning ovarian cancer patients [74]. Real-time NIR fluorescence imaging using tumor-targeted probes has the potential to accurately visualize tumor and its demarcation, hence to increase radical resection rates. The next steps should be clinical translation of pancreatic cancer specific probes, improving commercially available NIR fluorescence imaging systems and validation of the benefits for patients.

Nuclear imaging

Besides fluorophores, ligands can also be conjugated to radiotracers, which are directed to tumor-specific biomarkers eliciting tumor specific signals and enhancing tumor visualization (Figure 1D). These radioactive ligands are used in the preoperative setting with PET and SPECT and intraoperative with RadiolmmunoGuided Surgery (RIGS). RIGS was first described in 1984 by Aitken et al., who developed a hand-held gamma detector that can be used intra-operatively, but the technique has become relatively redundant due to the variable sensitivity, the delay in imaging of nearly a week (due to clearance of unbound antibody from the body) and difficulties in handling and disposing the radioactive material [75-78]. A relatively new nuclear imaging technique is freehand SPECT (FSPECT), which was lately introduced as a three-dimensional (3D) imaging and navigation technique that provides real-time images designed for use in the operating room to facilitate detection and resection [79]. However, this technique shows promising results in lymphatic mapping in breast cancer and for the visualization of thyroid diseases but not yet for pancreatic cancer where no known literature exists [79, 80].

DISCUSSION

The field of pancreatic cancer surgery is changing due to improvements in therapies and imaging modalities. These advances have not only led to better pancreatic cancer surgery, but also to limitations. The introduction of laparoscopic techniques, for example, has resulted in less postoperative pain, shorter hospital stay and lower morbidity [81, 82]. However, laparoscopy deprives the surgeon of tactile information, which is helpful during pancreatic cancer surgery. Another example is neoadjuvant therapy, after which a proportion of patients becomes eligible for curative-intended surgery [83]. However, preoperative imaging modalities, such as CT and MRI, drop in sensitivity and specificity in patients who received chemotherapy, for instance because they cannot accurately distinguish between vascular involvement or vascular encasement only due to periarterial stranding and fibrosis [6-9].

Intraoperative imaging modalities, which can accurately depict pancreatic cancer can overcome these limitations. Current available technologies, such

as US, have their own limitations. US-guided surgery failed to decrease the rate of R1 resections, possibly due to the fact that quality of obtained images is not high enough. The combination of different imaging modalities has proven to be a successful way to overcome separate limitations; PET/CT, for example, fuses anatomical and functional images in a single scan [84]. The combination of US with other techniques could increase functionality. A potential hybrid concept is FSPECT/US, which has already proven to be possible and easy to perform [80].

Molecular imaging is another promising research field where improvements may be expected. NIR fluorescence imaging offers visual guidance during surgery and can therefore potentially reduce the rate of positive resection margins. Fluorescence-guided laparoscopy during hepatopancreatobiliary surgery has already shown its potential to improve intraoperative identification and demarcation of tumors [85]. Remaining fluorescence signal in the resection wound can be an indication of irradical resection, which may make IFSA redundant. To date, no in-human trials have been done with pancreatic cancer specific contrast agents, but preclinical studies are very promising. A major restriction of NIR fluorescence imaging is its limited penetration depth; fluorescence signal is diminished within one centimeter tissue. This is an issue due to the retroperitoneal location of the pancreas. But again, fusing technologies could overcome this limitation. Radiolabeled NIR fluorescence probes may result in the best of two worlds: direct optical guidance and high penetration capacity of the radiotracer [86]. In addition, preoperative planning is possible with PET detection of the radiotracer [87]. Another improvement should be the development of novel probes that are highly specific for pancreatic cancer cells only, hence result in less background signal and lower false-positive rates. Improved fluorophores, which can easily be conjugated to different ligands are already available, such as ZW800-1 and CW800 [88]. Furthermore, improved imaging systems should become commercially available, making NIR fluorescence imaging available to a broader range of hospitals. But before NIR fluorescence imaging or a hybrid approach can lead to change in patient management, large multicenter studies are necessary to show if these intraoperative imaging modalities are beneficial for patients.

CONCLUSION

To improve surgical outcome, reduce irradical resections and improve patients' survival, novel intraoperative imaging strategies are necessary in pancreatic cancer surgery. Therefore, enhanced imaging technologies that can accurately visualize and delineate pancreatic cancer and its extension in real-time are currently being developed and tested. Tumor-specific targeted probes for near-infrared fluorescence imaging are very promising, but research in the next years will have to determine if these modalities are truly of added value for our patients.

Figure 1 Schematic overview of current and future intra-operative imaging modalities. A: Ultrasonography showing a pancreatic tumor (demarcated with red line). B: Intra-operative frozen section analysis and C: optical imaging using near-infrared imaging.

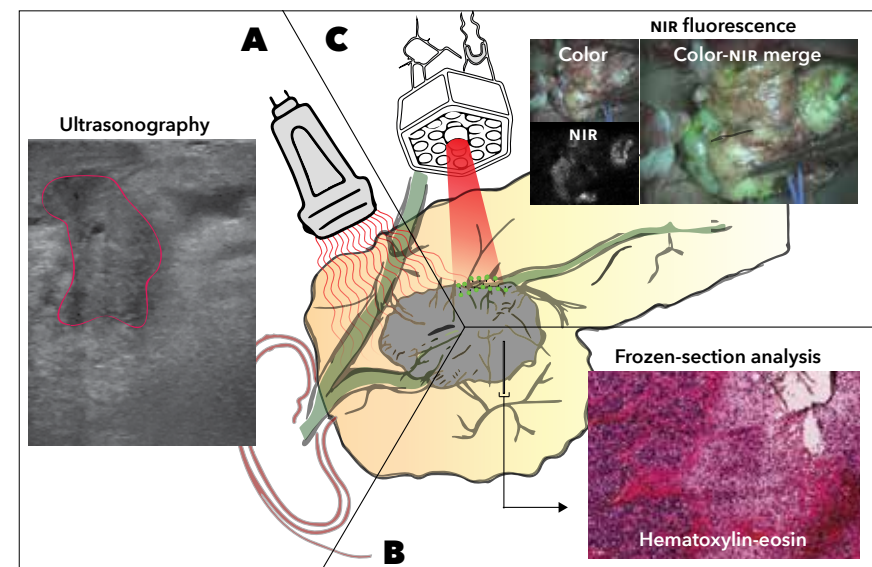
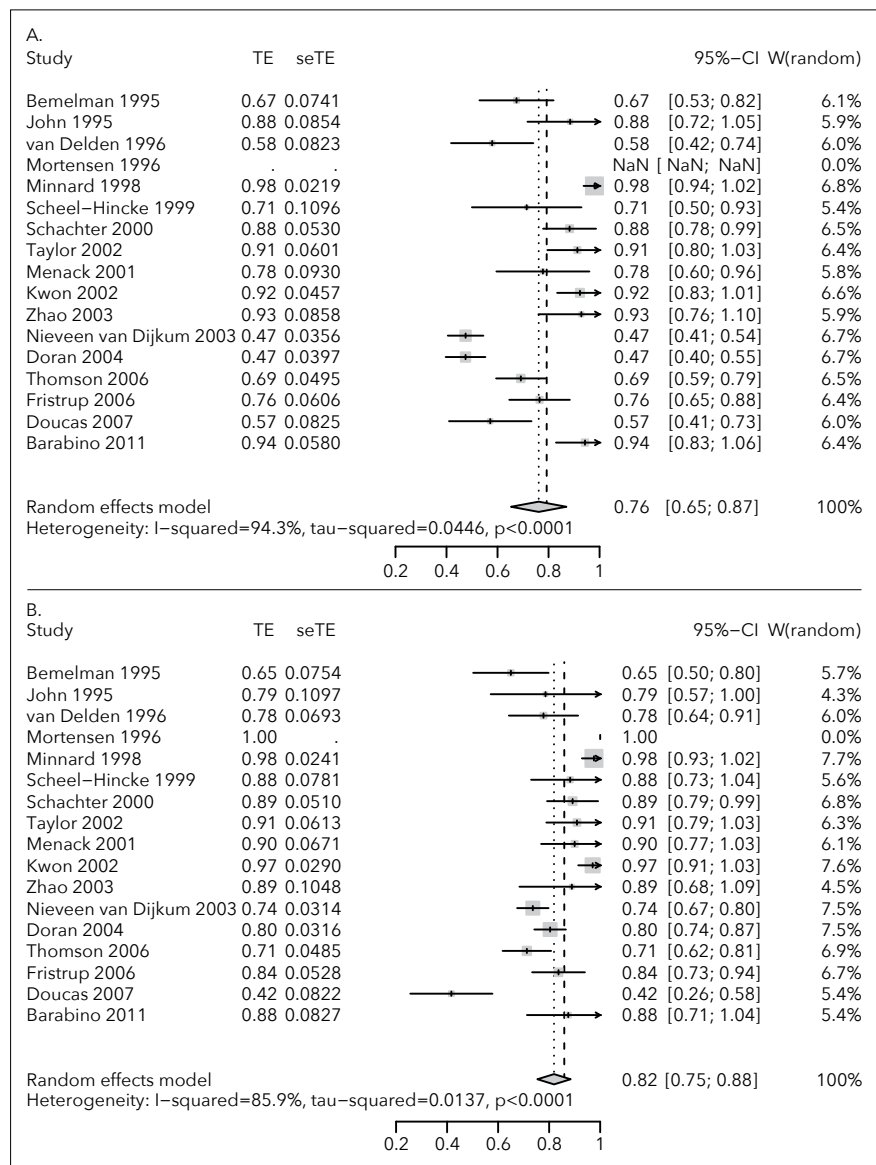


Figure 2 Forest plot of pooled data on (A) sensitivity and (B) negative predictive value of laparoscopic ultrasonography in predicting unresectability of pancreatic cancer, which is preoperatively considered to be resectable.



* Thomson et al. included 152 patients, 61% had pancreatic adenocarcinoma, 12% presumed pancreatic cancer, 11% ampullary cancer, 5% cholangiocarcinoma, 11% other diagnoses. No data solely describing pancreatic cancer patients was available.

REFERENCES

- Diener MK, Knaebel HP, Heukauf C, Antes G, Buchler MW and Seiler CM. A systematic review and meta-analysis of pylorus-preserving versus classical pancreaticoduodenectomy for surgical treatment of periampullary and pancreatic carcinoma. *Ann Surg.* 2007; 245(2):187-200.
- Hackert T, Buchler MW and Werner J. Surgical options in the management of pancreatic cancer. *Minerva Chir.* 2009; 64(5):465-476.
- Bilimoria KY, Bentrem DJ, Ko CY, Stewart AK, Winchester DP and Talamonti MS. National failure to operate on early stage pancreatic cancer. *Ann Surg.* 2007; 246(2):173-180.
- Barugola G, Partelli S, Marcucci S, Sartori N, Capelli P, Bassi C, Pederzoli P and Falconi M. Resectable pancreatic cancer: who really benefits from resection? *Ann Surg Oncol.* 2009; 16(12):3316-3322.
- Siegel R, Naishadham D and Jemal A. Cancer statistics, 2013. *CA Cancer J Clin.* 2013; 63(1):11-30.
- Egorov VI, Petrov RV, Solodina EN, Kar-mazanovsky GG, Starostina NS and Kuruschkina NA. Computed tomography-based diagnostics might be insufficient in the determination of pancreatic cancer unresectability. *World J Gastrointest Surg.* 2013; 5(4):83-96.
- Buchs NC, Chilcott M, Poletti PA, Buhler LH and Morel P. Vascular invasion in pancreatic cancer: Imaging modalities, preoperative diagnosis and surgical management. *World J Gastroenterol.* 2010; 16(7):818-831.
- Manak E, Merkel S, Klein P, Papadopoulos T, Bautz WA and Baum U. Resectability of pancreatic adenocarcinoma: assessment using multidetector-row computed tomography with multiplanar reformations. *Abdom Imaging.* 2009; 34(1):75-80.
- Cassinotto C, Cortade J, Belleanne G, Lapuyade B, Terrebonne E, Vendrely V, Laurent C and Sa-Cunha A. An evaluation of the accuracy of CT when determining resectability of pancreatic head adenocarcinoma after neoadjuvant treatment. *Eur J Radiol.* 2013; 82(4):589-593.
- Mortensen MB, Fristrup CW, Ainsworth AP, Pless T, Nielsen HO and Hovendal C. Combined preoperative endoscopic and laparoscopic ultrasonography for prediction of RO resection in upper gastrointestinal tract cancer. *Br J Surg.* 2006; 93(6):720-725.
- Mortensen MB, Fristrup C, Ainsworth A, Nielsen HO, Pless T and Hovendal C. Combined pretherapeutic endoscopic and laparoscopic ultrasonography may predict survival of patients with upper gastrointestinal tract cancer. *Surg Endosc.* 2011; 25(3):804-812.
- Menon KV, Gomez D, Smith AM, Anthony A and Verbeke CS. Impact of margin status on survival following pancreatoduodenectomy for cancer: the Leeds Pathology Protocol (LEPP). *HPB (Oxford).* 2009; 11(1):18-24.
- Verbeke CS and Gladhaug IP. Resection margin involvement and tumour origin in pancreatic head cancer. *Br J Surg.* 2012; 99(8):1036-1049.
- Schnelldorfer T, Ware AL, Sarr MG, Smyrk TC, Zhang L, Qin R, Gullerud RE, Donohue JH, Nagorney DM and Farnell MB. Long-term survival after pancreatoduodenectomy for pancreatic adenocarcinoma: is cure possible? *Ann Surg.* 2008; 247(3):456-462.
- Garcea G, Dennison AR, Pattenden CJ, Neal CP, Sutton CD and Berry DP. Survival following curative resection for pancreatic ductal adenocarcinoma. A systematic review of the literature. *JOP.* 2008; 9(2):99-132.
- Esposito I, Kleeff J, Bergmann F, Reiser C, Herpel E, Friess H, Schirmacher P and Buchler MW. Most pancreatic cancer resections are R1 resections. *Ann Surg Oncol.* 2008; 15(6):1651-1660.
- Verbeke CS, Leitch D, Menon KV, McMahon MJ, Guillou PJ and Anthony A. Redefining the R1 resection in pancreatic cancer. *Br J Surg.* 2006; 93(10):1232-1237.
- Hariharan D, Constantinides VA, Froeling FE, Tekkis PP and Kocher HM. The role of laparoscopy and laparoscopic ultrasound in the preoperative staging of pancreatico-biliary cancers--A meta-analysis. *Eur J Surg Oncol.* 2010; 36(10):941-948.
- Oshikawa O, Tanaka S, Ioka T, Nakaizumi A, Hamada Y and Mitani T. Dynamic sonography of pancreatic tumors: comparison with dynamic CT. *AJR Am J Roentgenol.* 2002; 178(5):1133-1137.
- D'Onofrio M, Gallotti A and Pozzi MR. Imaging techniques in pancreatic tumors. *Expert Rev Med Devices.* 2010; 7(2):257-273.
- Shrikhande SV, Barreto SG, Goel M and Arya S. Multimodality imaging of pancreatic ductal adenocarcinoma: a review of the literature. *HPB (Oxford).* 2012; 14(10):658-668.
- Donadon M and Torzilli G. Intraoperative Ultrasound in Patients with Hepatocellular Carcinoma: From Daily Practice to Future Trends. *Liver cancer.* 2013; 2(1):16-24.
- Menack MJ, Spitz JD and Arregui ME. Staging of pancreatic and ampullary cancers for resectability using laparoscopy with laparoscopic ultrasound. *Surg Endosc.* 2001; 15(10):1129-1134.
- Bemelman WA, de Wit LT, van Delden OM, Smits NJ, Obertop H, Rauws EJ and Gouma DJ. Diagnostic laparoscopy combined with laparoscopic ultrasonography in staging of cancer of the pancreatic head region. *Br J Surg.* 1995; 82(6):820-824.
- John TG, Greig JD, Carter DC and Garden OJ. Carcinoma of the pancreatic head and periampullary region. Tumor staging with laparoscopy and laparoscopic ultrasonography. *Ann Surg.* 1995; 221(2):156-164.

- 26 van Delden OM, Smits NJ, Bemelman WA, de Wit LT, Gouma DJ and Reeders JW. Comparison of laparoscopic and transabdominal ultrasonography in staging of cancer of the pancreatic head region. *J Ultrasound Med.* 1996; 15(3):207-212.
- 27 Mortensen MB, Scheel-Hincke JD, Madsen MR, Qvist N and Hovendal C. Combined endoscopic ultrasonography and laparoscopic ultrasonography in the pretherapeutic assessment of resectability in patients with upper gastrointestinal malignancies. *Scand J Gastroenterol.* 1996; 31(11):1115-1119.
- 28 Minnard EA, Conlon KC, Hoos A, Dougherty EC, Hann LE and Brennan MF. Laparoscopic ultrasound enhances standard laparoscopy in the staging of pancreatic cancer. *Ann Surg.* 1998; 228(2):182-187.
- 29 Durup Scheel-Hincke J, Mortensen MB, Qvist N and Hovendal CP. TNM staging and assessment of resectability of pancreatic cancer by laparoscopic ultrasonography. *Surg Endosc.* 1999; 13(10):967-971.
- 30 Schachter PP, Avni Y, Shimonov M, Gvirtz G, Rosen A and Czerniak A. The impact of laparoscopy and laparoscopic ultrasonography on the management of pancreatic cancer. *Arch Surg.* 2000; 135(11):1303-1307.
- 31 Taylor AM, Roberts SA and Manson JM. Experience with laparoscopic ultrasonography for defining tumour resectability in carcinoma of the pancreatic head and periampullary region. *Br J Surg.* 2001; 88(8):1077-1083.
- 32 Kwon AH, Inui H and Kamiyama Y. Preoperative laparoscopic examination using surgical manipulation and ultrasonography for pancreatic lesions. *Endoscopy.* 2002; 34(6):464-468.
- 33 Zhao ZW, He JY, Tan G, Wang HJ and Li KJ. Laparoscopy and laparoscopic ultrasonography in judging the resectability of pancreatic head cancer. *Hepatobiliary Pancreat Dis Int.* 2003; 2(4):609-611.
- 34 Doran HE, Bosonnet L, Connor S, Jones L, Garvey C, Hughes M, Campbell F, Hartley M, Ghaneh P, Neoptolemos JP and Sutton R. Laparoscopy and laparoscopic ultrasound in the evaluation of pancreatic and periampullary tumours. *Dig Surg.* 2004; 21(4):305-313.
- 35 Thomson BN, Parks RW, Redhead DN, Welsh FK, Madhavan KK, Wigmore SJ and Garden OJ. Refining the role of laparoscopy and laparoscopic ultrasound in the staging of presumed pancreatic head and ampullary tumours. *Br J Cancer.* 2006; 94(2):213-217.
- 36 Frstrup CW, Mortensen MB, Pless T, Durup J, Ainsworth A, Hovendal C and Nielsen HO. Combined endoscopic and laparoscopic ultrasound as preoperative assessment of patients with pancreatic cancer. *HPB (Oxford).* 2006; 8(1):57-60.
- 37 Doucas H, Sutton CD, Zimmerman A, Dennison AR and Berry DP. Assessment of pancreatic malignancy with laparoscopy and intraoperative ultrasound. *Surg Endosc.* 2007; 21(7):1147-1152.
- 38 Barabino M, Santambrogio R, Pisani CA, Scalzone R, Montorsi M and Opocher E. Is there still a role for laparoscopy combined with laparoscopic ultrasonography in the staging of pancreatic cancer? *Surg Endosc.* 2011; 25(1):160-165.
- 39 Nieveen van Dijkum EJ, Romijn MG, Terwee CB, de Wit LT, van der Meulen JH, Lameris HS, Rauws EA, Obertop H, van Eyck CH, Bossuyt PM and Gouma DJ. Laparoscopic staging and subsequent palliation in patients with peripancreatic carcinoma. *Ann Surg.* 2003; 237(1):66-73.
- 40 Stefanidis D, Grove KD, Schwesinger WH and Thomas CR, Jr. The current role of staging laparoscopy for adenocarcinoma of the pancreas: a review. *Ann Oncol.* 2006; 17(2):189-199.
- 41 White R, Winston C, Gonen M, D'Angelica M, Jarnagin W, Fong Y, Conlon K, Brennan M and Allen P. Current utility of staging laparoscopy for pancreatic and peripancreatic neoplasms. *J Am Coll Surg.* 2008; 206(3):445-450.
- 42 Vollmer CM, Drebin JA, Middleton WD, Teeffey SA, Linehan DC, Soper NJ, Eagon CJ and Strasberg SM. Utility of staging laparoscopy in subsets of peripancreatic and biliary malignancies. *Ann Surg.* 2002; 235(1):1-7.
- 43 Rifkin MD and Weiss SM. Intraoperative sonographic identification of nonpalpable pancreatic masses. *J Ultrasound Med.* 1984; 3(9):409-411.
- 44 Catheline JM, Turner R, Rizk N, Barrat C and Champault G. The use of diagnostic laparoscopy supported by laparoscopic ultrasonography in the assessment of pancreatic cancer. *Surg Endosc.* 1999; 13(3):239-245.
- 45 Long EE, Van DJ, Weinstein S, Jeffrey B, Desser T and Norton JA. Computed tomography, endoscopic, laparoscopic, and intra-operative sonography for assessing resectability of pancreatic cancer. *Surg Oncol.* 2005; 14(2):105-113.
- 46 Doran HE, Blanchard TH, Causey MW, Homann JF and Brown TA. Examining the accuracy and clinical usefulness of intraoperative frozen section analysis in the management of pancreatic lesions. *Am J Surg.* 2013; 205(5):613-617.
- 47 Dillhoff M, Yates R, Wall K, Muscarella P, Melvin WS, Ellison EC and Bloomston M. Intraoperative assessment of pancreatic neck margin at the time of pancreaticoduodenectomy increases likelihood of margin-negative resection in patients with pancreatic cancer. *J Gastrointest Surg.* 2009; 13(5):825-830.
- 48 Hernandez J, Mullinax J, Clark W, Toomey P, Villalobid D, Morton C, Ross S and Rosemurgy A. Survival after pancreaticoduodenectomy is not improved by extending resections to achieve negative margins. *Ann Surg.* 2009; 250(1):76-80.
- 49 Lad NL, Squires MH, Maithel SK, Fisher SB, Mehta VV, Cardona K, Russell MC, Staley CA, Adsay NV and Kooby DA. Is it time to stop checking frozen section neck margins during pancreaticoduodenectomy? *Ann Surg Oncol.* 2013; 20(11):3626-3633.
- 50 Verbeke CS and Smith AM. Survival after pancreaticoduodenectomy is not improved by extending resections to achieve negative margins. *Ann Surg.* 2010; 251(4):776-777.
- 51 D'Onofrio M, Zamboni G, Faccioli N, Capelli P and Pozzi MR. Ultrasonography of the pancreas. 4. Contrast-enhanced imaging. *Abdom Imaging.* 2007; 32(2):171-181.
- 52 Faccioli N, D'Onofrio M, Malago R, Zamboni G, Falconi M, Capelli P and Mucelli RP. Resectable pancreatic adenocarcinoma: depiction of tumoral margins at contrast-enhanced ultrasonography. *Pancreas.* 2008; 37(3):265-268.
- 53 Takeda K, Goto H, Hirooka Y, Itoh A, Hashimoto S, Niwa K and Hayakawa T. Contrast-enhanced transabdominal ultrasonography in the diagnosis of pancreatic mass lesions. *Acta Radiol.* 2003; 44(1):103-106.
- 54 Faccioli N, Crippa S, Bassi C and D'Onofrio M. Contrast-enhanced ultrasonography of the pancreas. *Pancreatol.* 2009; 9(5):560-566.
- 55 Koito K, Namieno T, Nagakawa T and Morita K. Inflammatory pancreatic masses: differentiation from ductal carcinomas with contrast-enhanced sonography using carbon dioxide microbubbles. *AJR Am J Roentgenol.* 1997; 169(5):1263-1267.
- 56 Torzilli G, Del FD, Palmisano A, Donadon M, Bianchi P, Roncalli M, Balzarini L and Montorsi M. Contrast-enhanced intraoperative ultrasonography during hepatectomies for colorectal cancer liver metastases. *J Gastrointest Surg.* 2005; 9(8):1148-1153.
- 57 Vahrmeijer AL, Hutteman M, van der Vorst JR, van de Velde CJ and Frangioni JV. Image-guided cancer surgery using near-infrared fluorescence. *Nat Rev Clin Oncol.* 2013; 10(9):507-518.
- 58 Chance B. Near-infrared images using continuous, phase-modulated, and pulsed light with quantitation of blood and blood oxygenation. *Ann N Y Acad Sci.* 1998; 838:29-45.
- 59 Yokoyama N, Otani T, Hashidate H, Maeda C, Katada T, Sudo N, Manabe S, Ikeno Y, Toyoda A and Katayangi N. Real-time detection of hepatic micrometastases from pancreatic cancer by intraoperative fluorescence imaging: preliminary results of a prospective study. *Cancer.* 2012; 118(11):2813-2819.
- 60 van der Vorst JR, Schaafsma BE, Hutteman M, Verbeek FP, Liefers GJ, Hartgrink HH, Smit VT, Lowik CW, van de Velde CJ, Frangioni JV and Vahrmeijer AL. Near-infrared fluorescence-guided resection of colorectal liver metastases. *Cancer.* 2013; 119(18):3411-3418.
- 61 Winer JH, Choi HS, Gibbs-Strauss SL, Ashitate Y, Colson YL and Frangioni JV. Intraoperative localization of insulinoma and normal pancreas using invisible near-infrared fluorescent light. *Ann Surg Oncol.* 2010; 17(4):1094-1100.
- 62 van der Vorst JR, Vahrmeijer AL, Hutteman M, Bosse T, Smit VT, van de Velde CJ, Frangioni JV and Borsing BA. Near-infrared fluorescence imaging of a solitary fibrous tumor of the pancreas using methylene blue. *World J Gastrointest Surg.* 2012; 4(7):180-184.
- 63 Hutteman M, van der Vorst JR, Mieog JS, Borsing BA, Hartgrink HH, Kuppen PJ, Lowik CW, Frangioni JV, van de Velde CJ and Vahrmeijer AL. Near-infrared fluorescence imaging in patients undergoing pancreaticoduodenectomy. *Eur Surg Res.* 2011; 47(2):90-97.
- 64 Matsuda Y, Kure S and Ishiwata T. Nestin and other putative cancer stem cell markers in pancreatic cancer. *Med Mol Morphol.* 2012; 45(2):59-65.
- 65 Wang T, Wentz SC, Ausborn NL, Washington MK, Merchant N, Zhao Z, Shyr Y, Chakravarthy AB and Xia F. Pattern of breast cancer susceptibility gene 1 expression is a potential prognostic biomarker in resectable pancreatic ductal adenocarcinoma. *Pancreas.* 2013; 42(6):977-982.
- 66 Tan X, Egami H, Nozawa F, Abe M and Baba H. Analysis of the invasion-metastasis mechanism in pancreatic cancer: involvement of plasmin(ogen) cascade proteins in the invasion of pancreatic cancer cells. *Int J Oncol.* 2006; 28(2):369-374.
- 67 Cantero D, Friess H, Deflorin J, Zimmermann A, Brundler MA, Riesel E, Korc M and Buchler MW. Enhanced expression of urokinase plasminogen activator and its receptor in pancreatic carcinoma. *Br J Cancer.* 1997; 75(3):388-395.
- 68 Chen Y, Zheng B, Robbins DH, Lewin DN, Mikhitarian K, Graham A, Rumpp L, Glenn T, Gillanders WE, Cole DJ, Lu X, Hoffman BJ and Mitas M. Accurate discrimination of pancreatic ductal adenocarcinoma and chronic pancreatitis using multimarker expression data and samples obtained by minimally invasive fine needle aspiration. *Int J Cancer.* 2007; 120(7):1511-1517.
- 69 Wang W, Lin J, Guha S, Tong Z, Cameron AG, Zhang F, Qiu X, Zou C, Gao X, Mawad ME and Ke S. Target-specific agents imaging ectopic and orthotopic human pancreatic cancer xenografts. *Pancreas.* 2011; 40(5):689-694.
- 70 Neeße A, Hahnenkamp A, Griesmann H, Buchholz M, Hahn SA, Maghnoou A, Fendrich V, Ring J, Sipos B, Tuveson DA, Bremer C, Gress TM and Michl P. Claudin-4-targeted optical imaging detects pancreatic cancer and its precursor lesions. *Gut.* 2013; 62(7):1034-1043.
- 71 Wayua C and Low PS. Evaluation of a Cholecystokinin 2 Receptor-Targeted Near-Infrared Dye for Fluorescence-Guided Surgery of Cancer. *Mol Pharm.* 2013.

- 72 Ji S, Xu J, Zhang B, Yao W, Xu W, Wu W, Xu Y, Wang H, Ni Q, Hou H and Yu X. RGD-conjugated albumin nanoparticles as a novel delivery vehicle in pancreatic cancer therapy. *Cancer Biol Ther.* 2012; 13(4):206-215.
- 73 Kaushal S, McElroy MK, Luiken GA, Talamini MA, Moossa AR, Hoffman RM and Bouvet M. Fluorophore-conjugated anti-CEA antibody for the intraoperative imaging of pancreatic and colorectal cancer. *J Gastrointest Surg.* 2008; 12(11):1938-1950.
- 74 van Dam GM, Themelis G, Crane LM, Harlaar NJ, Pleijhuis RG, Kelder W, Sarantopoulos A, de Jong JS, Arts HJ, van der Zee AG, Bart J, Low PS and Ntziachristos V. Intraoperative tumor-specific fluorescence imaging in ovarian cancer by folate receptor-alpha targeting: first in-human results. *Nat Med.* 2011; 17(10):1315-1319.
- 75 Di C, V, Badellino F, Stella M, De NP, Fazio F, Percivalè P, Bertoglio S, Schenone F, Benevento A, Carcano G and . Role of B72.3 iodine 125-labeled monoclonal antibody in colorectal cancer detection by radioimmunoguided surgery. *Surgery.* 1994; 115(2):190-198.
- 76 Stella M, De NP, Paganelli G, Magnani P, Mangili F, Sassi I, Baratti D, Gini P, Zito F, Cristallo M and . Avidin-biotin system in radioimmunoguided surgery for colorectal cancer. Advantages and limits. *Dis Colon Rectum.* 1994; 37(4):335-343.
- 77 Sun D, Bloomston M, Hinkle G, Al-Saif OH, Hall NC, Povoski SP, Arnold MW and Martin EW, Jr. Radioimmunoguided surgery (RIGS), PET/CT image-guided surgery, and fluorescence image-guided surgery: past, present, and future. *J Surg Oncol.* 2007; 96(4):297-308.
- 78 Aitken DR, Hinkle GH, Thurston MO, Tuttle SE, Martin DT, Olsen J, Haagensen DE, Jr., Houchens D and Martin EW, Jr. A gamma-detecting probe for radioimmune detection of CEA-producing tumors. Successful experimental use and clinical case report. *Dis Colon Rectum.* 1984; 27(5):279-282.
- 79 Wendler T, Herrmann K, Schnelzer A, Lasser T, Traub J, Kutter O, Ehlerding A, Scheidhauer K, Schuster T, Kiechle M, Schwaiger M, Navab N, Ziegler SI and Buck AK. First demonstration of 3-D lymphatic mapping in breast cancer using free-hand SPECT. *Eur J Nucl Med Mol Imaging.* 2010; 37(8):1452-1461.
- 80 Freesmeyer M, Opfermann T and Winkens T. Hybrid Integration of Real-time US and Freehand SPECT: Proof of Concept in Patients with Thyroid Diseases. *Radiology.* 2014;132415.
- 81 Jusoh AC and Ammori BJ. Laparoscopic versus open distal pancreatectomy: a systematic review of comparative studies. *Surg Endosc.* 2012; 26(4):904-913.
- 82 Gumbs AA, Rodriguez Rivera AM, Milone L and Hoffman JP. Laparoscopic pancreatoduodenectomy: a review of 285 published cases. *Ann Surg Oncol.* 2011; 18(5):1335-1341.
- 83 Herreros-Villanueva M, Hijona E, Cosme A and Bujanda L. Adjuvant and neoadjuvant treatment in pancreatic cancer. *World J Gastroenterol.* 2012; 18(14):1565-1572.
- 84 Townsend DW. Dual-modality imaging: combining anatomy and function. *J Nucl Med.* 2008; 49(6):938-955.
- 85 Verbeek FP, van der Vorst JR, Schaafsma BE, Hutteman M, Bonsing BA, van Leeuwen FW, Frangioni JV, van de Velde CJ, Swijnenburg RJ and Vahrmeijer AL. Image-guided hepatopancreatobiliary surgery using near-infrared fluorescent light. *J Hepatobiliary Pancreat Sci.* 2012; 19(6):626-637.
- 86 Lutje S, Rijkema M, Helfrich W, Oyen WJ and Boerman OC. Targeted Radionuclide and Fluorescence Dual-modality Imaging of Cancer: Preclinical Advances and Clinical Translation. *Mol Imaging Biol.* 2014.
- 87 Beer AJ, Kessler H, Wester HJ and Schwaiger M. PET Imaging of Integrin α v β 3 Expression. *Theranostics.* 2011; 1:48-57.
- 88 Choi HS, Gibbs SL, Lee JH, Kim SH, Ashitate Y, Liu F, Hyun H, Park G, Xie Y, Bae S, Henary M and Frangioni JV. Targeted zwitterionic near-infrared fluorophores for improved optical imaging. *Nat Biotechnol.* 2013; 31(2):148-153.

CHAPTER 3

Real-time near-infrared fluorescence guided surgery in gynecological oncology: A review of the current state of the art

Gynecol Oncol. 2014; 135(3):606-613

HJM HANDGRAAF, FPR VERBEEK, QRJG TUMMERS, LSF BOOGERD, CJH VAN DE VELDE, AL VAHRMEIJER, KN GAARENSTROOM

ABSTRACT

Near-infrared (NIR) fluorescence imaging has emerged as a promising complementary technique for intraoperative visualization of tumor tissue, lymph nodes and vital structures. In this review, the current applications and future opportunities of NIR fluorescence imaging in gynecological oncology are summarized. Several studies indicate that intraoperative sentinel lymph node identification in vulvar cancer using NIR fluorescence imaging outperforms blue dye staining and provides real-time intra-operative imaging of sentinel lymph nodes. Tumor-targeted probes are currently being developed and have the potential to improve surgical outcomes of cytoreductive and staging procedures, in particular in ovarian cancer. NIR fluorescence imaging can penetrate through several millimeters of tissue, revealing structures just below the tissue surface. Hereby, iatrogenic damage to vital structures, such as the ureter or nerves may be avoided by identification using NIR fluorescence imaging. Research in the near future will be necessary to determine whether this technology has additional value in order to facilitate the surgical procedure and improve surgical outcome.

INTRODUCTION

Advanced imaging technologies, such as multidetector computed tomography (MDCT) and three-dimensional magnetic resonance imaging (3D-MRI), have introduced a new era in preoperative planning and treatment of gynecological malignancies. However, as these imaging modalities are mainly used in the preoperative setting, translation of these images to the surgical theatre is often challenging and does not always correspond to the intraoperative findings.

Over the past years, near-infrared (NIR) fluorescence imaging has emerged as a promising complementary technique for intraoperative visualization of tumor tissue, sentinel lymph nodes (SLN) and vital structures. This technology provides real-time images, which allows accurate guidance during surgery. In gynecologic oncology, NIR fluorescence imaging has been used for intraoperative identification of SLN in vulvar, cervical and endometrial cancer, detection of ovarian tumors and abdominal or peritoneal metastases and imaging of vital structures such as the ureter [1]. NIR light has a wavelength range of 700 to 900 nanometers and is invisible to the naked eye. Therefore, it does not alter the surgical field when used. NIR fluorescence can penetrate several millimeters into blood or soft tissue, allowing identification of structures even when they are not yet directly exposed to the surface. This property is the consequence of less absorption of light within the NIR spectrum by water and most biomolecules, such as hemoglobin and lipid. Several NIR fluorescent probes are currently being evaluated in a preclinical setting [2]. Moreover, NIR fluorescence imaging systems for image-guided surgery are developing rapidly. It is expected that this technology will be of increasing importance in the field of cancer surgery in the following years.

This review aims to summarize current opportunities using NIR fluorescence imaging in gynecologic cancer surgery with special attention to SLN mapping, tumor imaging and imaging of vital structures.

NIR FLUORESCENCE IMAGING SYSTEMS AND CURRENTLY AVAILABLE FLUOROPHORES

NIR fluorescence imaging uses NIR light, which is safe when used at the relatively low intensity needed for this technique. Requirements are a NIR fluorescent probe (fluorophore) combined with an imaging system which is able to excite this fluorophore and to detect the emitted fluorescence. By displaying the detected fluorescence on a screen, it becomes visible to the human eye. Some systems are able to merge white light images with NIR fluorescence images, which enhances anatomical orientation. Due to the increasing opportunities in the surgical field, more fluorescence imaging systems are becoming available for both open and laparoscopic surgery. Most published clinical studies use the Photodynamic Eye (PDE, Hamamatsu Photonics Co., Hamatsu, Japan), Mini-FLARE (Beth Israel

Deaconess Hospital, Boston, MA, USA), SPY (Novadaq Technologies Inc., Toronto, Canada) or Fluobeam (Fluoptics, Grenoble, France). Currently available systems are described in Table 1 and reviewed by Gioux et al [3].

To date, indocyanine green (ICG) and methylene blue (MB) are the only fluorophores approved for clinical use by the Food and Drug Administration and the European Medicines Agency. ICG is cleared exclusively by the liver and emits light with a wavelength of approximately 820 nanometers [4]. MB is cleared simultaneously by liver and kidneys and emits light with a less optimal wavelength of approximately 700 nanometers, which has less tissue penetration capacity and more tissue autofluorescence [5]. Both ICG and MB are non-targeted dyes and their chemical structures do not allow conjugation to tumor specific ligands. Therefore, they are mainly suitable for indications such as SLN mapping, e.g. in vulvar and cervical cancer, since they do not bind to tumors, but only follow the lymphatic drainage pattern. Furthermore, they can be used for ureter or bile duct visualization.

SENTINEL LYMPH NODE MAPPING

Sentinel lymph node detection in vulvar cancer

Vulvar cancer accounts for approximately 5% of gynecological malignancies [6]. In case of early stage squamous cell cancer of the vulva less than 4 centimeters in diameter and unifocal tumor, SLN biopsy for identification of lymph node metastases to the groins has been proven safe [7]. Morbidity, such as lymphocele, recurrent erysipelas and lymphedema of the leg, decreases significantly if only SLN biopsy has been done, compared to full lymphadenectomy of the groins [7, 8]. Combining radiotracer ^{99m}Tc -nanocolloid and blue dye is currently regarded as standard-of-care for SLN detection and gives the highest identification rates (94.4%; 95% confidence interval 92.4 – 95.9) [9]. However, both modalities have several disadvantages. For example, although blue dye can be used for intraoperative imaging of the SLN, it cannot be seen through the skin or soft tissue and has a lower sensitivity (68.7%; 95% CI 63.1 – 74.0) compared to radioisotopes (94.0%; 95% CI 90.5 – 96.4) [10, 11]. Furthermore, radioisotopes can only be detected using a gamma counter, but real-time intraoperative visual guidance to exactly locate the SLN is lacking. When intraoperatively searching for the SLN, the radioactive signal can be disturbed by a high background signal originating from the injection spot around the vulvar tumor (shine effect) [12]. In recent years, NIR fluorescence imaging has been introduced in SLN mapping in vulvar cancer, because this technique has the potential for accurate, real-time, intraoperative SLN mapping [1]. Thus far, 70 patients with vulvar cancer have been described in five clinical studies, as shown in Table 2 [13-16]. Crane et al. [13] used a mixture of 1 mL patent blue and 1 mL indocyanine green (ICG; 0.5 mg/mL), which

was injected immediately prior to surgery. In 10 patients with vulvar cancer, 29 SLNs were detected using ^{99m}Tc -nanocolloid, of which 26 SLNs were also detected by fluorescence. In contrast, only 21 SLNs were stained blue. Given the disadvantage of the limited penetration depth of NIR fluorescence, Crane et al. suggested to restrict this technique to patients with a body mass index < 25 kg/m², since overlying adipose tissue masks the NIR fluorescent signal. In a preclinical study using 12 Yorkshire pigs, premixing ICG with human serum albumin (HSA) showed better overall performance than ICG alone with respect to retention in the SLN and fluorescence intensity [17]. Therefore, Hutteman et al. [14] used this combination in patients with vulvar cancer and tried to identify the optimal dose, using 500, 750 and 1,000 μM of ICG:HSA for NIR fluorescence imaging, combined with the golden standard using radiocolloid and blue dye. No significant differences between the tested doses of ICG:HSA were observed. A total of 9 patients were included in this dose finding study and in all patients the SN could be detected. Altogether 14 SLNs were detected; all of them were fluorescent, but only 11 (78.6%) stained blue. The authors suggested, considering safety, costs (only one vial of ICG is needed) and pharmacy preferences, to use 500 μM ICG:HSA for SLN detection. Since lymphatic vessels contain high concentrations of HSA and other proteins, Schaafsma et al. [15] hypothesized that premixing ICG with HSA might be redundant. They randomized 24 patients in 2 groups of 500 μM ICG:HSA and 500 μM ICG alone, again combined with the golden standard for SLN detection. The average SLN biopsy rate between these two groups was not significantly different ($P = 0.65$), which confirmed the authors' hypothesis. In 19 out of the 24 patients the SN could be found in this study, using all 3 modalities to find the SLN, which was lower than generally found. However, in those 19 patients in whom the sentinel node was detected, a total of 35 SLNs were detected, which were all radioactive and fluorescent, but only 27 (77.1%) stained blue. To combine the favorable features of NIR fluorescence imaging for real-time intraoperative imaging with radioguidance, a mixture of ICG and ^{99m}Tc -nanocolloid was created, showing the exact same lymphatic drainage pattern as ^{99m}Tc -nanocolloid alone [18]. Subsequently, Mathéron et al. [16] used this mixture in 14 patients with vulvar cancer and one patient with melanoma of the vulva. *In vivo* 95.7% and *ex vivo* 100% of detected SLNs using ^{99m}Tc -nanocolloid as the golden standard showed fluorescence. The authors concluded that this hybrid tracer was feasible and superior to blue dye alone because of its higher sensitivity. Verbeek and Tummers et al. (unpublished data), confirmed these results in 12 patients with vulvar cancer using the ICG- ^{99m}Tc -nanocolloid mixture. The SLN detection rate was 100% and all 21 SLNs were fluorescent *in vivo*. In contrast, only 13 SLNs (61.9%) stained blue.

Combining the results of these five studies, 96.6% of the SLNs detected by using ^{99m}Tc -nanocolloid were also fluorescent *in vivo*, in contrast to blue dye, which stained comparable with literature only 70.6% of the SLNs ($p < 0.001$) [11]. In conclusion, SLN detection in vulvar cancer using NIR fluorescence imaging appears

to be of added value because of its high sensitivity, which outperforms blue dye staining and is comparable with radioguidance using ^{99m}Tc -nanocolloid. In addition, NIR fluorescence imaging has the potential to exactly locate the SLN without disturbance by background signal, which can be a problem using radiocolloid. However, penetration capacity of NIR fluorescence is limited to approximately 8 millimeters. The use of radiotracers seems therefore still indispensable, since it allows preoperative scintigraphy and intraoperative identification of deeper located SLNs in the groin. In the near future, randomized controlled trials should confirm if ICG mixed with radiocolloid can replace the golden standard using the combination blue dyes and radiotracer.

Sentinel lymph node detection in cervical and in endometrial cancer

SLN biopsy has been proven as a valuable procedure to avoid extensive lymphadenectomy in melanoma, breast- and vulvar cancer. However, due to varying, bilateral and difficult predictable drainage patterns, this is challenging in cervical and in endometrial cancer. Nevertheless, consensus exists that SLN biopsy is a worthy area for further investigation in order to omit full lymphadenectomy and tailoring postoperative or additional treatment in patients with FIGO stage I cervical cancer [19, 20]. Traditional methods for SLN detection are blue dyes and/or radioactive tracers [21]. Using the combined technique of blue dye and radiotracers in uterine cancer, sensitivity of SLN biopsy reaches 91% - 93%, which is similar compared to SLN biopsy in breast cancer [20-23]. These data are encouraging and management might be changed in the future and lead to a decrease in the extent of necessary pelvic lymphadenectomy. One step closer to a decrease in the extent of pelvic lymphadenectomy may be a more accurate identification of SLNs. Especially blue dye can be difficult to detect when localized in the extrapelvic area or under layers of tissue. NIR fluorescence imaging may be of clinical value to increase the sensitivity and specificity of SLN detection.

Seven studies, described in Table 3, studied the use of ICG fluorescence imaging for the detection of SLNs in cervical and in endometrial cancer. They all used ICG and appointed the fluorescent lymph node(s) as SLN. After SLN biopsy, full pelvic lymphadenectomy was performed. No radiotracer was used in these studies. The first feasibility study was done in 2011 by Crane et al. [24] in 10 patients with cervical cancer. A mixture of ICG and patent blue was injected into the cervix during surgery. After resecting the SLN, pelvic lymphadenectomy was performed. In 6 out of 10 patients (60%), real-time NIR fluorescence lymph mapping was observed, resulting in the detection of 9 SLN. Ex vivo, 11 out of 197 lymph nodes showed NIR fluorescence in addition. SLN metastases were found only in 1 patient (11%) and no false-negative SLNs were detected. Although this shows the feasibility of NIR fluorescence imaging in SLN detection, the study population was

small. Similar results were found in a study with 10 patients by Furukawa et al. [25]. Furthermore, Van der Vorst et al. [26] randomized 9 cervical cancer patients in 500-, 750-, or 1000 μM ICG:HSA to assess the optimal dose for SLN mapping, without using other SLN detection methods. Lymph node metastases were found in 2 patients. Both these lymph nodes were fluorescent. Three fluorescent spots appeared to be false-positive: only adipose tissue, but no lymph node was found during histopathologic examination. No significant difference was found between the doses. In a subsequent study by Schaafsma et al. [27], no significant difference regarding SLN detection was found between two randomized groups ($n = 18$) with early stage cervical cancer using 500 μM ICG:HSA and 500 μM ICG alone, again without using radiocolloids or blue dye. One lymph node contained a metastasis, but did not show any fluorescence and was therefore false-negative. Five more SLNs contained metastases; 3 were detected by fluorescence *in vivo*, 2 were only detected by fluorescence *ex vivo*. The authors conclude that NIR fluorescence has an improved tissue penetration compared to blue dye for intraoperative real-time imaging, but sensitivity could be improved. They suggested that the most optimal tracer would therefore be a mixture of a radioactive tracer with ICG. Rossi et al. [28] used ICG fluorescence imaging using the da Vinci® robot for laparoscopic surgery in patients with cervical or endometrial cancer. SLNs were successfully identified in 17 of 20 patients (85%), although 1 SLN biopsy proved to be false-negative after lymphadenectomy. Holloway et al. [29] compared blue dye with ICG fluorescence imaging in robotic-assisted staging of patients with endometrial cancer. With ICG, bilateral SLN detection was significantly more successful compared to blue dye, in 97% and 77% of cases respectively ($p = 0.03$). Rossi et al. [30] compared cervical stromal versus hysteroscopic endometrial injection for sentinel lymph node mapping in 29 patients with endometrial cancer. Detection rate after cervical injection appeared to be superior compared to hysteroscopic injection (82% vs. 33% respectively, $p = 0.027$). There was 1 false-negative SLN biopsy after cervical injection.

In conclusion, seven studies showed the feasibility of ICG fluorescence imaging for the detection of SLNs in cervical and in endometrial cancer. This results in a sensitivity of 84.0% and a negative predictive value of 95.2% compared to the golden standard of performing a standard pelvic lymphadenectomy. Therefore, ICG fluorescence imaging appears to be a valuable method to replace blue dye. However, optimal patient selection may improve sensitivity and negative predictive value. In addition, further optimization, such as deeper tissue penetration, may improve *in vivo* SLN identification ratio. The multimodal approach of radiotracer mixed with ICG will therefore most likely give superior results and pave the way to SLN biopsy in early stage cervical and endometrial cancer for clinical use.

IMAGING OF VITAL STRUCTURES

Ureter visualization

Ureteral injury is a rare but serious complication during pelvic surgery. In gynecologic surgery, injury of the ureter is reported in 0.4% to 3% of the cases, being the highest in difficult procedures, i.e. in patients with malignant disease and after radiation therapy [31-33]. Different methods can be used to prevent ureteral injury, such as prophylactic ureteral catheterization. However, this is an invasive method and also associated with a risk of ureteral injury [34]. In case of intraoperative suspicion of ureteral injury, other methods are available, such as intravenous or retrograde contrast to show extravasation of contrast [35]. However, findings can be subtle and easily missed. NIR fluorescence may potentially be used for both preventing and detecting ureteral injury intraoperatively.

Methylene blue (MB) is a clinically available blue dye used for contrast. However, in lower dose and diluted, it becomes a fluorophore with a wavelength of approximately 700 nanometers [36]. It is cleared renally and thus very useful for visualizing the ureters. Verbeek et al. [5] reported the first in human experience in 12 patients who underwent lower abdominal surgery. The ureters were successfully visualized within 10 minutes after injecting MB and the signal lasted at least up to 60 minutes. The authors recommended 0.25 mg/kg of MB, approximately 7 times lower compared to the dose necessary for visualizing the ureters with the naked eye.

In conclusion, NIR fluorescence imaging using MB may decrease the risk of ureteral injury and provide valuable additional information about obstruction or leakage of the ureter during surgery.

Nerve visualization

During radical hysterectomy, surgical damage of autonomic nerves can result in postoperative pain and loss of function, such as bladder dysfunction. Different methods have been described which all attempt to preserve autonomic nerves [37]. However, nerve anatomy varies greatly between patients and nerves are often hidden beneath protective layers of tissue, which hampers correct identification. Nerve-targeted NIR fluorescence agents potentially allow intraoperative detection of nerves, such as the hypogastric nerves which can be damaged during radical hysterectomy.

To date, no in-human trials have been done. Whitney et al. [38] successfully imaged peripheral nerves in mice with nerve binding peptides conjugated to fluorescein-5(6)-carbonyl group (FAM) or to the deep red fluorophore Cy5. The nerve-to-background signal was up to tenfold, and a sufficient ratio lasted at least for 8 hours. Gibbs-Strauss et al. demonstrated the feasibility of nerve-targeted

fluorophores in rats and pigs [39]. They studied 4,49-[(2-methoxy-1,4-phenylene) di-(1E)-2,1-ethenediyl]bis-benzenamine (BMB) and 4-[(1E)-2-[4-[(1E)-2-[4-amino-phenyl]ethenyl]-3-methoxyphenyl]ethenyl]-benzonitrile (GE3082), which both accumulate in nerve tissue and emit light with wavelengths of 560 and 600 nanometers respectively. Although still a lot of work has to be done to bring nerve-specific fluorescent agents to the clinic, this new technique may be beneficial in sparing nerve tissue.

TUMOR IMAGING

Intraoperative imaging and detection of ovarian cancer

Ovarian cancer is the fifth cause of cancer related death in females [6]. In patients with clinically low stage disease, a staging procedure is performed to detect occult tumor spread in order to select those patients who need chemotherapy [40, 41]. In advanced stage ovarian cancer, treatment consists of the combination of cytoreductive surgery and chemotherapy. The amount of residual disease after surgery is inversely related with patient survival and one of the main prognostic factors [42, 43]. Preoperative CT and MRI are useful in treatment planning. However, these modalities have their limitations. First, CT is unable to accurately detect small-size peritoneal metastases; secondly, MRI and CT cannot detect cancer in normal sized lymph nodes or discriminate between hyperplastic lymph nodes and metastases; thirdly, the provided images do not provide real-time intraoperative guidance [44]. Therefore, accuracy of preoperative staging by these imaging modalities is limited. The only reliable staging method is therefore thorough inspection of the abdominal cavity by laparoscopy or laparotomy and histologic sampling. This is done by taking biopsies of suspected lesions or otherwise at random [40]. However, visual and tactile information is not ideal for detecting small tumors and clusters of cells invisible for the naked eye. In addition, as laparoscopy is gaining popularity, the use of laparoscopy deprives the surgeon of tactile feedback.

As the extent of cytoreduction greatly influences prognosis of patients with advanced ovarian cancer, detailed intraoperative visualization of tumorous tissue may be of added value and improve therapeutic efficacy of surgery. Therefore, intraoperative imaging using tumor-specific NIR fluorescent tracer may be used as a complementary modality for both staging and cytoreduction in ovarian cancer treatment. Essential for optimal visualization in NIR fluorescence imaging is a sufficient signal-to-background ratio (SBR). Too intense background signal would conceal targeted tumorous tissue. An ideal target for NIR fluorescence agents should therefore show high expression on tumors and be absent in healthy tissue.

Many tumor-targeting probes binding to diverse molecular targets are currently being validated in preclinical and clinical studies and reviewed by Luo et al. [2].

These include several targets for ovarian tumors. Cyclic RGD-peptide is a promising ligand, as it targets integrins such as $\alpha_V\beta_3$ and $\alpha_V\beta_5$, which are involved in neovascularization and up-regulated in many tumor types, such as breast, colorectal, pancreas, lung and ovarian cancer [45]. *In vivo* results show indeed binding to $\alpha_V\beta_3$ integrin, providing NIR fluorescence imaging through the skin of ovarian tumor bearing mice [46]. Besides tumor visualization, CRGD conjugated to the zwitterionic fluorophore ZW800-1, has demonstrated to enable simultaneous ureter visualization, since it is cleared renally [47]. Other tumor targeted-fluorophores cleared by the kidneys potentially also allow simultaneous ureter visualization. Folate receptor α (FR- α) is another promising target, as it overexpressed in 72% of primary and 81.5% of recurrent ovarian tumors [48]. A folate receptor ligand conjugated to a fluorophore was successfully tested in mice with xenograft ovarian tumors, showing NIR fluorescence signal in tumors after 1 hour after administration [49]. Besides $\alpha_V\beta_3$ integrin and folate receptor, other targets are currently being studied, such as, hypoxia-related proteins, vascular endothelial growth factor, epidermal growth factor, chemokine receptor 4, chemokine ligand 12 and matrix metalloproteinases [50]. In conclusion, in the literature, many preclinical studies have shown promising results using novel tumor specific contrast agents. Though, the focus within the field is currently shifting towards clinical translation.

In 2011, van Dam et al. successfully used a FR- α specific fluorescent probe for the intraoperative visualization of ovarian cancer cells in patients [51]. Ten patients undergoing staging or debulking laparotomy for suspected ovarian cancer received prior to surgery an intravenous injection of folate conjugated with fluorescein isothiocyanate (FITC). Only, four patients out of these ten patients were diagnosed with ovarian cancer, one with serous borderline tumor (FIGO I) and five with benign ovarian tumor. In three patients with malignant FR- η positive tumor, clearly fluorescence was shown, but absent in one patient with malignant tumor without increased FR- α expression. *Ex vivo*, tumor sized smaller than 1 millimeter could be visualized in the omentum and peritoneal cavity. These first in-human results are promising and await confirmation in larger multicenter studies. A limitation of FITC is its peak fluorescence emission of approximately 520 nanometers. Ideally, a fluorophore with NIR properties (700-900 nanometers) should be used to improve penetration depth and reduce background signal due to tissue autofluorescence.

In the near future it is expected that more tumor-targeted agents will become available, and together with improved imaging systems, this will possibly lead to higher sensitivity and a broader application of the technology. In addition, research is in progress to conjugate fluorophores and radiotracers to one ligand, creating a multimodal probe which enables preoperative and intraoperative imaging. Real-time visualization of tumors using tumor-targeted probes has the potential to optimize debulking and surgical staging procedures in gynecologic oncologic surgery.

CONCLUSIONS

Current available literature suggests a complementary role for intraoperative NIR fluorescence imaging in gynecological oncology. It has the potential to improve sentinel lymph node identification in vulvar cancer and possibly also in cervical and endometrial cancer. This may reduce the need for additional full lymphadenectomy and hereby reduce postoperative morbidity. Multiple studies indicate that SLN identification using ICG outperforms blue dye staining. The latter is important in countries where no ^{99m}Tc -nanocolloid is available for the SLN procedure and where only blue dye is used. The use of a radioactive tracer and ICG combined (multimodal approach) will most likely give superior results. Tumor-targeted probes are currently being developed and have the potential to identify tumor cells invisible to the naked eye. This can be a very helpful technique during laparoscopy, and more specific during staging procedures and possibly of added value in cytoreductive surgery in patients with ovarian cancer. Finally, intraoperative iatrogenic injury may be prevented by imaging ureters and nerves. However, optimization of fluorescent agents and imaging systems becoming commercially available is warranted. Finally, large multicenter trials are needed to investigate whether NIR fluorescence imaging is of additional use in improving and individualizing treatment and prognosis of patients with gynecologic cancer.

Table 1 Currently available NIR fluorescence imaging systems.

Imaging system	Excitation source	Working distance (cm)	Field of view (cm ²)	White light illumination of surgical field	NIR-colour overlay
Artemis	Laser diode 400-1000 nm, 4 mW/cm ²	1.5-25	60	Yes	Yes
FDPM imager	Laser diode 785 ± 10 nm, <1.9 mW/cm ²	<76.2	Max 900	No	No
Firefly for robotic surgery	NA	NA	NA	Yes	No
FLARE	LED 745-779 nm, 14mw/cm ²	45	3.7-169.5	Yes	Yes
Fluobeam	Laser 780 nm, 10 mW/cm ²	22	80	Yes	No
HyperEye	LED 760 nm, power NS	30-50	78.5	Yes	Yes
Karl Storz high definition fluorescence laparoscope	Xenon light, 760 nm	Varies	Varies	Yes	No
Kit-FLARE	Laser, 660 nm, 760nm	17.8 - 33.0	7.6-14.0	Yes	Yes
Mini-FLARE	LED 760 nm, 8.6 mW/cm ²	30	100	Yes	Yes
Munich/SurgOptix prototype camera system	Laser 750 nm, 300 mW	21	1.5-107	Yes	Yes
Photodynamic Eye (PDE)	Led 805 nm,	12-25	NA	No	No
PINPOINT Endoscopic Fluorescence Imaging	NA	NA	NA	Yes	Yes
SPY	Laser 806nm, 2.0W	30	56	No	No

Abbreviations: na=not available.

Table 2 Clinical studies of sentinel lymph node mapping with near-infrared fluorescence imaging in vulvar cancer.

Study	n	Injection	Detection of ≥ 1 SLN1	Total SLNS	Fluorescent <i>in vivo</i>	Fluorescent <i>ex vivo</i>	Sens.	NPV	Blue <i>in vivo</i>
Crane, 2011	10	1mL ICG 0,5mg/mL	10 (100%)	29	26 (89.7%)	28 (96.6%)	100%	100%	21 (72.4%)
Hutteman, 2012	9	1.6mL of 500, 750 or 1000 µM ICG:HSA	9 (100%)	14	14 (100%)	14 (100%)	100%	100%	11 (78.6%)
Schaafsma, 2013	24	1.6 mL of 500 µM ICG:HAS or 500 µM ICG	19 (79.2%)	35	35 (100%)	35 (100%)	100%	100%	27 (77.1%)
Mathéron, 2013	15 ²	ICG- ^{99m} Tc nanocolloid	14 (93.3%)	46	44 (95.7%)	46 (100%)	100%	100%	24 (64.9%) ³
Verbeek, unpublished data ⁴	12	ICG- ^{99m} Tc nanocolloid	12 (100%)	21	21 (100%)	21 (100%)	100%	100%	13 (61.9%)
Total	70		64 (91.4%; 84.9 - 98.0)	145	140 (96.6%; 93.6 - 99.5)	144 (99.3%; 98.0 - 100)	100%	100%	96 (70.6%; 62.9 - 78.3)

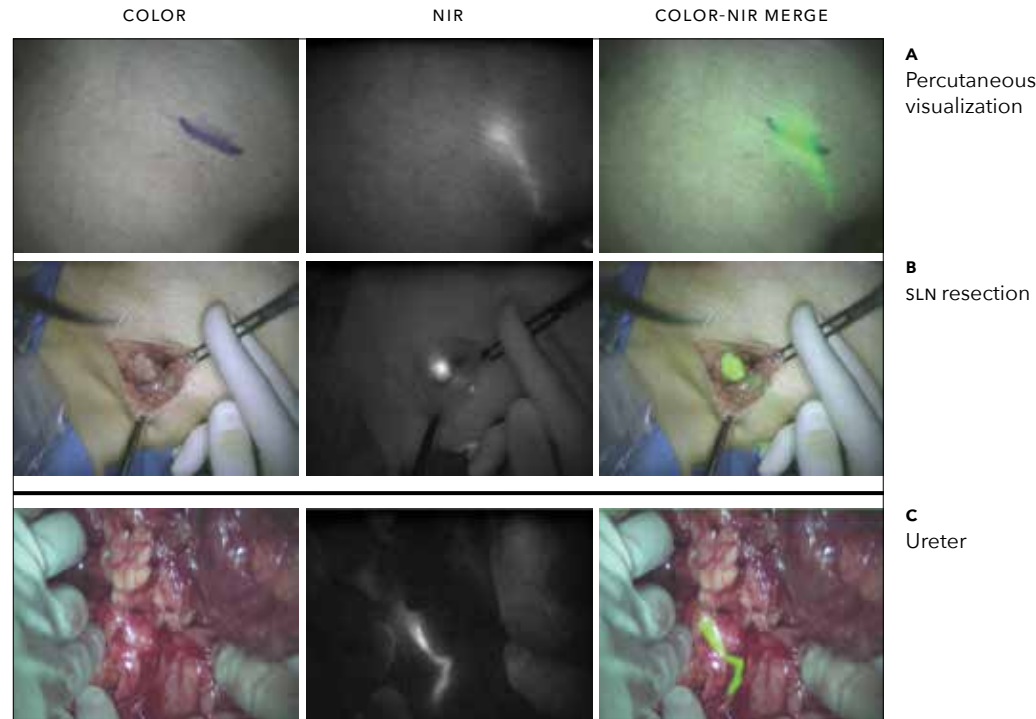
Abbreviations: ICG=indocyanine green; HAS=human albumin serum; Tc=technetium; Sens.=sensitivity; NPV=negative predictive value. Lymph nodes were appointed as slns in case they were radioactive and/or blue. Fourteen patients with vulvar cancer and one patient with melanoma of the vulva were included. Nine slns were harvested in two patients where no blue dye was injected prior to sln mapping. Thirty-six patients were analyzed, including 24 patients from the study by Schaafsma, 2013.

Table 3 Clinical studies of sentinel lymph node mapping in cervical and endometrial cancer using near-infrared fluorescence imaging.

Study	n	Indication	Injection	Detection of ≥ 1 SLN	Fluorescent SLNS	False-negative	Sens.	NPV
Crane, 2010	10	cc	2 mL ICG 0.5 mg/mL	6 (60.0%)	9	0	100%	100%
Furukawa, 2010	12	cc	0.2 mL 5mg/mL ICG	10 (83.3%)	NA ¹	0	100%	100%
Van der Vorst, 2011	9	cc	1.6 mL 500, 750 or 1000 µM ICG:HSA	9 (100%)	31	0	100%	100%
Schaafsma, 2012	18	cc	500 µM ICG:HSA or 500 µM ICG	14 (77.8%)	50	1 ²	83.3%	92.3%
Rossi, 2012	20	cc (n=4), EC (n=16)	1 - 3 mL 500 µg/mL ICG	17 (85.0%)	NA ³	1	50.0%	94.1%
Holloway, 2012	35	EC	2.5 mg ICG	34 (97.1%)	69	1	90.0%	96.2%
Rossi, 2013 ⁴	17	EC	1 mg 0.5 mg/mL ICG	14 (82.4%)	NA ⁵	1	50.0%	92.3%
Total	121			104 (86.0%; 79.8-92.1)	4		84.0% (69.6- 98.4)	95.2% (90.6- 99.8)

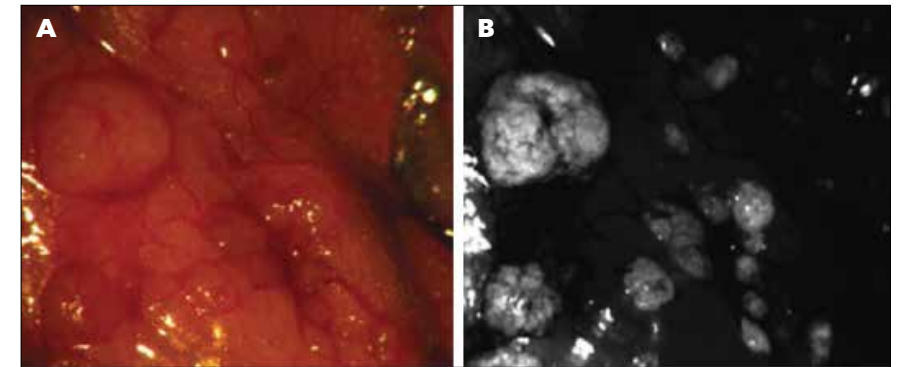
Abbreviations: Sens.=sensitivity; NPV=negative predicting value; cc=Cervical Cancer; EC=Endometrial Cancer; ICG=Indocyanine Green; NA=Not Available; SLN=Sentinel Lymph Node; LN=Lymph Node. Fluorescent lymph nodes were appointed as SLN. After SLN biopsy, pelvic lymphadenectomy was performed. A median of 7 SLNS (range 3 to 10) were identified per patient. Three out of 6 slns of patients contained metastases, but were *in vivo* not detected by fluorescence. In 2 of these patients, fluorescent metastasis containing nodes were only detected *ex vivo*. A median of 4.5 SLNS (range 0 to 9) were identified per patient. Seventeen patients received a cervical stromal injection and 12 a hysteroscopic endometrial injection. Hysteroscopic injection resulted in a detection rate of 33.3%, which was significantly lower than cervical injection (detection rate 82.4%; p=0.027). These patients are therefore excluded. A median of 5 SLNS (range 1 to 9) were identified.

Figure 1 NIR fluorescence imaging of sln in vulvar cancer and of the ureter during lower abdominal surgery. Color video, nir fluorescence and color-nir merge of intraoperative imaging. (A) NIR fluorescence signal of the sln is visible through the skin, enabling a precise incision. (B) Clear identification of the localization of the sln after incision. (C) Clear identification of right ureter with overlying blood and tissue, 15 minutes after administration of 0.5 mg/kg mb.



Reprinted by permission from Elsevier: The Journal of Urology [5]. © 2013.

Figure 2 Tumor deposits of ovarian cancer imaged with a fr- α specific ligand conjugated to the fluorophore fitc. (A,B) Color image with corresponding tumor-specific fluorescence image of the representative area in de abdominal cavity.



Reprinted by permission from Macmillan Publishers Ltd: Nature Medicine [51]. Copyright © 2011.

REFERENCES

- Vahrmeijer AL, Hutteman M, van der Vorst JR, van de Velde CJ and Frangioni JV. Image-guided cancer surgery using near-infrared fluorescence. *Nat Rev Clin Oncol.* 2013; 10(9):507-518.
- Luo S, Zhang E, Su Y, Cheng T and Shi C. A review of NIR dyes in cancer targeting and imaging. *Biomaterials.* 2011; 32(29):7127-7138.
- Gioux S, Choi HS and Frangioni JV. Image-guided surgery using invisible near-infrared light: fundamentals of clinical translation. *Mol Imaging.* 2010; 9(5):237-255.
- Kraft JC and Ho RJ. Interactions of indocyanine green and lipid in enhancing near-infrared fluorescence properties: the basis for near-infrared imaging *in vivo*. *Biochemistry.* 2014; 53(8):1275-1283.
- Verbeek FP, van der Vorst JR, Schaafsma BE, Swijnenburg RJ, Gaarenstroom KN, Elzevier HW, van de Velde CJ, Frangioni JV and Vahrmeijer AL. Intraoperative near infrared fluorescence guided identification of the ureters using low dose methylene blue: a first in human experience. *J Urol.* 2013; 190(2):574-579.
- Siegel R, Naishadham D and Jemal A. Cancer statistics, 2013. *CA Cancer J Clin.* 2013; 63(1):11-30.
- van der Zee AG, Oonk MH, de Hullu JA, Ansink AC, Vergote I, Verheijen RH, Maggioni A, Gaarenstroom KN, Baldwin PJ, van Dorst EB, van d, V, Hermans RH, van der Putten H, Drouin P, Schneider A and Sluiter WJ. Sentinel node dissection is safe in the treatment of early-stage vulvar cancer. *J Clin Oncol.* 2008; 26(6):884-889.
- Oonk MH, van Hemel BM, Hollema H, de Hullu JA, Ansink AC, Vergote I, Verheijen RH, Maggioni A, Gaarenstroom KN, Baldwin PJ, van Dorst EB, van d, V, Hermans RH, van der Putten HW, Drouin P, Runnebaum IB, et al. Size of sentinel-node metastasis and chances of non-sentinel-node involvement and survival in early stage vulvar cancer: results from GROINSS-V, a multicentre observational study. *Lancet Oncol.* 2010; 11(7):646-652.
- Hassanzade M, Attaran M, Treglia G, Yousefi Z and Sadeghi R. Lymphatic mapping and sentinel node biopsy in squamous cell carcinoma of the vulva: systematic review and meta-analysis of the literature. *Gynecol Oncol.* 2013; 130(1):237-245.
- Schaafsma BE, Mieog JS, Hutteman M, van der Vorst JR, Kuppen PJ, Lowik CW, Frangioni JV, van de Velde CJ and Vahrmeijer AL. The clinical use of indocyanine green as a near-infrared fluorescent contrast agent for image-guided oncologic surgery. *J Surg Oncol.* 2011; 104(3):323-332.
- Meads C, Sutton AJ, Rosenthal AN, Malysiak S, Kowalska M, Zapalska A, Rogozinska E, Baldwin P, Ganesan R, Borowiack E, Barton P, Roberts T, Khan K and Sundar S. Sentinel lymph node biopsy in vulvar cancer: systematic review and meta-analysis. *Br J Cancer.* 2014; 110(12):2837-2846.
- El-Ghobashy AE and Saidi SA. Sentinel lymph node sampling in gynaecological cancers: techniques and clinical applications. *Eur J Surg Oncol.* 2009; 35(7):675-685.
- Crane LM, Themelis G, Arts HJ, Buddingh KT, Brouwers AH, Ntziachristos V, van Dam GM and van der Zee AG. Intraoperative near-infrared fluorescence imaging for sentinel lymph node detection in vulvar cancer: first clinical results. *Gynecol Oncol.* 2011; 120(2):291-295.
- Hutteman M, van der Vorst JR, Gaarenstroom KN, Peters AA, Mieog JS, Schaafsma BE, Lowik CW, Frangioni JV, van de Velde CJ and Vahrmeijer AL. Optimization of near-infrared fluorescent sentinel lymph node mapping for vulvar cancer. *Am J Obstet Gynecol.* 2012; 206(1):89-85.
- Schaafsma BE, Verbeek FP, Peters AA, van der Vorst JR, de Kroon CD, van Poelgeest MI, Trimboos JB, van de Velde CJ, Frangioni JV, Vahrmeijer AL and Gaarenstroom KN. Near-infrared fluorescence sentinel lymph node biopsy in vulvar cancer: a randomised comparison of lymphatic tracers. *BJOG.* 2013; 120(6):758-764.
- Matheron HM, van den Berg NS, Brouwer OR, Kleinjan GH, van Driel WJ, Trum JW, Vegt E, Kenter G, van Leeuwen FW and Valdes Olmos RA. Multimodal surgical guidance towards the sentinel node in vulvar cancer. *Gynecol Oncol.* 2013; 131(3):720-725.
- Ohnishi S, Lomnes SJ, Laurence RG, Gogbashian A, Mariani G and Frangioni JV. Organic alternatives to quantum dots for intraoperative near-infrared fluorescent sentinel lymph node mapping. *Mol Imaging.* 2005; 4(3):172-181.
- Brouwer OR, Buckle T, Vermeeren L, Klop WM, Balm AJ, van der Poel HG, van Rhijn BW, Horenblas S, Nieweg OE, van Leeuwen FW and Valdes Olmos RA. Comparing the hybrid fluorescent-radioactive tracer indocyanine green-99mTc-nanocolloid with 99mTc-nanocolloid for sentinel node identification: a validation study using lymphoscintigraphy and SPECT/CT. *J Nucl Med.* 2012; 53(7):1034-1040.
- Levenback CF, van der Zee AG, Rob L, Plante M, Covens A, Schneider A, Coleman R, Solima E, Hertel H, Barranger E, Obermair A and Roy M. Sentinel lymph node biopsy in patients with gynecologic cancers Expert panel statement from the International Sentinel Node Society Meeting, February 21, 2008. *Gynecol Oncol.* 2009; 114(2):151-156.
- Cibula D, Abu-Rustum NR, Dusek L, Slama J, Zikan M, Zaal A, Sevcik L, Kenter G, Querleu D, Jach R, Bats AS, Dyduch G, Graf P, Klat J, Meijer CJ, Mery E, et al. Bilateral ultrastaging of sentinel lymph node in cervical cancer: Lowering the false-negative rate and improving the detection of micrometastasis. *Gynecol Oncol.* 2012; 127(3):462-466.
- van de Lande J, Torrens B, Raijmakers PG, Hoekstra OS, van Baal MW, Brolmann HA and Verheijen RH. Sentinel lymph node detection in early stage uterine cervix carcinoma: a systematic review. *Gynecol Oncol.* 2007; 106(3):604-613.
- Veronesi U, Paganelli G, Viale G, Luini A, Zurrada S, Galimberti V, Intra M, Veronesi P, Robertson C, Maisonneuve P, Renne G, De CC, De LF and Gennari R. A randomized comparison of sentinel-node biopsy with routine axillary dissection in breast cancer. *N Engl J Med.* 2003; 349(6):546-553.
- Ansari M, Rad MA, Hassanzadeh M, Gholami H, Yousefi Z, Dabbagh VR and Sadeghi R. Sentinel node biopsy in endometrial cancer: systematic review and meta-analysis of the literature. *Eur J Gynaecol Oncol.* 2013; 34(5):387-401.
- Crane LM, Themelis G, Pleijhuis RG, Harlaar NJ, Sarantopoulos A, Arts HJ, van der Zee AG, Ntziachristos V and van Dam GM. Intraoperative multispectral fluorescence imaging for the detection of the sentinel lymph node in cervical cancer: a novel concept. *Mol Imaging Biol.* 2011; 13(5):1043-1049.
- Furukawa N, Oi H, Yoshida S, Shigetomi H, Kanayama S and Kobayashi H. The usefulness of photodynamic eye for sentinel lymph node identification in patients with cervical cancer. *Tumori.* 2010; 96(6):936-940.
- van der Vorst JR, Hutteman M, Gaarenstroom KN, Peters AA, Mieog JS, Schaafsma BE, Kuppen PJ, Frangioni JV, van de Velde CJ and Vahrmeijer AL. Optimization of near-infrared fluorescent sentinel lymph node mapping in cervical cancer patients. *Int J Gynecol Cancer.* 2011; 21(8):1472-1478.
- Schaafsma BE, van der Vorst JR, Gaarenstroom KN, Peters AA, Verbeek FP, de Kroon CD, Trimboos JB, van Poelgeest MI, Frangioni JV, van de Velde CJ and Vahrmeijer AL. Randomized comparison of near-infrared fluorescence lymphatic tracers for sentinel lymph node mapping of cervical cancer. *Gynecol Oncol.* 2012; 127(1):126-130.
- Rossi EC, Ivanova A and Boggess JF. Robotically assisted fluorescence-guided lymph node mapping with ICG for gynecologic malignancies: a feasibility study. *Gynecol Oncol.* 2012; 124(1):78-82.
- Holloway RW, Bravo RA, Rakowski JA, James JA, Jeppson CN, Ingersoll SB and Ahmad S. Detection of sentinel lymph nodes in patients with endometrial cancer undergoing robotic-assisted staging: a comparison of colorimetric and fluorescence imaging. *Gynecol Oncol.* 2012; 126(1):25-29.
- Rossi EC, Jackson A, Ivanova A and Boggess JF. Detection of sentinel nodes for endometrial cancer with robotic assisted fluorescence imaging: cervical versus hysteroscopic injection. *Int J Gynecol Cancer.* 2013; 23(9):1704-1711.
- Cholkeri-Singh A, Narepalem N and Miller CE. Laparoscopic ureteral injury and repair: case reviews and clinical update. *J Minim Invasive Gynecol.* 2007; 14(3):356-361.
- Goodno JA, Jr., Powers TW and Harris VD. Ureteral injury in gynecologic surgery: a ten-year review in a community hospital. *Am J Obstet Gynecol.* 1995; 172(6):1817-1820.
- Garry R, Fountain J, Mason S, Hatt J, Napp V, Abbott J, Clayton R, Phillips G, Whittaker M, Lilford R, Bridgman S and Brown J. The eVALuate study: two parallel randomised trials, one comparing laparoscopic with abdominal hysterectomy, the other comparing laparoscopic with vaginal hysterectomy. *BMJ.* 2004; 328(7432):129.
- Kuno K, Menzin A, Kauder HH, Sison C and Gal D. Prophylactic ureteral catheterization in gynecologic surgery. *Urology.* 1998; 52(6):1004-1008.
- Brandes S, Coburn M, Armenakas N and McAninch J. Diagnosis and management of ureteric injury: an evidence-based analysis. *BJU Int.* 2004; 94(3):277-289.
- Ashtate Y, Lee BT, Laurence RG, Lunsford E, Hutteman M, Oketokoun R, Choi HS and Frangioni JV. Intraoperative prediction of postoperative flap outcome using the near-infrared fluorophore methylene blue. *Ann Plast Surg.* 2013; 70(3):360-365.
- de Kroon CD, Gaarenstroom KN, van Poelgeest MI, Peters AA and Trimboos JB. Nerve sparing in radical surgery for early-stage cervical cancer: yes we should! *Int J Gynecol Cancer.* 2010; 20(11 Suppl 2):S39-S41.
- Whitney MA, Crisp JL, Nguyen LT, Friedman B, Gross LA, Steinbach P, Tsien RY and Nguyen QT. Fluorescent peptides highlight peripheral nerves during surgery in mice. *Nat Biotechnol.* 2011; 29(4):352-356.
- Gibbs-Strauss SL, Nasr KA, Fish KM, Khullar O, Ashtate Y, Siclován TM, Johnson BF, Barnhardt NE, Tan Hehir CA and Frangioni JV. Nerve-highlighting fluorescent contrast agents for image-guided surgery. *Mol Imaging.* 2011; 10(2):91-101.
- Brockbank EC, Harry V, Kolomainen D, Mukhopadhyay D, Sohaib A, Bridges JE, Noppenhuis MA, Shepherd JH, Ind TE and Barton DP. Laparoscopic staging for apparent early stage ovarian or fallopian tube cancer. First case series from a UK cancer centre and systematic literature review. *Eur J Surg Oncol.* 2013; 39(8):912-917.
- Ghezzi F, Malzoni M, Vizza E, Cromi A, Perone C, Corrado G, Uccella S, Cosentino F, Mancini E and Franchi M. Laparoscopic staging of early ovarian cancer: results of a multi-institutional cohort study. *Ann Surg Oncol.* 2012; 19(5):1589-1594.
- Chang SJ, Hodeib M, Chang J and Bristow RE. Survival impact of complete cytoreduction to no gross residual disease for advanced-stage ovarian cancer: a meta-analysis. *Gynecol Oncol.* 2013; 130(3):493-498.

- 43 Bristow RE, Tomacruz RS, Armstrong DK, Trimble EL and Montz FJ. Survival effect of maximal cytoreductive surgery for advanced ovarian carcinoma during the platinum era: a meta-analysis. *J Clin Oncol.* 2002; 20(5):1248-1259.
- 44 Forstner R. Radiological staging of ovarian cancer: imaging findings and contribution of CT and MRI. *Eur Radiol.* 2007; 17(12):3223-3235.
- 45 Schittenhelm J, Klein A, Tatagiba MS, Meyermann R, Fend F, Goodman SL and Sipos B. Comparing the expression of integrins alphavbeta3, alphavbeta5, alphavbeta6, alphavbeta8, fibronectin and fibrinogen in human brain metastases and their corresponding primary tumors. *Int J Clin Exp Pathol.* 2013; 6(12):2719-2732.
- 46 Harlaar NJ, Kelder W, Sarantopoulos A, Bart J, Themelis G, van Dam GM and Ntziachristos V. Real-time near infrared fluorescence (NIRF) intra-operative imaging in ovarian cancer using an alpha(v)beta(3)-integrin targeted agent. *Gynecol Oncol.* 2013; 128(3):590-595.
- 47 Verbeek FP, van der Vorst JR, Tummers QR, Boonstra MC, de Rooij KE, Lowik CW, Valentijn AR, van de Velde CJ, Choi HS, Frangioni JV and Vahrmeijer AL. Near-Infrared Fluorescence Imaging of Both Colorectal Cancer and Ureters Using a Low-Dose Integrin Targeted Probe. *Ann Surg Oncol.* 2014.
- 48 Kalli KR, Oberg AL, Keeney GL, Christianson TJ, Low PS, Knutson KL and Hartmann LC. Folate receptor alpha as a tumor target in epithelial ovarian cancer. *Gynecol Oncol.* 2008; 108(3):619-626.
- 49 Tung CH, Lin Y, Moon WK and Weissleder R. A receptor-targeted near-infrared fluorescence probe for *in vivo* tumor imaging. *Chembiochem.* 2002; 3(8):784-786.
- 50 Crane LM, van OM, Pleijhuis RG, Motekallemi A, Dowdy SC, Cliby WA, van der Zee AG and van Dam GM. Intraoperative imaging in ovarian cancer: fact or fiction? *Mol Imaging.* 2011; 10(4):248-257.
- 51 van Dam GM, Themelis G, Crane LM, Harlaar NJ, Pleijhuis RG, Kelder W, Sarantopoulos A, de Jong JS, Arts HJ, van der Zee AG, Bart J, Low PS and Ntziachristos V. Intraoperative tumor-specific fluorescence imaging in ovarian cancer by folate receptor-alpha targeting: first in-human results. *Nat Med.* 2011; 17(10):1315-1319.

CHAPTER 4

Identification of malignant tumors in the liver

Chapter 30 in: Dip FD, Ishizawa T, Kokudo N and Rosenthal R, eds. Fluorescence Imaging for Surgeons (Springer): pp. 159-168

ABSTRACT

To date, surgery is the only curative treatment option for patients with resectable metastases in the liver and is regarded as standard-of-care. However, recurrence rates remain high, which might partly be explained by the inability of conventional technologies to detect small lesions. Near-infrared fluorescence imaging is able to detect lesions as small as one millimeter, but only if they are localized on or several millimeters below the liver surface. Several studies reported the identification of otherwise undetectable liver tumors using near-infrared fluorescence imaging. Research in the coming years will have to determine if this technology is truly beneficial for patients requiring resection of hepatic metastases.

INTRODUCTION

Prognosis and survival of patients with cancer deteriorates dramatically when metastases are present. Most metastases in the liver originate from colorectal cancer. 14.5% of colorectal cancer patients have liver metastases at the moment of diagnosis and 15.2% will develop liver metastases within 5 years after curative resection of the primary tumor [1]. Metastases are the leading cause of cancer-related death, with no survivors at 5 years if left untreated [2]. Besides advancements in radiotherapy, (neoadjuvant) chemotherapy and preoperative imaging, improvements in surgical techniques have led to improved prognosis and survival rate. In the past decades, hepatic metastasectomy has evolved from a high-risk procedure to a more commonly performed curative treatment. Surgical resection is currently the only potential curative therapy and is regarded as standard-of-care, but is only possible in patients with sufficient functional liver reserve, without unresectable extrahepatic disease and when liver metastases can be resected with a tumor-free margin. Unfortunately, only 10 to 20% of patients are potential candidates for curative resection. Even with strict patient selection, intrahepatic recurrence rates after hepatic metastasectomy remain high, ranging from 11% to 28%, of which 78% occurs within 1 year [3, 4]. Factors influencing the recurrence rate of colorectal cancer liver metastases are positive resection margins, extrahepatic disease, node-positive primary tumor, disease-free interval from primary tumor to metastases less than 12 months, more than one hepatic tumor, cases where the largest hepatic tumor is more than 5 centimeters, and a serum carcinoembryonic antigen level of more than 200 ng/ml [5]. The high recurrence rate could partly be explained by inability of available technologies to detect the presence of micrometastases during liver metastasectomy. In addition, positive resection margins (R1 and R2) are still a major issue, with reported rates ranging from 11% to 23% [5, 6]. In the preoperative setting, imaging technologies such as ultrasonography, computed tomography (CT), magnetic resonance imaging (MRI) and positron emission tomography (PET) are used for surgical planning. However, these technologies are less suitable for intraoperative use and are unable to provide real-time surgical guidance. In addition, technologies available during surgery, such as intraoperative ultrasonography (IOUS), visual inspection and palpation by the surgeon, are less suitable for the detection of small lesions [7]. Recently, the use of near-infrared (NIR) fluorescence imaging has emerged as an additional technique for real-time detection of small and superficial hepatic metastases [8]. This chapter focuses on the development and current applications of NIR fluorescence imaging in identifying metastases in the liver.

Conventional technologies for identification of metastases in the liver

Several imaging technologies can be used to detect hepatic abnormalities, though sensitivity and specificity can vary greatly. Among these technologies are ultrasound, CT, MRI, fluorodeoxyglucose positron emission tomography (FDG-PET) and FDG-PET/CT. CT is considered to be the preferred technology for staging of liver disease in the majority of hospitals, because it provides good coverage of the liver and, if necessary, the abdomen and thorax in the same scan [9]. However, CT is relatively expensive and requires ionizing radiation. In addition, lesions only several millimeters small are frequently missed [7]. MRI has a higher detection rate of lesions smaller than 10 millimeters compared to CT, with a sensitivity of 60.2% and 47.3% respectively [10]. However, for both modalities, this is still unacceptably low. Diagnostic accuracy of FDG-PET is strongly affected by neoadjuvant chemotherapy; treatment resulted in a drop in sensitivity from 81.3% to 54.5% [11].

All these preoperative imaging modalities have great value for planning surgical procedures, but the hands and eyes of the surgeon combined with IOUS are still the most important tools during surgery. Hata et al. analyzed retrospectively a prospectively collected and recorded database of intraoperative detected colorectal liver metastases [12]. A total of 270 new metastases were detected in 183 consecutive patients. Intraoperative palpation and/or visual inspection detected 77% (207/270) of the new lesions. IOUS also showed to be of great value. 12% (33/270) of the new detected metastases was detected solely by IOUS. The remaining 11% (30/270) were found in removed tissue. Most of the newly found metastases were located on or less than 1 centimeter underneath the liver surface. Although this obviously shows the benefit of IOUS, palpation and visual inspection, small tumors are still missed by all detection methods. Nomura et al. histologically examined resected liver specimen and concluded that IOUS misses 25% of liver tumors smaller than 5 millimeters [7]. The same rate applies to palpation and visual inspection, although, sensitivity may vary greatly, e.g. due to the experience of surgeons and size and depth of tumors. In conclusion, there is a strong need for technologies which can intraoperatively detect small and superficial metastases in the liver. During minimally invasive liver resections, surgeons are deprived of tactile information and their visibility is hampered, increasing the need for additional imaging modalities.

Intraoperative NIR fluorescence imaging

Near-infrared (NIR) fluorescence imaging is a promising technique that can be used to identify tumors and vital structures during surgery [13]. It uses light with wavelengths between 700-900 nanometers, which is invisible to the naked eye. Advantages of NIR light include high tissue penetration and low autofluorescence.

NIR fluorescence does not alter the surgical field, as it is invisible. It is safe to use as no ionizing radiation is used, and no tissue contact is needed. As NIR fluorescence images can be acquired in real-time, it allows the surgeon to operate under direct image-guidance.

Several NIR fluorescence imaging systems are already commercially available for both open and laparoscopic surgery [14, 15]. The demand for minimally invasive liver resection increases due to exponential growth of patients eligible for hepatic metastasectomies. Laparoscopic liver resection shows a more favorable outcome than open liver resection with regard to complications, hospital stay and blood loss [16]. However, minimally invasive surgery also limits visualization and palpability of the liver surface. NIR fluorescence imaging could therefore contribute to this field of surgery by providing additional information. Several NIR fluorescence imaging systems can simultaneously acquire the NIR fluorescence signal and color video signal, enabling a real-time overlay of NIR fluorescence signal and enhance anatomical orientation. Ishizawa et al. were the first to demonstrate the safety and convenience of a prototype fluorescent imaging system during laparoscopic hepatectomy in a patient with hepatocellular carcinoma (HCC) and underlying chronic hepatitis C [17]. Laparoscopic NIR fluorescence imaging facilitated visual inspection by clearly delineating the tumor on the liver surface. Tummers et al. showed that laparoscopic NIR fluorescence imaging identified additional uveal melanoma metastases in the liver in 2 out of 3 patients [18].

NIR fluorescent contrast agents

NIR fluorescence imaging of metastases in the liver can be challenging due to hepatic uptake and clearance of many fluorescent agents, resulting in fluorescent liver tissue and, hence, invisible metastases due to high background fluorescence. Furthermore, liver tissue absorbs a higher proportion of NIR fluorescent light compared to other human tissues, such as colon and breast, resulting in a lower signal [19]. Fluorophores emitting fluorescence with longer wavelengths achieve deeper tissue penetration. However, wavelengths longer than 900 nm suffer from more absorption by water. An ideal fluorescent agent for hepatic metastases should be tumor-specific, cause low background fluorescence by being cleared renally, and emit light within the NIR fluorescence window (700-900 nanometers). To date, no such fluorescent agent is available for clinical use. Methylene blue (MB) and indocyanine green (ICG) are currently the only suitable NIR fluorescence agent approved by the Food and Drug Administration (FDA) and the European Medicines Agency (EMA). MB is cleared simultaneously by liver and kidneys, while ICG is cleared solely by liver. Hepatic metastases are visualized by non-tumor-targeted dyes when this dye is cleared by healthy hepatocytes, while it retains in cancerous tissue. The fluorescent properties of MB make it a less favorable fluorophore; its peak emitted fluorescence wavelength is 700 nanometers and therefore

subject to higher tissue autofluorescence, more light absorption and less tissue penetration capacity. No study showed the capability of MB to identify metastases in the liver. The peak emitted fluorescence wavelength of ICG is 810 nanometers, making it a better candidate for NIR fluorescence imaging. In addition, since ICG is cleared exclusively by the liver, it results in stronger signal in the liver compared to MB. Extensive medical experience with ICG already exists, due to its use in a broad spectrum of other clinical applications, e.g. assessing coronary artery bypass graft patency, retinal angiography and liver function. Since ICG contains iodine, iodine allergy and thyrotoxicosis are contraindications for its use. ICG is not metabolized, is cleared exclusively by the liver and does not undergo enterohepatic recirculation, making it an ideal candidate for detecting liver dysfunction [20].

Tumor-targeting dyes

Both ICG and MB are non-targeted dyes and the chemical structures do not readily allow conjugation to tissue-specific ligands. The lack of other clinically available NIR fluorescent agents is a considerable limitation, since ICG is only capable of imaging metastases inside the liver; extrahepatic metastases will not show any fluorescent signal. In contrast, tumor-targeted dyes do have this property and offer therefore great advantages. NIR fluorescence imaging of metastases in the liver is challenging due to hepatic uptake and clearance of many fluorescent dyes. This may result in unfavorable tumor-to-liver ratio (TLR). For identification, tumorous tissue has to be more fluorescent than its background. Several academic and commercial parties are currently developing tumor-targeting dyes. Integrin $\alpha_V\beta_3$ is a potential target, as it shows overexpression in various cancer types, such as colorectal, ovarian and breast cancer, but low expression in hepatocytes [21]. Several integrin $\alpha_V\beta_3$ targeting agents have been studied, such as IntegriSense680 (Perkin Elmer, Waltham, Massachusetts), targeting integrin $\alpha_V\beta_3$. Hutteman et al. demonstrated the feasibility for detecting colorectal metastases using IntegriSense680 in a syngeneic rat model [18]. Another potential target is matrix metalloproteinase 2 (MMP-2), which is associated with metastatic capacity of colorectal cancer. By using the NIR fluorescence probe CY5.5-C6 in mice with induced colorectal cancer, tumors with increased expression of MMP-2 were successfully imaged [22]. Another excellent target for colorectal cancer is epidermal growth factor receptor (EGFR). Cetuximab, a human antibody binding specifically to EGFR, coupled with CY5.5 (cetuximab-CY5.5), resulted in the accurate detection of tumors [23]. Much more tumor-targeted dyes are currently under development and reviewed by Luo et al. [21]. However, as fluorescent dyes are excreted by liver and kidneys, this may result in high background signal. Therefore, optimal TLR should be studied for each new dye. Tumor-targeted dyes can potentially contribute during liver metastasectomy by visualizing not only intrahepatic, but, in contrast to non-targeted dyes, also extrahepatic tumors.

Dose and timing of ICG administration

After intravenous injection, ICG is absorbed by hepatocytes and eventually excreted into the bile. Therefore, the first period after intravenous administration results in highly fluorescent liver tissue, i.e. unfavorable TLR. Timing of administration before surgery is therefore crucial to reach an optimal TLR. Fluorescent intensity of the liver strongly decreases after 24 hours, although liver dysfunction may influence this rate [24]. In patients with an unfavorable ICG retention rate, e.g. in cirrhosis, steatosis and after chemotherapy, the fluorescence signal of noncancerous liver parenchyma is higher, which makes it more challenging to obtain an adequate TLR [25]. To determine optimal dose and timing of ICG administration, van der Vorst et al. performed a preclinical study with syngeneic rats with colorectal liver metastases [24]. The highest TLR was achieved 72 hours after intravenous injection. No significant effects were observed regarding doses, although a trend favoring 0.25 milligram per kilogram body weight (extrapolated to humans) was shown. Ishizwa et al. suggested that the interval between ICG administration and surgery should be longer than at least 2 days to obtain an optimal TLR, especially in patients with advanced cirrhosis [25]. However, as in most other studies, the used dose was 0.5 milligram per kilogram body weight. In a clinical trial, administration 24 hours and 48 hours before surgery as well as doses of 10 milligrams and 20 milligrams ICG all showed sufficient TLR and no significant difference in TLR [13]. A dose of 10 milligrams ICG administered 24 hours prior to surgery is therefore advised.

NIR fluorescence imaging of metastases in the liver

NIR fluorescence imaging of metastases in the liver started after the incidental finding that hepatocellular carcinoma (HCC) shows a very strong fluorescent signal in patients who have been given ICG several days prior to surgery as a routine preoperative liver function test. In a subsequent study by Gotoh et al., all primary HCCs in ten patients were identified as bright NIR fluorescent lesions and could be removed completely [26]. In addition, four new HCC nodules that were not detected by any preoperative examinations or IOUS were detected due to the use of NIR fluorescence imaging. Harada et al. were the first to demonstrate the feasibility during hepatectomy in a patient with colorectal hepatic metastasis [27]. Several other clinical studies followed, describing the detection of both HCC and metastatic liver cancer (Table 1) [13, 18, 25, 27-32]. A total of 167 patients with colorectal or pancreatic liver metastases have been included in eight studies. In these patients, ICG has been shown to accumulate as a rim around the tumor (Figure 1 and 2). This pattern differs from primary hepatic cancers, e.g. HCC, where ICG shows total or partial fluorescence of the tumor [13]. Since ICG is removed from circulation exclusively by the liver, the rim pattern is influenced by clearance by the liver and biliary

drainage. Ishizawa et al. showed microscopically that fluorescence did not exist in metastatic tissue itself, but in surrounding noncancerous liver tissue compressed by the tumor [25]. Compression by metastases not only leads to obstructed bile canaliculi, but also to changes in the liver parenchyma due to inflammation, ductular transformation and increased presence of immature hepatocytes [33]. Compared to well-differentiated hepatocytes, immature hepatocytes display less expression of organic anion transporters [34]. Multidrug resistance P-glycoprotein 2 (MDR2), an organic anion transporter in the hepatocyte canalicular membrane, is essential for the transport of certain hydrophobic organic anions such as ICG and thus for its excretion. In its absence, ICG excretion is reduced by 90% [35]. The rim pattern of fluorescence can therefore be explained by the fact that ICG can be transported from circulation into immature hepatocytes, but is retained intracellular and not cleared into the bile canaliculi. The rim pattern is specific for malignant lesions. Van der Vorst et al. could differentiate 25 benign lesions (8 hemangiomas, 13 cysts, and 4 bile duct hamartomas) from malignant lesions by a lack of a fluorescent signal rim (Figure 4). False-negative results have not been reported so far, resulting in a sensitivity of 100% on resected tissue *ex vivo*. However, several studies describe a combined total of 14 false-positive lesions, among which 4 large regenerative nodules and 1 bile duct proliferation [25, 30-32, 36]. The incidence and characteristics of false-positive lesions should be clarified in larger study populations.

One of the great challenges in NIR fluorescence imaging is still its limited capability to penetrate human tissue. None of the above described studies reported the ability to detect metastases more than 8 millimeters below the liver capsule. For colorectal liver metastases, however, this technique is very useful, as colorectal liver metastases are mostly located on the surface of liver parenchyma. Deeper localized metastases also show a fluorescent rim after resection and sectioning (Figure 2) [37], but detection of these tumors still needs conventional technologies. Although this is a great limitation, NIR fluorescence imaging also has major advantages. Conventional imaging technologies easily miss superficial liver metastases smaller than 10 millimeters [7, 10]. In NIR fluorescence imaging, the bright signal enables surgeons to detect lesions as small as one millimeter in real-time (Figure 3) [7, 13]. Indeed, additional, otherwise undetectable metastases were identified in 7 studies [13, 25, 26, 30-32, 36]. Van der Vorst et al. report identification of otherwise undetectable liver metastases in 5 of 40 patients (12.5%, 95% CI = 5.0-26.6) [13]. Combining contrast-enhanced IIOUS and NIR fluorescence imaging together with CT and MRI, Uchiyama et al. improved diagnostic sensitivity in 32 consecutive patients from 88.5% to 98.1% ($p=0.05$). [30] Yokoyama et al. showed the potential of using NIR fluorescence imaging by screening the hepatic surface during pancreatic surgery with curative intent [32]. In 49 patients without preoperative detected hepatic metastases, 13 abnormal fluorescent lesions were detected without any apparent tumor, and 8 of them contained micrometastases. Within 6 months after surgery, 10 patients with abnormal fluorescence developed

hepatic metastases, versus 1 of 36 patients in the fluorescence negative group, resulting in a positive predictive value of 77% and a negative predictive value of 97%. This outcome could possibly help surgeons select patients for either curative or palliative treatment.

Other applications of NIR fluorescence imaging during hepatectomy

Besides tumor demarcation, excretion of ICG into the bile can be used for real-time cholangiography of the biliary anatomy. Iatrogenic damage of bile ducts is a major issue in liver surgery. Bile leakage after hepatic resection is associated with high risk for liver failure and postoperative mortality [36]. During cholangiography, the feasibility is shown by Ishizawa et al. [38]. Potentially, bile leakage could also be detected during resection of hepatic metastasis, though no study reports the feasibility. Another novel and intraoperative technique is the use of ICG for image-guided liver segment identification for anatomical hepatic resection. Aoki et al. performed a study in 35 patients who underwent hepatectomy for hepatic malignancy [39]. After administration of 5 milligrams ICG into the portal vein, stained subsegments and segments of the liver were identified in 33 of 35 patients. Both cholangiography and identification of liver segments are very usable during hepatic metastectomy and are described in other chapters.

CONCLUSIONS

Surgical resection is currently the only potentially curative therapy and standard-of-care for metastases in the liver of selected patients. The high recurrence rate demands a technology which is able to detect lesions that are otherwise undetected by current visualization methods. Current available literature suggests an important complementary role for intraoperative NIR fluorescence imaging in the detection of metastatic and primary tumors in the liver. It enables the identification of otherwise undetectable metastases as small as one millimeter and localized on or up to 8 millimeters below the liver surface. Although several studies show promising results, larger clinical trials are required to truly validate the benefit for patients requiring hepatic metastectomy. In addition, optimization of NIR fluorescent contrast agents and imaging systems is necessary before NIR fluorescence imaging becomes standard-of-care.

Figure 1 In vivo near-infrared fluorescence imaging of a hepatic metastasis using the Mini-FLARE system (Beth Israel Deaconess Hospital, Boston, USA). A characteristic rim of fluorescence around the lesion is shown.



Figure 2 Ex vivo near-infrared fluorescence imaging of resected and sliced lesion at pathology department using the FLARE imaging system (Beth Israel Deaconess Hospital, Boston, USA).



Figure 3 Small, superficial, otherwise occult metastases are identified by near-infrared fluorescence imaging (arrow).



Figure 4 Benign lesions (arrow) can be differentiated from malignant lesions by a lack of a near-infrared fluorescent rim around the lesion.



Table 1 List of studies using near-infrared fluorescence imaging in surgery for hepatic metastases.

First author, year	Number of patients	Pre-operative diagnosis	Imaging system	Dose of ICG	Injection site	Time between injection and imaging	Intraoperative IR (tumors)	Additional metastases identified	False-positive lesions	Smallest tumor size
Harada, 2009	3	ICC (n=2); CLM (n=1)	PDE	0.5 mg/kg	i.v.	4 days (1,2) & 2 days (3)	3/3	-	0	20 mm
Ishizawa, 2009	49*	HCC (n=37); CLM (n=12)	PDE	0.5 mg/kg	i.v.	1-7 days for HCC & 1-14 days for CLM	21/41 HCCs & 16/16 CLM**	+	5	2 mm
Kasuya, 2010	1	CLM	PDE	500 µl mixed with ethanol	Locally	NA	NA	-	0	3 mm
Uchiyama, 2010	32	CLM	PDE	0.5 mg/kg	i.v.	<2 weeks	NA	+	2	4 mm
Yokoyama, 2011	49	PCM	PDE	25 mg	i.v.	1 day	NA	+	5	1.5 mm
Ishizuka, 2012	7	CLM	PDE	0.1 ml/kg	NA	NA	26/26	+	1	NA
Peloso, 2012	25	CLM	PDE	0.5 mg/kg	i.v.	24 h	NA/77	+	1	3 mm
van der Vorst, 2013	40	CLM	Mini-FLARE	10 and 20 mg	i.v.	24 and 48 h	71/97	+	0	1 mm
Tummers, 2015	3	UMM	Karl Storz Fluorescence laparoscope	10 mg	i.v.	24 h	NA	+	0	1 mm

HCC=Hepatocellular carcinoma; CLM=Colorectal Liver Metastases; ICC=Intrahepatic cholangiocarcinoma; PCM=pancreatic cancer metastasis; PDE=Photo Dynamic Eye; FLARE= Fluorescence-Assisted Resection and Exploration; NA=not available; IR=identification rate; i.v.=intravenous; UMM= uveal melanoma metastases. *)26 of 49 patients (20 with HCC and 6 with CLM) underwent near-infrared fluorescence imaging during surgery; **) Identification rate of 26 patients who were examined with near-infrared fluorescence imaging during surgery.

REFERENCES

- Manfredi S, Lepage C, Hatem C, Coatmeur O, Faivre J and Bouvier AM. Epidemiology and management of liver metastases from colorectal cancer. *Ann Surg.* 2006; 244(2):254-259.
- Goslin R, Steele G, Jr., Zamcheck N, Mayer R and MacIntyre J. Factors influencing survival in patients with hepatic metastases from adenocarcinoma of the colon or rectum. *Dis Colon Rectum.* 1982; 25(8):749-754.
- Abdalla EK, Vauthey JN, Ellis LM, Ellis V, Pollock R, Broglio KR, Hess K and Curley SA. Recurrence and outcomes following hepatic resection, radiofrequency ablation, and combined resection/ablation for colorectal liver metastases. *Ann Surg.* 2004; 239(6):818-825; discussion 825-817.
- Karanjia ND, Lordan JT, Fawcett WJ, Quiney N and Worthington TR. Survival and recurrence after neo-adjuvant chemotherapy and liver resection for colorectal metastases: a ten year study. *Eur J Surg Oncol.* 2009; 35(8):838-843.
- Fong Y, Fortner J, Sun RL, Brennan MF and Blumgart LH. Clinical score for predicting recurrence after hepatic resection for metastatic colorectal cancer: analysis of 1001 consecutive cases. *Ann Surg.* 1999; 230(3):309-318; discussion 318-321.
- Trancharit H, Chirica M, Faron M, Balladur P, Lefevre LB, Svrcek M, de Gramont A, Tiret E and Paye F. Prognostic impact of positive surgical margins after resection of colorectal cancer liver metastases: reappraisal in the era of modern chemotherapy. *World J Surg.* 2013; 37(11):2647-2654.
- Nomura K, Kadoya M, Ueda K, Fujinaga Y, Miwa S and Miyagawa S. Detection of hepatic metastases from colorectal carcinoma: comparison of histopathologic features of anatomically resected liver with results of preoperative imaging. *J Clin Gastroenterol.* 2007; 41(8):789-795.
- Vahrmeijer AL, Hutteman M, van der Vorst JR, van de Velde CJ and Frangioni JV. Image-guided cancer surgery using near-infrared fluorescence. *Nat Rev Clin Oncol.* 2013; 10(9):507-518.
- Bipat S, Niekel MC, Comans EF, Nio CY, Bemelman WA, Verhoef C and Stoker J. Imaging modalities for the staging of patients with colorectal cancer. *Neth J Med.* 2012; 70(1):26-34.
- Niekel MC, Bipat S and Stoker J. Diagnostic imaging of colorectal liver metastases with CT, MR imaging, FDG PET, and/or FDG PET/CT: a meta-analysis of prospective studies including patients who have not previously undergone treatment. *Radiology.* 2010; 257(3):674-684.
- van Kessel CS, Buckens CF, van den Bosch MA, van Leeuwen MS, van Hillegersberg R and Verkooijen HM. Preoperative imaging of colorectal liver metastases after neoadjuvant chemotherapy: a meta-analysis. *Ann Surg Oncol.* 2012; 19(9):2805-2813.
- Hata S, Imamura H, Aoki T, Hashimoto T, Akahane M, Hasegawa K, Bekku Y, Sugawara Y, Makuuchi M and Kokudo N. Value of visual inspection, bimanual palpation, and intraoperative ultrasonography during hepatic resection for liver metastases of colorectal carcinoma. *World J Surg.* 2011; 35(12):2779-2787.
- van der Vorst JR, Schaafsma BE, Hutteman M, Verbeek FP, Liefers GJ, Hartgrink HH, Smit VT, Lowik CW, van de Velde CJ, Frangioni JV and Vahrmeijer AL. Near-infrared fluorescence-guided resection of colorectal liver metastases. *Cancer.* 2013; 119(18):3411-3418.
- Schaafsma BE, Mieog JS, Hutteman M, van der Vorst JR, Kuppen PJ, Lowik CW, Frangioni JV, van de Velde CJ and Vahrmeijer AL. The clinical use of indocyanine green as a near-infrared fluorescent contrast agent for image-guided oncologic surgery. *J Surg Oncol.* 2011; 104(3):323-332.
- Gioux S, Choi HS and Frangioni JV. Image-guided surgery using invisible near-infrared light: fundamentals of clinical translation. *Mol Imaging.* 2010; 9(5):237-255.
- Topal B, Fieuws S, Aerts R, Vandeweyer H and Penninckx F. Laparoscopic versus open liver resection of hepatic neoplasms: comparative analysis of short-term results. *Surgical endoscopy.* 2008; 22(10):2208-2213.
- Ishizawa T, Bandai Y and Kokudo N. Fluorescent cholangiography using indocyanine green for laparoscopic cholecystectomy: an initial experience. *Archives of surgery (Chicago, Ill : 1960).* 2009; 144(4):381-382.
- Tummers QR, Verbeek FP, Prevoo HA, Braat AE, Baeten CI, Frangioni JV, van de Velde CJ and Vahrmeijer AL. First experience on laparoscopic near-infrared fluorescence imaging of hepatic uveal melanoma metastases using indocyanine green. *Surgical innovation.* 2015; 22(1):20-25.
- Stolik S, Delgado JA, Perez A and Anasagasti L. Measurement of the penetration depths of red and near infrared light in human "ex vivo" tissues. *J Photochem Photobiol B.* 2000; 57(2-3):90-93.
- Faybik P and Hetz H. Plasma disappearance rate of indocyanine green in liver dysfunction. *Transplantation proceedings.* 2006; 38(3):801-802.
- Luo S, Zhang E, Su Y, Cheng T and Shi C. A review of NIR dyes in cancer targeting and imaging. *Biomaterials.* 2011; 32(29):7127-7138.
- Lee CM, Jang D, Cheong SJ, Jeong MH, Kim EM, Kim DW, Lim ST, Sohn MH and Jeong HJ. Optical imaging of MMP expression and cancer progression in an inflammation-induced colon cancer model. *Int J Cancer.* 2012; 131(8):1846-1853.
- Rosenthal EL, Kulbersh BD, King T, Chaudhuri TR and Zinn KR. Use of fluorescent labeled anti-epidermal growth factor receptor antibody to image head and neck squamous cell carcinoma xenografts. *Mol Cancer Ther.* 2007; 6(4):1230-1238.
- van der Vorst JR, Hutteman M, Mieog JS, de Rooij KE, Kaijzel EL, Lowik CW, Putter H, Kuppen PJ, Frangioni JV, van de Velde CJ and Vahrmeijer AL. Near-infrared fluorescence imaging of liver metastases in rats using indocyanine green. *J Surg Res.* 2012; 174(2):266-271.
- Ishizawa T, Fukushima N, Shibahara J, Masuda K, Tamura S, Aoki T, Hasegawa K, Beck Y, Fukayama M and Kokudo N. Real-time identification of liver cancers by using indocyanine green fluorescent imaging. *Cancer.* 2009; 115(11):2491-2504.
- Gotoh K, Yamada T, Ishikawa O, Takahashi H, Eguchi H, Yano M, Ohigashi H, Tomita Y, Miyamoto Y and Imaoka S. A novel image-guided surgery of hepatocellular carcinoma by indocyanine green fluorescence imaging navigation. *J Surg Oncol.* 2009; 100(1):75-79.
- Harada N, Ishizawa T, Muraoka A, Ijichi M, Kusaka K, Shibasaki M, Yamamoto K, Hasegawa K, Bandai Y and Kokudo N. Fluorescence navigation hepatectomy by visualization of localized cholestasis from bile duct tumor infiltration. *Journal of the American College of Surgeons.* 2010; 210(6):e2-6.
- Ishizuka M, Kubota K, Kita J, Shimoda M, Kato M and Sawada T. Intraoperative observation using a fluorescence imaging instrument during hepatic resection for liver metastasis from colorectal cancer. *Hepatogastroenterology.* 2012; 59(113):90-92.
- Kasuya K, Sugimoto K, Kyo B, Nagakawa Y, Ikeda T, Mori Y, Wada T, Suzuki M, Nagai T, Itoi T, Shimazu M, Aoki T and Tsuchida A. Ultrasonography-guided hepatic tumor resection using a real-time virtual sonography with indocyanine green navigation (with videos). *Journal of hepatobiliary-pancreatic sciences.* 2011; 18(3):380-385.
- Peloso A, Franchi E, Canepa MC, Barbieri L, Briani L, Ferrario J, Bianco C, Quaretti P, Brugnatelli S, Dionigi P and Maestri M. Combined use of intraoperative ultrasound and indocyanine green fluorescence imaging to detect liver metastases from colorectal cancer. *HPB (Oxford).* 2013; 15(12):928-934.
- Uchiyama K, Ueno M, Ozawa S, Kiriyama S, Shigekawa Y and Yamaue H. Combined use of contrast-enhanced intraoperative ultrasonography and a fluorescence navigation system for identifying hepatic metastases. *World J Surg.* 2010; 34(12):2953-2959.
- Yokoyama N, Otani T, Hashidate H, Maeda C, Katada T, Sudo N, Manabe S, Ikeno Y, Toyoda A and Katayanagi N. Real-time detection of hepatic micrometastases from pancreatic cancer by intraoperative fluorescence imaging: preliminary results of a prospective study. *Cancer.* 2012; 118(11):2813-2819.
- Marchal GJ, Pylyser K, Tshibwabwa-Tumba EA, Verbeken EK, Oyen RH, Baert AL and Lauweryns JM. Anechoic halo in solid liver tumors: sonographic, microangiographic, and histologic correlation. *Radiology.* 1985; 156(2):479-483.
- Oshima H, Kon J, Ooe H, Hirata K and Mitaka T. Functional expression of organic anion transporters in hepatic organoids reconstructed by rat small hepatocytes. *J Cell Biochem.* 2008; 104(1):68-81.
- Huang L and Vore M. Multidrug resistance p-glycoprotein 2 is essential for the biliary excretion of indocyanine green. *Drug Metab Dispos.* 2001; 29(5):634-637.
- Ishizuka M, Kubota K, Kita J, Shimoda M, Kato M and Sawada T. Intraoperative observation using a fluorescence imaging instrument during hepatic resection for liver metastasis from colorectal cancer. *Hepatogastroenterology.* 2012; 59(113):90-92.
- Verbeek FP, van der Vorst JR, Schaafsma BE, Hutteman M, Bonsing BA, van Leeuwen FW, Frangioni JV, van de Velde CJ, Swijnenburg RJ and Vahrmeijer AL. Image-guided hepatopancreatobiliary surgery using near-infrared fluorescent light. *Journal of hepatobiliary-pancreatic sciences.* 2012; 19(6):626-637.
- Ishizawa T, Bandai Y, Ijichi M, Kaneko J, Hasegawa K and Kokudo N. Fluorescent cholangiography illuminating the biliary tree during laparoscopic cholecystectomy. *The British journal of surgery.* 2010; 97(9):1369-1377.
- Aoki T, Murakami M, Yasuda D, Shimizu Y, Kusano T, Matsuda K, Niiya T, Kato H, Murai N, Otsuka K, Kusano M and Kato T. Intraoperative fluorescent imaging using indocyanine green for liver mapping and cholangiography. *Journal of hepatobiliary-pancreatic sciences.* 2010; 17(5):590-594.

PART II

NON-TARGETED TRACERS

CHAPTER 5

Intraoperative Near-Infrared Fluorescence Imaging of Multiple Pancreatic Neuroendocrine Tumors: a Case Report

Pancreas. 2017 (in press)

HJM HANDGRAAF, LSF BOOGERD, S SHAHBAZI FESTHALI, A FARIÑA SARASQUETA,
M SNEL, RJ SWIJNENBURG, AL VAHRMEIJER, BA BONSING, JSD MIEOG

ABSTRACT

Multiple endocrine neoplasia type 1 syndrome (MEN1) can feature pancreatic neuroendocrine lesions that have the potential to degenerate into malignancies (pancreatic neuroendocrine tumors, PNETS). Resection is required in selected cases and aims to cure patients and to prevent metastasis. Preoperative imaging is important to assess the number, size and location of PNETS. However, sensitivity of preoperative imaging modalities to detect small lesions can be rather disappointing. This makes intraoperative reassessment of the pancreas crucial. Methylene blue (MB) accumulates in neuroendocrine lesions after intravenous administration. MB emits fluorescence around 700 nm and can be visualized using a dedicated near-infrared (NIR) fluorescence imaging system. We present a 58-year old male patient with MEN1 syndrome and two lesions suspect for PNETS identified during regular follow-up. Intraoperative administration of MB allowed successful NIR fluorescence imaging of multiple lesions missed by preoperative imaging. After confirmation by intraoperative ultrasound, this new finding led to a major change in treatment: from enucleations to total pancreatectomy. Histopathological examination confirmed that the fluorescent lesions were indeed neuroendocrine lesions ranging from microadenomas to PNETS. This case demonstrates that intraoperative assessment of neuroendocrine lesions can be improved by intraoperative NIR fluorescence imaging using MB, a safe and relatively easy technique.

INTRODUCTION

Multiple endocrine neoplasia type 1 syndrome (MEN1) is a rare genetic disorder characterized by the development of parathyroid, anterior pituitary and pancreatic islet cell hyperplasia and microadenomas.[1] Its primary life-threatening manifestation is the malignant degeneration of neuroendocrine lesions into pancreatic neuroendocrine tumors (PNETS). Surgery is recommended in case of symptomatic and hormonal active PNETS or if tumors are larger than 1 cm.[2] The aim of surgery is to obtain cure and prevent metastasis.[3] Pre- and intraoperative assessment of tumors in the pancreas remains difficult, leading to incomplete resections.[4] Near-infrared (NIR, wavelengths of 700-900 nm) fluorescence imaging has shown to identify lesions during surgery using a fluorescent dye and a dedicated imaging system.[5] Methylene blue (MB) is an FDA-approved agent and emits fluorescence around 700 nm. Preclinical studies suggest that a low dose of MB stains PNETS and allows intraoperative NIR fluorescence imaging.[6] Based on these results, we explored the feasibility to identify PNETS using MB and an intraoperative NIR fluorescence imaging system.

Case report

We present a 58-year old male patient with MEN1 syndrome with persistent mild hyperparathyroidism despite parathyroidectomy and two nonfunctional adrenal gland adenomas. In addition, two lesions suspect for PNETS were identified during regular follow-up using dedicated MRI. The lesions were sized 15 and 14 mm and located in the head and tail of the pancreas, respectively. ⁶⁸Ga-DOTATATE PET/CT identified six lesions in the head, body and tail of the pancreas (Figure 1A). No metastases were identified. Enucleation of the lesions was planned.

The local medical ethics committee approved this study and the patient provided informed consent. During routine surgery, after exposing the pancreas, NIR fluorescence imaging was performed using the Quest Spectrum™ Platform (Quest Medical Imaging B.V., The Netherlands). No autofluorescence was observed (Figure 2A). Subsequently, a dose of 0.5 mg/kg MB was administered intravenously. The infusion was done in 5 minutes to reduce pseudohypoxia caused by its blue color. No adverse reactions related to infusion of MB occurred. Within minutes after start of the infusion multiple lesions in the head, body and tail of the pancreas became fluorescent and remained visible for at least 30 minutes (Figure 2B). Ultrasound confirmed the presence of multiple (>20) lesions throughout the whole pancreas (Figure 1B). Due to the unexpected large number of lesions and their distribution, the planned enucleations would not cure the patient. The procedure was therefore canceled to discuss the results and consequences with the patient and the multidisciplinary team. As advised by the multidisciplinary team, the patient opted for a total pancreatectomy, which was planned five days

after the first procedure. A repeated dose of MB was administered approximately 20 min prior to dissection of the pancreatic vessels. Again, the same lesions could be identified using NIR fluorescence imaging (supplementary video).

After successful total pancreatectomy, the resected specimen was analyzed at the pathology department. The tissue was fixed in formalin and processed for further microscopic analysis. Faint fluorescence signals were still visible in tumors (Figure 2C). A total of ten PNETs sized 5 to 14 mm and countless microadenomas and islet hyperplasia were identified throughout the entire pancreas. The two largest fluorescent lesions showed strong, diffuse staining for synaptophysin and chromogranin in 100% of the lesional cells (Figure 3). Mitoses were not seen. The largest lesion was classified however as a PNET grade 2 with a tumor area with a proliferation rate of approximately 5% of Ki-67 positive cells, while the other lesion was classified as PNET grade 1 with less than 2% of Ki-67 positivity. A total of 18 lymph nodes were examined; none contained tumor cells (0/18).

DISCUSSION

This case report illustrates the difficulties of translating preoperative imaging to the intraoperative situation. Even with the latest advances in MRI and nuclear imaging, in this case preoperative imaging lacked sensitivity to identify all small lesions throughout the pancreas. Furthermore, it shows the importance of intraoperative assessment of PNETs, especially in MEN1 patients. NIR fluorescence imaging using MB can identify and demarcate neuroendocrine lesions (tumors and microadenomas) during surgery. Moreover, in this case it led to a major change in treatment: from enucleations to a total pancreatectomy.

Already in 1974 it became clear that high doses of MB (5 mg/kg) can stain insulinomas blue.[7] Later, selective intra-arterial administration of MB was used to stain PNETs blue up to 15 min after injection.[8] However, visualizing macroscopically blue tumors still required them to be exposed completely. More recently, intraoperative NIR fluorescence imaging of adenomas using MB became clinically feasible.[9] NIR fluorescence signals from MB can penetrate through approximately 5 mm of tissue, also allowing visualization of targets located just below the surface.[10] When contraindications, such as renal insufficiency and hypersensitivity, are taken into consideration, intravenous administration of MB is relatively safe. The sensitivity of dedicated fluorescence imaging systems allows detection of even low concentrations of MB and requires thus a tenfold lower dose. A lower dose decreases the risk of adverse reactions even further.

Although in this case MB and fluorescence imaging showed to be specific for neuroendocrine lesions, the mechanism of action is unclear and potentially unreliable. Furthermore, its wavelength (around 700 nm) is subject to reduced tissue penetration depth and more autofluorescence from surrounding tissue compared to the more optimal wavelengths around 800 nm.[5] The technique

may be improved by conjugating 800 nm fluorophores to targeting moieties. This method has already shown to be feasible in clinical studies with cetuximab-IRDYE-800CW for head and neck cancer and folate conjugated to a NIR fluorescent dye for ovarian cancer.[11, 12] Fluorescent tracers targeting the PNET-specific neurokinin-1 receptor or the somatostatin receptor showed *in vivo* high tumor uptake and low non-specific uptake in mouse xenograft models.[13, 14] However, clinical translation of new fluorescent tracers is costly, time-consuming and not much is known about safety. MB is safe, cheap, and clinically available for off-label use in combination with a dedicated fluorescence imaging system. Prices of such systems are starting from \$40,000 and have been reviewed previously.[15]

In conclusion, this case demonstrates that intraoperative assessment of neuroendocrine lesions can be improved by NIR fluorescence imaging using MB, a safe and relatively easy technique.

Figure 1 ^{68}Ga -DOTATATE PET/CT and intraoperative ultrasound. ^{68}Ga -DOTATATE PET/CT identified multiple metabolically active lesions in the head, body and tail of the pancreas. Intraoperative ultrasound confirmed the presence of multiple neuroendocrine lesions throughout the whole pancreas. White arrows: lesions suspect for pancreatic neuroendocrine lesions. Smaller microadenomas have not been marked.



Figure 2 Intraoperative and ex vivo near-infrared fluorescence imaging of the pancreas. Prior to intravenous administration of methylene blue. No autofluorescence was observed (exposure time 50 ms). Five minutes after start of the infusion of methylene blue. Multiple lesions in the head, body and tail of the pancreas are fluorescent (exposure time 50 ms). Ex vivo. Faint fluorescence signals are still visible (exposure time 200 ms) 3 days after resection and formalin fixation. White arrows: lesions suspect for pancreatic neuroendocrine tumors. * Head of the pancreas. ** Tail of the pancreas. Dashed arrow: this suspect lesion was stained for chromogranin and synaptophysin (see figure 3).

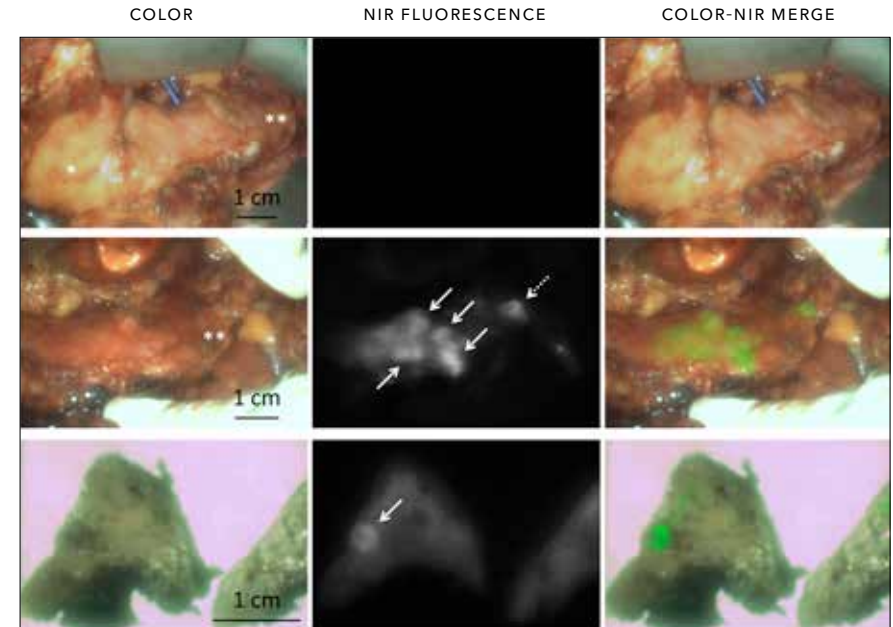
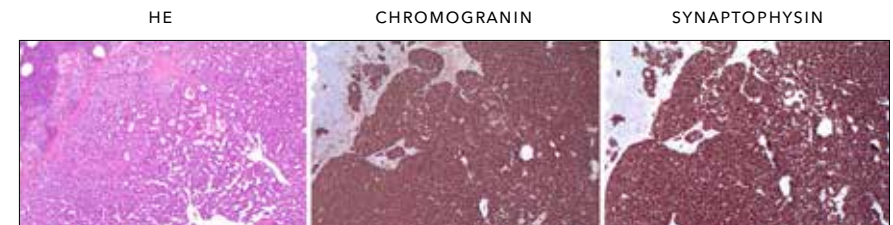


Figure 3 Histopathological examination of a fluorescent lesion. The fluorescent lesion (dashed arrow in figure 2B) showed strong, diffuse staining for synaptophysin and chromogranin in 100% of the lesional cells. Magnification: 25x.



REFERENCES

- 1 Brandi ML, Gagel RF, Angeli A, Bilezikian JP, Beck-
Peccoz P, Bordini C, Conte-Devolx B, Falchetti A,
Gheri RG, Libroia A, Lips CJ, Lombardi G, Mannelli
M, Pacini F, Ponder BA, Raue F, et al. Guidelines for
diagnosis and therapy of MEN type 1 and type 2. *J
Clin Endocrinol Metab.* 2001; 86(12):5658-5671.
- 2 Thakker RV, Newey PJ, Walls GV, Bilezikian J,
Dralle H, Ebeling PR, Melmed S, Sakurai A, Tonelli
F, Brandi ML and Endocrine S. Clinical practice
guidelines for multiple endocrine neoplasia
type 1 (MEN1). *J Clin Endocrinol Metab.* 2012;
97(9):2990-3011.
- 3 Giudici F, Nesi G, Brandi ML and Tonelli F. Surgical
management of insulinomas in multiple endocrine
neoplasia type 1. *Pancreas.* 2012; 41(4):547-553.
- 4 Handgraaf HJ, Boonstra MC, Van Erkel AR, Bonsing
BA, Putter H, Van De Velde CJ, Vahrmeijer AL
and Mieog JS. Current and future intraoperative
imaging strategies to increase radical resection
rates in pancreatic cancer surgery. *Biomed Res Int.*
2014; 2014:890230.
- 5 Vahrmeijer AL, Hutteman M, van der Vorst JR,
van de Velde CJ and Frangioni JV. Image-guided
cancer surgery using near-infrared fluorescence.
Nat Rev Clin Oncol. 2013; 10(9):507-518.
- 6 Winer JH, Choi HS, Gibbs-Strauss SL, Ashitate
Y, Colson YL and Frangioni JV. Intraoperative
localization of insulinoma and normal pancreas
using invisible near-infrared fluorescent light. *Ann
Surg Oncol.* 2010; 17(4):1094-1100.
- 7 Gordon DL, Airan MC and Suvanich S. Visual
identification of an insulinoma using methylene
blue. *The British journal of surgery.* 1974;
61(5):363-364.
- 8 Prinz RP. Selective intraarterial methylene blue for
pancreatic and duodenal endocrine tumors. *J Hep
Bil Pancr Surg.* 1994; 1:517-521.
- 9 van der Vorst JR, Schaafsma BE, Verbeek FP,
Swijnenburg RJ, Tummers QR, Hutteman M,
Hamming JF, Kievit J, Frangioni JV, van de Velde
CJ and Vahrmeijer AL. Intraoperative near-infrared
fluorescence imaging of parathyroid adenomas
with use of low-dose methylene blue. *Head Neck.*
2014; 36(6):853-858.
- 10 Verbeek FP, van der Vorst JR, Schaafsma BE,
Swijnenburg RJ, Gaarenstroom KN, Elzevier HW,
van de Velde CJ, Frangioni JV and Vahrmeijer
AL. Intraoperative near infrared fluorescence
guided identification of the ureters using low dose
methylene blue: a first in human experience. *J
Urol.* 2013; 190(2):574-579.
- 11 Hoogstins CE, Tummers QR, Gaarenstroom KN,
de Kroon CD, Trimpos JB, Bosse T, Smit VT, Vuyk J,
van de Velde CJ, Cohen AF, Low PS, Burggraaf J
and Vahrmeijer AL. A Novel Tumor-Specific Agent
for Intraoperative Near-Infrared Fluorescence
Imaging: A Translational Study in Healthy
Volunteers and Patients with Ovarian Cancer. *Clin
Cancer Res.* 2016; 22(12):2929-2938.
- 12 Rosenthal EL, Warram JM, de Boer E, Chung
TK, Korb ML, Brandwein-Gensler M, Strong TV,
Schmalbach CE, Morlandt AB, Agarwal G, Hartman
YE, Carroll WR, Richman JS, Clemons LK, Nabell
LM and Zinn KR. Safety and Tumor Specificity of
Cetuximab-IRDye800 for Surgical Navigation in
Head and Neck Cancer. *Clin Cancer Res.* 2015;
21(16):3658-3666.
- 13 Kanduluru AK, Srinivasarao M and Low PS. Design,
Synthesis, and Evaluation of a Neurokinin-1 Receptor-Targeted Near-IR Dye for Fluorescence-Guided
Surgery of Neuroendocrine Cancers. *Bioconjug
Chem.* 2016; 27(9):2157-2165.
- 14 Santini C, Kuil J, Bunschoten A, Pool S, de Blois E,
Ridwan Y, Essers J, Bernsen MR, van Leeuwen FW
and de Jong M. Evaluation of a Fluorescent and
Radiolabeled Hybrid Somatostatin Analog In Vitro
and in Mice Bearing H69 Neuroendocrine Xeno-
grafts. *J Nucl Med.* 2016; 57(8):1289-1295.
- 15 Handgraaf HJ, Verbeek FP, Tummers QR, Boogerd
LS, van de Velde CJ, Vahrmeijer AL and Gaaren-
stroom KN. Real-time near-infrared fluorescence
guided surgery in gynecologic oncology: a review
of the current state of the art. *Gynecol Oncol.* 2014;
135(3):606-613.

CHAPTER 6

Intraoperative fluorescence
imaging to localize tumors
and sentinel lymph nodes in
rectal cancer

Minim Invasive Ther Allied Technol. 2016; 25(1):48-53.

HJM HANDGRAAF, LSF BOOGERD, FPR VERBEEK, QRJG TUMMERS, JCH HARDWICK,
CIM BAETEN, JV FRANGIONI, CJH VAN DE VELDE, AL VAHRMEIJER

ABSTRACT

Tumor involvement at the resection margin remains the most important predictor for local recurrence in patients with rectal cancer. A careful description of tumor localization is therefore essential. Currently, endoscopic tattooing with ink is customary, but visibility during laparoscopic resections is limited. Near-infrared (NIR) fluorescence imaging using indocyanine green (ICG) could be an improvement. In addition to localize tumors, ICG can also be used to identify sentinel lymph nodes (SLNs). The feasibility of this new technique was explored in 5 patients undergoing laparoscopic low anterior resection for rectal cancer. Intraoperative tumor visualization was possible in 4 out of 5 patients. Fluorescence signal could be detected 32 ± 18 minutes after incision, while ink could be detected 42 ± 21 minutes after incision ($p=0.53$). No recurrence was diagnosed within 3 months after surgery. *Ex vivo* imaging identified a mean of 4.2 ± 2.7 fluorescent lymph nodes, which were appointed SLNs. One out of a total of 83 resected lymph nodes contained a micrometastasis. This node was not fluorescent.

This technical note describes the feasibility of endoscopic tattooing of rectal cancer using ICG:nanocolloid and NIR fluorescence imaging during laparoscopic resection. Simultaneous SLN mapping was also feasible, but may be less reliable due to neoadjuvant therapy.

INTRODUCTION

The introduction of total mesorectal excision (TME) combined with preoperative radiotherapy in patients with resectable rectal cancer has shown to reduce local recurrence rates from 11% to 5% compared to surgery alone [1]. Tumor involvement at the resection margin remains the most important predictor for local recurrence [2]. A careful description of the localization of the rectal tumor is therefore essential. In the era of laparoscopic surgery, this is even more challenging, especially when the tumor is small or located at the mesenteric intestinal border. Colonoscopy is the gold standard for diagnosis of colorectal cancer. However, its ability to localize cancer has been called into question [3]. Tumor localization can be wrongly assessed when the colonoscope is not completely straight. Endoscopic tattooing using ink to direct the surgeon has been performed since the 1960s [4]. It results in reliable intraoperative localization, but not all tattoos are visible, especially when the tumor can be found below the peritoneal reflection or adjacent to the mesorectal envelope [5].

Recently, near-infrared (NIR) fluorescence imaging has been introduced for real-time intraoperative visualization of tumors, sentinel lymph nodes (SLNs) and vital structures such as ureters [6]. Advantages of NIR light (wavelength 700-900 nm) include high tissue penetration (several millimeters) and low tissue autofluorescence, providing high signal-to-background ratios. Indocyanine green (ICG) is currently the only clinically available 800 nm fluorophore and has been used with success in several clinical studies [7, 8]. ICG could be a more suitable dye for tattooing, because of few side effects, relatively long absorption time and potentially increased detection using NIR fluorescence imaging compared to macroscopic color perception [9].

Besides endoscopic tattooing, injecting ICG may also assist in intraoperative detection of SLNs. Although surgery is often considered curative in node-negative rectal cancer, approximately 25% of these patients will develop disease recurrence [10]. This is most likely caused by understaging of the resected lymph nodes (LNs). Micrometastases are easily missed by conventional histopathological examination, but examination of all LNs to detect micrometastases is time consuming and expensive. Multilevel fine pathological examination of SLNs in colorectal cancer has been shown to improve tumor staging [11]. Several studies report high detection and sensitivity rates by using ICG for the SLN procedure in different types of cancer, including gastrointestinal cancer [12-18]. ICG is non-covalently absorbed by nanocolloid. The hydrodynamic diameter is thereby increased from 1 nm to approximately 50 nm [19, 20]. This improves accuracy, since molecules smaller than approximately 10 nm quickly flow through the SLN to second tier LNs, whereas larger molecules require multiple hours to days to reach beyond the SLN. Using ICG-nanocolloid whether or not combined with Technetium-99m to identify SLNs has already successfully been described in patients [21-23]. The aim of the present

study was to assess the feasibility to localize tumors and SLNS using NIR fluorescence imaging after endoscopic tattooing with ICG:nanocolloid.

MATERIALS AND METHODS

The study was approved by the Medical Ethics Committee of the Leiden University Medical Center and performed in accordance with the ethical standards of the Helsinki Declaration of 1975.

Laparoscopic fluorescence imaging system

Intraoperative NIR fluorescence imaging was performed using a laparoscopic high definition fluorescence imaging system (KARL STORZ GmbH & Co. KG, Tuttlingen, Germany). The system included a plasma light guide and a 30°, 10 mm laparoscope, applicable for white light (WL) and ICG imaging. Switching between WL and ICG mode was done by using a foot pedal.

Preparation and injection of the probe

ICG (25 mg vials, Pulsion Medical Systems, Munich, Germany) was dissolved in 5ml sterile water. Subsequently, 1 ml of 5 mg/ml ICG was diluted in 100 ml sterile water (50 µg/ml final concentration). Nanocolloid (0.5 mg vials, GE Healthcare, Eindhoven, the Netherlands) was dissolved in 3 ml saline. 1.5 ml 50 µg/ml ICG was then mixed with 0.9 ml of 0.167 mg/ml nanocolloid. After general anesthesia, prior to incision, 1.6ml ICG:nanocolloid containing 100 µg nanocolloid and 50 µg ICG was injected endoscopically at 4 peritumoral submucosal spots (0.4 ml per spot) by the gastroenterologist. A rectal tube was used to deflate the rectum after endoscopy.

Surgical technique

Included patients (Table 1) underwent standard-of-care laparoscopic low anterior resection performed by experienced surgeons. Peritumoral tattooing with India ink was performed by the gastroenterologist several weeks prior to surgery. In addition to the standard-of-care, NIR fluorescence imaging was performed at several time points during laparoscopic surgery to localize the tumor and SLNS.

Ex vivo imaging

After slicing of the specimen at least 1 day after surgery, fluorescence imaging was performed again at the Pathology Department with the previously described FLARE™ imaging system [24]. Fluorescent LNS were appointed as SLNS and

processed separately from non-fluorescent LNS. Standard pathologic assessment was performed by cytokeratin immunohistochemistry.

RESULTS

The tumor could clearly be localized in 4 out of 5 patients (Fig.1A). One patient (patient no.4) was injected with ICG:nanocolloid, but no intraoperative images were obtained due to an operator mistake that disabled the correct imaging settings. Fluorescence signal was in all other patients earlier visible than ink (Fig. 1B). Fluorescence signals could be detected 32±18 minutes after incision, while ink could be detected 42 ± 21 minutes after incision ($p = 0.53$). All resections were radical. No recurrence was diagnosed within 3 months after completion of the study. One patient (no. 2.) developed anastomotic leakage, which was closed surgically. No other complications regarding the use of ICG:nanocolloid or fluorescence imaging occurred.

Mean time between injection and end of the procedure, i.e. the time for ICG:nanocolloid to migrate to the SLN, was 189 ± 48 minutes. During the procedure, a mean of 2.0 ± 0.82 fluorescent LNS could be visualized (Fig. 2). *Ex vivo* imaging was performed in all 5 patients. Using the FLARE™ imaging system, a mean of 4.2 ± 2.7 fluorescent LNS per patient could be identified, which were appointed SLNS. The pathologist found 12.4 ± 8.0 additional LNS per patient by conventional method, which were appointed non-SLNS. One out of a total of 83 identified LNS contained a micrometastasis. However, this node (in patient no. 2) was not fluorescent.

DISCUSSION

Advances in the treatment of rectal cancer have not only led to improved patient outcome, but also to challenges. Laparoscopic surgery results in significantly lower mortality and morbidity compared to open surgery [25], but also deprives surgeons of tactile and visual feedback. Neoadjuvant radiochemotherapy decreases recurrence rates, but pathologic response makes identification of the primary tumor more difficult [5]. Both laparoscopy and neoadjuvant therapy complicate intraoperative localization of the tumor. These advances are especially an issue since incomplete resections are the single most important factor for rectal cancer recurrence [2]. Endoscopic tattooing using ink results in reliable intraoperative localization of colorectal cancer [26]. However, not all tattoos are visible, because ink can be masked easily by overlying tissue.

The present study shows that endoscopic tattooing with ICG:nanocolloid is technically feasible. NIR fluorescence signal was visible in all patients in whom imaging could be performed. In addition, the signal was not only seen earlier than ink, but also better visible throughout the entire procedure. This is the result

of a higher penetration depth of NIR light (several millimeters) compared to ink. Watanabe et al. [9] also used ICG for colonic tattooing. In all 10 patients, the tumor border could be identified using NIR fluorescence imaging. The signal remained visible for at least 72-120 hours after pre-operative endoscopic injection. However, we chose to perform endoscopic tattooing after general anesthesia to save our patients from discomfort of yet another colonoscopy and another visit to the hospital. Although the tumor could be localized 10 minutes earlier, the endoscopy during surgery neutralized this advantage. To be cost-effective, it should therefore be studied if the ICG injection can be combined with the standard-of-care endoscopic tattooing with ink or even replace it. This is however only possible if the retention time of ICG is sufficient enough.

In colorectal cancer patients, both blue dyes and radiotracers have been used as SLN tracers in *in vivo* and *ex vivo* settings, but both tracers have disadvantages [27]. The use of gamma ray-emitting radiotracers requires involvement of a nuclear physician and localization requires a handheld gamma probe, which does not permit real-time visualization. Blue dyes cannot be seen through overlying tissue and can diffuse through the true SLN to 2nd- and 3rd-tier nodes due to their small size. The use of ICG:nanocolloid may overcome these disadvantages and identify LNs which are a candidate for multilevel fine pathological examination[11]. Other studies describing the use of ICG and NIR fluorescence imaging in SLN identification in different types of cancer report detection rates of 90 to 100% and sensitivity rates of 82% to 100% [12-18]. The detection rate is similar (100%), but the only micrometastasis containing lymph node in the present study was not fluorescent (sensitivity: 0%). Although the included number of patients is not enough to draw extensive conclusions, the difference may be explainable by the long course of neoadjuvant chemoradiotherapy this patient (patient no.2) received, which has been shown to result in unreliable SLN procedures in rectal cancer [28]. SLN mapping in rectal cancer using ICG:nanocolloid and NIR fluorescence imaging appears to perform just like other SLN mapping methods in rectal cancer, i.e. unreliable. However, it can still assist in identifying the necessary number of LNs required for pathologic TNM staging [29]. In addition, in case no neoadjuvant therapy is given, e.g. in selected patients with stage cT1-cT2N0, this technique may have higher sensitivity. Arezzo et al. [25] showed the feasibility of SLN mapping using ICG and NIR fluorescence imaging during transanal endoscopic microsurgery (TEM) in 3 patients with T0/T1 rectal cancer.

The currently used laparoscope was only capable of showing one light modus at a time. However, there are already camera systems available that can depict white light and NIR channels at the same time, and even produce white light-NIR overlay video for better anatomical orientation.

ICG is not a tumor-targeted probe. Hence, no tumor-specific signal can be expected. The accuracy of the fluorescence signal depends therefore mainly on the accuracy of the gastroenterologist's injection. In the near future, tumor-specific

probes, such as CRGD-ZW800-1 which targets integrins associated with neoangiogenesis, may be expected [30]. Such probes have the potential to accurately localize tumor and its border in real-time during surgery. Furthermore, it makes endoscopic tattooing redundant, because these probes are injected intravenously prior to surgery.

CONCLUSION

This technical note describes the technical feasibility of endoscopic tattooing of rectal cancer using ICG:nanocolloid and NIR fluorescence imaging during laparoscopic resection. Simultaneous SLN mapping was also feasible, but may be less reliable.

Figure 1 A. Intraoperative laparoscopic NIR fluorescence imaging of the endoscopically injected probe ICG:nanocolloid in a patient with rectal cancer. India ink is not yet visible. B. Intraoperative macroscopic visualization of India ink in the rectum. NIR fluorescence signal is also visible.

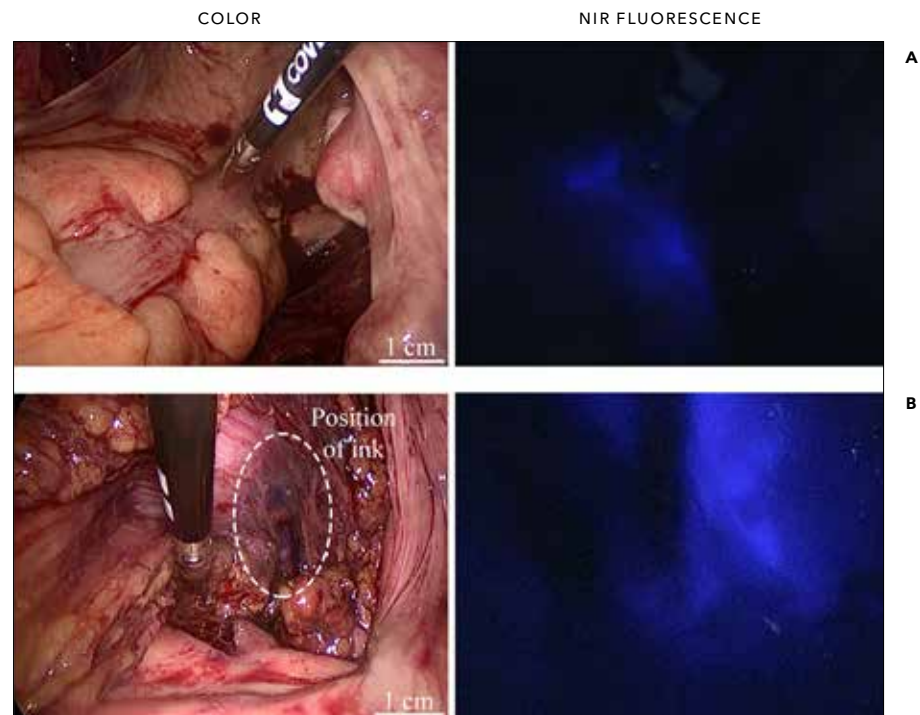


Figure 2. Ex vivo NIR fluorescence imaging of a resected and sliced rectum specimen using the FLARE™ camera system. Two fluorescent spots are visible (white arrows), which were appointed as SLNS.



Table 1 Patient characteristics.

Patient no.	Gender	Age (years)	Clinical tm Classification	Distance to dentate line (cm)	Neoadjuvant therapy	Localization of tumor by NIR fluorescence	SLNs detected by NIR fluorescence	SLNs identified at pathology	Blue ink visible
1	M	71	cT2N0M0	15	Radiotherapy	+	5	12	+
2	M	61	cT3N2M0	7	Chemoradiotherapy	+	2	15	+
3	F	65	cT3N1M0	18	Radiotherapy	+	3	12	+
4	F	70	cT3N2M0	7	Chemoradiotherapy	-	5	18	+
5	F	76	cT2N0M0	9	None	+	4	26	+
		69 ± 5.6		11.2 ± 5.0		80%	3.8 ± 1.3	16.6 ± 5.8	100%

REFERENCES

- van Gijn W, Marijnen CA, Nagtegaal ID, Kranenburg EM, Putter H, Wiggers T, Rutten HJ, Pahlman L, Glimelius B and van de Velde CJ. Preoperative radiotherapy combined with total mesorectal excision for resectable rectal cancer: 12-year follow-up of the multicentre, randomised controlled TME trial. *Lancet Oncol.* 2011; 12(6):575-582.
- Kellokumpu I, Vironen J, Kairaluoma M, Jantunen I, Kautiainen H and Nuorva K. Quality of surgical care, local recurrence, and survival in patients with low- and midrectal cancers following multimodal therapy. *Int J Colorectal Dis.* 2012; 27(1):111-120.
- Schoellhammer HF, Gregorian AC, Sarkisyan GG and Petrie BA. How important is rigid proctosigmoidoscopy in localizing rectal cancer? *American journal of surgery.* 2008; 196(6):904-908; discussion 908.
- HE K. The use of a tattooing instrument for marking colonic mucosa. *Am J Surg.* 1962; 103:83-85.
- Torres ML, McCafferty MH and Jorden J. The difficulty with localization of rectal cancer after neoadjuvant chemoradiation therapy. *Am Surg.* 2010; 76(9):974-976.
- Vahrmeijer AL, Hutteman M, van der Vorst JR, van de Velde CJ and Frangioni JV. Image-guided cancer surgery using near-infrared fluorescence. *Nat Rev Clin Oncol.* 2013; 10(9):507-518.
- van der Vorst JR, Schaafsma BE, Hutteman M, Verbeek FP, Liefers GJ, Hartgrink HH, Smit VT, Lowik CW, van de Velde CJ, Frangioni JV and Vahrmeijer AL. Near-infrared fluorescence-guided resection of colorectal liver metastases. *Cancer.* 2013; 119(18):3411-3418.
- Schaafsma BE, Mieog JS, Hutteman M, van der Vorst JR, Kuppen PJ, Lowik CW, Frangioni JV, van de Velde CJ and Vahrmeijer AL. The clinical use of indocyanine green as a near-infrared fluorescent contrast agent for image-guided oncologic surgery. *J Surg Oncol.* 2011; 104(3):323-332.
- Watanabe M, Tsunoda A, Narita K, Kusano M and Miwa M. Colonic tattooing using fluorescence imaging with light-emitting diode-activated indocyanine green: a feasibility study. *Surg Today.* 2009; 39(3):214-218.
- de Campos-Lobato LF, Stocchi L, de Sousa JB, Buta M, Lavery IC, Fazio VW, Dietz DW and Kalady MF. Less than 12 nodes in the surgical specimen after total mesorectal excision following neoadjuvant chemoradiation: it means more than you think! *Ann Surg Oncol.* 2013; 20(11):3398-3406.
- Vogelaar FJ, Reimers MS, van der Linden RL, van der Linden JC, Smit VT, Lips DJ, van de Velde CJ and Bosscha K. The Diagnostic Value of One-Step Nucleic acid Amplification (OSNA) for Sentinel Lymph Nodes in Colon Cancer Patients. *Ann Surg Oncol.* 2014.
- Ankersmit M, van der Pas MH, van Dam DA and Meijerink WJ. Near infrared fluorescence lymphatic laparoscopy of the colon and mesocolon. *Colorectal disease : the official journal of the Association of Coloproctology of Great Britain and Ireland.* 2011; 13 Suppl 7:70-73.
- Cahill RA, Anderson M, Wang LM, Lindsey I, Cunningham C and Mortensen NJ. Near-infrared (NIR) laparoscopy for intraoperative lymphatic road-mapping and sentinel node identification during definitive surgical resection of early-stage colorectal neoplasia. *Surgical endoscopy.* 2012; 26(1):197-204.
- van der Vorst JR, Hutteman M, Gaarenstroom KN, Peters AA, Mieog JS, Schaafsma BE, Kuppen PJ, Frangioni JV, van de Velde CJ and Vahrmeijer AL. Optimization of near-infrared fluorescent sentinel lymph node mapping in cervical cancer patients. *Int J Gynecol Cancer.* 2011; 21(8):1472-1478.
- Fujiwara M, Mizukami T, Suzuki A and Fukamizu H. Sentinel lymph node detection in skin cancer patients using real-time fluorescence navigation with indocyanine green: preliminary experience. *J Plast Reconstr Aesthet Surg.* 2009; 62(10):e373-378.
- Hirche C, Mohr Z, Kneif S, Doniga S, Murawa D, Strik M and Hunerbein M. Ultrastaging of colon cancer by sentinel node biopsy using fluorescence navigation with indocyanine green. *Int J Colorectal Dis.* 2012; 27(3):319-324.
- Crane LM, Themelis G, Arts HJ, Buddingh KT, Brouwers AH, Ntziachristos V, van Dam GM and van der Zee AG. Intraoperative near-infrared fluorescence imaging for sentinel lymph node detection in vulvar cancer: first clinical results. *Gynecol Oncol.* 2011; 120(2):291-295.
- Kusano M, Tajima Y, Yamazaki K, Kato M, Watanabe M and Miwa M. Sentinel node mapping guided by indocyanine green fluorescence imaging: a new method for sentinel node navigation surgery in gastrointestinal cancer. *Dig Surg.* 2008; 25(2):103-108.
- Ohnishi S, Lomnes SJ, Laurence RG, Gogbashian A, Mariani G and Frangioni JV. Organic alternatives to quantum dots for intraoperative near-infrared fluorescent sentinel lymph node mapping. *Mol Imaging.* 2005; 4(3):172-181.
- Buckle T, van Leeuwen AC, Chin PT, Janssen H, Muller SH, Jonkers J and van Leeuwen FW. A self-assembled multimodal complex for combined pre- and intraoperative imaging of the sentinel lymph node. *Nanotechnology.* 2010; 21(35):355101.
- Schaafsma BE, Verbeek FP, Rietbergen DD, van der Hiel B, van der Vorst JR, Liefers GJ, Frangioni JV, van de Velde CJ, van Leeuwen FW and Vahrmeijer AL. Clinical trial of combined radio- and fluorescence-guided sentinel lymph node biopsy in breast cancer. *Br J Surg.* 2013; 100(8):1037-1044.
- Matheron HM, van den Berg NS, Brouwer OR, Kleinjan GH, van Driel WJ, Trum JW, Vegt E, Kenter G, van Leeuwen FW and Valdes Olmos RA. Multimodal surgical guidance towards the sentinel node in vulvar cancer. *Gynecol Oncol.* 2013; 131(3):720-725.
- van der Poel HG, Buckle T, Brouwer OR, Valdes Olmos RA and van Leeuwen FW. Intraoperative laparoscopic fluorescence guidance to the sentinel lymph node in prostate cancer patients: clinical proof of concept of an integrated functional imaging approach using a multimodal tracer. *Eur Urol.* 2011; 60(4):826-833.
- Troyan SL, Kianzad V, Gibbs-Strauss SL, Gioux S, Matsui A, Oketokoun R, Ngo L, Khamene A, Azar F and Frangioni JV. The FLARE intraoperative near-infrared fluorescence imaging system: a first-in-human clinical trial in breast cancer sentinel lymph node mapping. *Ann Surg Oncol.* 2009; 16(10):2943-2952.
- Arezzo A, Passera R, Scozzari G, Verra M and Morino M. Laparoscopy for rectal cancer reduces short-term mortality and morbidity: results of a systematic review and meta-analysis. *Surg Endosc.* 2013; 27(5):1485-1502.
- Conaghan PJ, Maxwell-Armstrong CA, Garrioch MV, Hong L and Acheson AG. Leaving a mark: the frequency and accuracy of tattooing prior to laparoscopic colorectal surgery. *Colorectal disease : the official journal of the Association of Coloproctology of Great Britain and Ireland.* 2011; 13(10):1184-1187.
- van der Pas MH, Meijer S, Hoekstra OS, Riphagen II, de Vet HC, Knol DL, van Grieken NC and Meijerink WJ. Sentinel-lymph-node procedure in colon and rectal cancer: a systematic review and meta-analysis. *Lancet Oncol.* 2011; 12(6):540-550.
- Braat AE, Oosterhuis JW, Moll FC, de Vries JE and Wiggers T. Sentinel node detection after preoperative short-course radiotherapy in rectal carcinoma is not reliable. *Br J Surg.* 2005; 92(12):1533-1538.
- Kim YW, Kim NK, Min BS, Lee KY, Sohn SK and Cho CH. The influence of the number of retrieved lymph nodes on staging and survival in patients with stage II and III rectal cancer undergoing tumor-specific mesorectal excision. *Ann Surg.* 2009; 249(6):965-972.
- Verbeek FP, van der Vorst JR, Tummers QR, Boonstra MC, de Rooij KE, Lowik CW, Valentijn AR, van de Velde CJ, Choi HS, Frangioni JV and Vahrmeijer AL. Near-Infrared Fluorescence Imaging of Both Colorectal Cancer and Ureters Using a Low-Dose Integrin Targeted Probe. *Ann Surg Oncol.* 2014.

CHAPTER 7

Long-term follow-up after near-infrared fluorescence-guided resection of colorectal liver metastases: a retrospective multicenter analysis *Eur J Surg Oncol.* 2017;43(8):1463-1471

HJM HANDGRAAF, LSF BOOGERD, DJ HÖPPENER, A PELOSO, BG SIBINGA MULDER, CES HOOGSTINS, HH HARTGRINK, CJH VAN DE VELDE, JSD MIEOG, RJ SWIJNENBURG, H PUTTER, M MAESTRI, AE BRAAT, JV FRANGIONI, AL VAHRMEIJER

ABSTRACT

BACKGROUND Several studies demonstrated that intraoperative near-infrared fluorescence (NIRF) imaging using indocyanine green (ICG) identifies (sub)capsular colorectal liver metastases (CRLM) missed by other techniques. It is unclear if this results in any survival benefit. This study evaluates long-term follow-up after NIRF-guided resection of CRLM using ICG.

METHODS First, patients undergoing resection of CRLM with or without NIRF imaging were analyzed retrospectively. Perioperative details, liver-specific recurrence-free interval and overall survival were compared. Second, the prognosis of patients in whom additional metastases were identified solely by NIRF was studied.

RESULTS Eighty-six patients underwent resection with NIRF imaging and 87 without. In significantly more patients of the NIRF imaging cohort additional metastases were identified during surgery (25% vs. 13%, $p=0.04$). Tumors identified solely by NIRF imaging were significantly smaller compared to additional metastases identified also by inspection, palpation or intraoperative ultrasound (3.2 ± 1.8 mm vs. 7.4 ± 2.6 mm, $p<0.001$). Liver-specific recurrence-free survival at 4 years was 47% with NIRF imaging and 39% without (hazard ratio at multivariate analysis 0.73, 95%CI 0.42-1.28, $p=0.28$). Overall survival at 4 years was 62% and 59%, respectively ($p=0.79$). No liver recurrences occurred within 3 years follow-up in 52% of patients in whom additional metastases were resected based on only NIRF imaging.

CONCLUSIONS This study suggests that NIRF imaging identifies significantly more and smaller tumors during resection of CRLM, preventing recurrences in a subset of patients. Given its safety profile and low expense, routine use can be considered until tumor targeting fluorescent tracers are clinically available.

INTRODUCTION

Intrahepatic recurrence rates after resection of colorectal liver metastases (CRLM) remain high, despite improvements in preoperative imaging modalities and chemotherapy regimens.[1-3] The majority of patients develop recurrence within 12 months, suggesting that tumors were missed previously.[4] Indeed, current pre- and intraoperative imaging techniques have low sensitivity for subcentimeter lesions in the liver.[5-7] Near-infrared fluorescence (NIRF; wavelengths 700-900 nm) imaging with targeted or non-targeted fluorescent tracers empowers surgeons to improve contrast between structures and aids in differentiating malignant from benign tissue.[8] In general, NIRF imaging has the potential to improve clinical outcomes by improving radical resection rates and visualizing more malignant lesions, but most published studies are proof-of-concept designs. To date, randomized controlled trials have been performed only with 5-aminolevulinic acid (5-ALA) to guide brain surgery.[9] 5-ALA leads to intracellular accumulation of fluorescent protoporphyrin IX (emission peak at 635 nm, outside NIR) in malignant gliomas. Actually, the benefits of 5-ALA were evident in observational studies even before the start of a randomized controlled trial. Fluorescence imaging of malignant glioma had 85% sensitivity and 100% specificity, overall survival (OS) strongly correlated with residual intraoperative fluorescence, and no safety issues were recorded.[10, 11] Not unexpectedly, the randomized study had to be terminated prematurely due to 20% higher progression-free survival in the 5-ALA arm at 6 months.

Parallels can be drawn between 5-ALA for glioma surgery and indocyanine green (ICG, emission peak at 820 nm) for resection of CRLM, even though the diseases and consequences are different. NIRF imaging using ICG identifies (sub) capsular micrometastases missed by conventional modalities in up to 17% of CRLM patients.[12-17] In addition, screening of resection margins can detect residual tumor, enabling complete removal of all tumor tissue (RO resection).[17, 18] Intravenous administration of ICG is safe; adverse reactions are reported in less than 1 in 40,000 patients.[19] ICG is widely used for clinical applications (e.g. to test liver function prior to major liver surgery).

It seems unjustifiable to randomize patients into a control arm without NIRF imaging when previous studies have already shown that NIRF imaging identifies additional tumors in the context of an excellent safety profile. However, before NIRF imaging can be accepted and implemented in routine clinical practice, the optical imaging community must show long-term benefits, while also addressing safety and cost-effectiveness.[20] A key unanswered question is whether the (micro)metastases additionally identified by NIRF are indicative of otherwise undetectable, widespread metastases in the liver or if patients are in fact cured by resecting these lesions. This multicenter study is the first to report long-term follow-up after NIRF-guided resection of CRLM. In addition, perioperative data and

post-operative outcomes were compared with a cohort of patients that underwent resection of CRLM without intraoperative NIRF imaging.

PATIENTS AND METHODS

Patients

All patients undergoing resection of CRLM with or without NIRF imaging at Leiden University Medical Center (LUMC, Leiden, the Netherlands) between January 2010 and June 2016 were included and termed ‘analysis 1’. Patients received ICG and underwent NIRF imaging only if a NIRF imaging system and operator were available, if patients were willing to participate and if none of the exclusion criteria was met. Exclusion criteria consisted of contraindications for ICG: eGFR < 55; pregnancy; breastfeeding; hyperthyroidism; or an allergy to iodine, shellfish, or ICG. Patients with an eGFR < 55 or hyperthyroidism that underwent resection of CRLM without NIRF imaging were excluded to prevent selection bias. The local institutional review board approved the studies. All patients receiving ICG provided informed consent. Patients with a prior history of metastatic disease were excluded from analysis. Demographics, patient characteristics, Fong’s clinical risk score for predicting recurrence after hepatic resection of CRLM [21], perioperative and long-term follow-up data were collected. Patients were divided into 2 cohorts: a control cohort that underwent standard resection and an experimental cohorts that underwent NIRF-guided resection.

Intraoperative NIRF imaging (analysis 1)

Patients in the NIRF cohorts received a dose of 10 or 20 mg ICG 1 or 2 days prior to surgery. Four different NIRF imaging systems were used: Mini-FLARE® (Frangioni Laboratory, Harvard Medical School, Boston, MA, U.S., see Figure 1) [22], Kit-FLARE® (FLARE Foundation, defunct, previously Wayland, U.S.), Artemis (Quest Innovations BV, Middenmeer, the Netherlands) [23], and Storz HD laparoscope (KARL STORZ GmbH & Co. KGm, Tuttlingen, Germany).

Preoperative workup and surgical procedure (analysis 1)

All patients underwent computed tomography (CT) to detect hepatic and/or extrahepatic metastases. In selected cases, when deemed necessary by the medical team, magnetic resonance imaging (MRI) or positron emission tomography (PET) was performed. The protocol for imaging of CRLM was updated several times and new scanners were acquired by the hospitals during the period 2010-2016. Since 2015 Primovist-enhanced and diffusion weighted MRI was performed. Chemotherapy treatment was divided into 3 categories: (1) no chemotherapy, (2)

neoadjuvant chemotherapy was defined as chemotherapy treatment specifically aimed to decrease hepatic tumor load prior to the planned liver surgery and (3) adjuvant chemotherapy as chemotherapy treatment with curative intent aimed at reducing recurrence rate of CRLM following liver resection.

Surgery started with inspection and palpation (the latter during open surgery only), followed by intraoperative ultrasound (IOUS) performed by a dedicated radiologist. Subsequently, the accessible liver surface of patients in the experimental cohorts was screened by NIRF imaging. Note that with the currently available systems, only the accessible surface of the liver was interrogated. Metastases were considered additionally identified if they were not detected by any type of preoperative imaging. They were classified by their method of detection: standard (inspection, palpation and/or IOUS) or NIRF imaging alone. Intraoperative radiofrequency ablation (RFA) was – if deemed necessary – performed under IOUS-guidance by the interventional radiologist. Hemihepatectomy was defined by resection of liver segments 2, 3 and 4 or 5, 6, 7 and 8.

Perioperative details, including length of surgery, resected volume, reoperation rates and complications, were analyzed. The tumor volume was estimated by calculating the spherical volume using the maximum diameter of the resected tumor. Histopathological examination was considered the golden standard. When no tissue was obtained, e.g. if RFA was performed, the diagnosis was based on imaging.

Follow-up (Analysis 1)

A CT was performed with 4 months intervals in the first 2 years after surgery. If intraoperative RFA was performed an additional CT was performed directly after surgery. In case patients were disease-free at 2 years follow-up, assessment by CT was done each 6 months for an additional period of 3 years, after which the follow-up ended in case of no recurrence. Additional MRI and PET were used at the discretion of the specialist. The diagnosis of recurrence and/or progression was based on available radiologic imaging. Recurrences were divided into hepatic and extrahepatic recurrence.

Survival after resection of metastases identified solely by NIRF imaging (Analysis 2)

An additional cohort, termed ‘analysis 2’, was created to answer the question whether the (micro)metastases additionally identified by NIRF are indicative of otherwise undetectable, widespread metastases in the liver or if patients are in fact cured by resecting these lesions. Only patients in whom additional lesions were identified solely by NIRF imaging were included. To increase statistical power, also patients who underwent NIRF-guided resection of CRLM at the San

Matteo General Hospital (SMGH, Pavia, Italy) between August 2011 and June 2012 were included. Due to significant differences in baseline, adjuvant treatment protocols and follow-up, these patients could not be included in analysis 1. At the SMGH patients received a dose of 0.5 mg/kg ICG and the PhotoDynamic Eye (PDE, Hamamatsu Photonics K.K., Hamamatsu-city, Japan) was used. SMGH patients received an ultrasound at 3 months and a CT at 6 months follow-up. Subsequently, CT was performed annually for up to three years.

Statistical analyses

Baseline characteristics between cohorts were compared using an unpaired samples T-test for parametric continuous data, Mann-Whitney U-test for non-parametric continuous data and a Pearson's Chi-square test for dichotomous or categorical variables. Baseline characteristics of patients treated with fluorescence imaging at the LUMC and SMGH were compared with the cohort of patients treated without fluorescence imaging at the LUMC. Parametric continuous data was reported as mean \pm standard deviation (SD), non-parametric continuous data as median with range, and dichotomous or categorical variables as percentage. Liver-specific recurrence-free interval was considered the main outcome of this study as NIRF imaging using ICG can only be used to identify metastases located in the liver. All interval and survival curves were estimated using the Kaplan-Meier method. Long-term results were analyzed until only 25% of all cases were left. Multivariate regression was performed using to the Cox proportional hazards model. All statistical analyses were performed using the Statistical Package for the Social Sciences (SPSS® version 23; IBM, IL, USA). A p-value of <0.05 was considered statistically significant.

RESULTS

Patient demographics (Analysis 1 & 2)

A total of 209 patients was analyzed (Figure 2) of which 36 were excluded either due to a history of metastatic disease (n=7), no resection of metastases (n=15) or EGFR <55 (n=8; i.e. exclusion criterion for ICG administration). For 6 patients at the SMGH no follow-up was available. These patients were consequently also excluded. Baseline characteristics are presented in Table 1. Sixty-seven patients were included in the LUMC experimental cohort and 87 in the LUMC control cohort. The Mini-FLARE® was used in 43 patients, Kit-FLARE® in 1 patient, Artemis in 13 patients, and Storz HD laparoscope in 10 patients. No significant differences in baseline characteristics were observed between the LUMC experimental cohort and LUMC control cohort. Intraoperative results of some of the included patients have been reported previously.[15-17, 24] At the LUMC, adjuvant chemotherapy was no longer

standard-of-care since 2013, resulting in a significant difference between the LUMC and SMGH experimental cohorts. Furthermore, patients from SMGH had more comorbidity, including COPD, diabetes and cardiovascular events, resulting in a significantly higher ASA score.

Perioperative details (Analysis 1)

The LUMC experimental cohort was compared with the control cohort. Results are shown in Table 2. No significant differences in volume of resected tissue, time of procedure and complications were seen.

Tumor characteristics (Analysis 1)

Tumors resected in the LUMC experimental cohort were compared with those in the control cohort (Figure 3). The median number of preoperatively identified metastases did not differ significantly (1 [range 1-5] vs. 2 [1-7], respectively; $p=0.48$). The median number of resected or ablated tumors also did not differ significantly (2 [1-10] vs. 2 [1-7]; $p=0.81$). However, the percentage of patients in whom additional lesions were identified during surgery was significantly higher in the LUMC experimental cohort (25% vs. 13%; $p=0.04$). The difference was the result of lesions identified by NIRF only; there was no significant difference when using standard techniques only (15% vs. 13%; $p=0.68$). In 3% (n=2) additional metastases were identified by standard techniques, but also other metastases by NIRF imaging only. The mean size of additional tumors identified by NIRF imaging only was significantly smaller than the size of tumors identified by standard techniques (3.2 ± 1.8 mm vs. 7.4 ± 2.6 mm; $p<0.001$). Tumors in the LUMC experimental cohort were resected radically (RO resection) in 83% of cases vs. 79% of tumors in the control cohort ($p=0.41$). Overall, sensitivity of NIRF imaging was 83%. Sensitivity of only superficial (i.e. < 8 mm subcapsular) CRLM was 100%. Intraoperative identification of additional CRLM was not significantly correlated with the interval between last preoperative imaging and surgery.

Long-term follow-up results (Analysis 1)

The follow-up of the LUMC experimental cohort was compared with the control cohort (Figure 4). Median follow-up was 46 (range 4-80) and 43 (5-79) months, respectively. In the experimental cohort 47% did not have a recurrence in the liver at 4 years follow-up, compared to 39% in the control cohort ($p=0.40$). Overall survival at 4 years was 62% and 59%, respectively ($p=0.79$). A Cox proportional hazards regression analysis was performed, including use of NIRF imaging, age, gender, chemotherapy, ASA score, surgery type, and Fong's clinical risk score (0-4; CEA >200 ng/ml was excluded due to a high number of missing values). The

hazard ratio for liver-specific recurrence when using NIRF imaging was 0.73 (95% confidence interval [CI] 0.42-1.28; $p=0.28$). The hazard ratio for overall survival was 0.94 (95% CI 0.50-1.76, $p=0.85$).

Survival after resection of metastases identified solely by NIRF imaging (Analysis 2)

Additional subcapsular CRLM were visualized by fluorescence imaging only in 24% (21/86) of patients who underwent NIRF-guided resection of CRLM either at the LUMC ($n=9$) or the SMGH ($n=12$). At 3 years follow-up 52% of those patients did not have recurrent disease in the liver; 48% did not have any recurrence at all.

DISCUSSION

The only option to cure patients with CRLM is a complete resection of all lesions. Yet, intrahepatic recurrence rates after surgery using only white light remain high. [1-3] One of the main problems is the fact that subcentimeter lesions cannot be detected easily, neither before nor during surgery.[5-7, 17] Even with state-of-the-art scanners and up-to-date protocols, metastases are still being missed, as experienced in this study. Moreover, metastases may arise and/or grow in the period between preoperative imaging and surgery. Novel techniques for better intraoperative distinction between malignant and benign tissue are urgently needed. This is the first study that presents long-term follow-up after NIRF-guided resection of CRLM, although the non-randomized design limits its level of evidence. NIRF imaging of CRLM using ICG was safe and time-efficient, while significantly more and smaller tumors were identified during surgery. Removal of metastases solely identified by NIRF appears helpful; 52% of patients did not develop liver recurrence after resection of vital tumor cells. These additional metastases would – if not resected or treated by chemotherapy – almost certainly result in recurrence of liver metastases. In the Netherlands, neoadjuvant chemotherapy is not standard-of-care, since there is no clear survival benefit, while there are considerable side-effects.[25]

At the LUMC additional tumors were identified in 13% of all patients. Assuming that 52% of these patients (i.e. 7%) do not develop a recurrence, the number-needed-to-treat would be 14. ICG is inexpensive; a vial of 25 mg costs approximately \$85 USD. Leaving the costs of purchasing a fluorescence imaging system aside, 14 doses of ICG cost \$1190 USD, while treating a recurrence of CRLM will cost a plurality. Several NIRF imaging systems are already available for clinical use.[26]

This study failed however to show substantial evidence that the addition of NIRF imaging positively influences clinical outcome measures including recurrence-free interval and OS. A study powered to show a significant difference of 7% would require a total of >1,500 patients. This means that the current study is severely underpowered to show such a difference.

Although significantly more tumors were identified in the LUMC experimental cohort, patients still developed recurrences, of which the majority within the first year. This means that tumors were being missed by NIRF imaging, potentially due to the fact that not the entire liver surface was interrogated. During surgery it proved to be difficult to reach the posterior segments of the liver due to either the size of the camera head or because the liver was not always fully mobilized off the diaphragm. A smaller, hand-held camera head, or the combined use of open and minimally-invasive imaging systems, could increase the percentage of the liver surface that can be imaged. Furthermore, although tumors additionally identified by NIRF imaging are significantly smaller, submillimeter tumors might still be missed. Finally, tumors at a depth of more than 8 mm from the liver surface are currently not identifiable by NIRF imaging.[12] The technique can therefore only be applied in combination with IOUS, as done in this study.

No significant difference was shown in radical resection rates of both LUMC cohorts. Especially during open surgery, the fluorescence imaging systems were mostly used during screening of the liver surface and not during resection. Of note, no attempt was made to compare the performance among imaging systems, and it is possible that variation in detectability exist. All open space imaging systems, however, provided surgeons simultaneously with real-time color, NIRF and color-NIR merge images. The Storz HD laparoscope only had a color and NIRF modus. Switching was done using a foot pedal.

ICG can also be applied in combination with 5-ALA for the detection of CRLM.[14] Although combined use improved specificity, 5-ALA resulted in adverse events, including vomiting and serum AST elevation, in 14% of all patients. Furthermore, the emitted fluorescence of 5-ALA (peak at 635 nm) is subject to higher absorbance and penetrates only approximately 2 mm tissue. NIRF imaging with ICG for the detection of superficial CRLM is sensitive, but cannot detect extrahepatic metastases. Conjugation of fluorophores to targeting moieties, such as antibodies, can enable detection of all tumor lesions, regardless of location. This method was explored in several clinical trials, including breast, ovarian and head and neck cancer patients.[27-29] For CRLM a clinical trial with SGM-101, which targets CEA is currently ongoing (Netherlands Trial Register number NTR5673). Unfortunately, clinical translation of targeted fluorescent tracers is expensive and time-consuming and requires specific expertise. Until hurdles associated with clinical translation of novel tracers are overcome, ICG can be used as a safe, inexpensive and clinically available alternative. Moreover, as SGM-101 is fluorescent at approximately 700 nm, it could be simultaneously applied with ICG. Several NIRF imaging systems, including the Artemis and FLARE® systems, can perform dual-wavelength imaging.

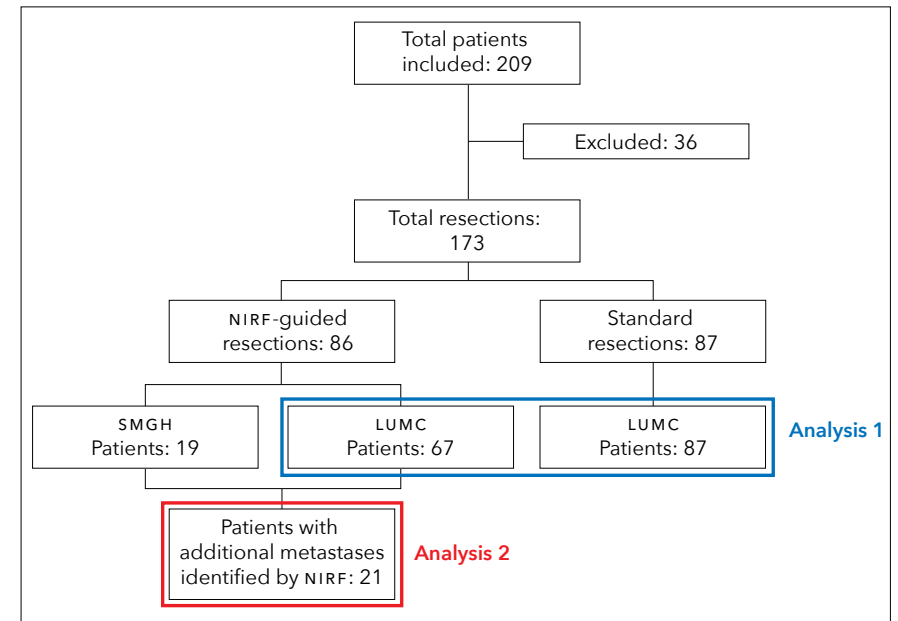
CONCLUSION

In conclusion, this study suggests that NIRF imaging during resection of CRLM identifies significantly more and smaller tumors, preventing recurrences in a subset of patients. Given its safety profile and low expense, routine use can be considered until tumor targeting fluorescent tracers are available for clinical use.

Figure 1 A liver metastasis identified by NIRF imaging only (white arrow) in a patient that received 10 mg indocyanine green one day prior to surgery. Tumors that were already identified by preoperative imaging (dashed arrow) can be demarcated by fluorescence imaging. Imaging was performed using the Mini-FLARE®.

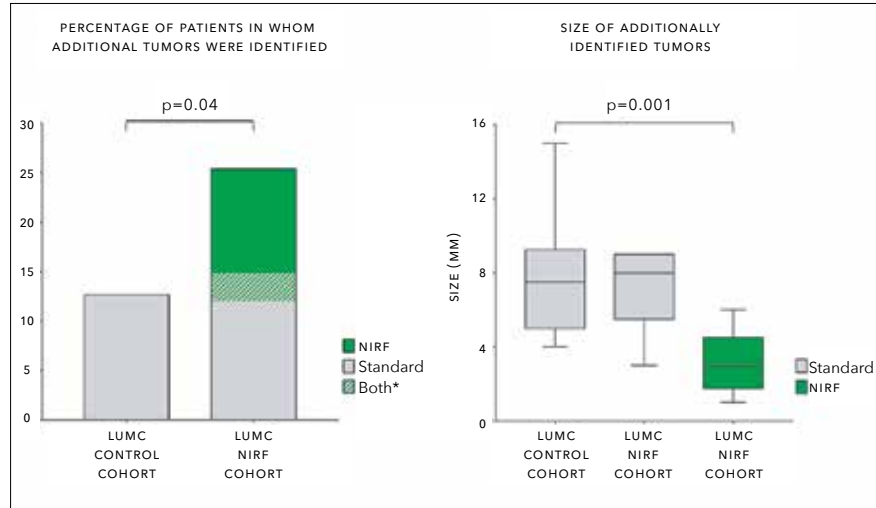


Figure 2 Patient selection.



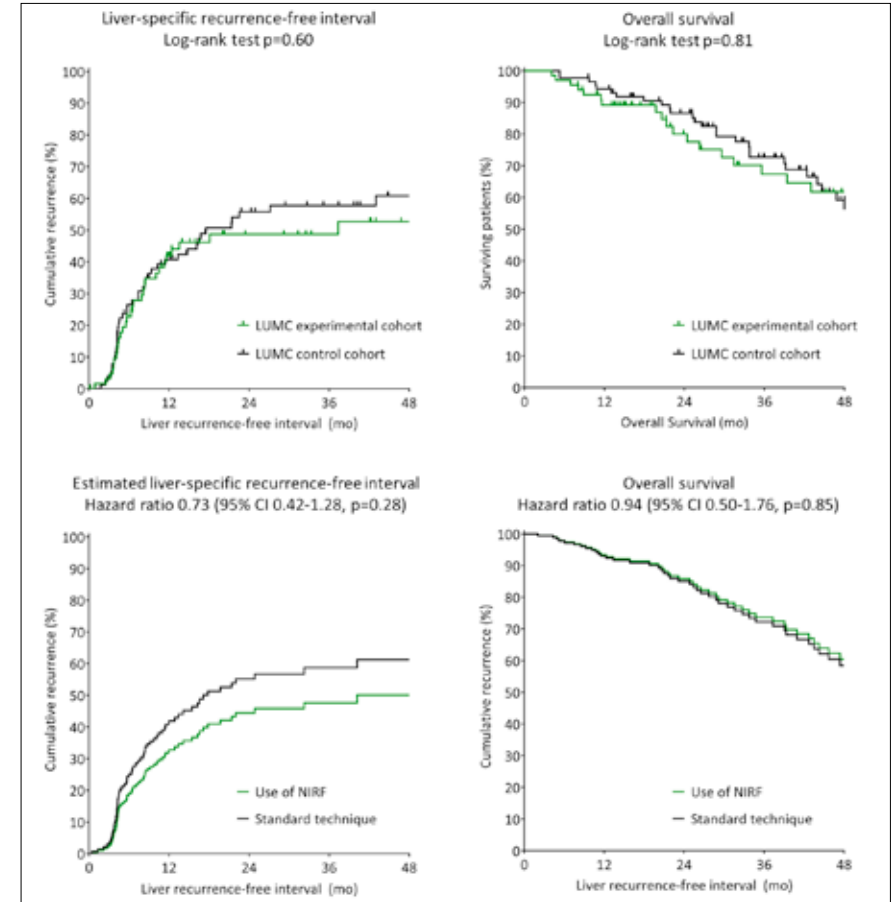
NIRF: near-infrared fluorescence; LUMC: Leiden University Medical Center; SMGH: San Matteo General Hospital. Analysis 1 assesses differences in perioperative details and survival between patients from LUMC who underwent surgery with or without guidance by near-infrared fluorescence. Analysis 2 includes only patients in whom additional metastases were identified solely by near-infrared fluorescence imaging.

Figure 3 Additionally identified colorectal liver metastases. The percentage of patients in whom additional metastases were identified during surgery was significantly higher in the LUMC experimental cohort compared to the LUMC control cohort. Tumors identified solely by near-infrared fluorescence imaging were significantly smaller compared to additional metastases identified using standard techniques.



*) In 3% (n=2) additional metastases were identified with standard techniques, but NIRF imaging identified even more unknown metastases.

Figure 4 (Estimated) liver-specific recurrence-free interval and overall survival.



LUMC: Leiden University Medical Center; SMGH: San Matteo General Hospital; NIRF: near-infrared fluorescence.

Table 1 Baseline characteristics.

	Cohorts for analysis 1		Comparison (p-value)		Additional patients for analysis 2
	LUMC Control % (n=87)	LUMC NIRF % (n=67)	LUMC Control vs NIRF (n=154)	SMGH NIRF % (n=19)	
Gender			0.33		
Female	36 (31/87)	43 (29/67)			42 (8/19)
Male	64 (56/87)	57 (38/67)			58 (11/19)
Age at surgery, mean ± SD (n)	63 ± 9.4 (87)	62 ± 9.2 (67)	0.55		61 ± 9.3 (19)
Chemotherapy			0.42		
No chemotherapy	28 (24/87)	36 (24/67)			0 (0/19)
Neoadjuvant	40 (35/87)	40 (27/67)			26 (5/19)
Adjuvant	32 (28/87)	24 (16/67)			74 (14/19)
Location of primary tumor					
Colon	33 (28/86)	40 (24/67)			42 (8/19)
Sigmoid	42 (36/86)	28 (19/67)			37 (7/19)
Rectum	26 (22/86)	36 (24/67)			21 (4/19)
Latest type of preoperative imaging			0.09		
CT	70 (61/87)	61 (41/67)			100 (100/19)
PET-CT	7 (6/87)	1 (1/67)			0 (0/19)
MRI	13 (11/87)	15 (10/67)			0 (0/19)
Primovist-enhanced MRI	10 (9/87)	22 (15/67)			0 (0/19)
Days between imaging and surgery, mean ± SD (n)	34 ± 18 (87)	38 ± 24 (67)	0.24		NA
ASA score			0.52		
I	12 (10/86)	9 (6/67)			0 (0/19)
II	80 (69/86)	78 (52/67)			53 (10/19)
III	8 (7/86)	13 (9/67)			47 (9/19)

Type of surgery	0.06			
Laparotomy	94 (82/87)	85 (57/67)		100 (19/19)
Laparoscopy	5 (4/87)	15 (10/67)		0 (0/19)
Conversion to laparotomy	1 (1/87)	0 (0/67)		0 (0/19)
Hemihepatectomy	16 (14/87)	10 (7/67)	0.31	32 (6/19)
RFA	28 (24/87)	24 (16/67)	0.60	5 (1/19)
Node positive primary*	51 (44/86)	56 (36/64)	0.54	68 (13/19)
Disease-free interval < 12 months*	76 (66/87)	78 (52/67)	0.80	68 (13/19)
More than 1 hepatic tumor*	59 (51/87)	49 (33/67)	0.25	42 (8/19)
Largest hepatic tumor > 5cm*	14 (12/87)	9 (6/67)	0.35	21 (4/19)
Preoperative CEA > 200ng/ml*	3 (2/72)	2 (1/55)	0.72	11 (2/19)
Synchronous metastases	53 (46/87)	43 (29/67)	0.24	32 (6/19)
No. of CRLM on CT/MRI, median; range (n)	1; 1 - 5 (67)	2; 1 - 7 (87)	0.48	1; 1 - 4 (19)
Comorbidities			0.25	
COPD	5 (4/87)	1 (1/67)		26 (5/19)
DVT or PE	2 (2/87)	3 (2/67)		11 (2/19)
CVE	9 (8/87)	1 (1/67)		42 (8/19)
DM	10 (9/87)	7 (5/67)		74 (14/19)
BMI, mean ± SD (n)	26 ± 3.8 (85)	26 ± 4.0 (67)	0.80	25 ± 3.9 (19)

NIRF: near-infrared fluorescence; LUMC: Leiden University Medical Center; SMGH: San Matteo General Hospital; SD: standard deviation; NA: not available; CRLM: colorectal liver metastases; RFA: radiofrequency ablation; COPD: chronic obstructive pulmonary disease; DM: diabetes mellitus; DVT: deep venous thrombosis; PE: pulmonary embolism; CVE: cardiovascular event; BMI: body mass index. *) Individual Fong criteria

Table 2 Perioperative details.

	LUMC Control (n=87) mean ± SD (n)	LUMC Experi- mental (n=67) mean ± SD (n)	p-value
Total resected volume (cm ³) / number of vital tumors resected			
Other*	62 ± 3.8 (66)	57 ± 4.5 (54)	0.76
Hemihepatectomy*	637 ± 2.4 (12)	657 ± 2.7 (7)	0.95
Volume of healthy tissue resected per tumor (cm ³)**			
Other*	26 ± 4.9 (128)	24 ± 7.5 (110)	0.79
Hemihepatectomy*	685 ± 2.2 (16)	596 ± 1.9 (11)	0.62
Length of surgery (min)	180 ± 53 (87)	183 ± 56 (67)	0.69
Estimated blood loss (ml)*	403 ± 2.8 (63)	416 ± 3.3 (48)	0.89
Duration of hospital stay (days) - median ; range (n)	6 ; 1 - 48 (87)	6 ; 4 - 87 (67)	0.99
Reoperation - % (n/n)	7 (6/87)	7 (5/67)	0.89
90-day mortality - % (n/n)	0 (0/87)	0 (0/67)	1.00
Complications (Clavien-Dindo) - % (n/n)			
Grade III	8 (7/87)	7 (5/67)	
Grade IV	5 (4/87)	7 (5/67)	

*) Logarithmic transformation was used in the analysis of the data, **) For each resected tumor (vital or non-vital) the spherical volume of the tumor diameter was subtracted from the estimated specimen volume.

REFERENCES

- Wei AC, Greig PD, Grant D, Taylor B, Langer B and Gallinger S. Survival after hepatic resection for colorectal metastases: a 10-year experience. *Ann Surg Oncol.* 2006; 13(5):668-676.
- Abdalla EK, Vauthey JN, Ellis LM, Ellis V, Pollock R, Broglio KR, Hess K and Curley SA. Recurrence and outcomes following hepatic resection, radiofrequency ablation, and combined resection/ablation for colorectal liver metastases. *Ann Surg.* 2004; 239(6):818-825; discussion 825-817.
- Rees M, Tekkis PP, Welsh FK, O'Rourke T and John TG. Evaluation of long-term survival after hepatic resection for metastatic colorectal cancer: a multifactorial model of 929 patients. *Ann Surg.* 2008; 247(1):125-135.
- Karanja ND, Lordan JT, Fawcett WJ, Quiney N and Worthington TR. Survival and recurrence after neo-adjuvant chemotherapy and liver resection for colorectal metastases: a ten year study. *Eur J Surg Oncol.* 2009; 35(8):838-843.
- Frankel TL, Gian RK and Jarnagin WR. Preoperative imaging for hepatic resection of colorectal cancer metastasis. *J Gastrointest Oncol.* 2012; 3(1):11-18.
- Khalil H, Patterson SA and Panicek DM. Hepatic lesions deemed too small to characterize at CT: prevalence and importance in women with breast cancer. *Radiology.* 2005; 235(3):872-878.
- Holzappel K, Reiser-Erkan C, Fingerle AA, Erkan M, Eiber MJ, Rummeny EJ, Friess H, Kleeff J and Gaa J. Comparison of diffusion-weighted MR imaging and multidetector-row CT in the detection of liver metastases in patients operated for pancreatic cancer. *Abdom Imaging.* 2011; 36(2):179-184.
- Vahrmeijer AL, Hutteman M, van der Vorst JR, van de Velde CJ and Frangioni JV. Image-guided cancer surgery using near-infrared fluorescence. *Nat Rev Clin Oncol.* 2013; 10(9):507-518.
- Stummer W, Pichlmeier U, Meinel T, Wiestler OD, Zanella F, Reulen HJ and Group AL-GS. Fluorescence-guided surgery with 5-aminolevulinic acid for resection of malignant glioma: a randomised controlled multicentre phase III trial. *Lancet Oncol.* 2006; 7(5):392-401.
- Stummer W, Novotny A, Stepp H, Goetz C, Bise K and Reulen HJ. Fluorescence-guided resection of glioblastoma multiforme by using 5-aminolevulinic acid-induced porphyrins: a prospective study in 52 consecutive patients. *J Neurosurg.* 2000; 93(6):1003-1013.
- Stummer W, Stocker S, Wagner S, Stepp H, Fritsch C, Goetz C, Goetz AE, Kiefmann R and Reulen HJ. Intraoperative detection of malignant gliomas by 5-aminolevulinic acid-induced porphyrin fluorescence. *Neurosurgery.* 1998; 42(3):518-525; discussion 525-516.
- Ishizawa T, Fukushima N, Shibahara J, Masuda K, Tamura S, Aoki T, Hasegawa K, Beck Y, Fukayama M and Kokudo N. Real-time identification of liver cancers by using indocyanine green fluorescent imaging. *Cancer.* 2009; 115(11):2491-2504.
- Ishizuka M, Kubota K, Kita J, Shimoda M, Kato M and Sawada T. Intraoperative observation using a fluorescence imaging instrument during hepatic resection for liver metastasis from colorectal cancer. *Hepatogastroenterology.* 2012; 59(113):90-92.
- Kaibori M, Matsui K, Ishizaki M, Iida H, Okumura T, Sakaguchi T, Inoue K, Ikeura T, Asano H and Kon M. Intraoperative Detection of Superficial Liver Tumors by Fluorescence Imaging Using Indocyanine Green and 5-aminolevulinic Acid. *Anticancer Res.* 2016; 36(4):1841-1849.
- van der Vorst JR, Schaafsma BE, Hutteman M, Verbeek FP, Liefers GJ, Hartgrink HH, Smit VT, Lowik CW, van de Velde CJ, Frangioni JV and Vahrmeijer AL. Near-infrared fluorescence-guided resection of colorectal liver metastases. *Cancer.* 2013; 119(18):3411-3418.
- Peloso A, Franchi E, Canepa MC, Barbieri L, Briani L, Ferrario J, Bianco C, Quaretti P, Brugnattelli S, Dionigi P and Maestri M. Combined use of intraoperative ultrasound and indocyanine green fluorescence imaging to detect liver metastases from colorectal cancer. *HPB (Oxford).* 2013; 15(12):928-934.
- Boogerd LS, Handgraaf HJ, Lam HD, Huurman VA, Farina-Sarasqueta A, Frangioni JV, van de Velde CJ, Braat AE and Vahrmeijer AL. Laparoscopic detection and resection of occult liver tumors of multiple cancer types using real-time near-infrared fluorescence guidance. *Surgical endoscopy.* 2016.
- Barabino G, Porcheron J, Cottier M, Cuilleron M, Coutard JG, Berger M, Molliex S, Beauchesne B, Phelip JM, Grichine A and Coll JL. Improving Surgical Resection of Metastatic Liver Tumors With Near-Infrared Optical-Guided Fluorescence Imaging. *Surgical innovation.* 2016; 23(4):354-359.
- Benya R, Quintana J and Brundage B. Adverse reactions to indocyanine green: a case report and a review of the literature. *Cathet Cardiovasc Diagn.* 1989; 17(4):231-233.
- Rosenthal EL, Warram JM, de Boer E, Basilion JP, Biel MA, Bogoyo M, Bouvet M, Brigman BE, Colson YL, DeMeester SR, Gurtner GC, Ishizawa T, Jacobs PM, Keereweer S, Liao JC, Nguyen QT, et al. Successful Translation of Fluorescence Navigation During Oncologic Surgery: A Consensus Report. *J Nucl Med.* 2016; 57(1):144-150.
- Fong Y, Fortner J, Sun RL, Brennan MF and Blumgart LH. Clinical score for predicting recurrence after hepatic resection for metastatic colorectal cancer: analysis of 1001 consecutive cases. *Ann Surg.* 1999; 230(3):309-318; discussion 318-321.
- Troyan SL, Kianzad V, Gibbs-Strauss SL, Gioux S, Matsui A, Oketokoun R, Ngo L, Khamene A, Azar F and Frangioni JV. The FLARE intraoperative

- near-infrared fluorescence imaging system: a first-in-human clinical trial in breast cancer sentinel lymph node mapping. *Ann Surg Oncol*. 2009; 16(10):2943-2952.
- 23 van Driel PB, van de Giessen M, Boonstra MC, Snoeks TJ, Keereweer S, Oliveira S, van de Velde CJ, Lelieveldt BP, Vahrmeijer AL, Lowik CW and Dijkstra J. Characterization and evaluation of the artemis camera for fluorescence-guided cancer surgery. *Mol Imaging Biol*. 2015; 17(3):413-423.
- 24 Boogerd LS, Handgraaf HJ, Lam HD, Braat AE, Baranski AG, Swijnenburg RJ, Frangioni JV, Vahrmeijer AL and Ringers J. Application of near-infrared fluorescence imaging during modified associating liver partition and portal vein ligation for staged hepatectomy. *Surgery*. 2016; 159(5):1481-1482.
- 25 Nordlinger B, Sorbye H, Glimelius B, Poston GJ, Schlag PM, Rougier P, Bechstein WO, Primrose JN, Walpole ET, Finch-Jones M, Jaeck D, Mirza D, Parks RW, Mauer M, Tanis E, Van Cutsem E, et al. Perioperative FOLFOX4 chemotherapy and surgery versus surgery alone for resectable liver metastases from colorectal cancer (EORTC 40983): long-term results of a randomised, controlled, phase 3 trial. *Lancet Oncol*. 2013; 14(12):1208-1215.
- 26 Handgraaf HJ, Verbeek FP, Tummers QR, Boogerd LS, van de Velde CJ, Vahrmeijer AL and Gaarenstroom KN. Real-time near-infrared fluorescence guided surgery in gynecologic oncology: a review of the current state of the art. *Gynecol Oncol*. 2014; 135(3):606-613.
- 27 Hoogstins CE, Tummers QR, Gaarenstroom KN, de Kroon CD, Trimbos JB, Bosse T, Smit VT, Vuyk J, van de Velde CJ, Cohen AF, Low PS, Burggraaf J and Vahrmeijer AL. A Novel Tumor-Specific Agent for Intraoperative Near-Infrared Fluorescence Imaging: A Translational Study in Healthy Volunteers and Patients with Ovarian Cancer. *Clin Cancer Res*. 2016; 22(12):2929-2938.
- 28 Rosenthal EL, Warram JM, de Boer E, Chung TK, Korb ML, Brandwein-Gensler M, Strong TV, Schmalbach CE, Morlandt AB, Agarwal G, Hartman YE, Carroll WR, Richman JS, Clemons LK, Nabell LM and Zinn KR. Safety and Tumor Specificity of Cetuximab-IRDye800 for Surgical Navigation in Head and Neck Cancer. *Clin Cancer Res*. 2015; 21(16):3658-3666.
- 29 Lamberts LE, Koch M, de Jong JS, Adams A, Glatz J, Kranendonk ME, Terwisscha van Scheltinga AG, Jansen L, de Vries J, Lub-de Hooge MN, Schroder CP, Jorritsma-Smit A, Linssen MD, de Boer E, van der Vegt B, Nagengast WB, et al. Tumor-specific uptake of fluorescent bevacizumab-IRDye800CW microdosing in patients with primary breast cancer: a phase I feasibility study. *Clin Cancer Res*. 2016.

CHAPTER 8

Staging laparoscopy with ultrasound and near-infrared fluorescence imaging to detect occult metastases in pancreatic and periampullary cancer *Submitted*

HJM HANDGRAAF*, BG SIBINGA MULDER*, S SHAHBAZI FESHTALI, LSF BOOGERD, MJM VAN DER VALK, A FARIÑA SARASQUETA, RJ SWIJNENBURG, BA BONSING, AL VAHRMEIJER, JSD MIEOG (*shared first authorship)

ABSTRACT

INTRODUCTION Up to 38% of pancreatic and periampullary cancer patients undergoing curative intended surgery turn out to have incurable disease. Therefore, staging laparoscopy (SL) prior to laparotomy is advised to spare patients the morbidity, inconvenience and expense of futile major surgery. The aim of this study was to assess the added value of SL with laparoscopic ultrasonography (LUS) and laparoscopic near-infrared fluorescence imaging (LFI).

METHODS All patients undergoing curative intended surgery of pancreatic or periampullary cancer were included prospectively in this single arm study. Patients received an intravenous infusion of 10 mg indocyanine green (ICG) one or two days prior to surgery to allow LFI. Suspect lesions were analyzed via biopsy or resection. Follow-up visits after surgery occurred every three months.

RESULTS A total of 25 patients were included. Suspect lesions were identified in 7 patients: liver metastases (n=2; identified by inspection, LUS, and LFI), peritoneal metastases (n=1; identified by inspection only), and benign lesions (n=4; identified by inspection or LUS). Quality of LFI was good in 67% (10/15) of patients dosed one day and 89% (8/9) dosed two days prior to surgery. Following SL the primary tumor was resected in 20 patients. Two patients (10%) developed metastases within 3 months after resection.

CONCLUSIONS Despite current preoperative imaging modalities metastases are still identified during surgery. The current study shows limited added value of LUS and LFI during SL of pancreatic or periampullary cancer patients.

INTRODUCTION

Pancreatic and periampullary cancers are dreadful diseases with a poor prognosis. At time of diagnosis only 10% to 20% of pancreatic cancer patients is eligible for curative intended surgery, but during explorative laparotomy up to 38% of those patients turn out to have distant metastases or an unresectable primary tumor [1]. Yet, even after resection with curative intent, 5-year survival rates are still disappointingly low between 6.8% and 32% [2]. Up to 70% of patients with resectable pancreatic cancer suffer from distant metastases, of which the majority occurs within 6 months after surgery [3]. These metastases may have been present during surgery without being detected. Preoperative imaging modalities, including computed tomography (CT) and magnetic resonance imaging (MRI), have low sensitivity for subcentimeter peritoneal and liver metastases [4]. Especially superficial metastases are difficult to detect. In a disease with such a dismal prognosis, it is important to spare patients with incurable disease the morbidity, inconvenience and expense of futile major surgery.

The Society of American Gastrointestinal and Endoscopic Surgeons (SAGES) advocates that staging laparoscopy (SL) should be considered in selected patients [5]. Compared to explorative laparotomy, SL results in less postoperative pain, a shorter hospital stay and chemo- and/or radiotherapy can be administered more often and sooner to patients [6]. The chance of an unnecessary laparotomy in patients who appear eligible for curative resection based on preoperative imaging decreases from 40% to 17% by performing SL [7]. Moreover, metal stents make biliary anastomosis abundant and other palliative bypass surgery can be done laparoscopically.

The yield of SL may be amplified by adding laparoscopic ultrasonography (LUS) and laparoscopic near-infrared fluorescence imaging (LFI). LUS enables identification of metastases located deep in the liver and, additionally, vascular involvement of the primary tumor can be assessed [8]. Open-space fluorescence imaging or LFI using indocyanine green (ICG) is a safe and easy method to identify microscopic (sub)capsular liver metastases not yet visible by any other means [9]. Yokoyama et al. previously demonstrated that open space fluorescence imaging is able to identify additional micrometastases in the liver in 16% of the patients with pancreatic cancer [10].

Although selection of patients for SL is being advised, there is no scientific support, nor a consensus on which selection criteria should be used [11, 12]. The current study combines SL with LUS and LFI and aims to determine the added value of these three modalities in all patients with pancreatic and periampullary cancer before undergoing surgery with curative intent.

METHODS

Patients

The clinical study protocol was approved by the local medical ethics review board and conducted in concordance with the Helsinki Declaration of 1975 (as amended in Tokyo, Venice, Hong Kong, Somerset West, Edinburgh, Washington, and Seoul), ICH-GCP guidelines, and the laws and regulations of the Netherlands. The study protocol has been registered at the Netherlands National Trial Register (registry number NTR6639). All subjects provided written informed consent prior to the start of any study-related procedure. All patients of 18 years or older undergoing resection of suspected pancreatic or periampullary cancer at the Leiden University Medical Center (LUMC) were eligible for inclusion. Exclusion criteria were contraindications for ICG administration: eGFR <55; hyperthyroidism; and allergy to iodine, shellfish or ICG. Included patients received standard-of-care, including pancreas-specific CT utilizing a thin-section, multi-phase technique with pancreatic phase and portal venous phase images. All patients received water as oral contrast. Additional imaging, for example contrast-enhanced MR with 3D-MRCP, (endoscopic) ultrasound or FDG-PET, was performed if deemed necessary by the multidisciplinary team. Patients who did not provide informed consent or those who were included in other trials still received SL, but without LUS and LFI.

Staging procedure

Patients received 4 mL 2.5 mg/mL (10 mg in total) ICG one day prior to surgery to allow intraoperative LFI of the liver surface. This dose and dosing time was based on previous experiences [13]. Before laparotomy, SL was performed via two ports of 10 mm and one port of 5 mm: a subumbilical port and two ports along the planned laparotomy line. Laparoscopic inspection of the abdomen was performed, including the parietal and visceral peritoneum, the pelvis, the liver, the porta hepatis, the gastrohepatic omentum, the duodenum, the transverse mesocolon and celiac region. Second, LUS (with or without Doppler; Toshiba Aplio 300, with a laparoscopic probe) of the liver was performed by a trained surgeon. LFI of the liver surface was performed lastly using a high-definition fluorescence imaging system (Karl Storz GmbH & Co. KG, Tuttlingen, Germany). Lesions with a fluorescent rim were considered suspect. Quality of fluorescence imaging was divided into three categories: good, meaning that healthy liver was dark and bile ducts and/or intestines were fluorescent; medium, meaning that healthy liver showed some remaining fluorescence; or bad, meaning that the liver was either totally fluorescent or totally dark and no fluorescence was seen in bile ducts nor intestines. The categories medium and bad were considered insufficient for adequate fluorescence imaging. We hypothesized that cholestasis would decrease

the quality of fluorescence imaging at one day after ICG administration. If so, dosing time would be extended to two days before surgery. Any lesions suspect for metastases based on inspection, LUS or LFI were sampled and analyzed, either by biopsy or by resection. In case of multiple lesions with similar appearance on inspection, LUS and LFI, only one biopsy was taken. Histopathological examination was considered the gold standard. The surgical procedure continued via laparotomy if the tumor appeared to be resectable and no metastases were identified.

Follow-up

Follow-up occurred according to the local standard protocol, including a visit every three months to the surgical outpatient clinic of surgery in conjunction with the department of oncology. A CT-scan was performed only if locoregional or metastatic disease was suspected.

Outcomes

Main outcome of this study was the percentage of averted futile laparotomies. Secondary outcome was the accuracy of the diagnostic modalities. Findings of SL, LUS, LFI were compared with histopathological examination of intraoperative biopsies, findings after laparotomy and finally, with follow-up results until at least the first visit to the outpatient clinic (i.e. approximately 3 months after surgery).

Statistics

Using A'Hern's single-stage phase II trial design and $\alpha=0.05$ and $\text{power}=80\%$, 25 patients were needed to distinguish between an averted laparotomy rate of 30% (worth exploring in a Phase III trial) and 10% or less (unacceptable outcome) [14]. This required at least six averted laparotomies to reach the positive endpoint. Comparing the means of two groups was performed using a two-tailed t-test in SPSS (version 23.0, IBM Statistics, US).

RESULTS

Patient characteristics

Twenty-five patients were included between January 2016 and April 2017. Patient and tumor characteristics are summarized in Table 1. Three patients received neoadjuvant therapy. One patient was treated with gemcitabine and radiotherapy, two patients with FOLFIRINOX. In one patient a liver metastasis was already suspected based on preoperative imaging, but no histopathological diagnosis could be obtained. During SL a liver metastasis was confirmed by histopathological examination.

Averted laparotomies and accuracy of sL

In 16% (n=4) the surgeon decided to stop the procedure after completion of the sL due to the detection of apparent metastases. Two patients had liver metastases, which could be identified with inspection, LUS and LFI. One patient had developed peritoneal metastases, which were – as expected – only visible with inspection. In the fourth patient LUS showed a suspect lesion in the liver, while inspection and LFI were negative (Figure 1). Intraoperative frozen section analysis suspected an adenocarcinoma, whereupon the surgical procedure was stopped. The pathological diagnosis was revised postoperatively into a bile duct adenoma after subsequent immunohistochemistry. The patient underwent a laparotomy and resection four days later and remained without metastases up to 4.5 months of follow-up.

Three other suspect lesions were resected in three other patients during sL, but turned out to be benign. All three were assessed as suspect based on inspection only. LFI did not result in false-positive outcomes. Altogether, accuracies were 57%, 57%, and 86% for inspection, LUS and LFI, respectively. In 8% (n=2) a laparotomy was performed, but the primary tumor appeared to be locally irresectable due to vascular involvement.

Quality of near-infrared fluorescence imaging

Results are shown in Figure 2. None of the patients experienced any adverse events related to administration of ICG. Fifteen patients received their dose of ICG one day prior to surgery. In 67% of the patients (n=10) the quality was good, resulting in sufficient visualization of potential liver lesions. Due to reduced ICG clearance in 20% of the patients (n=3), the quality was medium, while in 13% (n=2) the liver was still completely fluorescent. No significant differences were seen in laboratory tests for cholestasis between patients with sufficient or insufficient quality of LFI. ICG was cleared sufficiently by the liver in eight out of nine patients (89%) who were administered ICG two days prior to surgery. The surgical procedure of one patient was postponed after ICG administration with five days due to clinical reasons. During sL no fluorescence signal was detected at all.

Follow-up

The median follow-up time of all included patients was 7.8 months (range 2.7-12.6). Liver metastases were diagnosed in 20% (n=5) of the patients in whom the primary tumor was resected. In two patients, liver metastases were diagnosed within three months after surgery. None were detected during sL or subsequent laparotomy. When including these lesions, accuracies of diagnostic modalities decreased to 44%, 44% and 67% for inspection, LUS and LFI, respectively. In hindsight, abnormal fluorescence spots were visible in one patient who developed

miliary liver metastases (Figure 3). However, since no suspect fluorescence rim pattern was observed, no biopsies were taken.

DISCUSSION

Several attempts have been made to increase the yield of sL in pancreatic and periampullary cancer patients, including use of contrast-enhanced ultrasound, LUS, and selection based on preoperative imaging or blood values [8, 15-20]. This is the first study to combine sL with LUS and LFI, but not with the desired result. As mentioned, an unselected population of patients with periampullary cancer was included in this study. This may have resulted in a low *a priori* probability of metastases (12%; 3/25). In hindsight, including only patients with CA 19.9 > 150 U/L or a tumor sized > 3 cm, as suggested in a systematic review covering 24 studies [21], would increase the incidence to 21% (3/14). However, it remains disputable if selection of patients for sL should be performed. During this study period all patients with pancreatic or periampullary cancer who were not included also received sL (without LUS or LFI) before exploratory laparotomy (data not shown). Metastases were detected in 16% (5/31) of these patients. Two of these five patients would not have received sL with the above mentioned selection criteria. Risking that patients with metastases do not undergo sL should be weighed against delaying all procedures with 10 to 15 minutes.

In surgery for colorectal liver metastases, the addition of NIRF imaging to inspection and ultrasound doubled the intraoperative detection rate of additional liver metastases from 13% to 25% [22]. In the current study, we aimed to increase the yield of intraoperative screening for metastases of pancreatic or periampullary cancers by adding fluorescence imaging, but without success. One issue could be that, in contrast to patients with colorectal liver metastases, patients with pancreatic or periampullary cancer are more likely to have reduced ICG clearance. Reduced ICG clearance results in nonspecific background fluorescence, which can hamper detection of micrometastases. Our study suggest that within this population dosing ICG two days prior to surgery results in improved quality of fluorescence imaging than one day, regardless of cholestasis laboratory tests.

Apparently, LFI in patients with pancreatic or periampullary cancer has a certain learning curve. During open-space fluorescence imaging, Yokoyama et al. [10] observed abnormal fluorescence spots (larger than 1.5 mm) in 4 patients, but no malignancies could be confirmed by histopathological examination. Three of these patients developed liver metastases within six months. In the current study, only a rim pattern was considered suspect, based on previous experiences with fluorescence imaging of liver metastases [9, 13]. However, abnormal fluorescent spots were seen in two patients (Figure 3) and both developed hepatic metastases shortly after surgery. The yield of LFI may have been higher if also abnormal spots without a rim pattern were analyzed.

LUS was expected to identify intrahepatic metastases and to assess resectability before exploratory laparotomy. However, the technique failed to deliver. Instead, it even resulted in a false-positive biopsy. The added value of LUS is minimized even further when combined with MRI, which is already very sensitive for small, intrahepatic metastases [23]. However, superficial liver metastases remain difficult to distinguish on preoperative imaging. These metastases can be detected with inspection and LFI. The current results suggest that there is no added value of LUS during SL when optimal preoperative imaging has been performed.

In conclusion, this study showed limited added value of LUS during SL in patients with pancreatic or periampullary cancers. Even though LFI had a learning curve, it had the highest accuracy compared to inspection and LUS. If ICG is administered two days prior to surgery it may have more value in a selected patient population.

Figure 1 Quality of near-infrared fluorescence imaging. Upper figures: In the majority of patients ICG was cleared sufficiently from healthy liver tissue (star) if administered 2 days before to surgery. The gall bladder (arrow) was used as a positive control. In 33%, the liver still showed significant background fluorescence if ICG was administered 1 day prior to surgery. Lower figures: ICG administered 1 day showed insufficient clearance regardless of cholestatic laboratory values.

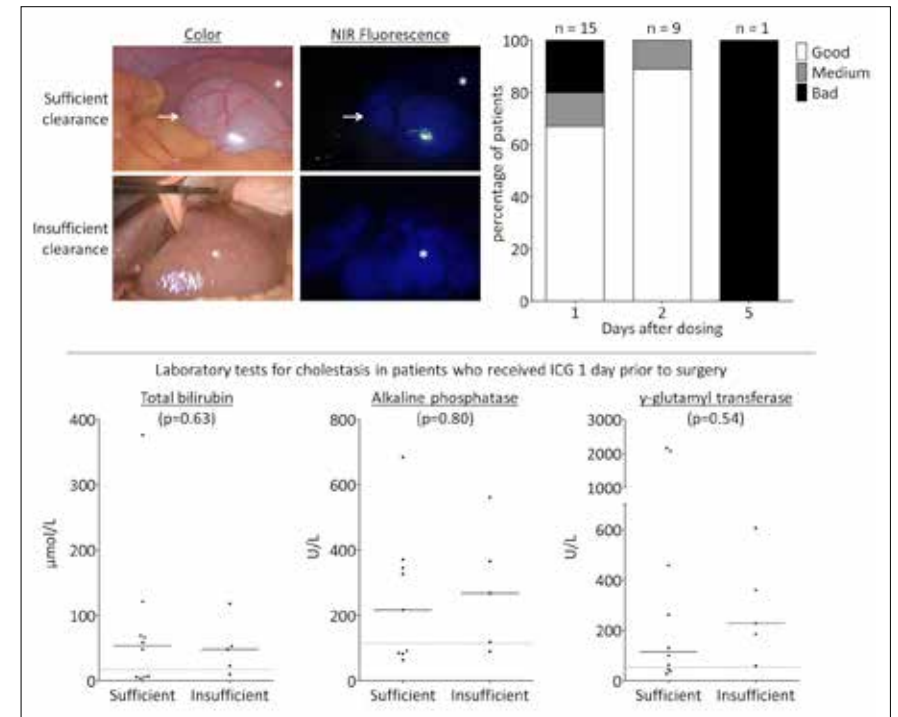


Figure 2 Laparoscopic near-infrared fluorescence imaging. Laparoscopic near-infrared fluorescence imaging could demarcate liver metastases (note the characteristic fluorescent rim), but not peritoneal metastases. Furthermore, discrimination between malignant and benign lesions such as bile duct hamartoma was clear due to the absence of fluorescence in the latter (arrow). In two patients, abnormal fluorescent spots were visible, without a characteristic rim (arrow heads). These lesions were not biopsied, but the patients developed liver metastases within 3 months after surgery..



Figure 3 False-positive lesion. A lesion suspected to be a metastasis was detected and biopsied with laparoscopic imaging (arrow). Near-infrared fluorescence imaging did not show any fluorescence signal, even though the lesion was located 7 mm below the liver capsule. The final diagnosis was a bile duct hamartoma.

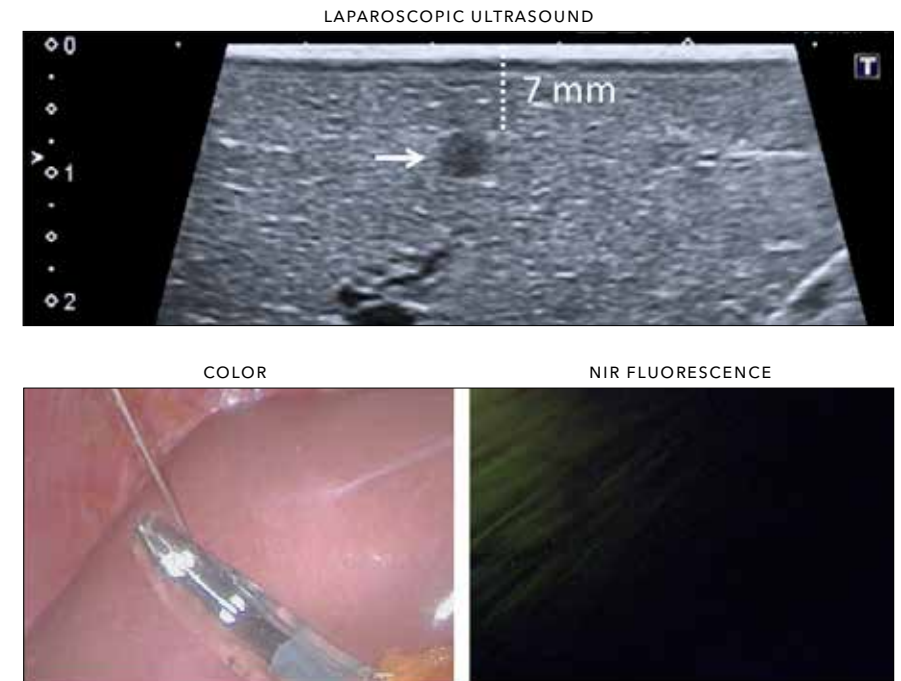


Table 1 Patient and tumor characteristics

Gender, % (n)	
Female	32 (8)
Male	68 (17)
Age at surgery, median (range)	67 (51-83)
Origin of primary tumor, % (n)	
Pancreas	78 (17)
Duodenum	12 (3)
Ampulla of Vater	12 (3)
Distal common bile duct	8 (2)
Radiological characteristics, % (n)	
≥ cT3*	28 (7)
cN1	16 (4)
Neoadjuvant therapy, % (n)	
Chemotherapy	12 (3)
Radiotherapy	4 (1)
Size of tumor (mm), % (n)*	
Not measurable	24 (6)
≥ 3 cm	36 (9)
< 3 cm	40 (10)
Laboratory values, median (range)	
CEA (µg/L)	3.0 (0.2-18.8)
cA19.9 (kU/L)	132 (3-3426)
Total bilirubin (µMol/L)	48 (6-376)
Alkaline phosphatase (U/L)	243 (57-684)
γ-glutamyl transpeptidase (U/L)	182 (12-2159)

* The tumor could not be measured

REFERENCES

- Gaujoux S, Allen PJ. Role of staging laparoscopy in peri-pancreatic and hepatobiliary malignancy. *World J Gastrointest Surg.* 2010;2(9):283-90. doi: 10.4240/wjgs.v2.i9.283. PubMed PMID: 21160897; PubMed Central PMCID: PMC2999692.
- Hsu CP, Hsu JT, Liao CH, Kang SC, Lin BC, Hsu YP, et al. Three-year and five-year outcomes of surgical resection for pancreatic ductal adenocarcinoma: Long-term experiences in one medical center. *Asian J Surg.* 2016. doi: 10.1016/j.asjsur.2016.11.009. PubMed PMID: 28010955.
- Fujioka S, Misawa T, Okamoto T, Gocho T, Futagawa Y, Yanaga K. Predictors for postoperative liver metastasis in patients with resectable pancreatic cancer. *Int Surg.* 2008;93(6):324-30. PubMed PMID: 20085041.
- Holzapfel K, Reiser-Erkan C, Fingerle AA, Erkan M, Eiber MJ, Rummeny EJ, et al. Comparison of diffusion-weighted MR imaging and multidetector-row CT in the detection of liver metastases in patients operated for pancreatic cancer. *Abdom Imaging.* 2011;36(2):179-84. doi: 10.1007/s00261-010-9633-5. PubMed PMID: 20563868.
- Hori Y, Committee SG. Diagnostic laparoscopy guidelines : This guideline was prepared by the SAGES Guidelines Committee and reviewed and approved by the Board of Governors of the Society of American Gastrointestinal and Endoscopic Surgeons (SAGES), November 2007. *Surgical endoscopy.* 2008;22(5):1353-83. doi: 10.1007/s00464-008-9759-5. PubMed PMID: 18389320.
- Velanovich V, Wollner I, Ajlouni M. Staging laparoscopy promotes increased utilization of postoperative therapy for unresectable intra-abdominal malignancies. *Journal of gastrointestinal surgery : official journal of the Society for Surgery of the Alimentary Tract.* 2000;4(5):542-6. PubMed PMID: 11077332.
- Allen VB, Gurusamy KS, Takwoingi Y, Kalia A, Davidson BR. Diagnostic accuracy of laparoscopy following computed tomography (CT) scanning for assessing the resectability with curative intent in pancreatic and periampullary cancer. *Cochrane Database Syst Rev.* 2016;7:CD009323. doi: 10.1002/14651858.CD009323.pub3. PubMed PMID: 27383694.
- Handgraaf HJ, Boonstra MC, Van Erkel AR, Bonsing BA, Putter H, Van De Velde CJ, et al. Current and future intraoperative imaging strategies to increase radical resection rates in pancreatic cancer surgery. *Biomed Res Int.* 2014;2014:890230. doi: 10.1155/2014/890230. PubMed PMID: 25157372; PubMed Central PMCID: PMC4123536.
- Boogerd LS, Handgraaf HJ, Lam HD, Huurman VA, Farina-Sarasqueta A, Frangioni JV, et al. Laparoscopic detection and resection of occult liver tumors of multiple cancer types using real-time near-infrared fluorescence guidance. *Surgical endoscopy.* 2016. doi: 10.1007/s00464-016-5007-6. PubMed PMID: 27357928.
- Yokoyama N, Otani T, Hashidate H, Maeda C, Katada T, Sudo N, et al. Real-time detection of hepatic micrometastases from pancreatic cancer by intraoperative fluorescence imaging: preliminary results of a prospective study. *Cancer.* 2012;118(11):2813-9. doi: 10.1002/cncr.26594. PubMed PMID: 21990070.
- Alexakis N, Gomatos IP, Sbarounis S, Toutouzias K, Katsaragakis S, Zografos G, et al. High serum CA 19-9 but not tumor size should select patients for staging laparoscopy in radiologically resectable pancreas head and peri-ampullary cancer. *Eur J Surg Oncol.* 2015;41(2):265-9. doi: 10.1016/j.ejso.2014.09.006. PubMed PMID: 25266999.
- Stefanidis D, Grove KD, Schwesinger WH, Thomas CR, Jr. The current role of staging laparoscopy for adenocarcinoma of the pancreas: a review. *Ann Oncol.* 2006;17(2):189-99. doi: 10.1093/annonc/mdj013. PubMed PMID: 16236756.
- van der Vorst JR, Schaafsma BE, Hutteman M, Verbeek FP, Liefers GJ, Hartgrink HH, et al. Near-infrared fluorescence-guided resection of colorectal liver metastases. *Cancer.* 2013;119(18):3411-8. doi: 10.1002/cncr.28203. PubMed PMID: 23794086; PubMed Central PMCID: PMC3775857.
- A'Hern RP. Sample size tables for exact single-stage phase II designs. *Stat Med.* 2001;20(6):859-66. doi: 10.1002/sim.721. PubMed PMID: 11252008.
- Garcea G, Cairns V, Berry DP, Neal CP, Metcalfe MS, Dennison AR. Improving the diagnostic yield from staging laparoscopy for periampullary malignancies: the value of preoperative inflammatory markers and radiological tumor size. *Pancreas.* 2012;41(2):233-7. doi: 10.1097/MPA.0b013e31822432ee. PubMed PMID: 21946812.
- de Werra C, Quarto G, Aloia S, Perrotta S, Del Giudice R, Di Filippo G, et al. The use of intraoperative ultrasound for diagnosis and stadiation in pancreatic head neoplasms. *Int J Surg.* 2015;21 Suppl 1:S55-8. doi: 10.1016/j.ijsu.2015.04.091. PubMed PMID: 26118609.
- Levy J, Tahir M, Vanounou T, Maimon G, Bergman S. Diagnostic Laparoscopy with Ultrasound Still Has a Role in the Staging of Pancreatic Cancer: A Systematic Review of the Literature. *HPB Surg.* 2016;2016:8092109. doi: 10.1155/2016/8092109. PubMed PMID: 27122655; PubMed Central PMCID: PMC4829723.
- Lin LZ, Li F, Liu Y, Xing LX, Du LF. Contrast-Enhanced Ultrasound for differential diagnosis of pancreatic mass lesions: a meta-analysis. *Med Ultrason.* 2016;18(2):163-9. doi: 10.11152/mu.2013.2066.182.ceu. PubMed PMID: 27239649.

- 19 Grossjohann HS, Rappeport ED, Jensen C, Svendsen LB, Hillingsø JG, Hansen CP, et al. Usefulness of contrast-enhanced transabdominal ultrasound for tumor classification and tumor staging in the pancreatic head. *Scand J Gastroenterol.* 2010;45(7-8):917-24. doi: 10.3109/00365521003702718. PubMed PMID: 20441527.
- 20 Maithel SK, Maloney S, Winston C, Gonen M, D'Angelica MI, Dematteo RP, et al. Preoperative CA 19-9 and the yield of staging laparoscopy in patients with radiographically resectable pancreatic adenocarcinoma. *Ann Surg Oncol.* 2008;15(12):3512-20. doi: 10.1245/s10434-008-0134-5. PubMed PMID: 18781364.
- 21 De Rosa A, Cameron IC, Gomez D. Indications for staging laparoscopy in pancreatic cancer. *HPB (Oxford).* 2016;18(1):13-20. doi: 10.1016/j.hpb.2015.10.004. PubMed PMID: 26776846; PubMed Central PMCID: PMC4750228.
- 22 Handgraaf HJ, Boogerd LS, Höppener DJ, Peloso A, Sibinga Mulder BG, Hoogstins CE, et al. Long-term follow-up after near-infrared fluorescence-guided resection of colorectal liver metastases: a retrospective multicenter analysis. *Eur J Surg Oncol.* 2017. doi: 10.1016/j.ejso.2017.04.016.
- 23 Kim HW, Lee JC, Paik KH, Kang J, Kim YH, Yoon YS, et al. Adjunctive role of preoperative liver magnetic resonance imaging for potentially resectable pancreatic cancer. *Surgery.* 2017;161(6):1579-87. doi: 10.1016/j.surg.2016.12.038. PubMed PMID: 28237643.

PART III

TARGETED TRACERS

CHAPTER 9

Detecting tumor-positive resection margins after oral cancer surgery by spraying a fluorescent tracer activated by gamma-glutamyltranspeptidase

Oral Oncology. 2017 (in press)

MD SLOOTER*, HJM HANDGRAAF*, MC BOONSTRA, LA VAN DER VELDEN, SS BHAIROSINGH, I QUE, LM DE HAAN, S KEEREWEER, PBAA VAN DRIEL, A CHAN, H KOBAYASHI, AL VAHRMEIJER, CWGM LÖWIK (*shared first authorship)

ABSTRACT

OBJECTIVES Tumor-positive resection margins are a major problem during oral cancer surgery. GGLU-HMRG is a tracer that becomes fluorescent upon activation by gamma-glutamyltranspeptidase (GGT). This study aims to investigate the combination of GGLU-HMRG and a clinical fluorescence imaging system for the detection of tumor-positive resection margins.

MATERIALS AND METHODS The preclinical Maestro and clinical Artemis imaging systems were compared *in vitro* and *ex vivo* with cultured human head and neck cancer cells (OSC19, GGT-positive; and FADU, GGT negative) and tumor-bearing nude mice. Subsequently, frozen sections of normal and oral cancer tissues were *ex vivo* sprayed with GGLU-HMRG to determine the sensitivity and specificity. Finally, resection margins of patients with suspected oral cancer were *ex vivo* sprayed with GGLU-HMRG to detect tumor-positive resection margins.

RESULTS Both systems could be used to detect GGLU-HMRG activation *in vitro* and *ex vivo* in GGT positive cancer cells. Sensitivity and specificity of GGLU-HMRG and the Artemis on frozen tissue samples was 80% and 87%, respectively. Seven patients undergoing surgery for suspected oral cancer were included. In three patients fluorescence was observed at the resection margin. Those margins were either tumor-positive or within 1 mm of tumor. The margins of the other patients were clear (≥ 8 mm).

CONCLUSION This study demonstrates the feasibility to detect tumor-positive resection margins with GGLU-HMRG and a clinical fluorescence imaging system. Applying this technique would enable intraoperative screening of the entire resection margin and allow direct re-resection in case of tumor-positivity.

INTRODUCTION

Surgery remains the treatment of choice for the curative therapy of squamous cell carcinoma (SCC), including oral cancer. A resection requires wide margins to ensure no residual tumour tissue is left behind after surgery. However, such resections often cause functional loss. In the case of oral cancer, inadequate resection margins (i.e. close and positive margins) are reported in up to 85% of these patients [1, 2]. These patients more often develop local recurrences and regional neck metastases, resulting in decreased survival rates [3]. Patients with oral cancer often have leucoplakia, which makes intraoperative discrimination between benign and malignant tissue challenging. Intraoperative frozen section analysis is sometimes used in oral cancer surgery to assess whether the resection margin is free of tumour. However, this method has certain drawbacks. Sampling errors can result in incorrect diagnosis. A pathologist is required for histopathological examination where the subsequent processing of the biopsy would then delay the surgical procedure [4, 5]. Ideally, the entire resection surface should be evaluated during the operation, but this is not possible with current strategies.

Recently, several clinical studies with tumour-targeted fluorescent tracers demonstrated the feasibility to visualize tumours, and more importantly their margins, during surgery [6-8]. Cetuximab was conjugated to the near-infrared fluorescent dye IRDye800CW. The combination enabled demarcation of tumours with millimetre-resolution in oral cancer patients [9]. These results are promising, but these tracers have several disadvantages. First, intravenous administration may lead to adverse reactions. Cetuximab, for example, can cause severe infusion reactions and other harmful side effects [10]. Second, antibody-based tracers have long plasma half-lives, and intravenous administration requires relatively high doses to have sufficient tracers reach the tumour. Unbound tracers in the systemic circulation result in non-specific background fluorescence. This reduces the signal-to-background ratio (SBR) and potentially hampers visualization of specific fluorescence. Third, administration of labelled antibodies to patients needs to be applied several days before surgery, which requires an additional visit or earlier admission to the hospital. This requires additional planning and is inconvenient for patients. Fourth, clinical translation of novel fluorescent tracers is costly, time-consuming and requires specific expertise.[11]

All these issues can be solved by topically applying activatable fluorescent tracers instead. This strategy requires a much lower dose and does not suffer from nonspecific fluorescence from unbound tracers. Moreover, spraying activatable tracers on only resected tissue only would not require costly translational research. Furthermore, such an approach would completely diminishes the risk of adverse events.

Recently, γ -glutamyl hydroxymethyl rhodamine green (gglu-HMRG) was developed for the detection and diagnosis of preclinical cancer [12]. HMRG remains quenched until cleaved in the presence of the enzyme γ -glutamyltranspeptidase (GGT). After activation HMRG emits fluorescence with a peak at 525 nm. Application of gglu-HMRG on resected material was investigated to identify tumour-positive resection margins in breast cancer patients [13]. Mizushima et al. [14] showed that fluorescence imaging with gglu-HMRG could be useful for screening of early-stage head and neck SCC. Shimane et al. demonstrated that gglu-HMRG has high sensitivity for ex vivo detection of oral SCC [15]. However, to have clinical significance for oral cancer patients during surgery, intraoperative detection of microscopic tumour-positive margins of SCC is required.

The feasibility of this technique was demonstrated with a preclinical fluorescence imaging system [12], which cannot be used in the operating room. To investigate if an intraoperative clinical imaging system such as the Artemis [16] can be used to image the activation of gglu-HMRG, we compared the sensitivity with the Maestro preclinical imaging system. The aims of this study are outlined as follows: (A) to compare those aforementioned combinations using human head and neck cancer cell lines, (B) to determine the sensitivity and specificity of gglu-HMRG on ex vivo frozen human oral cancer tissues, and (C) to study the feasibility to detect microscopic tumour-positive resection margins in oral cancer patients.

MATERIALS AND METHODS

Flow cytometry and fluorescence microscopy

The protocol adopted for this study was described previously by Urano et al. [12]. Flow cytometry was performed with the BD LSR-II Flow Cytometer for cell evaluation and subsequent cell measurements were analysed with FlowJo software (FlowJo, LLC, Ashland, OR, USA). Two human SCC cell lines, OSC19 (oral cancer; GGT overexpressing) and FaDu (hypopharyngeal cancer; GGT low expressing), were used. After incubation with gglu-HMRG, the cells were nuclear stained with Hoechst fluorescent stain (Invitrogen). Images were obtained every 5 minutes for 1 hour after application using the Leica microsystems LAS AF6000 modular systems at 20x magnification. Quantification of the signal over time was assessed using the in-house developed software program, called 'Stacks', which operates using the Microsoft Windows operating system. Each measurement was corrected to make translation between separate images possible after which a mask was created based on the last image ($t=60$). Within the mask the average intensity was measured for all images and the standard deviation was calculated as a percentage of the intensity.

Imaging systems

Two imaging systems were compared. The preclinical CRI Maestro imaging system (CRI Inc., Woburn, MA, Perkin Elmer, Waltham, MA, USA) consists of a 300 W xenon-based excitation light source with seven possible excitation and emission filter pairs, covering the complete spectral range from 500 to 950 nm. Every pixel can be analysed by a process called spectral unmixing, in which the signals from the background and fluorophore are separated. The software quantifies each pixel and determines relative concentration of the fluorophore present in that pixel [17, 18].

The Artemis fluorescence imaging system [16] (Quest Medical Imaging B.V., The Netherlands) used in this study consisted of a "white" light source, and a light source at 490 nm. Colour video and fluorescence images are simultaneously acquired on separate sensors and displayed in real-time. A pseudo-coloured (lime green) merged image of the colour video and fluorescence images is also displayed. The intensities of the light sources and exposure times could be controlled with the Artemis software.

In vitro imaging of GGLU-HMRG

OSC19 or FaDu cells (2×10^4 cells/well) were seeded into a 12-well plate. The cells were incubated at a timepoint of 48 h after seeding, with gglu-HMRG at five different concentrations (1, 2, 10, 50, and 100 μ M) in PBS for 30 min. PBS without cells, but with similar concentrations of gglu-HMRG was used as the background signal to calculate a SBR. Images were obtained using the Maestro and Artemis camera system, and analysed by measuring ROIs with the Maestro and ImageJ software (v.1.48, National Institutes of Health, USA), respectively.

In vivo imaging of GGLU-HMRG

The local animal welfare committee of Leiden University Medical Center approved the animal experiments. OSC19 cancer cells (60,000 cells/10 μ l medium) were injected into the submucosa of the tip of the tongue of six to eight weeks-old female nude Balb/c mice (Charles River laboratories, France). Health and tumour growth was monitored by weighing and inspecting the mice at least twice a week. Tongue inspections were carried out under isoflurane gas anaesthesia.

One to two weeks after cell injection, when the tumour diameter had reached approximately 5 mm, gglu-HMRG (100 μ l, 50 μ M in PBS) was sprayed on the tongue under general anaesthesia ($n=4$). A control tongue ($n=1$) was sprayed with PBS. The

tongues were imaged by the Maestro imaging system 30 minutes after topical application. Mice were sacrificed and tongues were directly harvested for *ex vivo* imaging both by Maestro and Artemis. SBRs were calculated with ImageJ.

To confirm signal and tumour overlay, the tongues were cut into cryosections of 10 µm after which were stained by haematoxylin and eosin (H&E).

Ex vivo evaluation of patient-derived cancer specimen

Frozen tissues of 15 patients with oral cancer were analysed to assess sensitivity and specificity. Normal tissue of the oral cavity of each patient was used as a negative control. Tissues were obtained from the Erasmus Medical Center (Rotterdam, The Netherlands) tissue bank. Cryosections were cut into slices of 10 µm. The cryosections were imaged by fluorescence microscopy (Leica microsystems DM5500 B, Eindhoven, The Netherlands) at 0, 1, 5 and 10 min after application of gglu-HMRG (50 µl of 50 µM in PBS). Fluorescence intensity (negative, weak, or positive) was scored independently by two authors (MS & HH). Subsequently, each slice was stained using an anti-GGT1 antibody (dilution 1:800; ab55138, Abcam, Cambridge, UK). The staining of epithelium was also scored (negative, weak, or positive) by two authors (LH&HH). Concordance between fluorescence and GGT status was subsequently evaluated.

Ex vivo evaluation of resection margins during oral cancer surgery

Patients with suspected or biopsy-proven oral cancer and scheduled to undergo resection with curative intent were eligible for inclusion. Patients were excluded if they received: (A) radiotherapy, (B) had undergone previous surgery in the oral cavity, or (C) diagnosed with multiple primary oral tumours or any active autoimmune diseases (e.g. Sjögren or lichen planus). The latter category was excluded for their diffuse abnormalities in the oral cavity.

The local medical ethical committee decided no formal approval from patients was required, because the spray was applied *ex vivo*, the tissue was handled anonymously, the outcomes did not influence treatment, and the surgeon and pathologist were blinded for the study. This pilot study was designed to prevent any potentially harmful change in standard care.

Directly after surgery the resection margins of the resected specimen were sprayed with 1 ml of 50 µM gglu-HMRG per 6 cm². Upcoming fluorescent spots were marked with ink. Subsequently, the epithelial side was sprayed, which functioned as a positive control. Fluorescence imaging was performed with the Artemis only. The resection margins were assessed for tumour positivity after embedding into paraffin using standard of care. The tissue was cut into slices of 10 µm and stained for H&E staining and GGT (dilution 1:1600). Spots marked with ink were checked for tumour and GGT status.

RESULTS

Activation and uptake of gglu-HMRG

Both the oral cancer cell line OSC19 and the hypopharyngeal cancer cell line FaDu, were evaluated for tracer uptake by flow cytometry. OSC19 was found to provide activation of gglu-HMRG, while the FaDu cell line was identified as almost negative in responding to GGT (Figure 1A and 1B). More than 70% of the total intracellular activation of gglu-HMRG already occurred within 1 minute (Figure 1C), but the signal continued to increase up to 60 minutes (figure 1D). The relatively high standard deviations are explained by the translation between the images at different times and the movement of cells. Activation and internalization of gglu-HMRG by OSC19 cells was clearly visible with fluorescence microscopy (Figure 1D).

Maestro vs. Artemis

Tracer activation by OSC19 and FaDu cells was imaged by comparing the performance of the Maestro, allowing spectral unmixing, and the clinical Artemis imaging system. The Maestro, which facilitates spectral unmixing, was capable of generating higher SBRs in OSC19 cells, whilst the Artemis showed already an increase of SBRs at lower concentrations (Figure 2A and 2C). The highest SBRs were achieved at an applied concentration of 100 µM performed on the Maestro instrument. However, even when a concentration of 50 µM was applied, the difference in detection between the two systems did not prove to be statically significant ($p=0.15$). The latter concentration was therefore considered optimal and used for further experiments. Moreover, 50 µM resulted in the highest SBR with the Artemis. FaDu showed very weak fluorescence originating from activated gglu-HMRG with both fluorescence systems (Figure 2B and 2D).

Figure 3 demonstrates the visual and numeral differences between the preclinical Maestro and the clinical Artemis system in an orthotopic oral cancer model. SBRs of *ex vivo* tongues were 22.3 ± 2.7 (control tongue: 1.4) and 4.1 ± 1.2 (control tongue: 1.1) after spraying gglu-HMRG for the Maestro and Artemis, respectively.

In brief, both systems could be used to recognize GGT positive cancer cells of *in vitro* and *in vivo* studies.

Ex vivo evaluation of patient-derived cancer specimen

Fifteen frozen tissue slices with oral cancer were included: 10 with tongue cancer and 5 with cancer of the floor of the mouth (Table 1). Fifteen tissue slices without cancer from the same patients were included. Twelve out of 15 malignant lesions showed fluorescence after spraying with gglu-HMRG (sensitivity 80%). Thirteen normal tissue slices showed either none or only weak fluorescence (specificity

87%). Twelve out of 14 fluorescent lesions (86%) were either weak or positive for GGT. None of the normal tissues stained positive for GGT, while none of the matching malignant lesions were negative for GGT. In five tissue samples some stromal cells showed expression of GGT. However, no fluorescence was observed in these samples and the epithelial cells did not show expression of GGT.

Ex vivo evaluation of resection margins during oral cancer surgery

Seven patients undergoing surgery for suspected oral cancer were included (Table 2). In three patients fluorescence was observed at the resection margin (Figure 5). In those patients, routine pathological examination demonstrated resection margins that were either tumour-positive or within 1 mm of tumour. The margins of the other four patients were at least 8 mm tumour-free. The epithelial side showed fluorescence in all except one patient. That patient turned out to have no malignancy, but parakeratosis, hyperplasia and a chronic lymphocytic inflammatory infiltrate.

Following fluorescence imaging, both the epithelial side and resection margin of 16 tissue slices were histopathologically evaluated, resulting in 32 measurements. A total of 11 slices contained oral cancer at the epithelial side and all were fluorescent. Three slices with fluorescent spots at the epithelial side did not contain tumour. Three patients had an inadequate resection margin. Two slices with fluorescent spots contained tumour-positive margins. Four slices were obtained near fluorescent spots in the resection margins of two patients, but no cancer cells could be detected. However, routine histopathological examination in both patients diagnosed a tumour-positive resection margin. Overall, the sensitivity, specificity and accuracy of fluorescence imaging were 100% (13/13), 63% (12/19) and 78% (25/32), respectively.

DISCUSSION

This study demonstrates that fluorescence imaging of resection margins using topically applied activatable tracers can enable detection of microscopic tumour-positive resection margins. Our results pave the way for a larger future study, to include more oral cancer patients, where sensitivity and specificity may be determined. Additionally, the factoring in of recurrence-free and disease-free survival would also help validate this tool., where we could diagnose tumour positive resection margins during surgery. This would permit for the surgeon to directly attempt another resection.. Moreover, if the utility of the technique is proven, this could mean a major reduction of costs and time, because intraoperative frozen section analysis will become unnecessary.

Even though assessing the margins of resected tissue with fluorescence imaging could already mean an improvement for surgeons and patients, it would even

be better if also the *in vivo* resection margin could be screened with gglu-HMRG. This requires certain toxicology studies prior to human use, but topical applications require less extensive and cheaper studies compared to intravenous administered tracers. Systemic uptake will probably be very low, which generally results in favourable safety.

Our work with gglu-HMRG is not the first activatable tracer to be used clinically for resection. 5-aminolevulinic acid (5-ALA), a non-fluorescent precursor of haemoglobin, is already being used clinically [19, 20]. Oral administration of 5-ALA induces accumulation of fluorescent protoporphyrin IX (emission peak at 635 nm) inside malignant tumours. A randomized controlled trial demonstrated that 5-ALA and fluorescence imaging enables a more complete resection and improved progression-free survival in patients with malignant glioma [21]. Even though the diseases and the consequences are not comparable, gglu-HMRG has the potential to have a similar effect on radical resection rates and thereby on surgical outcomes.

In this study no GGT-negative oral tumours were encountered in a total of 21 tumours. Comparably, all ten tumours with oral SCC included in the *ex vivo* study by Shimane et al. were GGT positive and showed fluorescence 10 minutes after applying gglu-HMRG [15]. This is in concordance with literature; most SCCs demonstrate intense GGT overexpression [14, 22]. However, in the unlikely case of GGT-negative tumours, applying gglu-HMRG would result in false-negative results. This can be detected easily by using the epithelial side of the tumour as a positive control, as shown in this study.

The fluorescence signals did not align perfectly in all *ex vivo* frozen tissues (Figure 4). There are several explanations. Tissue slices sprayed with gglu-HMRG stained afterwards negative for GGT. We therefore used consecutive, but not identical, slices. Furthermore, gglu-HMRG is internalized *in vivo* after activation. However, this process does not occur *ex vivo* in frozen tissue, which may cause activated HMRG to spread. Lastly, a GGT1 antibody was used, whereas gglu-HMRG may be specific for only certain subtypes of GGT. This hypothesis is reinforced by the finding that some stromal cells expressed GGT, but did not show any fluorescence. Nevertheless, fluorescence signals strongly correlated with GGT expression.

Seven tissue slices obtained from the proximity of fluorescent spots did not contain cancer cells. These results were either false-positive, or caused by sampling errors. Some fluorescent spots were very small (see Figure 5), which made it challenging and sometimes impossible to identify them in a single slice. Unfortunately, the tissue blocks could not completely used, because sufficient tissue needed to be preserved for other research purposes and additional routine histopathological examination.

It was sometimes difficult to discriminate between tissue autofluorescence and fluorescence from activated gglu-HMRG (see figure 5). More research is required to understand the nature of false-positive fluorescence signals. For example, in this study we chose to subjectively discriminate between negative, weak and positive

fluorescence (Table 1). The latter two were considered to be positive, hence the sensitivity of 80% and the specificity of 87%. However, if only positive fluorescence would be considered to be positive, the sensitivity would be 93%, with a specificity of 53%. One method to reduce non-specific (auto)fluorescence is to use different fluorophores. For intraoperative imaging, fluorescence with a wavelength around 800 nm is considered optimal [23]. That wavelength is capable of deeper tissue penetration compared to 500 nm [6]. Moreover, tissue autofluorescence is reduced to a minimum, which will increase sensitivity and specificity.

Discrimination between zero measurements and activated fluorescence signals were currently performed by visual inspection. Technology exists that compares spectral differences over time, for example to detect premalignant cervical lesions after spraying acetic acid.[24] This method could allow more accurate detection of gglu-HMRG activation by tumour-positive resection margins.

CONCLUSION

In conclusion, this study demonstrates the feasibility of being able to detect microscopic tumour-positive resection margins using an activatable tracer, gglu-HMRG, in conjunction with a clinical fluorescence imaging system. Applying this technique would allow intraoperative screening of the entire resection margin and facilitate direct re-resection in case of tumour-positivity.

Figure 1 Flow cytometry of the GGT-positive cell line OSC19 (A) and the negative cell line FADU (B). The majority of the activation of GGLU-HMRG on OSC19 cells occurs within the first ten minutes (C). HMRG is internalized after activation (D; 40 times enlarged).

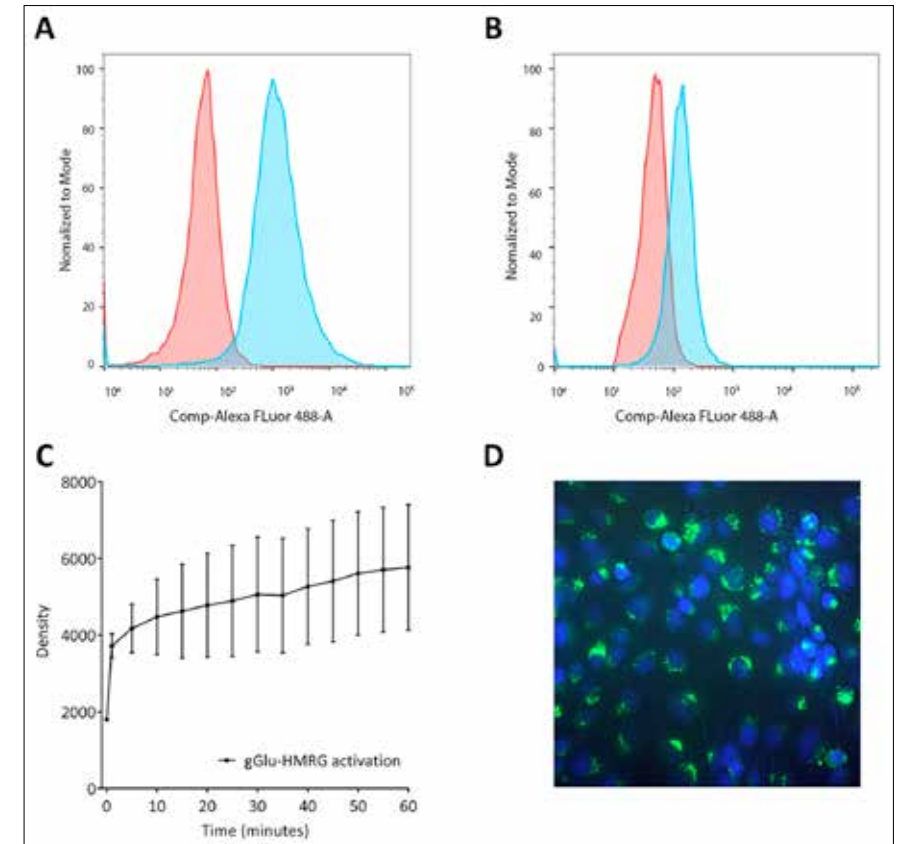


Figure 2 The Maestro was capable of generating high signal-to-background ratios (SBR) in OSC19 cells, especially with 50 μ M and 100 μ M (A). The Artemis demonstrated already an increase of SBRs at lower concentrations (C). FaDu showed very weak fluorescence originating from activated GGLU-HMRG with both fluorescence systems (B&D).

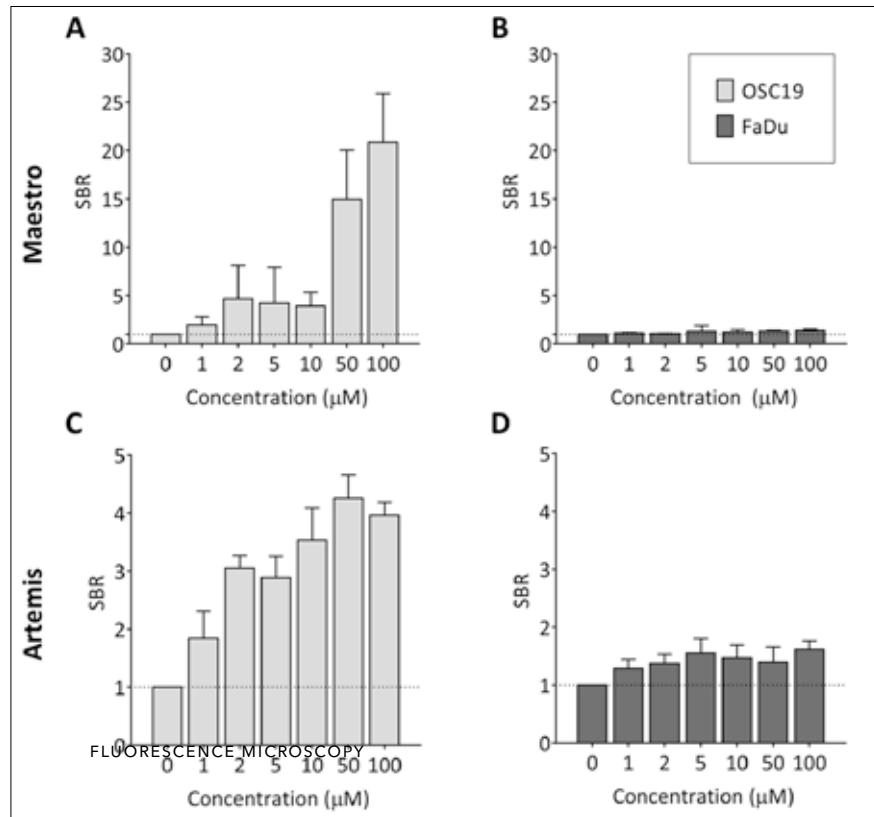


Figure 3 Shown are examples of *in vivo* and *ex vivo* measurements with the Maestro and colour and fluorescence images made *ex vivo* with the Artemis. On the right matching signal-to-background ratios of a control (n=1) and tongues sprayed with GGLU-HMRG (n=4). Both systems could be used to recognize GGT positive cancer cells of *in vitro* and *in vivo* studies.

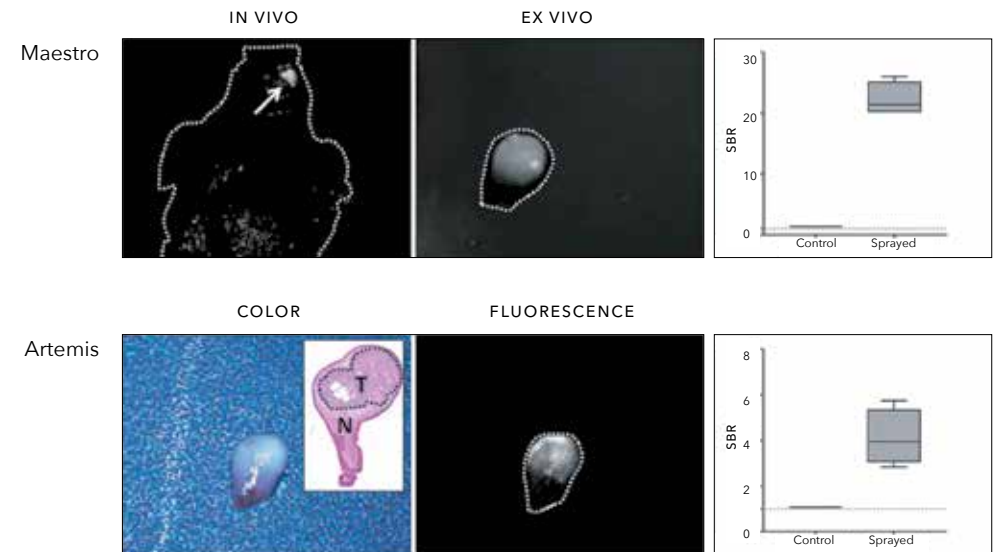


Figure 4 Example of fluorescence microscopy of normal and malignant frozen tissue (2.5 times enlarged). Ten minutes after spraying GGLU-HMRG the normal tissue shows weak fluorescence. Malignant tissue became clearly fluorescent, which correlated with positive GGT staining.

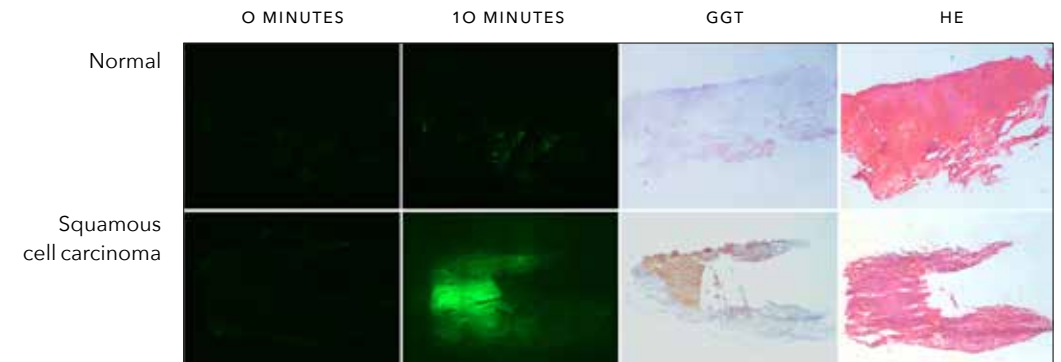


Figure 5 Example of resection margin assessment with GGLU-HMRG and the clinical Artemis imaging system (upper two panels). Ten minutes after spraying on the tissue several spots became fluorescent in the resection margin (arrows). In one patient with squamous cell carcinoma, focal expansion of a carcinoma in situ < 1 mm from the resection margin was diagnosed with fluorescence imaging (dashed arrow). The epithelial side was used as a positive control. A patient with suspected oral cancer turned out to have parakeratosis and hyperplasia instead. No fluorescence was observed in both the epithelial side and resection margin (data not shown). The tissue did not show overexpression of GGT (lower panel).

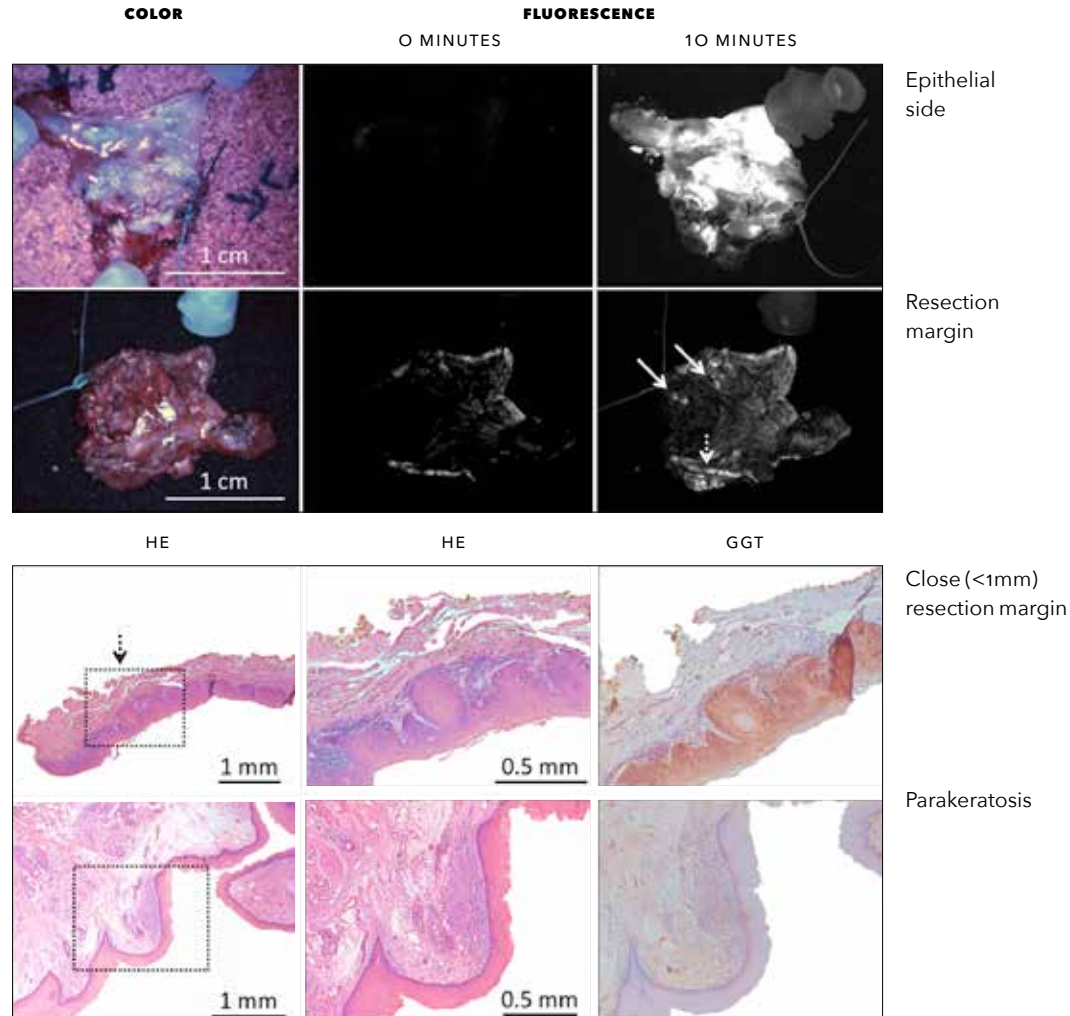


Table 1 Scoring results

	Normal	Malignant						
		Fluorescence			Fluorescence			
		Negative	Weak	Positive	GGT	Negative	Weak	Positive
GGT	Negative	6	5	2	GGT	Negative	0	0
	Weak	2	0	0	GGT	Weak	0	2
	Positive	0	0	0	GGT	Positive	1	0
							0	9

Table 2 Fluorescence imaging and histopathological evaluation of the resection margin

No.	Histopathology	Margin	Fluorescence		GGT (tumour)
			RM	ES	
1	Keratinizing squamous cell carcinoma	Clear (8 mm)	-	+	+
2	Parakeratosis, hyperplasia	NA	-	-	-
3	Keratinizing squamous cell carcinoma	Tumour-positive	+	+	+
4	Keratinizing squamous cell carcinoma	Tumour-positive	+	++	+
5	Keratinizing squamous cell carcinoma	Clear (8 mm)	-	+	+
6	Squamous cell carcinoma	Clear (8 mm)	-	++	+
7	Squamous cell carcinoma, well differentiated	Close (4 mm); focal expansion cis (1 mm)	+	++	+

RM: resection margin; ES: epithelial side; NA: not applicable; CIS: carcinoma in situ.

REFERENCES

- 1 Smits RW, Koljenovic S, Hardillo JA, Ten Hove I, Meeuwis CA, Sewnaik A, Dronkers EA, Bakker Schut TC, Langeveld TP, Molenaar J, Hegt VN, Puppels GJ and Baatenburg de Jong RJ. Resection margins in oral cancer surgery: Room for improvement. *Head Neck*. 2016; 38 Suppl 1:E2197-2203.
- 2 Woolgar JA and Triantafyllou A. A histopathological appraisal of surgical margins in oral and oropharyngeal cancer resection specimens. *Oral Oncol*. 2005; 41(10):1034-1043.
- 3 Hinni ML, Ferlito A, Brandwein-Gensler MS, Takes RP, Silver CE, Westra WH, Seethala RR, Rodrigo JP, Corry J, Bradford CR, Hunt JL, Strojan P, Devaney KO, Gnepp DR, Hartl DM, Kowalski LP, et al. Surgical margins in head and neck cancer: a contemporary review. *Head Neck*. 2013; 35(9):1362-1370.
- 4 Du E, Ow TJ, Lo YT, Gersten A, Schiff BA, Tassler AB and Smith RV. Refining the utility and role of Frozen section in head and neck squamous cell carcinoma resection. *Laryngoscope*. 2016; 126(8):1768-1775.
- 5 Wenig BM. Intraoperative consultation (IOC) in mucosal lesions of the upper aerodigestive tract. *Head Neck Pathol*. 2008; 2(2):131-144.
- 6 Hoogstins CE, Tummers QR, Gaarenstroom KN, de Kroon CD, Trimbos JB, Bosse T, Smit VT, Vuyk J, van de Velde CJ, Cohen AF, Low PS, Burggraaf J and Vahrmeijer AL. A Novel Tumor-Specific Agent for Intraoperative Near-Infrared Fluorescence Imaging: A Translational Study in Healthy Volunteers and Patients with Ovarian Cancer. *Clin Cancer Res*. 2016; 22(12):2929-2938.
- 7 Lamberts LE, Koch M, de Jong JS, Adams A, Glatz J, Kranendonk ME, Terwisscha van Scheltinga AG, Jansen L, de Vries J, Lub-de Hooge MN, Schroder CP, Jorritsma-Smit A, Linssen MD, de Boer E, van der Vegt B, Nagengast WB, et al. Tumor-specific uptake of fluorescent bevacizumab-IRDYE800CW microdosing in patients with primary breast cancer: a phase I feasibility study. *Clin Cancer Res*. 2016.
- 8 Burggraaf J, Kamerling IM, Gordon PB, Schrier L, de Kam ML, Kales AJ, Bendixsen R, Indrevoll B, Bjerke RM, Moestue SA, Yazdanfar S, Langers AM, Swaerd-Nordmo M, Torheim G, Warren MV, Morreau H, et al. Detection of colorectal polyps in humans using an intravenously administered fluorescent peptide targeted against c-Met. *Nat Med*. 2015; 21(8):955-961.
- 9 Rosenthal EL, Warram JM, de Boer E, Chung TK, Korb ML, Brandwein-Gensler M, Strong TV, Schmalbach CE, Morlandt AB, Agarwal G, Hartman YE, Carroll WR, Richman JS, Clemons LK, Nabell LM and Zinn KR. Safety and Tumor Specificity of Cetuximab-IRDYE800 for Surgical Navigation in Head and Neck Cancer. *Clin Cancer Res*. 2015; 21(16):3658-3666.
- 10 Thomas M. Cetuximab: adverse event profile and recommendations for toxicity management. *Clin J Oncol Nurs*. 2005; 9(3):332-338.
- 11 Keereweer S, Van Driel PB, Snoeks TJ, Kerrebijn JD, Baatenburg de Jong RJ, Vahrmeijer AL, Sterenberg HJ and Lowik CW. Optical image-guided cancer surgery: challenges and limitations. *Clin Cancer Res*. 2013; 19(14):3745-3754.
- 12 Urano Y, Sakabe M, Kosaka N, Ogawa M, Mitsunaga M, Asanuma D, Kamiya M, Young MR, Nagano T, Choyke PL and Kobayashi H. Rapid cancer detection by topically spraying a gamma-glutamyltranspeptidase-activated fluorescent probe. *Sci Transl Med*. 2011; 3(110):110ra119.
- 13 Ueo H, Shinden Y, Tobo T, Gamachi A, Udo M, Komatsu H, Nambara S, Saito T, Ueda M, Hirata H, Sakimura S, Takano Y, Uchi R, Kurashige J, Akiyoshi S, Iguchi T, et al. Rapid intraoperative visualization of breast lesions with gamma-glutamyl hydroxymethyl rhodamine green. *Sci Rep*. 2015; 5:12080.
- 14 Mizushima T, Ohnishi S, Shimizu Y, Hatanaka Y, Hatanaka KC, Hosono H, Kubota Y, Natsuzaka M, Kamiya M, Ono S, Homma A, Kato M, Sakamoto N and Urano Y. Fluorescent imaging of superficial head and neck squamous cell carcinoma using a gamma-glutamyltranspeptidase-activated targeting agent: a pilot study. *BMC Cancer*. 2016; 16:411.
- 15 van Driel PB, van de Giessen M, Boonstra MC, Snoeks TJ, Keereweer S, Oliveira S, van de Velde CJ, Lelieveldt BP, Vahrmeijer AL, Lowik CW and Dijkstra J. Characterization and evaluation of the artemis camera for fluorescence-guided cancer surgery. *Mol Imaging Biol*. 2015; 17(3):413-423.
- 16 Levenson RM, Lynch DT, Kobayashi H, Backer JM and Backer MV. Multiplexing with multispectral imaging: from mice to microscopy. *ILAR J*. 2008; 49(1):78-88.
- 17 Mansfield JR, Gossage KW, Hoyt CC and Levenson RM. Autofluorescence removal, multiplexing, and automated analysis methods for in-vivo fluorescence imaging. *J Biomed Opt*. 2005; 10(4):41207.
- 18 Stummer W, Novotny A, Stepp H, Goetz C, Bise K and Reulen HJ. Fluorescence-guided resection of glioblastoma multiforme by using 5-aminolevulinic acid-induced porphyrins: a prospective study in 52 consecutive patients. *J Neurosurg*. 2000; 93(6):1003-1013.
- 19 Stummer W, Stocker S, Wagner S, Stepp H, Fritsch C, Goetz C, Goetz AE, Kiefmann R and Reulen HJ. Intraoperative detection of malignant gliomas by 5-aminolevulinic acid-induced porphyrin fluorescence. *Neurosurgery*. 1998; 42(3):518-525; discussion 525-516.
- 20 Stummer W, Pichlmeier U, Meinel T, Wiestler OD, Zanella F, Reulen HJ and Group AL-GS. Fluorescence-guided surgery with 5-aminolevulinic acid for resection of malignant glioma: a randomised controlled multicentre phase III trial. *Lancet Oncol*. 2006; 7(5):392-401.
- 21 Pompella A, De Tata V, Paolicchi A and Zunino F. Expression of gamma-glutamyltransferase in cancer cells and its significance in drug resistance. *Biochem Pharmacol*. 2006; 71(3):231-238.
- 22 Vahrmeijer AL, Hutteman M, van der Vorst JR, van de Velde CJ and Frangioni JV. Image-guided cancer surgery using near-infrared fluorescence. *Nat Rev Clin Oncol*. 2013; 10(9):507-518.
- 23 Louwers J, Zaal A, Kocken M, Ter Harmsel W, Grazioti G, Spruijt J, Berkhof J, Balas C, Papagiannakis E, Srijders P, Meijer C, van Kemenade F and Verheijen R. Dynamic spectral imaging colposcopy: higher sensitivity for detection of premalignant cervical lesions. *BJOG*. 2011; 118(3):309-318.

CHAPTER 10

Real-time near-infrared fluorescence imaging using CRGD-ZW800-1 for intraoperative visualization of multiple cancer types

Oncotarget. 2017; 8(13):21054-21066,.Supplementary data available online.

HJM HANDGRAAF*, MC BOONSTRA*, HAJM PREVОО, J KUIL, MW BORDO,
LSF BOOGERD, BG SIBINGA MULDER, CFM SIER, ML VINKENBURG-VAN SLOOTEN,
ARPM VALENTIЈN, J BURGGRAAF, CJH VAN DE VELDE, JV FRANGIONI, AL VAHRMEIJER.
(* shared first authorship)

ABSTRACT

Incomplete resections and damage to critical structures increase morbidity and mortality of patients with cancer. Targeted intraoperative fluorescence imaging aids surgeons by providing real-time visualization of tumors and vital structures. This study evaluated the tumor-targeted zwitterionic near-infrared fluorescent peptide CRGD-ZW800-1 as tracer for intraoperative imaging of multiple cancer types. CRGD-ZW800-1 was validated *in vitro* on glioblastoma (U-87 MG) and colorectal (HT-29) cell lines. Subsequently, the tracer was tested in orthotopic mouse models with HT-29, breast (MCF-7), pancreatic (BXP-3), and oral (OSC-19) tumors. Dose-ranging studies, including doses of 0.25, 1.0, 10, and 30 nmol, in xenograft tumor models suggest an optimal dose of 10 nmol, corresponding to a human equivalent dose of 63 µg/kg, and an optimal imaging window between 2 and 24 h post-injection. The mean half-life of CRGD-ZW800-1 in blood was 25 min. Biodistribution at 4 h showed the highest fluorescence signals in tumors and kidneys. *In vitro* and *in vivo* competition experiments showed significantly lower fluorescence signals when U-87 MG cells (minus 36%, $p=0.02$) or HT-29 tumor bearing mice (TBR at 4 h 3.2 ± 0.5 vs 1.8 ± 0.4 , $p=0.03$) were simultaneously treated with unlabeled CRGD. CRGD-ZW800-1 visualized *in vivo* all colorectal, breast, pancreatic, and oral tumor xenografts in mice. Screening for off-target interactions, CRGD-ZW800-1 showed only inhibition of COX-2, likely due to binding of CRGD-ZW800-1 to integrin $\alpha_V\beta_3$. Due to its recognition of various integrins, which are expressed on malignant and neoangiogenic cells, it is expected that CRGD-ZW800-1 will provide a sensitive and generic tool to visualize cancer during surgery.

INTRODUCTION

Accurate and real-time detection of tumors and vital structures during surgery remains challenging. Similar to radioisotopes for single-photon emission computed tomography (SPECT) and positron emission tomography (PET), tumor targeting ligands can also be conjugated to near-infrared (NIR, 700–900 nm) fluorophores. These fluorescent tracers allow real-time visualization of tumors during surgery using dedicated intraoperative imaging systems [1, 2]. The advantage of NIR fluorescence is that it can penetrate through 8 mm into tissue, allowing identification of targets even when they are not yet fully exposed [3]. Several NIR fluorophore-labeled ligands have been introduced in clinical trials, including the labeled antibodies cetuximab-IRDYE800CW [4] for the epidermal growth factor receptor (EGFR), bevacizumab-IRDYE800CW (ClinicalTrials.gov Identifier NCT01508572) for vascular endothelial growth factor (VEGF), and SGM-101 (Netherlands Trial Register number NTR5673) for carcinoembryonic antigen (CEA). Antibodies have high affinity to specific targets, but they can cause immunogenic reactions and have a relatively slow biodistribution and low clearance rates [5, 6]. On the other hand, peptides possess more favorable pharmacokinetic properties, but often have lower affinity compared to antibodies. Clinical trials using the small NIR fluorescent molecules OTL-38 (1.4 kDa) targeting the folate receptor α (FR α) and GE-137 (3.7 kDa) targeting human tyrosine kinase c-MET [7, 8] have already been reported. However, these targets are selectively overexpressed and may only be applicable for a limited number of tumor types.

In this study we evaluate CRGD-ZW800-1, a cyclic pentapeptide conjugated to the 800 nm NIR fluorophore ZW800-1. RGD is clinically well known and binds to various integrins ($\alpha_V\beta_1$, $\alpha_V\beta_3$, $\alpha_V\beta_5$, $\alpha_V\beta_6$, $\alpha_V\beta_8$, $\alpha_5\beta_1$, $\alpha_8\beta_1$ and $\alpha_{11}\beta_3$). Expression of particular integrins can be found on tumor cells and tumor-associated vascular endothelium and correlates with neoangiogenesis [9]. Overexpression is found in almost all solid tumors, including breast, colorectal, pancreas, brain, lung, and other cancers [10]. CRGD-ZW800-1 may therefore act as a generic tracer for a broad variety of solid tumors. Indeed, various phase I and II clinical trials with RGD-based PET tracers have shown uptake in multiple tumor types, including melanomas, glioblastomas, breast, colorectal, ovarian, cervical, non-small cell lung, neuroendocrine, head and neck, and pancreatic cancer [11–14]. Preliminary work on the development of CRGD-ZW800-1 showed low non-specific uptake and excellent *in vivo* properties in tumor xenograft mouse models [15, 16]. Moreover, due to its predominant renal clearance, ureters could also be recognized, which can prevent damage to these structures during surgery in the lower pelvis.

This study aims to characterize the *in vitro* properties, optimize dosage and timing, study pharmacokinetics, and to evaluate the feasibility of using CRGD-ZW800-1 as a generic tracer for intraoperative near-infrared fluorescence imaging of solid tumors.

RESULTS

The expression of $\alpha_V\beta_3$, $\alpha_V\beta_5$ and $\alpha_V\beta_6$ on tumor cell lines

Table 1 reports the measured antigenic sites per cell for three RGD binding integrins on clinically relevant tumor cell lines. Pancreatic BXP-3 cells expressed all 3 integrins, while colorectal HT-29, glioblastoma U-87 MG, and oral OSC-19-GFP cells expressed 2 of the integrins evaluated. Breast MCF-7 cells showed only expression of integrin $\alpha_V\beta_5$. Overall, U-87 MG cells showed the highest and MCF-7 cells the lowest number of the three integrin antigenic sites combined.

Binding assay and *in vitro* and *in vivo* competition experiments

Binding assays with CRGD-ZW800-1 on intermediate integrin-expressing HT-29 cells showed an almost linear increase in fluorescence intensity with increasing concentrations (Figure 1A). Significantly lower signals were observed when cells were incubated at 4°C, which prevents internalization of the agent. *In vitro* competition for binding CRGD-ZW800-1 (500 nM) with a 1:1 molar ratio of unlabeled CRGD (500 nM) resulted in a reduction of 32% on the HT-29 cells and 36% on the high integrin-expressing U-87 MG cells compared to cells treated without unlabeled CRGD (Figure 1B).

In vivo competition using a 200 times higher dose of unlabeled CRGD compared to CRGD-ZW800-1 (2.0 μ Mol vs. 10 nmol) in the orthotopic HT-29 model (Figure 1C) resulted in a significant decrease in tumor-to-background ratio (TBR) at 4 and 24 h (42%, $p=0.02$ and 54%, $p=0.007$, respectively).

Identification of off-target interactions

Out of 44 selected targets, CRGD-ZW800-1 resulted in significant inhibition (62%) of control-specific binding of cyclooxygenase-2 (COX-2). Weak to moderate inhibition was seen in 5-hydroxytryptamine (serotonin) receptor 2B (5-HT_{2B}, 29%), lymphocyte-specific protein tyrosine kinase (LCK, 28%), and dopamine receptor D₂₅ (22%) (Table S1, supplementary data).

In vivo validation using HT-29 ($\alpha_V\beta_3$ negative) colorectal tumors

Four doses were explored using both the Pearl® Impulse small animal imaging system (LI-COR, Biosciences, Lincoln, NE, U.S.A.) and the prototype Fluorescence-Assisted Resection and Exploration (FLARE®, Curadel, LLC, MA, U.S.A.) system as indicated (Figure 2A). TBRs at 4 and 24 h post injection were sufficient (i.e. >2) in the 1, 10 and 30 nmol dose groups (Figure 2B and 2C). The FLARE showed clear fluorescence signals in the 10 and 30 nmol dose groups. The optimal dose was therefore set at 10 nmol.

In vivo validation using BXP-3 ($\alpha_V\beta_3$ positive) pancreatic tumors

Tumor specific signals (TBRs >2) were observed in all three dose groups using FLARE® and Pearl® at 4 h post injection (Figure 3A and 3B). Fluorescence microscopy of the pancreatic tumors showed that NIR fluorescence signals originate from inside malignant cells.

In vivo validation using OSC-19 ($\alpha_V\beta_3$ negative) oral tumors

The optimal dose of 10 nmol CRGD-ZW800-1 was administered in the well-established tongue orthotopic cancer model and resulted in clear tumor demarcation with a mean TBR of 5.4 ± 1.1 using Pearl® (Figure 3C and 3D). Fluorescence microscopy of the tumor showed a clear demarcation between malignant and normal tissue.

In vivo validation using MCF-7 ($\alpha_V\beta_3$ negative) breast tumors

The optimal dose of 10 nmol CRGD-ZW800-1 was administered to mice bearing orthotopic breast tumors. Compared to 0.5 h post injection fluorescence intensity of tumors decreased by $61\% \pm 8\%$ and by $77\% \pm 4\%$ at 4 and 24 h post injection (Figure 4C) Using the Pearl® and the skin as background tissue TBRs reached values slightly higher than 2 between 1 and 48 h post injection (Figure 4B). These relatively low TBRs compared to the other models were due to the relatively high fluorescence of the skin. Removal of the skin in a single mouse resulted in significant higher TBRs: 3.0 ± 0.3 vs. 1.5 ± 0.1 at 4 h post injection ($p=0.02$, Figure S1, supplementary data).

In vivo biodistribution

In both HT-29 and BXP-3 tumor models an increased dose of CRGD-ZW800-1 resulted in stronger fluorescence signals in the tumors (Figure 5A). The calculated organ-to-tumor ratios in these mice showed that for all doses the BXP-3 tumor was at least twice as fluorescent as the skin, intestines, lungs, muscle, gallbladder, brain, and blood at 4 h post injection (Figure 5B). The large intestines and liver showed fluorescence ratios of around half compared with BXP-3 tumors. Fluorescence signals in kidneys were equal to or higher than tumors, reflecting renal clearance of CRGD-ZW800-1.

As described before, at 24 h the intensity of fluorescence signals in HT-29 tumors decreased compared to 4 h (Figure 5C). However, in all dose groups the HT-29 tumor was still more than twice as fluorescent compared to signals observed in lungs, pancreas, muscle, gallbladder, brain, and blood (Figure 5D). Compared to the HT-29 tumor, the fluorescence signal was higher in kidneys (all dose groups), and liver and skin (only 10 and 30 nmol dose groups). Significant differences between dose groups were seen in kidneys only.

Pharmacokinetics

Peripheral blood concentrations were measured after injection of 10 nmol CRGD-ZW800-1 per mouse (n=5). These mice did not have tumors. The measured fluorescence values were validated by a calibration curve (Figure S2, supplementary data). The maximal concentration of CRGD-ZW800-1 in serum measured at 1 minute post injection was 1.17 μ M (Figure 6). Decrease of CRGD-ZW800-1 serum concentrations followed a biphasic pattern with a distribution and elimination phase with a mean terminal half-life of 71.1 ± 9.4 min. Mean systemic clearance was 0.25 ± 0.06 ml/min.

DISCUSSION

NIR fluorescent tracers offer significant potential for accurate and real-time tumor visualization during resection. This study shows that CRGD-ZW800-1 is specific for integrins expressed on multiple tumor types providing an imaging window between 2 to 24 h post injection. Due to its clearance via kidneys rather than the liver, CRGD-ZW800-1 could be used for NIR fluorescence imaging of almost all solid cancers and their metastases.

Research on RGD peptides for cancer targeting has mainly focused on the $\alpha_v\beta_3$ integrin and neoangiogenic endothelial cells, often using the glioblastoma U-87 MG cell line as proof of concept in animal models. Indeed, our inventory shows that U-87 MG cells contain the highest level of $\alpha_v\beta_3$ integrin, confirming its frequent use as positive control for RGD binding. However, 7 other integrins are also able to bind the RGD sequence, including $\alpha_v\beta_5$ and $\alpha_v\beta_6$ which are overexpressed on malignant cells from various tumor types [17-19]. This explains why CRGD-ZW800-1 accumulates in HT-29, MCF-7, and OSC-19 tumors: All are $\alpha_v\beta_3$ negative, but express integrins $\alpha_v\beta_5$ and/or $\alpha_v\beta_6$. The specificity of the fluorescence signals was previously demonstrated [16] and could also be extracted from *in vitro* and *in vivo* competition experiments, ruling out possible non-specific accumulation, e.g. due to the enhanced permeability and retention (EPR) effect [20]. CRGD thus offers potential for visualization of almost any type of solid cancer.

CRGD has previously been conjugated to the fluorophores indocyanine green (ICG), IRDYE800CW, and CY5.5 for optical imaging applications [21-25]. A study using CRGD-IRDYE800CW showed delineation of U-87 MG tumors in mice and underscored the relative simplicity and low cost of the synthesis [21]. Another study showed *in vitro* the binding capacity of CRGD-ICG using MCF-7 cells as a negative control [24]. In our study, we showed that CRGD-ZW800-1 targets *in vivo* even the low integrin expressing cell line MCF-7. In addition to expression of integrin $\alpha_v\beta_5$ by MCF-7 cancer cells, this could also be explained by expression of RGD-binding integrins by tumor-associated vascular endothelium and stromal cells. NIR fluorescence imaging of tumors using CRGD conjugated to

IRDYE800CW, CY5.5, or ICG is feasible, but compared to CRGD-ZW800-1 these tracers show higher non-specific uptake in normal tissues and organs due to their anionic charge [16]. For example, CRGD-ICG showed significant uptake in liver and colon, which can hamper identification of gastrointestinal tumors [25]. CRGD-ZW800-1 has a balanced charge distribution and a net charge of 0, which likely shields its hydrophobicity and minimizes interactions with serum proteins [26]. In our biodistribution study ratios between tumor and relevant organs, such as intestines, lung, pancreas, muscle, or brain, were more than sufficient for accurate discrimination. Moreover, increasing the dose to 30 nmol did not result in more non-specific uptake, whereas fluorescence in tumors was enhanced. Our group previously showed that CRGD-ZW800-1 is renally cleared, allowing identification of ureters [15]. This study confirms that kidneys are the exclusive clearance route. First, the measured clearance of CRGD-ZW800-1 is identical to basal glomerular filtration rate in mice (i.e. 0.25 ml/min) [27]. Second, there was a significant difference in fluorescence signals between doses in the kidneys. Third, all mice showed high signals in the bladder up to 4 h post injection, as shown for example in MCF-7 model. In contrast, no significant differences were seen between the dose groups in the gallbladder or intestines, making hepatic clearance unlikely. Clearance patterns are important, because limited target expression often constrains maximal tumor specific uptake [26]. For imaging colorectal or pancreatic tumors, renal clearance is beneficial, as it reduces background signals from liver and intestines and thereby improves TBRs. On the other hand, imaging tumors of the genitourinary tract might be impeded due to the renal excretion of CRGD-ZW800-1.

CRGD-ZW800-1 is internalized into cells after binding as shown in previous studies and recognizable in the *in vitro* binding assays at 4 and 37°C. The continuous process of internalization and recruitment of fresh integrins to the cell membrane results in a relatively large imaging window between 2 to 24 h post injection. After internalization, the majority of integrins are recycled back to the cellular membrane in approximately 45 min [28]. Based on the mean blood half-life of 25 min, we can rationalize that the majority of CRGD-ZW800-1 is internalized during the first hours. The MCF-7 model confirms this; TBRs increase up to 2 h post injection. The absolute signal in tumors depends therefore on the amount of initially available agent and integrins rather than accumulation of the agent over time. Although the central oxygen linking modality of ZW800-1 might be vulnerable for degradation *in vivo*, the intracellular signals remained visible up to 48 h post dosing [29]. For optimal results in a clinical study CRGD-ZW800-1 should be administered several hours prior to imaging. This is a major advantage compared to labeled antibodies, which have to be administered several days prior to surgery, requiring an additional visit or earlier admission to the hospital.

Besides interacting with extracellular matrix proteins, integrin $\alpha_v\beta_3$ can also modulate intracellular pathways essential for COX-2 expression [30]. The inhibition of COX-2 as shown in the *in vitro* off-target screening may be the result of

binding CRGD-ZW800-1 to integrin $\alpha_V\beta_3$. Potentially, inhibition of COX-2 in blood vessels can lead to higher blood pressure and increase the risk of cardiovascular events because of decreased prostacyclin production [31]. This seems unlikely to occur after a single low dose in humans, also because COX-2 inhibition by CRGD-ZW800-1 was observed in the micromolar range. Following these preclinical findings a toxicology study in rats (unpublished data) is already performed and neither clinical symptoms, nor treatment-related histopathological, biochemical, and hematological abnormalities were seen after intravenous injection of 5.0 mg/kg CRGD-ZW800-1. We can therefore conclude that the no observable adverse event level (NOAEL) in rats is at least 5.0 mg/kg. This confirms the absence of significant off-target inhibition by CRGD-ZW800-1, even at relatively high doses. A single, low dose of CRGD-ZW800-1 is therefore not expected to result in relevant clinical effects. The NOAEL of 5.0 mg/kg in rats is adjusted for body surface area a human equivalent dose (HED) of 0.80 mg/kg [32]. The US Food and Drug Administration (FDA) recommends to use 10% of the HED of the NOAEL to determine a safe starting dose [33]. A dose of 80 μ g/kg can therefore be considered as a safe starting dose for first-in-human studies. Furthermore, the dye ZW800-1 was separately evaluated (unpublished data) and showed no toxicity or adverse events in animal toxicity studies using doses of 24.5 mg/kg (HED 3.9 mg/kg). The RGD integrin-binding site is evolutionary conserved in vertebrates, including humans, mice, and rats [34]. Due to these similarities, animal models provide realistic expectations for first-in-patient studies. Adjusting the optimal dose in mice (10 nmol) into the HED shows the same dose range (63 μ g/kg). In a clinical study with a RGD-PET tracer the tumor uptake was $5.1 \pm 3.6\%$ injected dose per liter [35]. Assuming that the tumor uptake of CRGD-ZW800-1 will be comparable, the concentration inside tumors after administering 63 μ g/kg CRGD-ZW800-1 will be approximately 0.2 μ M. The FLARE[®] prototype system and other clinical systems can easily detect such concentrations (See also Figure S2, Supplementary data) [36]. Furthermore, this dose range is comparable to the optimal clinical dose of the similar sized fluorescent peptide OTL-38 for intraoperative fluorescence imaging of FRA α -positive ovarian cancer: 12.5 to 50 μ g/kg [8]. We conclude that targeting RGD-binding integrins appears to be safe. This is also suggested by a previous clinical study in which the CRGD-based integrin inhibitor cilengitide was intravenously administered at a dose of 2.0 g twice a week for a period up to 2 years without serious side effects [37].

CONCLUSION

In conclusion, due to its recognition of multiple integrins and its high affinity binding to a wide range of malignant and neoangiogenic cells, CRGD-ZW800-1 has the potential to become a sensitive and generic tool to visualize cancer during surgery.

MATERIALS AND METHODS

CRGD-ZW800-1 synthesis

The synthesis of CRGD-ZW800-1 was previously described [16].

Human cancer cell-lines

Human colorectal (HT-29-LUC2), pancreatic (BXPc-3-LUC2), squamous tongue (OSC-19-LUC2-CGFP), breast carcinoma (MCF-7-LUC2-CGFP), and glioblastoma (U-87 MG) cell line have been described previously [38, 39] (see also Supplementary Data).

Flow cytometry

Qifikit (DAKO) was used to determine the number of antigenic sites for the three most commonly described integrins $\alpha_V\beta_3$, $\alpha_V\beta_5$, and $\alpha_V\beta_6$ in the four cell lines with flow cytometry. Cells were grown to 90% confluence, detached with trypsin/EDTA (PAA), and counted using trypan blue. Cells were resuspended in DMEM/0.1%BSA/0.1%NaN₃ (wash- and dilution buffer), adjusted to 0.25×10^6 cells per tube, and incubated with anti- $\alpha_V\beta_3$ (Millipore, Clone LM609), $\alpha_V\beta_5$ (Millipore, Clone P1F6), $\alpha_V\beta_6$ (Millipore CLONE10D5), and isotype control antibody MOPC21 (BioXcell) at saturated conditions, for 30 min on ice. Cells and set-up and calibration beads were washed twice with wash buffer, followed by incubation with FITC-conjugated secondary antibody for 45 min on ice. After washing twice, propidium iodide was added to the cells. Cells and beads were measured on a BD LSRII flow cytometer (BD Biosciences). With the mean fluorescence intensity values of the calibration beads, a calibration curve was constructed. Using this curve the antigen density per cell for the different integrins was calculated.

In vitro binding and competition experiments

To evaluate the binding capacity of CRGD-ZW800-1, U-87 MG cells were plated in a 96-well plate at a density of ~40,000 cells per well. At 90-100% confluence, cells were washed and incubated with various concentrations of CRGD-ZW800-1 at 4°C or 37°C for 1 h (binding assay). CRGD-ZW800-1 was added to the U-87 MG cells in various concentrations: 0, 125, 250, 500, and 1000 nM.

For *in vitro* competition, U-87 MG ($\alpha_V\beta_3$ and $\alpha_V\beta_5$ positive, $\alpha_V\beta_6$ negative) and HT-29 ($\alpha_V\beta_3$ negative, $\alpha_V\beta_5$ and $\alpha_V\beta_6$ positive) cells were plated in a 96-well plate at a density of ~40,000 and ~60,000 cells per well, respectively. Subsequently, 500 nM of CRGD-ZW800-1 was simultaneously added to the cells and incubated at 37°C for 2 h. At the same time, half of the cells were also incubated with 500 nM unlabeled ("cold") CRGD.

Both the cells in the binding and the competition experiment were then washed twice and imaged with the Odyssey NIR scanner (LI-COR Biosciences, Lincoln, Nebraska: focus offset 3 mm; 800-nm channel). Next, cells were permeabilized with a 40/60 mixture of acetone and methanol followed by a washing step and a 5 min incubation with ToPro3 (1/2000, Invitrogen), a far red fluorescent dye (642/661nm). The wells were then washed and again imaged with the Odyssey scanner (focus offset 3 mm; 700-nm channel) to quantify the number of cells in each well. The experiments were performed in triplicate.

Identification of off-target interactions

Off-target interactions are binding of tracers to other components on the cell surface than the actual target site. These non-specific interactions are often of low affinity and easily missed, but can have significant effects. We outsourced the screening for *in vitro* for off-target interactions of CRGD-ZW800-1 to Eurofins Cerep SA, Le bois l'Évêque, France. They assessed the percentage of inhibition of a reference compound in 44 selected targets, including G protein-coupled receptors (GPCRs), transporters, ion channels, nuclear receptors, kinases and other non-kinase enzymes. These targets were recommended by four major pharmaceutical companies [40]. The complete list is included in Table S1 of the supplementary data. Each assay was performed twice using 10 μ M CRGD-ZW800-1 and a reference compound. Inhibition higher than 50% was considered to represent a significant effect of CRGD-ZW800-1. Results showing between 20% and 50% were considered weak to moderate effects, while lower than 20% was not considered significant and mostly attributable to variability of the signal around the control level.

Animal models

Six week-old athymic female mice (CD1-Foxn1^{NU}, Charles River Laboratories, Wilmington, MA, U.S.A.) were used and housed in ventilated cages. Normal pellet food and sterilized water were provided *ad libitum*. Throughout tumor inoculation and imaging procedures, animals were anesthetized with isoflurane. Each group consisted of 3 or more mice. The Animal Welfare Committee of Leiden University Medical Center approved all animal experiments for animal health, ethics, and research. All animals received humane care and maintenance in compliance with the “Code of Practice Use of Laboratory Animals in Cancer Research” (Inspectie WandV, July 1999).

To induce subcutaneous tumors, colorectal cancer cells (HT-29) were injected at 4 sites on the back (500,000 cells per spot). Subsequently, these colorectal tumor cells were transplanted on the colon of other mice, as described by Tseng *et al.* [41]. Approximately 500,000 pancreatic tumor cells (BXPc-3) were injected into the pancreas, as previously described by Kim *et al.* [42]. Approximately 40,000

oral tumor cells (OSC-19) were injected in the tongue, as previously described by van Driel *et al.* [39]. Approximately 500,000 breast tumor cells (MCF-7) were injected in both sides of the mammary fat pad to induce breast cancer tumors.

All animals were imaged using a Pearl[®] imager (LI-COR, Lincoln, NE) and an original FLARE[®] prototype. Animals with HT-29 tumors were imaged at 4 and 24 h post injection; animals with BXPc-3 and OSC-19 tumors at 4 h only. Animals with MCF-7 tumors were imaged at 0.5, 1, 2, 4, 6, 8, 24 and 48 h post injection. The specific and control images were normalized and regions of interest (ROIs) were selected using associated software. TBRs were calculated by dividing the tumor signal by the background signal. Based on our experience a TBR ≥ 2 is sufficient to discriminate between tumor and surrounding tissue [38].

After imaging, mice were sacrificed and OSC-19 and BXPc-3 tumors were quickly frozen in isopentane at -80°C for histological evaluation. Tissues were sectioned at 10 μ M and fluorescence imaging was performed using fluorescence microscopy (Nikon eclipse e800, Nikon, Amsterdam, The Netherlands). All histologic sections were stained with standard hematoxylin-eosin stain (HE). Organs of mice with colorectal and pancreatic cancer were collected and imaged using the Pearl[®] to evaluate biodistribution.

In vivo specificity

The binding specificity of CRGD-ZW800-1 was explored in a competition experiment using an excess of unlabeled CRGD (200-fold excess) co-injected with a standard dose of 10 nmol CRGD-ZW800-1 (n=4). Simultaneously, mice (n=3) were injected with 10 nmol CRGD-ZW800-1 as positive control. All mice had orthotopic HT-29 colon tumors. Images were acquired at 4 and 24 h post-injection after which animals were sacrificed and organs were resected and scanned with Pearl[®].

In vivo binding characteristics and biodistribution

Mice were administered with 0.25 (HT-29 model only), 1.0, 10, or 30 nmol CRGD-ZW800-1 to evaluate tumor signals, biodistribution, and to calculate TBRs (n=3 per dose group). At 4 h (BXPc-3 model) and 24 h (HT-29 model) after injection, mice were fully dissected and fluorescence intensity of their organs was measured.

Mice bearing orthotopic OSC-19 tumors (n=2) were administered with 10 nmol CRGD-ZW800-1 and imaged at 4 h. Mice bearing orthotopic MCF-7 tumors (n=2) were injected with 10 nmol CRGD-ZW800-1 and imaged at 0.5, 1, 2, 4, 6, 8, 24, and 48 h post injection. One mouse with 2 MCF-7 tumors was administered with 10 nmol CRGD-ZW800-1 and imaged at 4 h post injection while its skin was partially removed. In vivo TBRs were calculated by dividing the mean fluorescence signals of tumors by the mean of surrounding tissue. Ex vivo organ-to-tumor ratios were calculated by dividing the fluorescence intensity of the organ by that of the tumor.

Pharmacokinetics

CRGD-ZW800-1 was diluted in 0.05 mM HEPES buffered mouse serum to the concentrations 5.00, 4.50, 4.00, 3.50, 3.00, 2.50, 2.00, 1.50, 1.00, 0.50, 0.25, 0.13, 0.06, 0.03, and 0.02 μM . A calibration curve was created by measuring each concentration in 60 μL capillary tubes (Hirschmann® Laborgeräte GmbH and co. KG, Eberstadt, Germany) using the FLARE® with exposure times of: 1, 2, 5, 10, 25, 50, 100, 200, 500, 1000, and 2000 msec. Data were plotted in fluorescence intensity over concentration (μM) (Figure s2, supplementary data). For each exposure time, the formula of the linear regression line was calculated. Subsequently, 5 mice without tumors were injected with 10 nmol CRGD-ZW800-1 via the lateral tail vein. The contralateral lateral tail vein was used to draw blood on the time points -5, 1, 6, 10, 20, 30, 40, 50, 60, 90, 120, and 240 min. post injection. Blood samples were absorbed using 60 μL capillary tubes and immediately measured using the FLARE® with the same exposure times. Saturated images and those under the detection limit were excluded from analysis. Each measurement was calculated back to its concentration using the matching formulas (Figure s3, supplementary data). The mean of each formula output was used as the concentration. Data was analyzed using NONMEM® software (Icon Development Solutions, Ellicott City, MD, u.s.a.). Data were plotted in logarithmic and linear concentration (μM) over time (min).

Statistical analysis

For statistical analysis and the generation of graphs, GraphPad Prism software (version 5.01, GraphPad Software Inc., La Jolla, California, u.s.a.) was used. All values were reported using mean and standard deviation. Statistical significance for binding assay, *in vitro* and *in vivo* competition experiments, comparison of TBRS of the Pearl® and FLARE®, and comparison of fluorescence intensity of tumors was determined using the Holm-Sidak method. Differences in the biodistribution were calculated by two-way analysis of variance (ANOVA) and Dunnett for post-hoc testing. Group means were calculated for continuous data and medians were calculated for discrete data (scores). Test statistics were calculated on the basis of exact values for means and pooled variances. All tests were two-sided and in all an alpha of 5.0% was used.

Figure 1 Binding assay and *in vitro* and *in vivo* competition experiments. Binding assay of CRGD-ZW800-1 on intermediate integrin-expressing HT-29 cells shows an almost linear increase in fluorescence intensity with increasing applied concentrations. In addition, fluorescence signals are increased when cells are incubated at 37°C compared to 4°C with the various concentrations ($p < 0.0001$). This may be the result of enhanced internalization of the agent. *In vitro* competition experiment (1:1 ratio) using unlabeled CRGD (competition group) showing decreased NIR fluorescent signals in both the $\alpha_V\beta_3$ positive U-87 MG (* $p < 0.05$) as well as the $\alpha_V\beta_3$ negative HT-29 cell line compared to the control without unlabeled CRGD. Healthy colon was used as background. *In vivo* competition experiment using a 200 times higher dose of unlabeled CRGD compared to the dose of CRGD-ZW800-1 (1.24 mg, 2.0 μMol vs. 15.5 μg , 10 nmol) in the orthotopic HT-29 model. Compared to mice in the control group, a significant decrease in TBR was seen at 4 h (* $p = 0.02$) and 24 h (** $p = 0.007$). Healthy colon was used as background.

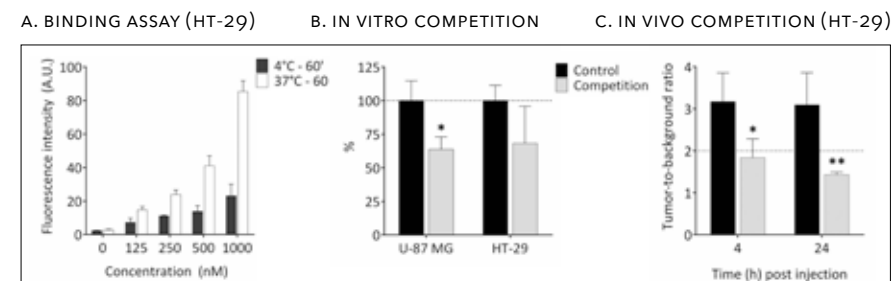
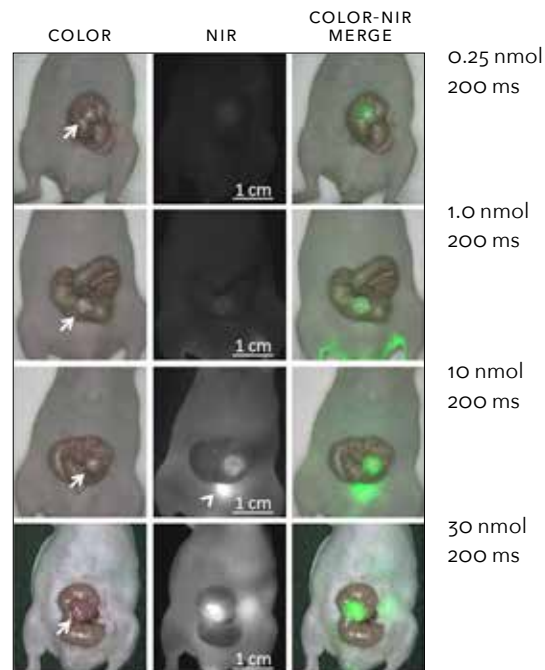
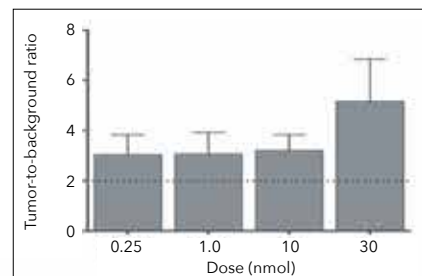


Figure 2 Near-infrared fluorescence imaging of colorectal cancer (HT-29). Representative images captured using the original FLARE® prototype of the various concentrations at 4 h post injection. For the 30 nmol dose group the exposure time had to be set at 50 msec due to saturation of the near-infrared fluorescence images. For the other dose groups 200 msec was sufficient. NIR fluorescence signals are clearly visible in 10 and 30 nmol groups only. Arrow=tumor; arrowhead=bladder. Near-infrared fluorescence imaging at 4 h post injection showed sufficient tumor-to-background ratios (i.e. ≥ 2) already in the 0.25 nmol (0.39 μg) dose group using the Pearl®. Surrounding tissue was used as background. Near-infrared fluorescence imaging using the Pearl® at 24 h post injection still showed sufficient tumor-to-background ratios in the 1.0, 10 and 30 nmol dose groups. Healthy tongue tissue was used as background.

A. IMAGING OF COLERECTAL CANCER (FLARE®)



B. IMAGING AT 4 H POST INJECTION (PEARL®)



C. IMAGING AT 24 H POST INJECTION (PEARL®)

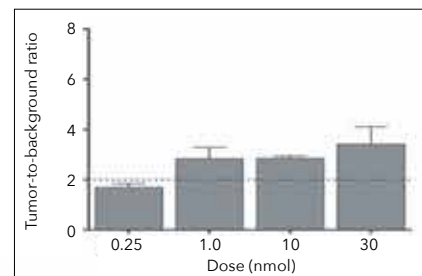
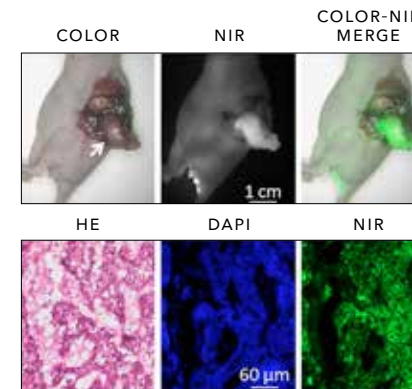
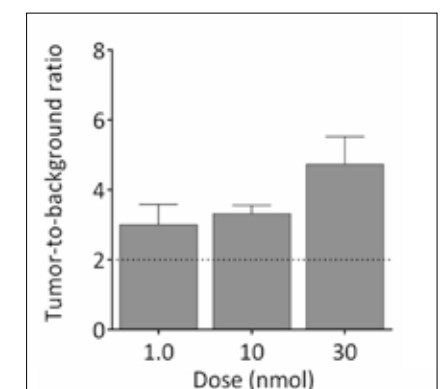


Figure 3 Near-infrared fluorescence imaging of pancreatic (BXPc-3) and oral cancer (OSC-19). Upper panel: example showing the in vivo images of 30 nmol CRGD-ZW800-1 in the orthotopic pancreas model at 4 h post injection using the original FLARE® prototype. Arrow=tumor. Lower panel: NIR fluorescence microscopy of the tumor shows fluorescence inside the cells. Mean tumor-to-background ratios at 4 h post injection in the BXPc-3 model with the Pearl®. Skin was used as background. Upper panel: example of images from the orthotopic OSC-19 model at 4 h using the original FLARE® prototype. Arrow=tumor. Lower panel: NIR fluorescence microscopy shows the border of a resected OSC-19 tumor. Clear fluorescent demarcation between normal and tumor tissue is shown (white dotted line). T=tumor; N=normal tissue surrounding the tumor. Mean tumor-to-background ratios of the optimal dose 10 nmol at 4 h in the orthotopic head-and-neck cancer model using the Pearl®.

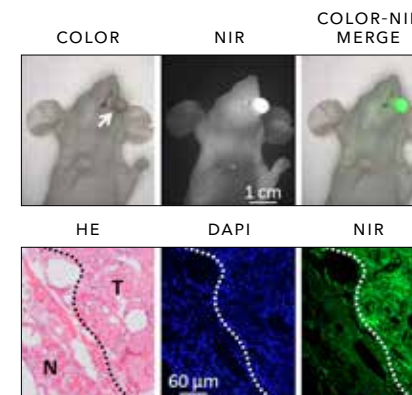
A. IMAGING OF PANCREATIC CANCER (FLARE®)



B. IMAGING AT 4 H POST INJECTION (PEARL®)



C. IMAGING OF ORAL CANCER (FLARE®)



D. IMAGING AT 24 H POST INJECTION (PEARL®)

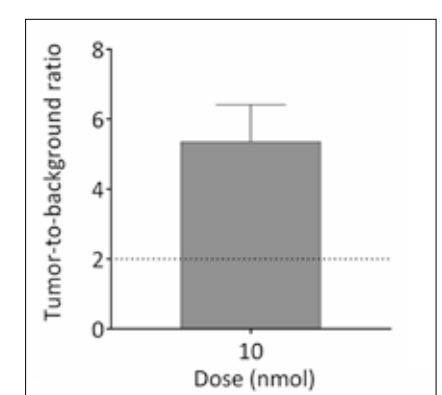


Figure 4 Near-infrared fluorescence imaging of breast cancer (MCF-7). Representative images captured with the Pearl® of the various time points after administration of 10 nmol CRGD-ZW800-1 in a xenograft breast cancer model. Arrowhead: bladder, arrows: tumors. All images are identically scaled. Tumor-to-background ratios over time measured using the Pearl®. Fluorescence intensity of tumors compared with 0.5 h post injection using the Pearl®.

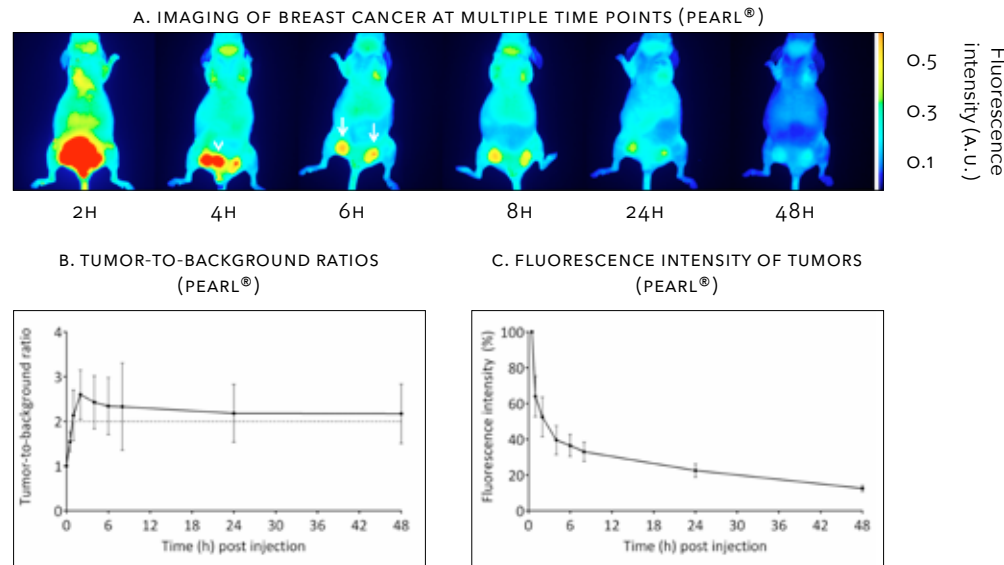


Figure 5 Biodistribution of crgd-zw800-1. *In vivo* fluorescence intensity of BxPC-3 and HT-29 tumors at 4 h post injection of several doses of CRGD-ZW800-1 using the Pearl®. Significant differences (* $p < 0.05$; ** $p < 0.01$) were seen in the 10 nmol dose group ($p < 0.05$). The *ex vivo* fluorescence intensity of BxPC-3 tumors were used to calculate the organ-to-tumor ratios at 4 h post injection. Compared to the 10 nmol dose group, significant differences were seen between kidneys (1.0 nmol: $p < 0.05$; 30 nmol: $p < 0.01$), liver (1.0 nmol: $p < 0.05$) and large intestines (1.0 nmol: $p < 0.05$). In all dose groups, tumors were more than twice as fluorescent compared to skin, intestines, lungs, muscle, brain, gallbladder, and blood. *In vivo* fluorescence intensity of HT-29 tumors at 4 and 24 h post injection of several doses. Significant differences (*) were seen in the 10 nmol dose group ($p < 0.05$). The *ex vivo* fluorescence intensity of HT-29 tumors were used to calculate the organ-to-tumor ratios at 24 h post injection. Compared to the 10 nmol dose group, significant differences (*) were seen between kidneys (1.0 nmol and 30 nmol: $p < 0.05$). In all dose groups, tumors were more than twice as fluorescent compared to lungs, pancreas, muscle, gallbladder, brain, and blood.

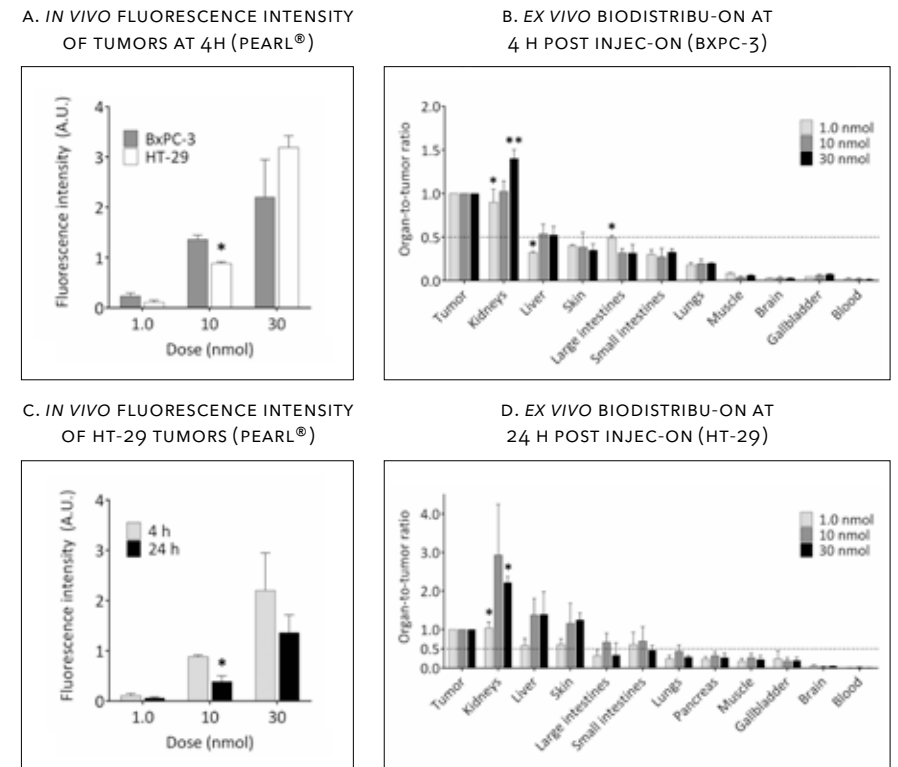


Figure 6 Pharmacokinetics of 10 nmol CRGD-ZW800-1. Graph shows the mean absolute concentrations (in μM) after intravenous administration of 10 nmol CRGD-ZW800-1 up to 240 min post injection. 1) AUC calculated via trapezoid rule. 2) Half-life calculated via $\ln(2)/k_{10}$.

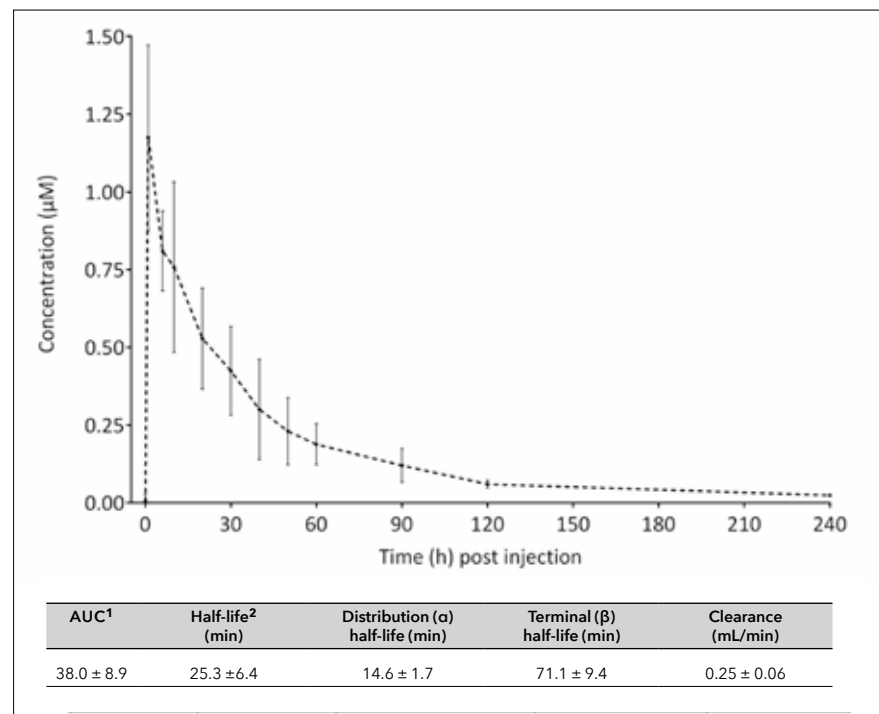


Table 1 The expression of integrins $\alpha_v\beta_3$, $\alpha_v\beta_5$ and $\alpha_v\beta_6$ on tumor cell lines

	U-87 MG	HT-29	MCF-7	BXPC-3	OSC-19
$\alpha_v\beta_3$	59,500	0	0	4,500	0
$\alpha_v\beta_5$	17,500	32,500	19,500	4,000	2,000
$\alpha_v\beta_6$	0	10,500	0	18,500	20,000

The number of antigenic sites for $\alpha_v\beta_3$, $\alpha_v\beta_5$, and $\alpha_v\beta_6$ integrins per individual cell of the U-87 MG, HT-29, BXPC3, MCF-7, and OSC-19 cell lines using Qifikit (DAKO) for quantitative flow cytometric analysis.

REFERENCES

- Vahrmeijer AL, Hutteman M, van der Vorst JR, van de Velde CJ and Frangioni JV. Image-guided cancer surgery using near-infrared fluorescence. *Nat Rev Clin Oncol.* 2013; 10(9):507-518.
- Sevick-Muraca EM, Houston JP and Gurfinkel M. Fluorescence-enhanced, near infrared diagnostic imaging with contrast agents. *Curr Opin Chem Biol.* 2002; 6(5):642-650.
- Ishizawa T, Fukushima N, Shibahara J, Masuda K, Tamura S, Aoki T, Hasegawa K, Beck Y, Fukayama M and Kokudo N. Real-time identification of liver cancers by using indocyanine green fluorescent imaging. *Cancer.* 2009; 115(11):2491-2504.
- Rosenthal EL, Warram JM, de Boer E, Chung TK, Korb ML, Brandwein-Gensler M, Strong TV, Schmalbach CE, Morlandt AB, Agarwal G, Hartman YE, Carroll WR, Richman JS, Clemons LK, Nabell LM and Zinn KR. Safety and Tumor Specificity of Cetuximab-IRDye800 for Surgical Navigation in Head and Neck Cancer. *Clin Cancer Res.* 2015; 21(16):3658-3666.
- Warram JM, de Boer E, Sorace AG, Chung TK, Kim H, Pleijhuis RG, van Dam GM and Rosenthal EL. Antibody-based imaging strategies for cancer. *Cancer Metastasis Rev.* 2014; 33(2-3):809-822.
- Frangioni JV. New technologies for human cancer imaging. *J Clin Oncol.* 2008; 26(24):4012-4021.
- Burggraaf J, Kamerling IM, Gordon PB, Schrier L, de Kam ML, Kales AJ, Bendiksen R, Indrevoll B, Bjerke RM, Moestue SA, Yazdanfar S, Langers AM, Swaerd-Nordmo M, Torheim G, Warren MV, Morreau H, et al. Detection of colorectal polyps in humans using an intravenously administered fluorescent peptide targeted against c-Met. *Nat Med.* 2015; 21(8):955-961.
- Hoogstins CE, Tummers QR, Gaarenstroom KN, de Kroon CD, Trimbos JB, Bosse T, Smit VT, Vuyk J, van de Velde CJ, Cohen AF, Low PS, Burggraaf J and Vahrmeijer AL. A Novel Tumor-Specific Agent for Intraoperative Near-Infrared Fluorescence Imaging: A Translational Study in Healthy Volunteers and Patients with Ovarian Cancer. *Clin Cancer Res.* 2016; 22(12):2929-2938.
- Desgrosellier JS and Cheresh DA. Integrins in cancer: biological implications and therapeutic opportunities. *Nat Rev Cancer.* 2010; 10(1):9-22.
- Schittenhelm J, Klein A, Tatagiba MS, Meyermann R, Fend F, Goodman SL and Sipos B. Comparing the expression of integrins $\alpha_v\beta_3$, $\alpha_v\beta_5$, $\alpha_v\beta_6$, $\alpha_v\beta_8$, fibronectin and fibrinogen in human brain metastases and their corresponding primary tumors. *Int J Clin Exp Pathol.* 2013; 6(12):2719-2732.
- Sharma R, Kallur KG, Ryu JS, Parameswaran RV, Lindman H, Avril N, Gleeson FV, Lee JD, Lee KH, O'Doherty MJ, Groves AM, Miller MP, Somers EJ, Coombes CR and Aboagye EO. Multicenter Reproducibility of 18F-Fluciclatide PET Imaging in Subjects with Solid Tumors. *J Nucl Med.* 2015; 56(12):1855-1861.
- Beer AJ, Haubner R, Sarbia M, Goebel M, Luderschmidt S, Grosu AL, Schnell O, Niemeyer M, Kessler H, Wester HJ, Weber WA and Schwaiger M. Positron emission tomography using [18F]Galacto-RGD identifies the level of integrin $\alpha_v\beta_3$ expression in man. *Clin Cancer Res.* 2006; 12(13):3942-3949.
- Beer AJ, Lorenzen S, Metz S, Herrmann K, Watzlowik P, Wester HJ, Peschel C, Lordick F and Schwaiger M. Comparison of integrin $\alpha_v\beta_3$ expression and glucose metabolism in primary and metastatic lesions in cancer patients: a PET study using 18F-galacto-RGD and 18F-FDG. *J Nucl Med.* 2008; 49(1):22-29.
- Beer AJ, Niemeyer M, Carlsen J, Sarbia M, Nahrig J, Watzlowik P, Wester HJ, Harbeck N and Schwaiger M. Patterns of $\alpha_v\beta_3$ expression in primary and metastatic human breast cancer as shown by 18F-Galacto-RGD PET. *J Nucl Med.* 2008; 49(2):255-259.
- Verbeek FP, van der Vorst JR, Tummers QR, Boonstra MC, de Rooij KE, Lowik CW, Valentijn AR, van de Velde CJ, Choi HS, Frangioni JV and Vahrmeijer AL. Near-infrared fluorescence imaging of both colorectal cancer and ureters using a low-dose integrin targeted probe. *Ann Surg Oncol.* 2014; 21 Suppl 4:S528-537.
- Choi HS, Gibbs SL, Lee JH, Kim SH, Ashitate Y, Liu F, Hyun H, Park G, Xie Y, Bae S, Henary M and Frangioni JV. Targeted zwitterionic near-infrared fluorophores for improved optical imaging. *Nat Biotechnol.* 2013; 31(2):148-153.
- Ruoslahti E. RGD and other recognition sequences for integrins. *Annu Rev Cell Dev Biol.* 1996; 12:697-715.
- Brooks PC, Montgomery AM, Rosenfeld M, Reisfeld RA, Hu T, Klier G and Cheresh DA. Integrin $\alpha_v\beta_3$ antagonists promote tumor regression by inducing apoptosis of angiogenic blood vessels. *Cell.* 1994; 79(7):1157-1164.
- Humphries JD, Byron A and Humphries MJ. Integrin ligands at a glance. *J Cell Sci.* 2006; 119(Pt 19):3901-3903.
- Fang J, Nakamura H and Maeda H. The EPR effect: Unique features of tumor blood vessels for drug delivery, factors involved, and limitations and augmentation of the effect. *Adv Drug Deliv Rev.* 2011; 63(3):136-151.
- Huang R, Vider J, Kovar JL, Olive DM, Mellinghoff IK, Mayer-Kuckuk P, Kircher MF and Blasberg RG. Integrin $\alpha_v\beta_3$ -targeted IRDye 800CW near-infrared imaging of glioblastoma. *Clin Cancer Res.* 2012; 18(20):5731-5740.
- Ke S, Zhang F, Wang W, Qiu X, Lin J, Cameron AG, Zou C, Gao X, Zou C, Zhu VF and Li M. Multiple target-specific molecular imaging agents detect

- liver cancer in a preclinical model. *Curr Mol Med.* 2012; 12(8):944-951.
- 23 Yoon Y, Mohs AM, Mancini MC, Nie S and Shim H. Combination of an Integrin-Targeting NIR Tracer and an Ultrasensitive Spectroscopic Device for Intraoperative Detection of Head and Neck Tumor Margins and Metastatic Lymph Nodes. *Tomography.* 2016; 2(3):215-222.
 - 24 Cao J, Wan S, Tian J, Li S, Deng D, Qian Z and Gu Y. Fast clearing RGD-based near-infrared fluorescent probes for in vivo tumor diagnosis. *Contrast Media Mol Imaging.* 2012; 7(4):390-402.
 - 25 Cheng H, Chi C, Shang W, Rengaowa S, Cui J, Ye J, Jiang S, Mao Y, Zeng C, Huo H, Chen L and Tian J. Precise integrin-targeting near-infrared imaging-guided surgical method increases surgical qualification of peritoneal carcinomatosis from gastric cancer in mice. *Oncotarget.* 2016.
 - 26 Choi HS, Nasr K, Alyabyev S, Feith D, Lee JH, Kim SH, Ashitate Y, Hyun H, Patonay G, Strekowski L, Henary M and Frangioni JV. Synthesis and in vivo fate of zwitterionic near-infrared fluorophores. *Angew Chem Int Ed Engl.* 2011; 50(28):6258-6263.
 - 27 Sasaki Y, Iwama R, Sato T, Heishima K, Shimamura S, Ichijo T, Satoh H and Furuhashi K. Estimation of glomerular filtration rate in conscious mice using a simplified equation. *Physiol Rep.* 2014; 2(8).
 - 28 Morgan MR, Hamidi H, Bass MD, Warwood S, Ballestrem C and Humphries MJ. Syndecan-4 phosphorylation is a control point for integrin recycling. *Dev Cell.* 2013; 24(5):472-485.
 - 29 Hyun H, Owens EA, Narayana L, Wada H, Gravier J, Bao K, Frangioni JV, Choi HS and Henary M. Central C-C Bonding Increases Optical and Chemical Stability of NIR Fluorophores. *RSC Adv.* 2014; 4(102):58762-58768.
 - 30 Ruegg C, Dormond O and Mariotti A. Endothelial cell integrins and COX-2: mediators and therapeutic targets of tumor angiogenesis. *Biochim Biophys Acta.* 2004; 1654(1):51-67.
 - 31 Crofford LJ, Breyer MD, Strand CV, Rushitzka F, Brune K, Farkouh ME and Simon LS. Cardiovascular effects of selective COX-2 inhibition: is there a class effect? The International COX-2 Study Group. *J Rheumatol.* 2006; 33(7):1403-1408.
 - 32 Reagan-Shaw S, Nihal M and Ahmad N. Dose translation from animal to human studies revisited. *FASEB J.* 2008; 22(3):659-661.
 - 33 FDA. Estimating the safe starting dose in clinical trials for therapeutics in adult healthy volunteers. pp. 2340-2341.
 - 34 Piha-Gossack A, Sossin W and Reinhardt DP. The evolution of extracellular fibrillins and their functional domains. *PLoS One.* 2012; 7(3):e33560.
 - 35 Beer AJ, Haubner R, Goebel M, Luderschmidt S, Spilker ME, Wester HJ, Weber WA and Schwaiger M. Biodistribution and pharmacokinetics of the alphavbeta3-selective tracer 18F-galacto-RGD in cancer patients. *J Nucl Med.* 2005; 46(8):1333-1341.
 - 36 van Driel PB, van de Giessen M, Boonstra MC, Snoeks TJ, Keereweer S, Oliveira S, van de Velde CJ, Lelieveldt BP, Vahrmeijer AL, Lowik CW and Dijkstra J. Characterization and evaluation of the artemis camera for fluorescence-guided cancer surgery. *Mol Imaging Biol.* 2015; 17(3):413-423.
 - 37 Stupp R, Hegi ME, Gorlia T, Erridge SC, Perry J, Hong YK, Aldape KD, Lhermitte B, Pietsch T, Grunjevic D, Steinbach JP, Wick W, Tarnawski R, Nam DH, Hau P, Weyerbrock A, et al. Cilengitide combined with standard treatment for patients with newly diagnosed glioblastoma with methylated MGMT promoter (CENTRIC EORTC 26071-22072 study): a multicentre, randomised, open-label, phase 3 trial. *Lancet Oncol.* 2014; 15(10):1100-1108.
 - 38 Boonstra MC, Tolner B, Schaafsma BE, Boogerd LS, Prevoo HA, Bhavsar G, Kuppen PJ, Sier CF, Bosing BA, Frangioni JV, van de Velde CJ, Chester KA and Vahrmeijer AL. Preclinical evaluation of a novel CEA-targeting near-infrared fluorescent tracer delineating colorectal and pancreatic tumors. *Int J Cancer.* 2015; 137(8):1910-1920.
 - 39 van Driel PB, van der Vorst JR, Verbeek FP, Oliveira S, Snoeks TJ, Keereweer S, Chan B, Boonstra MC, Frangioni JV, van Bergen en Henegouwen PM, Vahrmeijer AL and Lowik CW. Intraoperative fluorescence delineation of head and neck cancer with a fluorescent anti-epidermal growth factor receptor nanobody. *Int J Cancer.* 2014; 134(11):2663-2673.
 - 40 Bowes J, Brown AJ, Hamon J, Jarolimek W, Sridhar A, Waldron G and Whitebread S. Reducing safety-related drug attrition: the use of in vitro pharmacological profiling. *Nat Rev Drug Discov.* 2012; 11(12):909-922.
 - 41 Tseng W, Leong X and Engleman E. Orthotopic mouse model of colorectal cancer. *J Vis Exp.* 2007; (10):484.
 - 42 Kim MP, Evans DB, Wang H, Abbruzzese JL, Fleming JB and Gallick GE. Generation of orthotopic and heterotopic human pancreatic cancer xenografts in immunodeficient mice. *Nat Protoc.* 2009; 4(11):1670-1680.

CHAPTER 11

Real-time near-infrared fluorescence imaging with ZW800-1 and CRGD-ZW800-1: a translational study in healthy human volunteers

ABSTRACT

INTRODUCTION ZW800-1 is a new “zwitterionic” fluorophore that can be used for near-infrared fluorescence (NIRF) imaging of the urinary tract. Moreover, it is easily conjugated to targeting moieties, such as CRGD, a protein targeting integrins associated with neoangiogenesis. The aim of this translational study was to determine toxicity of both ZW800-1 and CRGD-ZW800-1 in animals, and to assess their tolerability and pharmacokinetics of single doses in healthy human volunteers.

METHODS ZW800-1 and CRGD-ZW800-1 were studied separately. Preclinical toxicology studies were performed to assess a safe starting dose for first-in-human studies. Subsequently, safety, tolerability and pharmacokinetics were assessed in two phase 1 studies in healthy volunteers. We performed randomized, double blind, placebo-controlled, single intravenous dose studies. Safety was assessed by recording pre-administration events, adverse events (AEs), clinical laboratory parameters, vital signs, ECGs, physical examination and injection site monitoring. Fluorescence imaging of the skin was performed frequently to assess the perfusion.

RESULTS Safe starting doses were 0.39 mg/kg and 0.08 mg/kg for ZW800-1 and CRGD-ZW800-1, respectively. None of the healthy volunteers experienced any acute or chronic toxicity, and specifically no hypersensitivity reactions were seen. Doses up to 5.0 mg ZW800-1 and 0.005 mg/kg CRGD-ZW800-1 were well-tolerated. The majority of both tracers could be retrieved in urine within 1 hour after administration.

CONCLUSION This translational study demonstrates that single IV administration of ZW800-1 or CRGD-ZW800-1 is safe. Subsequent Phase 2 studies need to assess the feasibility and the optimal doses to identify ureters with ZW800-1 and various tumors with CRGD-ZW800-1.

INTRODUCTION

Intraoperative near-infrared (NIR) fluorescence imaging is in the midst of a Renaissance. Multiple imaging systems are commercially available for preclinical and clinical purposes and their sensitivity has improved greatly over the past years. However, success of these systems goes hand-in-hand with the quality of NIR fluorophores. An important challenge in NIR fluorescence imaging is the development of fluorophores with optimal optical and *in vivo* properties. The well-known NIR fluorophore indocyanine green (ICG) is safe, clinically available and has been used extensively, e.g. for bile duct imaging and assessment of tissue or skin perfusion.[1] However, ICG is far from ideal due to the exclusive hepatic clearance, resulting in high uptake in liver and contamination of the gastrointestinal (GI) tract.[2] Moreover, ICG cannot be conjugated to targeting moieties. Other anionic fluorophores, including IRDYE800CW and CY5.5, are conjugatable, but show similar uptake in the liver and the GI tract.[3] Elimination patterns are important especially when imaging GI tumors, e.g. colorectal, pancreatic or liver cancer. Hepatic clearance results in nonspecific background fluorescence, which can reduce the target-to-background ratio (TBR). Recently, the zwitterionic fluorophore ZW800-1 has been introduced.[4] ZW800-1 exhibits low non-specific uptake and exclusive renal clearance. A preclinical study in rats demonstrated that the ureters became fluorescent within minutes after a low dose of ZW800-1 and remained visible for several hours. These characteristics combined with its extraordinary brightness (i.e. quantum yield times extinction coefficient) make ZW800-1 an ideal candidate to visualize the urinary tract during surgery. Iatrogenic ureteral injury is a rare but serious complication of lower abdominal surgery, with incidences varying from 0.4% up to 10%.[5-7] Since NIR light can penetrate through 5-10 mm of tissue, even ureters that are not fully exposed can be detected with ZW800-1. Furthermore, ZW800-1 can easily be conjugated through N-hydroxysuccinimide (NHS) esters, tetrafluorophenyl (TFP) esters, or maleimide to any ligand. ZW800-1 can therefore be used to target tumors in the GI tract. For instance, CRGD-ZW800-1 has shown to be useful in identifying colorectal and pancreatic tumors in animal cancer models without contamination of the liver and intestines.[8] The aim of this translational study was to determine toxicity of both ZW800-1 and CRGD-ZW800-1 in animals, and assess their tolerability and pharmacokinetics of a single dose in healthy volunteers.

METHODS

Ethical committee approval

Both studies were approved by a certified medical ethics review board and conducted in concordance with the Helsinki Declaration of 1975 (as amended in Tokyo,

Venice, Hong Kong, Somerset West, Edinburgh, Washington, and Seoul), ICH-GCP guidelines, and the laws and regulations of the Netherlands. All subjects provided written informed consent prior to the start of any study-related procedure.

PART I: ZW800-1

Investigational product

ZW800-1 (molecular formula $C_{51}H_{66}N_4O_9S_2$; molecular weight 943 Da) is a small zwitterionic molecule fluorescent at approximately 800 nm. It was manufactured in the Peptide Laboratory of the Interdivisional GMP Facility of the Leiden University Medical Center (IGFL) using methods that were previously described. [9] The product was aseptically lyophilized in sterile single dose vials, each containing 5.1 mg ZW800-1 without additional excipients. ZW800-1 was ready for intravenous (IV) administration after aseptic reconstitution in 5% dextrose in water. Placebo consisted of 0.9% sodium chloride solution.

Toxicology

Preclinical toxicity studies were conducted to characterize the toxicity of ZW800-1. Specific studies to characterize the safety profile included: 1) off-target receptor binding assay, recommended by four major pharmaceutical companies [10]; 2) bacterial mutation assay; 3) single infusion range-finding toxicity studies in rats and dogs to support definitive single IV infusion toxicity study in rats (with a genotoxicity and functional observation assessment) and single dose toxicity study in dogs; 4) a single IV infusion study to evaluate cardiovascular and respiratory function in conscious telemetered dogs.

Safety and tolerability

A single dose, randomized, placebo-controlled study in healthy volunteers was designed to determine the tolerability and pharmacokinetics in humans. The study was performed double-blinded: investigator, staff, and subjects were blinded with respect to the treatment until the end of the study. The placebo and ZW800-1 were formulated identically and syringes were wrapped in aluminum foil. The IV lines were covered during dosing and flushed directly afterwards with saline. Independent physicians administered ZW800-1 or placebo and performed NIR fluorescence imaging.

Preclinical studies demonstrated that ureter visualization in rats was possible with 40 nmol/kg [4], which corresponds to a human equivalent dose (HED; based on Reagan-Shaw formula [11]) of 0.5 mg for a 70 kg adult. Three dose levels of ZW800-1 were investigated in three non-overlapping cohorts (0.5, 2.5 and 5.0 mg).

Within the first cohort a sentinel approach was used: on the first day, two subjects were administered the study drug in a 1:1 ratio for ZW800-1 and placebo. The other subjects in this cohort were randomized to a 3:1 ratio for ZW800-1 and placebo. In the following cohorts five subjects were randomized in a ratio of 4:1 for ZW800-1 and placebo.

Safety was assessed by recording pre-administration events, adverse events (AEs), clinical laboratory parameters, vital signs, ECGs, physical examination and injection site monitoring.

Pharmacokinetics

Pharmacokinetics was assessed by collecting blood and urine samples at defined time points. Blood and urine samples were measured with the Pearl Impulse (LI-COR, Biosciences, Lincoln, NE, US) and ZW800-1 concentrations were estimated using calibration curves in fresh human blood and phosphate-buffered saline (PBS), respectively. Results were analyzed with software dedicated for PK analysis.

NIR fluorescence imaging of the feet of volunteers was performed frequently with the Lab-FLARE® Model R1 Open Space Imaging System (Curadel ResVet Imaging, LLC, Marlborough, MA) to assess the perfusion and uptake of ZW800-1 in the skin. The signal-to-baseline ratio (SBR) was calculated by dividing the signal of the skin by the signal at baseline.

PART II: CRGD-ZW800-1

Investigational product

ZW800-1 was conjugated to CRGDYK, resulting in CRGD-ZW800-1 (molecular formula $C_{78}H_{106}N_{13}O_{16}S_2$; molecular weight 1729 Da). It was manufactured in the Peptide Laboratory of the Interdivisional GMP Facility of the Leiden University Medical Center (IGFL). The product was aseptically lyophilized in sterile single dose vials each containing 0.725 mg without additional excipients. ZW800-1 was ready for IV administration after aseptic reconstitution into 0.9% sodium chloride solution. Placebo consisted of 0.9% sodium chloride solution.

Toxicology

Preclinical studies demonstrated that tumor visualization in mice was possible after IV administration of 10 nmol [12], which corresponds to a HED of 0.06 mg/kg. Based on these results, a generic extended non-clinical toxicity study in rats was designed, including control groups and two treatment groups with single doses 15.0 mg/kg and 5.0 mg/kg CRGD-ZW800-1 according to ICH M3 (R2), FDA, EMEA and GLP regulations. Both dose groups consisted of 10 males and 10 females,

which were subjected to a full *post mortem* examination on day 2 post dosing. In addition, 5 recovery animals per sex were added in the control and 5.0 mg/kg dose group and were followed for 14 days post dosing.

Safety and tolerability

A single dose, randomized, placebo-controlled study in healthy volunteers was designed to determine tolerability and pharmacokinetics in healthy volunteers. The study was performed double-blinded: investigator, staff, and subjects were blinded with respect to the treatment until the end of the study. The placebo and CRGD-ZW800-1 were formulated identically and syringes were wrapped in aluminum foil. The IV lines were covered during dosing and flushed directly afterwards with saline. Independent physicians administered the test substance and performed NIR fluorescence imaging.

Two dose levels of CRGD-ZW800-1 were investigated in two non-overlapping cohorts. Within the first cohort a sentinel approach with microdosing (0.001 mg/kg) was used: on the first day, two subjects were administered the study drug in a 1:1 ratio for CRGD-ZW800-1 and placebo. The other subjects in this cohort were randomized to a 3:1 ratio for CRGD-ZW800-1 and placebo. In the second cohort five subjects were randomized in a ratio of 4:1 for 0.005 mg/kg CRGD-ZW800-1 and placebo.

Safety was assessed by recording pre-administration events, adverse events (AEs), clinical laboratory parameters, vital signs, ECGs, physical examination and injection site monitoring.

Pharmacokinetics

Pharmacokinetics was assessed by collecting blood and urine samples at defined time points. Blood and urine samples were measured with the Pearl Impulse (LI-COR, Biosciences, Lincoln, NE, US) and CRGD-ZW800-1 concentrations were estimated using calibration curves in fresh human blood and phosphate-buffered saline (PBS), respectively. Results were analyzed with software dedicated for PK analysis.

NIR fluorescence imaging of the volunteer's hand was performed frequently with the Lab-FLARE® Model R1 Open Space Imaging System to assess the perfusion and uptake of CRGD-ZW800-1 in the skin. The signal-to-baseline ratio (SBR) was calculated by dividing the signal of the skin by the signal at baseline.

RESULTS

PART I: ZW800-1

Toxicology

ZW800-1 showed no significant inhibition of 44 selected targets. No evidence of genotoxicity was observed in the *in vitro* bacterial mutation assay, *in vivo* micronucleus using hematopoietic cells or Comet assays for the assessment of DNA strand breakage in liver cells.

The No Observable Adverse Event Level (NOAEL) in rats was 24.5 mg/kg. The HED of that NOAEL was set at 3.95 mg/kg. The Maximum Tolerated Dose (MTD) in rats was 1,000 mg/kg. The NOAEL in dogs was 14 mg/kg (HED 7.78 mg/kg) and the MTD was 280 mg/kg.

The cardiovascular and respiratory study in dogs indicated that administration of a single IV 30 minute infusion of ZW800-1 at doses of 0.7 and 7.0 mg/kg does not elicit any acute effects on the cardiovascular, pulmonary, or body temperature parameters.

Based on these nonclinical studies, a safe starting dose for IV administration in humans could be recommended. The rat was considered the more sensitive species based on the NOAEL. It was recommended to use 10% of the HED derived from the rat NOAEL as a starting dose for a Phase 1 clinical trial.[13] Thus, a safe starting dose would be $1/10 * 3.9 = 0.39 \text{ mg/kg} = 27.3 \text{ mg}$ for a 70 kg adult.

Safety and tolerability

In the phase 1 study, a total of 16 healthy volunteers were enrolled. There were no serious adverse events reported during the study and no volunteers experienced an AE leading to discontinuation. Seven volunteers reported a total of 10 AEs, all scored with a mild severity. Four of the 10 reported AEs were considered possibly related to the study drug: headache at 6 hours post dosing of 2.5 mg ZW800-1, which was successfully treated with paracetamol; tiredness at 1 hour post dosing of 2.5 mg ZW800-1, which was resolved the next morning after a good night sleep; urinary tract infection with positive nitrite in urine diagnosed at 48 hours post dosing of 2.5 mg ZW800-1; and an increased appetite starting 2 hours post-dosing of 5 mg ZW800-1.

Five reported AEs were procedural complications, including infusion site discomfort due to blood withdrawal, hematoma at the cannula site, subcutaneous infusion (n=2) and skin irritation at the ECG sticker sites. One AE was considered unrelated: influenza diagnosed during follow-up (placebo group). No clinically significant changes were observed in the vital signs, clinical laboratory tests or ECGs after dosing. Overall, all three doses were tolerated well.

Pharmacokinetics

ZW800-1 concentrations were measurable up to 24 to 48 hours post dose in blood and urine samples. The results are shown in Figure 1. Of the 16 included healthy volunteers, two volunteers (one from the 5 mg dosing group and one from the 2.5 mg dosing group) were completely excluded due to subcutaneous infusion of the study drug. Subcutaneous infusion did not lead to local side effects. Blood PK data from one volunteer (2.5 mg dose cohort) was excluded because the blood was drawn from the ZW800-1 infusion cannula, tampering with the accuracy of the fluorescence data. However, the urine and skin data was included. Skin data from the second volunteer in the 0.5 mg dose cohort was excluded due to suboptimal imaging settings.

The maximum blood plasma concentration in the included healthy volunteers was achieved at 6 min post dosing. After peaking directly after intravenous administration, the ZW800-1 serum concentration declined with a biphasic pattern with a distribution and an elimination phase. The cumulative excretion of ZW800-1 decreased with increasing dose. The majority of the injected dose was cleared renally within the first four hours after dosing. In the lowest dose group (0.5 mg) an average cumulative excretion of 93% ZW800-1 was observed at 12 hours post dosing. In the higher dosing cohorts, 2.5 mg and 5 mg, the average cumulative excretion of ZW800-1 12 hours post dosing was 70% and 63% respectively. No differences were observed between males and females.

PART II: CRGD-ZW800-1

Toxicology

No treatment-related mortality occurred, and no significant clinical signs, changes in clinical pathology or macroscopic and microscopic alterations were seen in the rats. Discolored (green) urine was observed in both the 5.0 and 15.0 mg/kg dose groups on the day of treatment. No effects compared to the control group on body weight, food consumption, hematology, clinical biochemistry or macroscopic and microscopic alterations were observed. One accidental death (control male at day 2) occurred due to blood sampling and no clinical signs, no findings on clinical pathology, or microscopic findings indicating cause of death were noted. Routine hematology parameters and clinical biochemistry remained within the normal range and were considered not toxicologically relevant. Histopathological examination did not raise a safety signal. Microscopic findings at the injection site (tail vein) included perivascular inflammation, perivascular hemorrhage and vascular necrosis and were present at similar incidence and severity in control and treated rats. These were considered procedure-related rather than treatment-related.

Based on these results, it was concluded that a single dose of 5.0 mg/kg and 15.0 mg/kg (with a NOAEL of at least 5.0 mg/kg) is well tolerated in rats. The HED was set at 0.8 mg/kg. Thus, a safe starting dose would be $1/10 * 0.8 = 0.08$ mg/kg = 5.6 mg for a 70 kg adult.

Safety and tolerability

None of the healthy volunteers showed signs of acute or chronic toxicity, and in particular no hypersensitivity reactions were encountered. During the study no significant clinical changes were seen in the volunteers after dosing. There were no evident clinical effects on the supine systolic and diastolic blood pressure or heart rate after dosing. The ECGs did not show clinically significant changes after dosing and no untoward effects on any analysis of blood chemistry or hematology were observed.

Pharmacokinetics

CRGD-ZW800-1 concentrations were measurably up to 6 hours post dose in the 0.005 mg/kg group. In the lower dose group (0.001 mg/kg) CRGD-ZW800-1 concentrations were measurable up to 1 hour post dosing. Samples measured after these time points were below the detection limit. The maximum blood plasma concentration was achieved at approximately 5 min post dosing. The cumulative excretion of CRGD-ZW800-1, expressed as the percentage of the injected dose, decreased with increasing dose. In the lowest dosing group (0.001 mg/kg) an average cumulative excretion of 83% CRGD-ZW800-1 was observed at 8 hours post dosing. In the higher dosing cohort, 0.005 mg/kg, the average cumulative excretion of CRGD-ZW800-1 8 hours post dosing was 68%.

Interestingly, one human volunteer in the 0.005 mg/kg cohort had a recent cut on the hand, with a scab present at the time of CRGD-ZW800-1 injection. This study subject had measurable fluorescence at the site of the lesion, which became visible within 15 minutes and remained above background up to 24 hours (Figure 2). The scab resolved within two weeks without sequelae.

DISCUSSION

Incomplete resections and avoidable iatrogenic damage during surgery increase morbidity and mortality rates.[14] Although advances in preoperative imaging modalities have improved adequate patient selection and surgical planning, during procedures surgeons rely mainly on inspection and palpation. This strategy is however highly variable and subjective. NIR fluorescence imaging can enhance contrast of tissue that needs to be resected or vital structures that need to be spared.[15] Using targeted or non-targeted fluorophores, such as CRGD-ZW800-1

and ZW800-1, surgeons have the potential to increase radical resection rates, while reducing avoidable iatrogenic damage.

Translational studies are costly and time-consuming. This study demonstrates that there are several strategies to do so. For ZW800-1, the total package of toxicology studies was performed, including the assessment of the NOAEL and MTD. Especially the latter costed huge amount of ZW800-1. The results were not really meaningful; the anticipated dose for clinical studies was well below the safe starting dose assessed in the toxicology studies. Therapeutic drugs often require a maximally tolerated dose to sort optimal effect. Optimal intraoperative imaging requires a much lower dose that should not give any side effects [16].

Extensive clinical experience with CRGD in PET and therapeutic applications [17-21] together with the now available experience with ZW800-1 justified a different approach for CRGD-ZW800-1. The toxicology studies aimed specifically to determine the safety of the anticipated clinical doses. The MTD and NOAEL in rats were not assessed. Followed by a microdose approach in healthy volunteers, this strategy costed minimal amounts of CRGD-ZW800-1 and was less expensive.

ZW800-1 is unique; it is the first and only clinically tested fluorophore that is exclusively eliminated via the kidneys. Doses up to 5.0 mg did not elicit any acute or chronic toxicity, nor to any hypersensitivity reactions. As expected, it did however result in highly fluorescent urine. The Lab-FLARE Model R1 was able to detect ZW800-1 solutions of 0.5 µg/ml (data not shown). This means that the urine of the 0.5 mg dose group was already detectable for at least the first 2 hours after administration. However, ureter and other covering tissue scatters and absorbs the fluorescence signal during surgery. Being able to detect the ureters even if they are not yet fully exposed therefore requires maximal fluorescence in the ureters, while background fluorescence is minimized.

Fluorescence intensity of ZW800-1 increases exponentially with the concentration up to 16 µg/ml, after which a plateau is reached up to 125 µg/ml. Higher concentrations lead to quenching, which reduces the fluorescence intensity. Maximal signal in the ureters and minimal signal in the background is therefore reached with a concentration ZW800-1 in urine of approximately 16 µg/ml. Higher concentrations would lead to similar fluorescence in urine, but higher background fluorescence and thus lower SBRs.

Concentrations between 10 and 20 µg/ml in urine were observed in one healthy volunteer of the 2.5 mg dose group and in three healthy volunteers of the 5.0 mg dose group. The intersubject variability can be explained by differences in hydration status of the healthy volunteers. The volunteer in the 2.5 mg dose group produced 33 ml urine within the first hour, while the average in all volunteers in the first hour was 167 ml. Such differences will be minimized during surgery, as the hydration status of patients is carefully monitored and maintained at a certain level.

Not 100% of the injected dose could be retrieved in urine, even though ZW800-1 demonstrates no known receptor binding. The decrease in excretion in higher doses can be explained by the breakdown of ZW800-1 over time, which is known to occur in blood.[22] Other clearance routes are unlikely, as the clearance rate correlates with the glomerular filtration rate.

The Phase 1 results allow the design of a Phase 2 study with ZW800-1 in patients. This study should assess the feasibility to detect ureters during surgery and further optimized the dose. It is expected that ZW800-1 allows imaging of the ureters within a short period of time after IV administration. This is advantageous; other methods for intraoperative ureter detection, including, double-J stents, lighted catheters or intraoperative retrograde pyelograms, require certain preparations and can delay surgery.[23, 24] If a surgeon is uncertain about the anatomy of the urinary tract, an IV bolus of ZW800-1 could be sufficient to highlight the ureters within a couple of minutes.

It cannot be emphasized enough that clearance patterns of targeted fluorophores are of paramount importance. The limited expression of receptors also limits the maximal intensity of fluorescence in tumors. After saturation of all receptors, the only other method to increase SBR is by reducing nonspecific background fluorescence. CRGD-ZW800-1 demonstrated, similar to ZW800-1 alone, renal clearance in mice and rats.[12, 25] This Phase 1 study confirms that the tracers is being cleared renally. The majority of the injected dose in healthy volunteers was retrieved in urine. A significant portion, however, will target available integrins and be internalized. In addition, similar to ZW800-1, CRGD-ZW800-1 is broken down by serum proteins in blood, which explains the observation that not 100% of the injected dose was retrieved in urine.

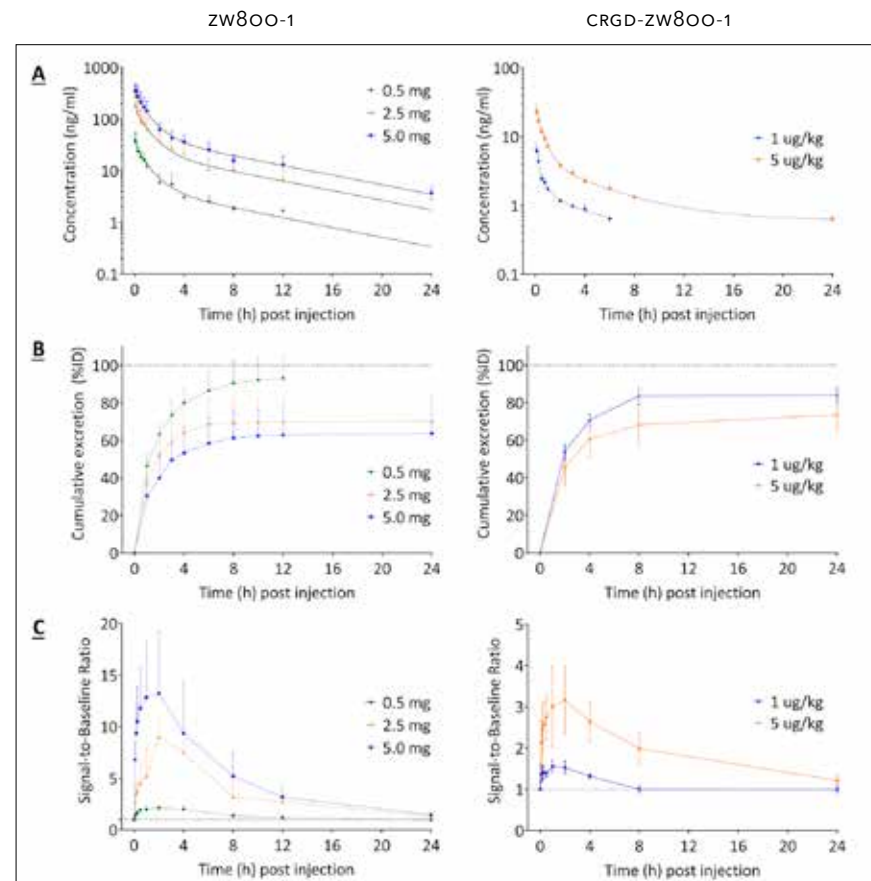
CRGD targets integrins that are also expressed by normal tissue, albeit in a lower density. Integrins are known to be upregulated in neovasculature, which occurs at the site of skin injuries [26]. The finding in the healthy volunteer with the scab provides indirect evidence that CRGD-ZW800-1 is hitting its target. On the other hand, it also demonstrates that it is not tumor-specific. A subsequent Phase 2 study should therefore study sensitivity and specificity.

Furthermore, the Phase 2 study should continue to optimize dose and dosing time. Based on preclinical and clinical results, it is expected that SBRs are optimal between 2 and 24 hours post dosing. Targeted fluorophores such as cetuximab-IRDYE800CW and bevacizumab-IRDYE800CW need to be dosed several days prior to surgery due to their long serum half-lives.[27, 28] This requires an additional visit or earlier admission to the hospital. Smaller sized fluorescent tracers, such as CRGD-ZW800-1, can be dosed on the day of surgery. This is much more convenient for patients.

CONCLUSION

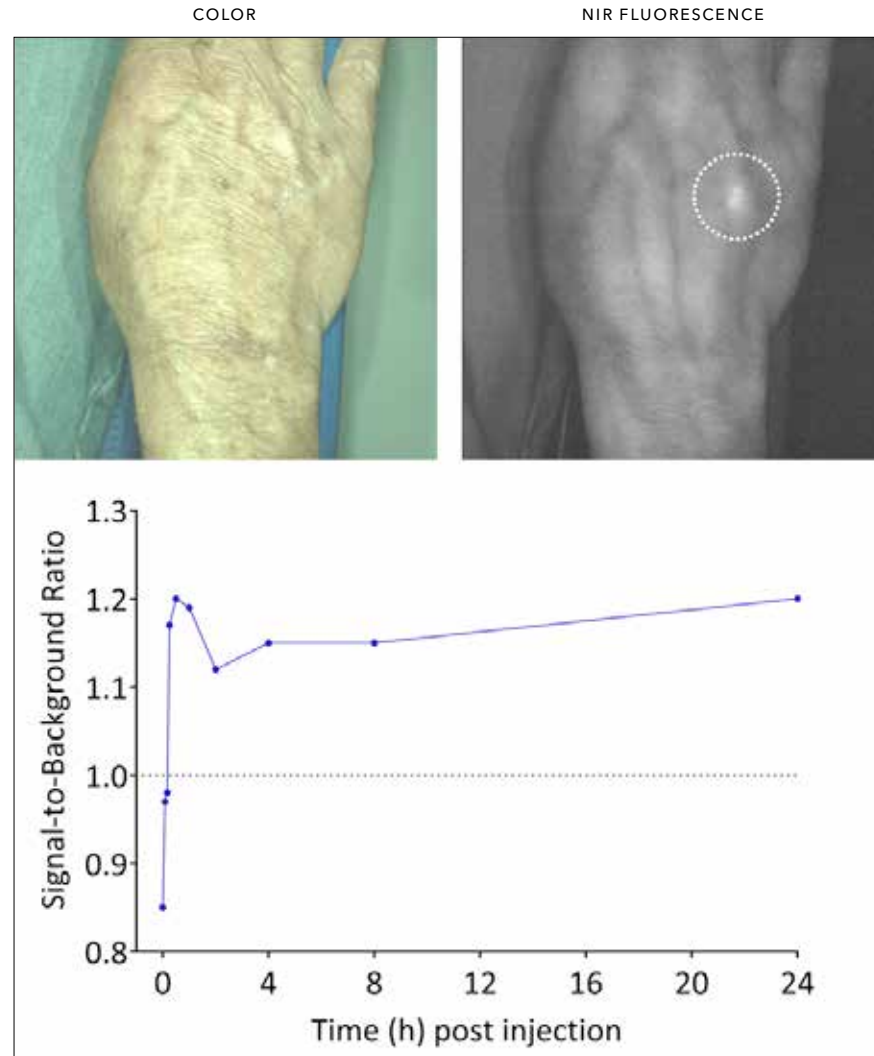
This translational study demonstrates that single IV administrations of ZW800-1 and CRGD-ZW800-1 are safe. Subsequent Phase 2 studies need to assess the feasibility and the optimal dose to identify ureters with ZW800-1 and tumors with CRGD-ZW800-1.

Figure 1 Blood concentrations.



Cumulative urine excretion. Signal-to-background ratios of skin measurements.

Figure 2 Fluorescence imaging of a scab in a healthy volunteer dosed 0.005 mg/kg CRGD-zw800-1. Fluorescence signal in the scab remained well above background between 15 minutes and 24 hours after intravenous administration.



REFERENCES

- Boogerd LS, Handgraaf HJ, Lam HD, Huurman VA, Farina-Sarasqueta A, Frangioni JV, van de Velde CJ, Braat AE and Vahrmeijer AL. Laparoscopic detection and resection of occult liver tumors of multiple cancer types using real-time near-infrared fluorescence guidance. *Surgical endoscopy*. 2016.
- Schaafsma BE, Mieog JS, Hutteman M, van der Vorst JR, Kuppen PJ, Lowik CW, Frangioni JV, van de Velde CJ and Vahrmeijer AL. The clinical use of indocyanine green as a near-infrared fluorescent contrast agent for image-guided oncologic surgery. *J Surg Oncol*. 2011; 104(3):323-332.
- Choi HS, Gibbs SL, Lee JH, Kim SH, Ashitate Y, Liu F, Hyun H, Park G, Xie Y, Bae S, Henary M and Frangioni JV. Targeted zwitterionic near-infrared fluorophores for improved optical imaging. *Nat Biotechnol*. 2013; 31(2):148-153.
- Choi HS, Nasr K, Alyabyev S, Feith D, Lee JH, Kim SH, Ashitate Y, Hyun H, Patonay G, Strekowski L, Henary M and Frangioni JV. Synthesis and in vivo fate of zwitterionic near-infrared fluorophores. *Angew Chem Int Ed Engl*. 2011; 50(28):6258-6263.
- Delacroix SE, Jr. and Winters JC. Urinary tract injuries: recognition and management. *Clin Colon Rectal Surg*. 2010; 23(2):104-112.
- Andersen P, Andersen LM and Iversen LH. Iatrogenic ureteral injury in colorectal cancer surgery: a nationwide study comparing laparoscopic and open approaches. *Surgical endoscopy*. 2015; 29(6):1406-1412.
- Engel O, Rink M and Fisch M. Management of iatrogenic ureteral injury and techniques for ureteral reconstruction. *Curr Opin Urol*. 2015; 25(4):331-335.
- Handgraaf HJ, Boonstra MC, Prevoo HA, Kuil J, Bordo MW, Boogerd LS, Sibinga Mulder BG, Sier CF, Vinkenburger-van Slooten ML, Valentijn AR, Burggraaf J, Van de Velde CJ, Frangioni JV and Vahrmeijer AL. Real-time near-infrared fluorescence imaging using cRGD-ZW800-1 for intraoperative visualization of multiple cancer types *Oncotarget*. 2017:14.
- Hyun H, Bordo MW, Nasr K, Feith D, Lee JH, Kim SH, Ashitate Y, Moffitt LA, Rosenberg M, Henary M, Choi HS and Frangioni JV. cGMP-Compatible preparative scale synthesis of near-infrared fluorophores. *Contrast Media Mol Imaging*. 2012; 7(6):516-524.
- Bowes J, Brown AJ, Hamon J, Jarolimek W, Sridhar A, Waldron G and Whitebread S. Reducing safety-related drug attrition: the use of in vitro pharmacological profiling. *Nat Rev Drug Discov*. 2012; 11(12):909-922.
- Reagan-Shaw S, Nihal M and Ahmad N. Dose translation from animal to human studies revisited. *FASEB J*. 2008; 22(3):659-661.
- Handgraaf HJM, Boonstra MC, Prevoo H, Kuil J, Bordo MW, Boogerd LSF, Sibinga Mulder BG, Sier CFM, Vinkenburger-van Slooten ML, Valentijn A, Burggraaf J, van de Velde CJH, Frangioni JV and Vahrmeijer AL. Real-time near-infrared fluorescence imaging using cRGD-ZW800-1 for intraoperative visualization of multiple cancer types. *Oncotarget*. 2017; 8(13):21054-21066.
- FDA. Estimating the safe starting dose in clinical trials for therapeutics in adult healthy volunteers. pp. 2340-2341.
- Hinni ML, Ferlito A, Brandwein-Gensler MS, Takes RP, Silver CE, Westra WH, Seethala RR, Rodrigo JP, Corry J, Bradford CR, Hunt JL, Strojjan P, Devaney KO, Gnepp DR, Hartl DM, Kowalski LP, et al. Surgical margins in head and neck cancer: a contemporary review. *Head Neck*. 2013; 35(9):1362-1370.
- Vahrmeijer AL, Hutteman M, van der Vorst JR, van de Velde CJ and Frangioni JV. Image-guided cancer surgery using near-infrared fluorescence. *Nat Rev Clin Oncol*. 2013; 10(9):507-518.
- Rosenthal EL, Warram JM, de Boer E, Basilion JP, Biel MA, Bogoyo M, Bouvet M, Brigman BE, Colson YL, DeMeester SR, Gurtner GC, Ishizawa T, Jacobs PM, Keereweer S, Liao JC, Nguyen QT, et al. Successful Translation of Fluorescence Navigation During Oncologic Surgery: A Consensus Report. *J Nucl Med*. 2016; 57(1):144-150.
- Sharma R, Kallur KG, Ryu JS, Parameswaran RV, Lindman H, Avril N, Gleeson FV, Lee JD, Lee KH, O'Doherty MJ, Groves AM, Miller MP, Somer EJ, Coombes CR and Aboagye EO. Multicenter Reproducibility of 18F-Fluciclatide PET Imaging in Subjects with Solid Tumors. *J Nucl Med*. 2015; 56(12):1855-1861.
- Beer AJ, Haubner R, Sarbia M, Goebel M, Luderschmidt S, Grosu AL, Schnell O, Niemyer M, Kessler H, Wester HJ, Weber WA and Schwaiger M. Positron emission tomography using [18F]Galacto-RGD identifies the level of integrin alpha(v) beta3 expression in man. *Clin Cancer Res*. 2006; 12(13):3942-3949.
- Beer AJ, Lorenzen S, Metz S, Herrmann K, Watzlowik P, Wester HJ, Peschel C, Lordick F and Schwaiger M. Comparison of integrin alphaVbeta3 expression and glucose metabolism in primary and metastatic lesions in cancer patients: a PET study using 18F-galacto-RGD and 18F-FDG. *J Nucl Med*. 2008; 49(1):22-29.
- Beer AJ, Niemyer M, Carlsen J, Sarbia M, Nahrig J, Watzlowik P, Wester HJ, Harbeck N and Schwaiger M. Patterns of alphaVbeta3 expression in primary and metastatic human breast cancer as shown by 18F-Galacto-RGD PET. *J Nucl Med*. 2008; 49(2):255-259.
- Stupp R, Hegi ME, Gorlia T, Erridge SC, Perry J, Hong YK, Aldape KD, Lhermitte B, Pietsch T, Grujicic D, Steinbach JP, Wick W, Tarnawski R, Nam DH, Hau P, Weyerbrock A, et al. Cilengitide combined with standard treatment for patients with newly

- diagnosed glioblastoma with methylated MGMT promoter (CENTRIC EORTC 26071-22072 study): a multicentre, randomised, open-label, phase 3 trial. *Lancet Oncol.* 2014; 15(10):1100-1108.
- 22 Hyun H, Owens EA, Narayana L, Wada H, Gravier J, Bao K, Frangioni JV, Choi HS and Henary M. Central C-C Bonding Increases Optical and Chemical Stability of NIR Fluorophores. *RSC Adv.* 2014; 4(102):58762-58768.
- 23 Chahin F, Dwivedi AJ, Paramesh A, Chau W, Agrawal S, Chahin C, Kumar A, Tootla A, Tootla F and Silva YJ. The implications of lighted ureteral stenting in laparoscopic colectomy. *JSLs.* 2002; 6(1):49-52.
- 24 Brandes S, Coburn M, Armenakas N and McAninch J. Diagnosis and management of ureteric injury: an evidence-based analysis. *BJU Int.* 2004; 94(3):277-289.
- 25 Verbeek FP, van der Vorst JR, Tummers QR, Boonstra MC, de Rooij KE, Lowik CW, Valentijn AR, van de Velde CJ, Choi HS, Frangioni JV and Vahrmeijer AL. Near-infrared fluorescence imaging of both colorectal cancer and ureters using a low-dose integrin targeted probe. *Ann Surg Oncol.* 2014; 21 Suppl 4:S528-537.
- 26 Humphries JD, Byron A and Humphries MJ. Integrin ligands at a glance. *J Cell Sci.* 2006; 119(Pt 19):3901-3903.
- 27 Lamberts LE, Koch M, de Jong JS, Adams A, Glatz J, Kranendonk ME, Terwisscha van Scheltinga AG, Jansen L, de Vries J, Lub-de Hooge MN, Schroder CP, Jorritsma-Smit A, Linssen MD, de Boer E, van der Vegt B, Nagengast WB, et al. Tumor-specific uptake of fluorescent bevacizumab-IRDye800CW microdosing in patients with primary breast cancer: a phase I feasibility study. *Clin Cancer Res.* 2016.
- 28 Rosenthal EL, Warram JM, de Boer E, Chung TK, Korb ML, Brandwein-Gensler M, Strong TV, Schmalbach CE, Morlandt AB, Agarwal G, Hartman YE, Carroll WR, Richman JS, Clemons LK, Nabell LM and Zinn KR. Safety and Tumor Specificity of Cetuximab-IRDye800 for Surgical Navigation in Head and Neck Cancer. *Clin Cancer Res.* 2015; 21(16):3658-3666.

PART IV

SUMMARIES AND APPENDICES

CHAPTER 12

Summary and discussion

Surgery is the cornerstone of curative treatment of many malignancies. However, incomplete resections and avoidable iatrogenic damage during surgery increase morbidity and mortality rates in patients. Although advances in preoperative imaging modalities have improved adequate patient selection and surgical planning, during procedures surgeons rely mainly on inspection and palpation. It is often very difficult to distinguish between fibrotic, inflamed, or malignant tissues [1]. Inspection and palpation are highly subjective and have low sensitivity for detecting cancer, especially for subcentimeter lesions [2].

Near-infrared fluorescence (NIRF) imaging is a technique that enhances contrast of certain structures during surgery and thereby improves their detectability [3, 4]. It uses targeted and non-targeted fluorescent tracers in combination with dedicated NIRF imaging systems. These tracers consist of fluorophores; molecules that emit fluorescence with a certain wavelength upon excitation by an external light source. These fluorescence signals can be captured by an imaging system optimized for that specific wavelength. Especially near-infrared wavelengths (i.e. 700-900 nm) have excellent characteristics, including relatively high tissue penetration capacity and low tissue autofluorescence, and are therefore preferably used for clinical applications [5]. NIRF imaging can identify targets covered by up to 10 mm tissue.

Non-targeted fluorescent tracers such as indocyanine green (ICG; emission peak 830 nm) and methylene blue (emission peak 700 nm) have been available for several decades, albeit for different indications. Their off-label use is safe and cheap, which contributed significantly to clinical experience and enabled NIRF imaging research to get momentum (chapter 2 and 3). NIRF imaging systems could be developed simultaneously with improved fluorophores. In general, NIRF-guided surgery has the potential to increase radical resection rates, while reducing avoidable iatrogenic damage. Both non-targeted as well as targeted tracers will be discussed, followed by the future perspectives of NIRF imaging.

NON-TARGETED TRACERS

Non-targeted tracers are not a natural ligand for receptors, but can be used for various indications due to their (pharmacokinetic characteristics). Representatives of this class of tracers are ICG, methylene blue and ZW800-1 and these will be discussed in detail.

Indocyanine green

The most used fluorophore in clinical studies is ICG [6]. ICG has a remarkable safety record with adverse events reported only in 1 out of 40,000 patients [7]. Due to its short serum half-life of only three minutes combined with its hepatic clearance, intravenous administration of ICG enables NIRF imaging during various indications.

Peritumoral injection of ICG allows sentinel lymph node (SLN) mapping (chapter 5), in some cases even percutaneously [8, 9]. Current standard-of-care includes preoperative ^{99m}Tc-technetium-nanocolloid injection to detect SLN via scintigraphy, followed by intraoperative patent blue injection. This strategy has certain disadvantages. For instance, only a gamma probe can detect ^{99m}Tc-technetium; visual guidance is lacking. Patent blue is only visible if the lymph node is fully exposed. Furthermore, only 70% of all SLN eventually stains blue. NIRF imaging with ICG outperforms patent blue and enables visual feedback during SLN mapping (chapter 2) [4].

An intravenous bolus injection of ICG during surgery almost immediately shows the difference between well-perfused tissue and areas that are deprived from blood flow. Anastomotic leakage after colorectal surgery is a feared complication with high morbidity and mortality rates. NIRF assessment of anastomoses can influence intraoperative decision-making and potentially prevent anastomotic leakage caused by ischemia [10]. Multiple injections of ICG can be given during surgery, since ICG has a short serum half-life. Currently, a multicenter study is performed to determine the difference in anastomotic leakage rate with or without NIRF assessment after low anterior resections (clinicaltrials.gov number NCT02205307).

ICG is cleared exclusively by the liver [11]. Within minutes after intravenous administration the liver becomes fluorescent. ICG is subsequently excreted into the bile. It is therefore a very useful fluorophore for bile duct imaging during (laparoscopic) cholecystectomy. Most clinical trials studying this strategy dosed ICG one hour prior to fluorescence imaging, but this approach is suboptimal as it results in high background fluorescence of the liver. The best approach for fluorescence imaging of the biliary tree is therefore to dose ICG a couple of hours prior to surgery [12]. This yields higher bile concentrations of ICG and lower fluorescence of the liver, thus a higher signal-to-background ratio.

An important goal of NIRF imaging is to prevent iatrogenic damage. Bile duct injury is a rare, but very serious complication [13]. Potentially, enhancing visibility with NIRF imaging during cholecystectomy can prevent iatrogenic bile duct injuries. However, designing a study to determine if bile duct injuries can be prevented would require a huge amount of patients. A multicenter randomized controlled study was therefore designed with alternative endpoints, including time until identification of the cystic duct, total surgical time and conversion to open surgery rate (clinicaltrials.gov number NCT02558556).

In 2009 it was shown that defective biliary clearance caused uptake and retention of ICG in a rim around hepatic malignancies [14]. Days after ICG administration tumors could be detected with NIRF imaging. Importantly, not only preoperatively identified tumors, but also small, superficial metastases missed by all other imaging modalities became visible in up to 17% of the patients [2, 15, 16]. Compared to standard-of-care, NIRF imaging identifies significantly more and smaller hepatic metastases of colorectal cancer, without safety concerns or delaying

the procedure (chapter 6) [17]. Of note, 48% of the patients in whom additional malignancies were resected remained disease-free up to three years follow-up. It can be argued that NIRF imaging prevented recurrence in these patients, but no randomized controlled trial was performed. The technique can be improved if a larger portion of the liver surface, including posterior segments, can be screened. Because NIRF imaging only identifies superficial metastases, the technique should be used in combination with a modality with a greater penetration capacity, such as intraoperative ultrasound.

Because millimeter-sized hepatic metastases were better visible with NIRF imaging, it was hypothesized that this method could increase the yield of staging laparoscopy in patients with suspected pancreatic or periampullary cancer (chapter 7) [18]. Although, no additional malignancies were discovered in 25 patients, NIRF imaging could accurately discriminate between malignant and benign hepatic lesions, due to the presence or absence of a characteristic fluorescent rim.

Methylene blue

Methylene blue is a suboptimal fluorophore compared to ICG. Its emitted fluorescence peaks around 700 nm, a wavelength associated with more absorption and tissue autofluorescence. Furthermore, its quantum yield is almost 2.5 times lower than ICG. However, methylene blue has the advantage that it is partially cleared by the kidneys, which allows ureter imaging even after a low intravenous dose [19]. Because methylene blue fluoresces at a different wavelength it can be used simultaneously with ICG, allowing dual-wavelength imaging.

Although the mechanism is not yet fully understood, methylene blue also accumulates in certain tumors, including neuroendocrine tumors and parathyroid adenomas [20-22]. In some patients this may influence intraoperative decision-making, as illustrated in a case report of a patient with multiple endocrine neoplasia type 1 (MEN1) syndrome (chapter 4). NIRF imaging with methylene blue revealed multiple additional microadenomas and neuroendocrine tumors in the pancreas, making total pancreatectomy instead of enucleation the only curative option.

ZW800-1

As methylene blue is a suboptimal fluorophore and only partially renally cleared, alternative compounds have been developed for ureter imaging. One of these compounds is the fluorophore ZW800-1. ZW800-1 emits fluorescence with a peak at 788 nm and shows an exclusive renal clearance pattern [23]. The quantum yield of ZW800-1 is approximately four times higher than methylene blue [11]. These characteristics make ZW800-1 particularly suitable to visualize ureters during surgery. Another advantage of ZW800-1 is that it can be conjugated to targeting moieties, such as CRGD. First-in-human studies with doses up to 5.0 mg

demonstrated no clinically significant adverse events and a favorable pharmacokinetic profile (chapter 10). The majority of the injected dose was renally excreted within the first two hours, but ZW800-1 could be detected in urine up to 12 hours post dosing.

TARGETED TRACERS

Targeted fluorescent tracers can be divided into three major classes:

- » fluorophores conjugated to ligands that specifically bind to a target – these tracers are always fluorescent [24];
- » activatable tracers, molecules that become fluorescent only upon activation by a specific target. This should result in lower nonspecific fluorescence and therefore higher tumor-to-background ratios [25];
- » structure-inherent targeted fluorophores, single compact molecules which both target and fluoresce [26].

Fluorophores conjugated to ligands

The first exploratory clinical study was performed with the folate receptor α (FRA) specific fluorescent tracer EC17 that consists of the fluorophore fluorescein isothiocyanate (FITC) conjugated to folate. The tracer was tested in patients with ovarian cancer metastases and it was shown that tumor deposits smaller than one millimeter could be detected with NIRF imaging [27]. Although proof-of-concept for a ligand targeted approach was obtained, important obstacles for EC17 remain. The majority of solid tumors do not overexpress FRA and FITC is fluorescent at 500 nm, thus has low tissue penetration capacity and high tissue autofluorescence. Indeed, a follow-up study with EC17 demonstrated the limited value of the compound [28]. FITC was therefore replaced by an 800 nm fluorophore [29], which has improved tissue penetration and less autofluorescence. However, this study also showed that the presumed selectivity of the tracer for FRA is questionable. This limits the applicability of FRA-targeted fluorescent tracers even further.

Shortly after these clinical studies, other fluorescent tracers became available, including cetuximab-IRDye800CW targeting the epidermal growth factor (EGFR) and bevacizumab-IRDye800CW for the vascular endothelial growth factor (VEGF). Even though IRDYE800CW emits bright fluorescence, anionic fluorophores increase the chance that tracers are being cleared by the liver [30]. This results in contamination of the gastrointestinal tract, and thus nonspecific background fluorescence, which reduces the tumor-to-background ratio. This is especially bothersome during imaging of colorectal, periampullary pancreatic or hepatic cancer. Other disadvantages of these antibody-based tracers are their propensity to cause serious adverse reactions and their long plasma half-lives [31]. Indeed, the chimeric antibody cetuximab can cause severe infusion reactions and other

serious side effects [32]. The long plasma half-lives will result in a long residence time of inbound tracers in the systemic circulation, causing high nonspecific background fluorescence. This can only be overcome by administration of these compounds several days before surgery, which is burdensome. It thus appears that smaller targeting moieties with better pharmacokinetic properties are therefore preferred.

One such tracer may be CRGD; a small peptide that targets integrins associated with neoangiogenesis and can be conjugated to NIRF dyes such as ZW800-1 [30]. It was shown that CRGD-ZW800-1 targets multiple tumor types, including pancreatic, colorectal, and breast cancer, with optimal tumor-to-background ratios between two and 24 hours after administration, most likely because this tracer shows rapid and exclusive renal clearance (chapter 9) [24]. First-in-human studies did not show any clinically relevant adverse events (chapter 10). Interestingly, one human volunteer had a recent cut in the hand, with a scab present at the time of CRGD-ZW800-1 administration. This lesion became fluorescent after two hours and the fluorescence signal remained above background up to 24 hours. Neovascularization occurs at the site of injuries and this result is therefore indirect evidence that CRGD-ZW800-1 is reaching its target.

Other alternative targeting moieties are antibody fragments, such as so-called Fab fragments. These tracers consist only of the antigen-binding region (Fab) of an antibody and are approximately three times smaller than a complete antibody. A preclinical study compared a Fab fragment with a complete antibody and demonstrated similar binding to tumors, but lower nonspecific background fluorescence due to improved biodistribution and pharmacokinetics [33]. For instance, liver uptake of the Fab fragment at 72 hours after injection was well below the tumor signal, while the intact antibody demonstrated twice as much fluorescence in the liver compared to the tumor.

Activatable tracers

A disadvantage of “always-on” fluorophores is that unbound tracers in the background cause non-specific fluorescence, which results in lower tumor-to-background ratios. Reducing nonspecific background fluorescence is important to obtain higher tumor-to-background ratios, also because the fluorescence intensity of tumors is limited by the amount of available receptors on tumor cells [23]. GGLU-HMRG is a fluorescent tracer that contains the quenched (i.e. inactive) fluorophore HMRG. HMRG is rapidly unquenched by gamma-glutamyltranspeptidase (GGT), which is overexpressed on multiple tumor types, including squamous cell carcinoma. Instead of intravenous administration, GGLU-HMRG can be sprayed on resected tissue, enabling detection of tumor-positive resection margins within ten minutes with no systemic exposure (chapter 8).

Structure-inherent targeting

A completely different approach to develop targeted fluorescent tracers is to create molecules that are both fluorescent and able to target specific structures. In essence, methylene blue accumulation in neuroendocrine tumors (chapter 4) or parathyroid glands can be considered a form of structure-inherent targeting [20, 21]. Other examples are T700-F and T800-F, small molecules that specifically target thyroid and parathyroid glands [26]. Because the mechanism of uptake and retention for these molecules is currently unknown, it is possible that non-specific uptake occurs. Furthermore, the indications for such molecules are limited, as the amount of molecules with structure-inherent targeting characteristics is also limited.

FUTURE PERSPECTIVES

The future of NIRF imaging seems promising. Several fluorescent tracers have proven their effectiveness and are moving towards phase 3 clinical trials. Simultaneously, sensitive, handy, and CE-marked imaging systems have been developed for intraoperative use. The next steps for NIRF imaging should be further improvement of tracers and imaging systems, but more importantly implementing the technique in standard-of-care, overcoming inherent limitations and broadening its applicability as discussed below.

Towards clinical implementation

NIRF imaging has demonstrated to make the invisible visible by enhancing contrast with targeted or non-targeted fluorescent tracers. Yet, implementation of this technique occurs tremendously slow, which is surprisingly given the current alternative; the decision for resection is based on the variable and subjective visual and tactile assessment by surgeons. An explanation for the slow implementation is that randomized controlled trials studying long-term clinical benefits of NIRF imaging are sparse. It can however be debated if such expensive trials are really necessary to demonstrate the obvious [34]. For example, completeness of cytoreductive surgery is an important prognostic factor for survival of patients with ovarian cancer and it is demonstrated that NIRF imaging reveals more metastases compared to visual and tactile inspection [29, 35, 36]. Another example is brain surgery guided by 5-aminovulnic acid (5-ALA), a fluorophore that accumulates in gliomas. The survival benefits of improving contrast between tumor and normal brain tissue were evident in observational studies [37, 38]. Not unexpectedly, a randomized controlled trial had to be terminated prematurely due to 20% higher progression-free survival in the 5-ALA arm at 6 months [39].

Nevertheless, NIRF imaging must undeniably demonstrate its value before it can be accepted and implemented. Alternative meaningful endpoints of trials

with fluorescent tracers that have advanced beyond safety, feasibility and optimization studies include the robust ability to locate and outline normal structures or to distinguish accurately between diseased and healthy tissue (i.e. sensitivity and specificity) [40]. These endpoints are accepted by US Food and Drug Administration (FDA) guidelines for the approval of imaging products and do not require additional information regarding clinical usefulness. Importantly, this can be demonstrated without randomizing patients, because they can serve as their own control. Using ICG for the detection of colorectal liver metastases is an ideal candidate for clinical implementation, as it is safe, inexpensive, and identifies additional tumors in up to 17% of the patients undergoing resection [2, 17].

Another issue is standardization. A broad variety of fluorescence imaging systems is available, all with different light sources, optical filters and software [4]. As a consequence, data output per system is completely different. Outcomes of studies with fluorescent tracers are depending on the type of imaging system used, which potentially raises the demand that imaging systems and fluorescent tracers are submitted as one package to the FDA and European Medicines Agency (EMA) for market authorization [40]. There is currently no objective way to determine the total performance of an imaging system [41, 42]. Suggested solutions include using standardized fluorescent phantoms or physical standards. The optical imaging community must address this issue and propose appropriate standards and recommendations.

Overcoming limitations

Even though NIRF imaging has great potential, important limitations should not be ignored. Structures located deeper than 5-10 mm into tissue are not (yet) visible. Several possibilities to improve the depth penetration of NIRF are currently being developed, including photoacoustic imaging, fluorophores in the near-infrared 2 (NIR-2) spectrum and multimodal tracers. Photoacoustic imaging offers visualization of targets several centimeters deep by detecting ultrasound waves caused by thermoelastic expansion of fluorophores [43]. Fluorophores in the NIR-2 spectrum (emission peaks at 1,000-1,700 nm) offer a great improvement in imaging quality due to diminished tissue autofluorescence, reduced scattering, and low levels of absorption [44]. Alternatively, fluorescent tracers can be conjugated to radioisotopes for positron emission tomography (PET) or single-photon emission tomography (SPECT) to allow multimodal imaging [45]. Such tracers can be used to locate targets before surgery and improve surgical planning, while using fluorescence imaging during surgery to ensure a radical resection.

Broaden the applicability

This thesis discussed the use of NIRF imaging during surgery, but its potential extends beyond that application. Notable examples are its utilization in accurate and early diagnosis for colorectal cancer, arthritis and assessment of cardiac and renal function. Fluorescent tracers for colorectal polyps are already available and demonstrated that polyps not visible with normal light could be detected with NIRF imaging [46]. Implementing this strategy in the national population screening program for colorectal cancer could enhance detection of flat or difficult to detect lesions. Diagnosing early-stage arthritis is difficult, as signs and symptoms are sometimes vague. Joint destruction can be diagnosed noninvasively by placing the affected joints under an imaging system after injecting a tracer targeting matrix metalloproteinases [47]. Cardiac and renal functions can be measured transcutaneously by assessing the distribution of fluorescence after bolus injection of ZW800-1 [48]. Research of these examples is in an early stage, but using NIRF imaging outside the surgical theatre will most likely demonstrate its usefulness to be greater than at present envisaged.

GENERAL CONCLUSIONS

Fluorescence imaging during surgery has the potential to make surgery better, faster and less expensive. ICG and methylene blue are safe, inexpensive and already useful for several indications. Major advantages can be expected especially from targeted tracers that highlight invisible metastases or tumor-positive resection margins. Several fluorescent tracers and clinical imaging systems are already available and more will follow shortly. Dozens of clinical trials studying several fluorescent tracers are currently ongoing. The optical imaging community must now demonstrate benefits for patients, safety, and cost-effectiveness, while also addressing issues such as standardization. These topics will be of critical importance to clinical implementation and acceptance of NIRF imaging in the coming years.

REFERENTIES

- 1 Handgraaf HJ, Boonstra MC, Van Erkel AR, Bonsing BA, Putter H, Van De Velde CJ, Vahrmeijer AL, Mieog JS. Current and future intraoperative imaging strategies to increase radical resection rates in pancreatic cancer surgery. *Biomed Res Int.* 2014; 2014: 890230. doi: 10.1155/2014/890230.
- 2 Boogerd LSF, Handgraaf HJM, Lam HD, Huurman VA, Farina-Sarasqueta A, Frangioni JV, van de Velde CJH, Braat AE, Vahrmeijer AL. Laparoscopic detection and resection of occult liver tumors of multiple cancer types using real-time near-infrared fluorescence guidance. *Surg Endosc.* 2017; 31: 952-61. doi: 10.1007/s00464-016-5007-6.
- 3 Vahrmeijer AL, Hutteman M, van der Vorst JR, van de Velde CJ, Frangioni JV. Image-guided cancer surgery using near-infrared fluorescence. *Nat Rev Clin Oncol.* 2013; 10: 507-18. doi: 10.1038/nrclinonc.2013.123.
- 4 Handgraaf HJ, Verbeek FP, Tummers QR, Boogerd LS, van de Velde CJ, Vahrmeijer AL, Gaarenstroom KN. Real-time near-infrared fluorescence guided surgery in gynecologic oncology: a review of the current state of the art. *Gynecol Oncol.* 2014; 135: 606-13. doi: 10.1016/j.ygyno.2014.08.005.
- 5 Patterson MS, Chance B, Wilson BC. Time resolved reflectance and transmittance for the non-invasive measurement of tissue optical properties. *Appl Opt.* 1989; 28: 2331-6. doi: 10.1364/AO.28.002331.
- 6 Schaafsma BE, Mieog JS, Hutteman M, van der Vorst JR, Kuppen PJ, Lowik CW, Frangioni JV, van de Velde CJ, Vahrmeijer AL. The clinical use of indocyanine green as a near-infrared fluorescent contrast agent for image-guided oncologic surgery. *J Surg Oncol.* 2011; 104: 323-32. doi: 10.1002/jso.21943.
- 7 Benya R, Quintana J, Brundage B. Adverse reactions to indocyanine green: a case report and a review of the literature. *Cathet Cardiovasc Diagn.* 1989; 17: 231-3. doi: 10.1111/1471-0528.12173.
- 8 Schaafsma BE, Verbeek FP, Peters AA, van der Vorst JR, de Kroon CD, van Poelgeest MI, Trimbos JB, van de Velde CJ, Frangioni JV, Vahrmeijer AL, Gaarenstroom KN. Near-infrared fluorescence sentinel lymph node biopsy in vulvar cancer: a randomised comparison of lymphatic tracers. *BJOG.* 2013; 120: 758-64. doi: 10.1111/1471-0528.12173.
- 9 Verbeek FP, Troyan SL, Mieog JS, Liefers GJ, Moffitt LA, Rosenberg M, Hirshfield-Bartek J, Gioux S, van de Velde CJ, Vahrmeijer AL, Frangioni JV. Near-infrared fluorescence sentinel lymph node mapping in breast cancer: a multicenter experience. *Breast Cancer Res Treat.* 2014; 143: 333-42. doi: 10.1007/s10549-013-2802-9.
- 10 Jafari MD, Waxner SD, Martz JE, McLemore EC, Margolin DA, Sherwinter DA, Lee SW, Senagore AJ, Phelan MJ, Stamos MJ. Perfusion assessment in laparoscopic left-sided/anterior resection (PILLAR II): a multi-institutional study. *J Am Coll Surg.* 2015; 220: 82-92.e1. doi: 10.1016/j.jamcollsurg.2014.09.015.
- 11 Chopra A. (2004). ZW800-1, a zwitterionic near-infrared fluorophore, and its cyclic RGD peptide derivative cyclo-(RGDyK)-ZW800-1. *Molecular Imaging and Contrast Agent Database (MICAD)*. (Bethesda (MD)).
- 12 Boogerd LSF, Handgraaf HJM, Huurman VAL, Lam HD, Mieog JSD, van der Made WJ, van de Velde CJH, Vahrmeijer AL. The Best Approach for Laparoscopic Fluorescence Cholangiography: Overview of the Literature and Optimization of Dose and Dosing Time. *Surg Innov.* 2017: 1553350617702311. doi: 10.1177/1553350617702311.
- 13 Nuzzo G, Giuliani F, Giovannini I, Ardito F, D'Acapito F, Vellone M, Murazio M, Capelli G. Bile duct injury during laparoscopic cholecystectomy: results of an Italian national survey on 56 591 cholecystectomies. *Arch Surg.* 2005; 140: 986-92. doi: 10.1001/archsurg.140.10.986.
- 14 Ishizawa T, Fukushima N, Shibahara J, Masuda K, Tamura S, Aoki T, Hasegawa K, Beck Y, Fukayama M, Kokudo N. Real-time identification of liver cancers by using indocyanine green fluorescent imaging. *Cancer.* 2009; 115: 2491-504. doi: 10.1002/cncr.24291 [doi].
- 15 van der Vorst JR, Schaafsma BE, Hutteman M, Verbeek FP, Liefers GJ, Hartgrink HH, Smit VT, Lowik CW, van de Velde CJ, Frangioni JV, Vahrmeijer AL. Near-infrared fluorescence-guided resection of colorectal liver metastases. *Cancer.* 2013; 119: 3411-8. doi: 10.1002/cncr.28203.
- 16 Boogerd LS, Handgraaf HJ, Lam HD, Braat AE, Baranski AG, Swijnenburg RJ, Frangioni JV, Vahrmeijer AL, Ringers J. Application of near-infrared fluorescence imaging during modified associating liver partition and portal vein ligation for staged hepatectomy. *Surgery.* 2016; 159: 1481-2. doi: 10.1016/j.surg.2015.11.024.
- 17 Handgraaf HJ, Boogerd LS, Höppener DJ, Peloso A, Sibinga Mulder BG, Hoogstins CE, Hartgrink HH, van de Velde CJ, Mieog JS, Swijnenburg RJ, Putter H, Maestri M, Braat AE, et al. Long-term follow-up after near-infrared fluorescence-guided resection of colorectal liver metastases: a retrospective multicenter analysis. *Eur J Surg Oncol.* 2017. doi: 10.1016/j.ejso.2017.04.016.
- 18 Handgraaf HJ, Sibinga Mulder BG, Shahbazi Festhali S, Boogerd LS, van der Valk MJ, Farina Sarasqueta A, Swijnenburg RJ, Bonsing BA, Vahrmeijer AL, Mieog JS. Staging laparoscopy with ultrasound and near-infrared fluorescence imaging to detect occult metastases in pancreatic and periampullary cancer. Submitted. 2017. doi: 10.1007/978-94-007-5105-4_9-13.
- 19 Verbeek FP, van der Vorst JR, Schaafsma BE, Swijnenburg RJ, Gaarenstroom KN, Elzevier HW, van de Velde CJ, Frangioni JV, Vahrmeijer AL. Intraoperative near infrared fluorescence guided identification of the ureters using low dose methylene blue: a first in human experience. *J Urol.* 2013; 190: 574-9. doi: 10.1016/j.juro.2013.02.3187.
- 20 Handgraaf HJM, Boogerd LS, Shahbazi Festhali S, Farina Sarasqueta A, Snel M, Swijnenburg RJ, Vahrmeijer AL, Bonsing BA, Mieog JS. Intraoperative near-infrared fluorescence imaging of multiple pancreatic neuroendocrine tumors: a case report. *Pancreas.* 2017. doi: 10.1007/s12220-017-0011-1.
- 21 van der Vorst JR, Schaafsma BE, Verbeek FP, Swijnenburg RJ, Tummers QR, Hutteman M, Hamming JF, Kievit J, Frangioni JV, van de Velde CJ, Vahrmeijer AL. Intraoperative near-infrared fluorescence imaging of parathyroid adenomas with use of low-dose methylene blue. *Head Neck.* 2014; 36: 853-8. doi: 10.1002/hed.23384.
- 22 Tummers QR, Schepers A, Hamming JF, Kievit J, Frangioni JV, van de Velde CJ, Vahrmeijer AL. Intraoperative guidance in parathyroid surgery using near-infrared fluorescence imaging and low-dose Methylene Blue. *Surgery.* 2015; 158: 1323-30. doi: 10.1016/j.surg.2015.03.027.
- 23 Choi HS, Nasr K, Alyabyev S, Feith D, Lee JH, Kim SH, Ashitate Y, Hyun H, Patonay G, Strekowski L, Henary M, Frangioni JV. Synthesis and in vivo fate of zwitterionic near-infrared fluorophores. *Angew Chem Int Ed Engl.* 2011; 50: 6258-63. doi: 10.1002/anie.201102459.
- 24 Handgraaf HJM, Boonstra MC, Prevoo H, Kuil J, Bordo MW, Boogerd LSF, Sibinga Mulder BG, Sier CFM, Vinkenburg-van Slooten ML, Valentijn A, Burggraaf J, van de Velde CJH, Frangioni JV, et al. Real-time near-infrared fluorescence imaging using cRGD-ZW800-1 for intraoperative visualization of multiple cancer types. *Oncotarget.* 2017; 8: 21054-66. doi: 10.18632/oncotarget.15486.
- 25 Urano Y, Sakabe M, Kosaka N, Ogawa M, Mitsunaga M, Asanuma D, Kamiya M, Young MR, Nagano T, Choyke PL, Kobayashi H. Rapid cancer detection by topically spraying a gamma-glutamyltranspeptidase-activated fluorescent probe. *Sci Transl Med.* 2011; 3: 110ra9. doi: 10.1126/scitranslmed.3002823.
- 26 Hyun H, Park MH, Owens EA, Wada H, Henary M, Handgraaf HJ, Vahrmeijer AL, Frangioni JV, Choi HS. Structure-inherent targeting of near-infrared fluorophores for parathyroid and thyroid gland imaging. *Nat Med.* 2015; 21: 192-7. doi: 10.1038/nm.3728.
- 27 van Dam GM, Themelis G, Crane LM, Harlaar NJ, Pleijhuis RG, Kelder W, Sarantopoulos A, de Jong JS, Arts HJ, van der Zee AG, Bart J, Low PS, Ntziachristos V. Intraoperative tumor-specific fluorescence imaging in ovarian cancer by folate receptor-alpha targeting: first in-human results. *Nat Med.* 2011; 17: 1315-9. doi: 10.1038/nm.2472.
- 28 Tummers QR, Hoogstins CE, Gaarenstroom KN, de Kroon CD, van Poelgeest MI, Vuyk J, Bosse T, Smit VT, van de Velde CJ, Cohen AF, Low PS, Burggraaf J, Vahrmeijer AL. Intraoperative imaging of folate receptor alpha positive ovarian and breast cancer using the tumor specific agent EC17. *Oncotarget.* 2016; 7: 32144-55. doi: 10.18632/oncotarget.8282.
- 29 Hoogstins CE, Tummers QR, Gaarenstroom KN, de Kroon CD, Trimbos JB, Bosse T, Smit VT, Vuyk J, van de Velde CJ, Cohen AF, Low PS, Burggraaf J, Vahrmeijer AL. A Novel Tumor-Specific Agent for Intraoperative Near-Infrared Fluorescence Imaging: A Translational Study in Healthy Volunteers and Patients with Ovarian Cancer. *Clin Cancer Res.* 2016; 22: 2929-38. doi: 10.1158/1078-0432.CCR-15-2640.
- 30 Choi HS, Gibbs SL, Lee JH, Kim SH, Ashitate Y, Liu F, Hyun H, Park G, Xie Y, Bae S, Henary M, Frangioni JV. Targeted zwitterionic near-infrared fluorophores for improved optical imaging. *Nat Biotechnol.* 2013; 31: 148-53. doi: 10.1038/nbt.2468.
- 31 Slooter MD, Handgraaf HJ, Boonstra MC, van der Velden LA, Bhariosingh SS, Que I, De Haan LM, Keereweer S, van Driel PB, Chan A, Kobayashi H, Vahrmeijer A, Löwik CW. Detecting microscopic tumour-positive resection margins after oral cancer surgery by spraying a fluorescent tracer activated by gamma-glutamyltranspeptidase. Submitted. 2017. doi: 10.1101/161111.
- 32 Thomas M. Cetuximab: adverse event profile and recommendations for toxicity management. *Clin J Oncol Nurs.* 2005; 9: 332-8. doi: 10.1188/05.cjon.332-338.
- 33 Boogerd LS, Boonstra MC, Prevoo HA, Handgraaf HJ, Kuppen PJ, van de Velde CJ, MacDonald GC, Cizeau J, Premsukh A, Vinkenburg-van Slooten ML, Burggraaf J, Sier CF, Vahrmeijer AL. Fluorescence-guided tumor detection with a novel anti-EpCAM targeted antibody fragment: preclinical validation. Submitted. 2017. doi: 10.1101/161111.
- 34 Smith GC, Pell JP. Parachute used to prevent death and major trauma related to gravitational challenge: systematic review of randomised controlled trials. *BMJ.* 2003; 327: 1459-61. doi: 10.1136/bmj.327.7429.1459.
- 35 Chang SJ, Bristow RE, Ryu HS. Impact of complete cytoreduction leaving no gross residual disease associated with radical cytoreductive surgical procedures on survival in advanced ovarian cancer. *Ann Surg Oncol.* 2012; 19: 4059-67. doi: 10.1245/s10434-012-2446-8.
- 36 Bristow RE, Tomacruz RS, Armstrong DK, Trimble EL, Montz FJ. Survival effect of maximal cytoreductive surgery for advanced ovarian carcinoma during the platinum era: a meta-analysis. *J Clin Oncol.* 2002; 20: 1248-59. doi: 10.1200/JCO.2002.20.5.1248.
- 37 Stummer W, Novotny A, Stepp H, Goetz C, Bise K, Reulen HJ. Fluorescence-guided resection of glioblastoma multiforme by using 5-aminolevulinic acid-induced porphyrins: a prospective study in

- 52 consecutive patients. *J Neurosurg.* 2000; 93: 1003-13. doi: 10.3171/jns.2000.93.6.1003.
- 38 Stummer W, Stocker S, Wagner S, Stepp H, Fritsch C, Goetz C, Goetz AE, Kiefmann R, Reulen HJ. Intraoperative detection of malignant gliomas by 5-aminolevulinic acid-induced porphyrin fluorescence. *Neurosurgery.* 1998; 42: 518-25; discussion 25-6. doi:
- 39 Stummer W, Pichlmeier U, Meinel T, Wiestler OD, Zanella F, Reulen HJ, Group AL-GS. Fluorescence-guided surgery with 5-aminolevulinic acid for resection of malignant glioma: a randomised controlled multicentre phase III trial. *Lancet Oncol.* 2006; 7: 392-401. doi: 10.1016/S1470-2045(06)70665-9.
- 40 Rosenthal EL, Warram JM, de Boer E, Basilion JP, Biel MA, Bogyo M, Bouvet M, Brigman BE, Colson YL, DeMeester SR, Gurtner GC, Ishizawa T, Jacobs PM, et al. Successful Translation of Fluorescence Navigation During Oncologic Surgery: A Consensus Report. *J Nucl Med.* 2016; 57: 144-50. doi: 10.2967/jnumed.115.158915.
- 41 Snoeks TJ, van Driel PB, Keereweer S, Aime S, Brindle KM, van Dam GM, Lowik CW, Ntziachristos V, Vahrmeijer AL. Towards a successful clinical implementation of fluorescence-guided surgery. *Mol Imaging Biol.* 2014; 16: 147-51. doi: 10.1007/s11307-013-0707-y.
- 42 Tummers WS, Warram JM, Tipirneni KE, Fengler J, Jacobs P, Shankar L, Henderson L, Ballard B, Pogue BW, Weichert JP, Bouvet M, Sorger J, Contag CH, et al. Regulatory Aspects of Optical Methods and Exogenous Targets for Cancer Detection. *Cancer Res.* 2017; 77: 2197-206. doi: 10.1158/0008-5472.CAN-16-3217.
- 43 Zackrisson S, van de Ven SM, Gambhir SS. Light in and sound out: emerging translational strategies for photoacoustic imaging. *Cancer Res.* 2014; 74: 979-1004. doi: 10.1158/0008-5472.CAN-13-2387.
- 44 Antaris AL, Chen H, Cheng K, Sun Y, Hong G, Qu C, Diao S, Deng Z, Hu X, Zhang B, Zhang X, Yaghi OK, Alamparambil ZR, et al. A small-molecule dye for NIR-II imaging. *Nat Mater.* 2016; 15: 235-42. doi: 10.1038/nmat4476.
- 45 Muselaers CH, Rijpkema M, Bos DL, Langenhuijsen JF, Oyen WJ, Mulders PF, Oosterwijk E, Boerman OC. Radionuclide and Fluorescence Imaging of Clear Cell Renal Cell Carcinoma Using Dual Labeled Anti-Carbonic Anhydrase IX Antibody G250. *J Urol.* 2015; 194: 532-8. doi: 10.1016/j.juro.2015.02.041.
- 46 Burggraaf J, Kamerling IM, Gordon PB, Schrier L, de Kam ML, Kales AJ, Bendiksen R, Indrevoll B, Bjerke RM, Moestue SA, Yazdanfar S, Langers AM, Swaerd-Nordmo M, et al. Detection of colorectal polyps in humans using an intravenously administered fluorescent peptide targeted against c-Met. *Nat Med.* 2015; 21: 955-61. doi: 10.1038/nm.3641.
- 47 Cho H, Bhatti FU, Lee S, Brand DD, Yi AK, Hasty KA. In Vivo Dual Fluorescence Imaging to Detect Joint Destruction. *Artif Organs.* 2016; 40: 1009-13. doi: 10.1111/aor.12685.
- 48 Ikeda M, Wakasaki R, Schenning KJ, Swide T, Lee JH, Miller MB, Choi HS, Anderson S, Hutchens MP. Determination of renal function and injury using near-infrared fluorimetry in experimental cardiorenal syndrome. *Am J Physiol Renal Physiol.* 2017; 312: F629-F39. doi: 10.1152/ajprenal.00573.2016.

CHAPTER 13

Nederlandse samenvatting

Incomplete resecties van tumoren en vermijdbare iatrogene schade tijdens chirurgie verhogen morbiditeit en mortaliteit bij patiënten. Tijdens operaties bepalen chirurgen met name door inspectie en/of palpatie of weefsel maligne, ontstoken of gezond is. Deze interpretatie is echter lastig, variabel en subjectief. Nabij-infrarode fluorescentiebeeldvorming is een techniek die structuren in real-time duidelijker zichtbaar maakt. Deze techniek detecteert fluorescentie afkomstig van moleculen, zogeheten fluoroforen, die geëxciteerd worden door een externe lichtbron. Door toediening van specifieke of niet-specifieke fluoroforen wordt in weefsel het contrast tussen target en achtergrond ('*target-to-background ratio*') verhoogd. Chirurgen kunnen hierdoor nauwkeuriger opereren, waardoor zij uiteindelijk een hoger percentage radicale resecties bereiken en/of minder vermijdbare schade veroorzaken. Dit proefschrift beschrijft met name de toepassing van fluorescentiebeeldvorming tijdens chirurgie, maar er zijn nog andere toepassingen waarbij deze techniek van meerwaarde kan zijn. Bijvoorbeeld tijdens colonoscopie voor de screening op (pre)maligne laesies in het bevolkingsonderzoek naar darmkanker.

Deel I schetst de actuele uitdagingen en oplossingen om tumoren andere weefseltypen te lokaliseren tijdens verschillende chirurgische ingrepen. **Hoofdstuk 1** beschrijft de pancreaschirurgie. Met de huidig beschikbare technieken blijft het zeer lastig om intra-operatief onderscheid te maken tussen maligne, ontstoken en gezond pancreasweefsel. Mede hierdoor is tot 75% van de resecties irradicaal. Dit kan leiden tot recidieven en daarmee een slechtere prognose. Nieuwe technieken, waaronder fluorescentiebeeldvorming, zouden hiervoor een oplossing kunnen zijn. **Hoofdstuk 2** gaat in op het gebruik van fluorescentiebeeldvorming tijdens gynaecologische ingrepen. Met behulp van indocyanine groen (ICG) kunnen schildwachtklieren beter gevonden worden. Een meta-analyse van de literatuur toont dat met behulp van ICG er meer schildwachtklieren gevonden worden dan met de huidige standaard techniek. Met behulp van methyleen blauw kunnen de ureters in beeld worden gebracht, waardoor iatrogene schade vermeden kan worden. Tumor-specifieke stoffen kunnen uitzaaiingen van het ovariumcarcinoom nauwkeuriger detecteren. **Hoofdstuk 3** gaat in op het detecteren van tumoren in de lever. ICG wordt na intraveneuze toediening hepatisch geklaard, maar hoopt zich op rondom maligne laesies in de lever. Eén of meerdere dagen na intraveneuze toediening toont het gezonde deel van de lever geen fluorescentie meer, terwijl rondom metastasen een fluorescente ring zichtbaar blijft. Op deze manieren kunnen bekende tumoren beter afgegrensd worden, terwijl er ook extra tumoren gedetecteerd worden die door andere technieken gemist zijn.

Deel II gaat in op de toepassingen van niet-specifieke fluoroforen. **Hoofdstuk 4** beschrijft een patiënt met meerdere neuroendocriene tumoren in de pancreas

ten gevolge van multipole endocriene neoplasia type 1 (MEN1) syndroom. In de literatuur is beschreven dat door hoge doseringen methyleen blauw sommige neuroendocriene tumoren blauw verkleuren. In deze casus is een relatief lage dosering methyleen blauw peroperatief toegediend, waarna met fluorescentiebeeldvorming de afwijkingen duidelijk zichtbaar werden. **Hoofdstuk 5** toont aan dat ICG ook gebruikt kan worden om tumoren te markeren. Tijdens laparoscopische rectumchirurgie is het lastig om de tumor te lokaliseren. De gastro-enteroloog markeert preoperatief endoscopisch de locatie met inkt. Echter, is inkt niet altijd zichtbaar voor de chirurg, bijvoorbeeld als de tumor bedekt is met weefsel of bloed. In deze studie was de fluorescente spot 10 minuten eerder zichtbaar dan de inkt. Daarnaast kon fluorescentiebeeldvorming *ex vivo* ook lymfeklieren zichtbaar maken. Uit **hoofdstuk 6** blijkt dat fluorescentiebeeldvorming tijdens resectie van colorectale levermetastasen de operatie niet vertraagt en geen extra complicaties veroorzaakt. Daarnaast werden er peroperatief met fluorescentiebeeldvorming in 13% van de patiënten extra metastasen aangetroffen die anders niet te detecteren waren. In 48% van die patiënten kwam de ziekte na resectie van de extra gevonden metastasen niet terug. In **hoofdstuk 6** is geprobeerd om met behulp van fluorescentiebeeldvorming de opbrengst van stadiëringslaparoscopie bij patiënten met een pancreascarcinoom te verhogen. De hypothese was dat fluorescentiebeeldvorming gecombineerd met echografie meer (lever)metastasen zichtbaar zou maken dan wanneer er alleen inspectie zou plaatsvinden. In 25 patiënten werden er geen extra tumoren gevonden, maar bleek de techniek wel bruikbaar bij het onderscheid tussen benigne en maligne laesies. De accuratesse van visuele inspectie, laparoscopische echografie en nabij-infrarode fluorescentiebeeldvorming was respectievelijk 57%, 57% en 86%.

Deel III gaat in op de toepassingen van specifieke fluoroforen. In **hoofdstuk 8** is een tracer onderzocht die pas fluorescent wordt op het moment dat het in aanraking komt met gamma-glutamyltranspeptidase, een enzym dat tot overexpressie komt bij onder andere plaveiselcelcarcinomen. Doordat inactieve fluoroforen niet fluorescent zijn, wordt aspecifieke achtergrondfluorescentie tot een minimum beperkt. Daarnaast, door deze tracer niet intraveneus toe te dienen maar te sprayen op geresecteerd weefsel wordt het risico op bijwerkingen geëlimineerd en zijn kostbare en tijdrovende translationele onderzoeken niet vereist. **Hoofdstuk 9** beschrijft het preklinische onderzoek naar CRGD, een eiwit dat bindt aan integrines betrokken bij neoangiogenese, gekoppeld aan ZW800-1, een nieuw type 800 nm fluorofoor. CRGD-ZW800-1 kan meerdere tumortypen zichtbaar maken. In **hoofdstuk 10** werd deze tracer getest in gezonde vrijwilligers. Ook werd ZW800-1 los getest, omdat deze fluorofoor volledig renaal geklaard wordt. Hierdoor zouden de ureters zichtbaar gemaakt kunnen worden. Er traden bij beide tracers geen klinisch relevante bijwerkingen op. Aan de hand van deze resultaten zijn inmiddels fase 2 studies in patiënten ontworpen.

Fluorescentiebeeldvorming is in staat om intra-operatief het contrast van tumoren, lymfeklieren en vitale structuren te verhogen, waardoor ze beter te detecteren zijn. Dit proefschrift beschrijft een aantal studies die vereist zijn om nieuwe, specifieke en niet-specifieke fluorescente tracers te transleren naar de kliniek. De techniek lijkt een veilige, effectieve en goedkope manier om de prognose en de kwaliteit van de zorg voor chirurgische patiënten te verbeteren.

Curriculum vitae

Henricus Johannes Marinus (Hein) Handgraaf werd geboren op 4 juli 1988 te Boxtel. Na het behalen van het Gymnasium diploma in 2006 aan het Jacob Roelandslyceum te Boxtel startte hij met de studie Geneeskunde aan de Universiteit Maastricht. In het collegejaar 2009-2010 onderbrak hij de studie één jaar en was hij fulltime vicevoorzitter van Studentenvereniging KoKo. Tijdens zijn hierop volgende coschappen bezocht hij onder andere Borneo in Indonesië (coschap Tropische Geneeskunde) en Zuid-Afrika (coschap Gynaecologie en Obstetrie). Gedurende de coschappen ontwikkelde hij affiniteit voor de chirurgie, waardoor hij in het laatste jaar koos voor een praktijk- en wetenschapsstage bij de afdeling Chirurgie in het Atrium Medisch Centrum (het huidige Zuyderland Medisch Centrum) te Heerlen. Dat jaar was hij tevens voorzitter van het KNMG Studentenplatform, de landelijke belangenbehartiger van geneeskundestudenten. Aansluitend startte hij in 2013 zijn promotieonderzoek bij de afdeling Heelkunde in het Leids Universitair Medisch Centrum (promotores: prof. dr. C.J.H. van de Velde en prof. dr. J. Burggraaf, co-promotor: dr. A.L. Vahrmeijer). In die tijd schreef hij mee aan meerdere grants, waaronder die voor KWF Kankerbestrijding en de National Institutes of Health. Sinds juni 2017 is hij arts-assistent bij de afdeling Chirurgie in het Jeroen Bosch Ziekenhuis te Den Bosch. Hein is gelukkig samen met Tina van Loon, met wie hij een gezamenlijke passie voor onder andere eten, reizen, winter- en duiksport heeft.

LIST OF PUBLICATIONS

Handgraaf HJM, Boonstra MC, Prevoo H, Kuil J, Bordo MW, Boogerd LSF, Sibinga Mulder BG, Sier CFM, Vinkenburg-van Slooten ML, Valentijn A, Burggraaf J, van de Velde CJH, Frangioni JV, Vahrmeijer AL. Real-time near-infrared fluorescence imaging using CRGD-zw800-1 for intraoperative visualization of multiple cancer types. *Oncotarget*. 2017;8(13):21054-66.

Handgraaf HJM, Boogerd LSF, Höppener DJ, Peloso A, Sibinga Mulder BG, Hoogstins CES, Hartgrink HH, Van De Velde CJH, Mieog JSD, Swijnenburg RJ, Putter H, Maestri M, Braat AE, Frangioni JV, Vahrmeijer AL. Long-term follow-up after near-infrared fluorescence-guided resection of colorectal liver metastases: a retrospective multicenter analysis. *Eur J Surg Oncol*. 2017;43(8):1463-71.

Boogerd LSF, Hoogstins CES, Schaap DP, Kusters M, **Handgraaf HJM**, van der Valk MJM, Hilling DE, Holman FA, Peeters KCMJ, van de Velde CJH, Farina-Sarasqueta A, van Lijnschoten I, Framery B, Pelegrin A, Gutowski M, Nienhuijs SW, de Hingh IHJT, Nieuwenhuijzen GAP, Rutten HJT, Cailler F, Burggraaf J, Vahrmeijer AL. Intraoperative tumor-targeted detection of primary, recurrent and peritoneal metastases of colorectal cancer using a fluorescent antibody targeting carcinoembryonic antigen. *Lancet Gastroenterol Hepatol*. 2017 [in press]

Slooter MD, **Handgraaf HJM**, Boonstra MC, van der Velden LA, Bhairosingh SS, Que I, Keereweer S, van Driel PBAA, Chan A, Kobayashi H, Vahrmeijer AL, Löwik CWGM. Detecting tumor-positive resection margins after oral cancer surgery by spraying a fluorescent tracer activated by gamma-glutamyltranspeptidase. *Oral Oncology*. 2017 [in press]

Handgraaf HJM, Boogerd LSF, Shahbazi Feshali S, Farina Sarasqueta A, Snel M, Swijnenburg RJ, Vahrmeijer AL, Bonsing BA, Mieog JSD. Intraoperative near-infrared fluorescence imaging of multiple pancreatic neuroendocrine tumors: a case report. *Pancreas*. 2017 [in press]

Boogerd LSF, **Handgraaf HJM**, Lam HD, Huurman VA, Farina-Sarasqueta A, Frangioni JV, van de Velde CJH, Braat AE, Vahrmeijer AL. Laparoscopic detection and resection of occult liver tumors of multiple cancer types using real-time near-infrared fluorescence guidance. *Surgical endoscopy*. 2017;31(2):952-61.

Boogerd LSF, **Handgraaf HJM**, Huurman VAL, Lam HD, Mieog JSD, van der Made WJ, van de Velde CJH, Vahrmeijer AL. The Best Approach for Laparoscopic Fluorescence Cholangiography: Overview of the Literature and Optimization of Dose and Dosing Time. *Surgical innovation*. 2017;24(4):386-96.

Sibinga Mulder BG, Mieog JSD, **Handgraaf HJM**, Farina Sarasqueta A, Vasen HF, Potjer TP, Swijnenburg RJ, Luelmo SA, Feshali S, Inderson A, Vahrmeijer AL, Bonsing BA, van Wezel T, Morreau H. Targeted next-generation sequencing of FNA-derived DNA in pancreatic cancer. *J Clin Pathol*. 2017;70(2):174-8.

Hoogstins CES, **Handgraaf HJM**, Boogerd LSF, Burggraaf J, Vahrmeijer AL. Image-guided surgery using near-infrared fluorescence: road to clinical translation of novel probes for real-time tumor visualization. *Proc of SPIE*. 2017;10049:100490X-1.

Boogerd LSF, Vuijk FA, Hoogstins CES, **Handgraaf HJM**, van der Valk MJM, Kuppen PJK, Sier CFM, van de Velde CJH, Burggraaf J, Farina-Sarasqueta A, Vahrmeijer AL. Correlation between preoperative serum carcinoembryonic antigen levels and expression on pancreatic and rectal cancer tissue. *Biomark Cancer*. 2017;9:1-7

Sibinga Mulder BG, Mieog JSD, Farina Sarasqueta A, **Handgraaf HJM**, Vasen HFA, Sijnenburg RJ, Luelmo SAC, Feshali S, Inderson A, Vahrmeijer AL, Bonsing BA, Wezel TV, Morreau H.

Diagnostic value of targeted next-generation sequencing in patients with suspected pancreatic or periampullary cancer. *J Clin Pathol*. 2017;70(2):174-8.

Tummers QR, Boogerd LSF, de Steur WO, Verbeek FPR, Boonstra MC, **Handgraaf HJM**, Frangioni JV, van de Velde CJH, Hartgrink HH, Vahrmeijer AL. Near-infrared fluorescence sentinel lymph node detection in gastric cancer: A pilot study. *World J Gastroenterol*. 2016;22(13):3644-51.

Handgraaf HJM, Boogerd LSF, Verbeek FPR, Tummers QR, Hardwick JC, Baeten CI, Frangioni JV, van de Velde CJH, Vahrmeijer AL. Intraoperative fluorescence imaging to localize tumors and sentinel lymph nodes in rectal cancer. *Minim Invasive Ther Allied Technol*. 2016;25(1): 48-53.

Boogerd LSF, **Handgraaf HJM**, Lam HD, Braat AE, Baranski AG, Swijnenburg RJ, Frangioni JV, Vahrmeijer AL, Ringers J. Application of near-infrared fluorescence imaging during modified associating liver partition and portal vein ligation for staged hepatectomy. *Surgery*. 2016;159(5):1481-2.

Bongers PJ, Boogerd LSF, **Handgraaf HJM**, Hoogstins CES, van de Velde CJH, Burggraaf J, Vahrmeijer AL. Image-guided surgery using fluorescence: road to clinical translation of novel probes. *SPIE BIOS*. 2016.

Boogerd LSF, **Handgraaf HJM**, Boonstra MC, Vahrmeijer AL, van de Velde CJH. Image-Guided Surgery. In: Poston GJ, Wyld L, Audisio A, editors. *Surgical Oncology: Theory and Multidisciplinary Practice*. Second ed: CRC Press; 2016.

Handgraaf HJM, Verbeek FPR, van de Velde CJH, Hutteman M, Vahrmeijer AL. Identification of malignant tumors in the liver. In: Dip FD, Ishizawa T, Kokudo N, Rosenthal R, editors. *Fluorescence Imaging for Surgeons*. First ed: Springer; 2015. p. 159-68.

Hyun H, Park MH, Owens EA, Wada H, Henary M, **Handgraaf HJM**, Vahrmeijer AL, Frangioni JV, Choi HS. Structure-inherent targeting of near-infrared fluorophores for parathyroid and thyroid gland imaging. *Nat Med*. 2015;21(2):192-7.

Handgraaf HJM, Ashton D, Favretti F, Segato G, van Ramshorst B, Meesters B, Greve JW. The Gastric Band That Is Not to Be : Efficacy, Safety and Performance of the Easyband: a Multicenter Experience. *Obes Surg*. 2015;25(12):2239-44.

Boogerd LSF, **Handgraaf HJM**, van de Velde CJH, Vahrmeijer AL. Image-guided surgery using near-infrared fluorescent light: from bench to bedside. *SPIE BIOS*. 2015;93110U-U-11.

Handgraaf HJM, Verbeek FPR, Tummers QR, Boogerd LSF, van de Velde CJH, Vahrmeijer AL, Gaarenstroom KN. Real-time near-infrared fluorescence guided surgery in gynecologic oncology: a review of the current state of the art. *Gynecol Oncol*. 2014;135(3):606-13.

Handgraaf HJM, Boonstra MC, Van Erkel AR, Bonsing BA, Putter H, van de Velde CJH, Vahrmeijer AL, Mieog JSD. Current and future intraoperative imaging strategies to increase radical resection rates in pancreatic cancer surgery. *Biomed Res Int*. 2014;2014:890230.

Vugts G, **Handgraaf HJM**, Marcelissen TAT, Rijkers K, Stoot MPC, Siroen J. Een opmerkelijke perforatie. *Ned Tijdschr Heelkd*. 2014;23(3):17-8.

Handgraaf HJM, Nelissen RM, Bianchi R, Meesters B, Greve JW. [A gastric pacemaker in obese type 2 diabetic patients]. *Ned Tijdschr Geneesk*. 2013;157(0):A5929.

Handgraaf HJM. Loten is zo gek nog niet. *Medisch Contact* 2012;67(26):1621.

DANKWOORD

Dit proefschrift is het resultaat van een intensieve en bijzonder leerzame periode die zonder de hulp van velen niet tot een succesvol einde was gekomen. Ik wil hier graag stilstaan bij iedereen die een belangrijke bijdrage heeft geleverd.

Allereerst zou ik alle patiënten willen bedanken die, ondanks hun ziekte, vertrouwen in ons hebben gehad. Zonder hun deelname zou dit onderzoek niet mogelijk zijn geweest. Ook dank voor de gezonde vrijwilligers die bereid waren om onze middelen te testen.

Dr. Vahrmeijer, beste Lex, dank voor je steun en de ruimte die je me als arts-onderzoeker bood. Een betere mentor kan ik me niet voorstellen. Je prettige begeleiding heeft me veel handvatten geboden waar ik in mijn verdere carrière nog veel profijt van zal hebben.

Prof. van de Velde, dank voor de kansen die u me als student uit het verre Maastricht heeft geboden. Uw uitgebreide staat van dienst was een enorme inspiratie tijdens onze regelmatige gesprekken.

Prof. Burggraaf, beste Koos, dank voor de begeleiding vanuit het Centre for Human Drug Research. Door jouw fijne manier van werken en je pragmatisch handelen hebben we in korte tijd veel mooie studies kunnen verrichten.

Prof. Frangioni, thank you for your guidance over the past years. You are the only one who can correct a manuscript within one hour at any time. Your support has been truly remarkable.

Iedereen van het Greenteam, bedankt voor de samenwerking en de fantastische tijd die we hebben gehad. Congressen, zoals die in Honolulu, New York en Sao Paulo, zijn om nooit te vergeten. Speciale dank voor Noor, onze gezamenlijke wetenschappelijke output telt inmiddels meer dan tien PubMed publicaties! Mark en Babs, jullie (ver)strekken de hulp bij alle muizenexperimenten was onmisbaar. Charlotte en Kim, bedankt voor de fijne samenwerking en alle peren in het CHDR. Daarnaast nog dank voor Thomas, Marion, Willemieke en Maxime voor alle verloren tijd in de Hepatho.

Alle betrokken collega's van het LUMC en met name Kees, beide Mariekes en Shadhvi, dank voor jullie belangrijke bijdrage.

Mijn beste vrienden van Festglede, dank voor het luisterend oor en het plezier wat we in de afgelopen jaren hebben gehad. Jullie zorgden voor de nodige balans tussen ontspanning en werk. Mijn paranimfen Rob en Lars wil ik specifiek bedanken voor hun tomeloze inzet rondom mijn promotie. Ondanks dat we na onze tijd in Maastricht ieder een ander pad zijn gaan bewandelen ben ik blij dat we elkaar nog zo vaak zien.

Mijn Amsterdamse huisgenoten, Anna, Mark, Steven, Cas, de lol die we samen hebben gehad is met geen pen te beschrijven. Dank voor alle mooie avonden.

Mijn zussen Annemarie en Eline, ik ben trots dat ik uit zo'n warm en liefdevol gezin kom. Onze band is heel bijzonder en die moeten we blijven koesteren! Annemarie, ik waardeer het enorm dat je zoveel tijd en moeite in de mooie kaft van dit proefschrift hebt gestoken.

Pap, mam, ik prijs mij gelukkig met jullie onvoorwaardelijke steun en belangstelling. Jullie stabiele basis en de vanzelfsprekendheid waarmee jullie me altijd met raad en daad bijstaan hebben heeft het voor mij mogelijk gemaakt om te doen wat ik nu doe.

En tot slot, de allerbelangrijkste, mijn liefste Tina. Jij bent in al die jaren van onschatbare waarde voor mij geweest. Jouw steun, begrip en liefde hebben me regelmatig overeind gehouden.

